



Universiteit
Leiden
The Netherlands

Essentiality of conserved amino acid residues in β -lactamase

Chikunova, A.

Citation

Chikunova, A. (2022, May 31). *Essentiality of conserved amino acid residues in β -lactamase*. Retrieved from <https://hdl.handle.net/1887/3304732>

Version: Publisher's Version

License: [Licence agreement concerning inclusion of doctoral thesis in the Institutional Repository of the University of Leiden](#)

Downloaded from: <https://hdl.handle.net/1887/3304732>

Note: To cite this publication please use the final published version (if applicable).

Essentiality of conserved amino acid residues in β -lactamase

Aleksandra Chikunova

Essentiality of conserved amino acid residues in β -lactamase

Proefschrift

ter verkrijging van
de graad van doctor aan de Universiteit Leiden,
op gezag van rector magnificus prof. dr. ir. H. Bijl,
volgens besluit van het college voor promoties
te verdedigen op dinsdag 31 mei 2022
klokke 15:00 uur

door

Aleksandra Chikunova
geboren te Moskou, Rusland
in 1993

Promotores:

Prof. dr. M. Ubbink
Prof. dr. A. Perrakis (Het Nederlands Kanker Instituut, Amsterdam)

Promotiecommissie:

Prof. dr. H. S. Overkleeft
Prof. dr. R. T. Dame
Dr. A. S. Wentink
Prof. dr. N. Doucet (Institut National de la Recherche Scientifique, Quebec, Canada)
Dr. T. den Blaauwen (Universiteit van Amsterdam)

Table of contents

List of abbreviations		6
Chapter 1.	Introduction	7
Chapter 2.	The roles of highly conserved, non-catalytic residues in class A β -lactamases	25
Chapter 3.	The N214-D233-D246 motif is essential for correct positioning of the active site residues in BlaC	69
Chapter 4.	Conserved residues Glu37 and Trp229 play an essential role in protein folding of β -lactamase	89
Chapter 5.	Mutations in two highly conserved residues are beneficial for BlaC	117
Chapter 6.	Crystal structures of single-point mutants of BlaC	141
Chapter 7.	General conclusions	159
References		166
Summary		181
Curriculum Vitae		185
List of Publications		186

List of abbreviations

BCG	Bacille Calmette-Guerin
CD	Circular dichroism
CSP	Chemical shift perturbation
DTT	Dithiothreitol
EDO	Ethylene glycol
EDTA	Ethylenediaminetetraacetic acid
ESBL	Extended spectrum β -lactamases
HSQC	Heteronuclear single quantum coherence
IPTG	Isopropyl β -D-1-thiogalactopyranoside
MDR	Multidrug resistant
MIC	Minimal inhibitory concentration
Mtb	<i>Mycobacterium tuberculosis</i>
NMR	Nuclear magnetic resonance
PA	Polyacrylamide
PAS	Para-aminosalicylic acid
PBP	Penicillin-binding protein
PEG	Polyethylene glycol
RMSD	Root-mean-square deviation
SDS	Sodium dodecyl sulfate
TEV	Tobacco Etch Virus
TROSY	Transverse relaxation optimized spectroscopy
TSA	Thermal shift assay
TSP	Trimethylsilylpropanoic acid
WHO	World Health Organization
XDR	Extensively drug resistant

Chapter 1
Introduction

Protein evolution

“...it is not the most intellectual of the species that survives; it is not the strongest that survives; but the species that survives is the one that is able best to adapt and adjust to the changing environment in which it finds itself.”

Leon C. Megginson, 1963

All organisms are optimized for their environment and are found in a state that shows little or no morphological change over time. This state is called stasis and represents the best phenotype in a given condition. However, if the environment changes, it forces organisms to change too. These changes were believed to occur gradually and continuously via a process called anagenesis, transforming the whole species into another¹. This phyletic gradualism model was later transformed into a punctuated equilibria model, which was proposed by Niels Eldredge and Stephen Jay Gould in 1972². In contrast to anagenesis, according to the punctuated equilibria model, species are changing via cladogenesis, dividing into two distinct species. Cladogenesis is a response to a rare and rapid environmental change and happens in a short period of time. However, our perception of “short” and “rapid” is different from the evolutionary time scale. Charles Darwin wrote that “although each species must have passed through numerous transitional stages, it is probable that the periods, during which each underwent modification, though many and long as measured by years, have been short in comparison with the periods during which each remained in an unchanged condition”³, so the transition from one stasis to another still happens gradually, with no noticeable difference between generations.

Under changed conditions organisms need to be able to adapt, so their proteins need to evolve, and they have been doing it successfully for billions of years. Our understanding of protein evolution is far from complete. While we might have obtained a great portion of knowledge about molecular mechanisms involved, we still lack the full knowledge of fundamental aspects of it.

The evolutionary process in proteins is determined by three main components: mutation in the DNA code, which occurs randomly and is the mechanism of evolution, selection, which determines the viability of mutations, and drift, which allows for a fixation of neutral mutations. Each single mutation, in order to persist, needs to be “accepted” by a functional protein. This was first proposed by John Maynard Smith in 1970. According to his concept, for evolution by natural selection to occur, functional proteins must form a continuous network in sequence space with single mutation steps without passing through nonfunctional intermediates⁴. A selective model of evolution was for a long time the main model. It suggested that all mutations are either detrimental for a protein and, therefore are not carried on, or beneficial. In 1968, Motoo Kimura for the first time proposed the neutral

model of evolution, arguing that most mutations arising during evolution are actually neutral^{5,6}, a theory that is well-accepted today. Although initially he based his theory on a very small dataset, later he was able to find proof for its relevance in the facts that conservative substitutions (changes to another amino acid of the same group) occur more often than non-conservative and that the rate of synonymous mutations (DNA changes in a gene that do not affect the amino acid sequence) are almost always higher than non-synonymous ones (DNA changes leading to changes in the amino acid sequence)⁷.

Proteins populate fitness peaks, which are the local optima in the fitness landscape. Fitness is a quantitative representation of an evolutionary selection process, and as such fitness peaks can be considered phenotypes that are more successful in present conditions than other phenotypes. Changing environmental conditions affect the fitness of the organism and thus may change the fitness landscape of its proteins. A number of fitness criteria for proteins have been proposed, such as foldability, folding rate, stability, substrate affinity and, for enzymes, accessibility of active site residues⁸⁻¹². If a protein adopts a new function, it needs to traverse the fitness landscape from one fitness peak to another. That means it must pass through lower fitness intermediates, an adaptive valley. Weak selection that purges only detrimental mutations aids in crossing from one fitness peak to another, because it allows for accumulation of neutral mutations. That was experimentally demonstrated with in-lab evolution performed on TEM-1 β -lactamase¹³. Crossing through this valley requires a close coaction of two important evolutionary properties: evolvability and evolutionary robustness.

Evolvability and evolutionary robustness

Evolvability and evolutionary robustness are fundamental features of biological systems on all levels of organization. Evolvability or adaptability describes the capability of a system to acquire a new trait. Evolutionary robustness or neutrality describes the phenotypical resistance to changes, in terms of proteins, the ability to accumulate mutations without losing the original function (Figure 1.1). Enzymes are often highly robust to mutations. It was shown for example, for bacteriophage T4 lysozyme that mutations in more than half of the sequence are well tolerated¹⁴. Evolvability on the other hand is not a basic property of enzymes, some families are known for their high evolvability and are able to acquire a new function relatively easy, such as β -lactamases^{15,16}, and some enzyme families are highly specific and invariable, such as dihydrofolate reductase¹⁷. Robustness and evolvability may appear to be contractionary traits at first, but evolvability is heavily dependent on robustness^{18,19}. To obtain a new functional mutation, proteins must sample various non-functional mutations without losing the native phenotype, and, most importantly, in a robust system a phenotype is presented by an ensemble of genotypes (neutral network), which increases the number of pathways evolution can take to generate a new phenotype.

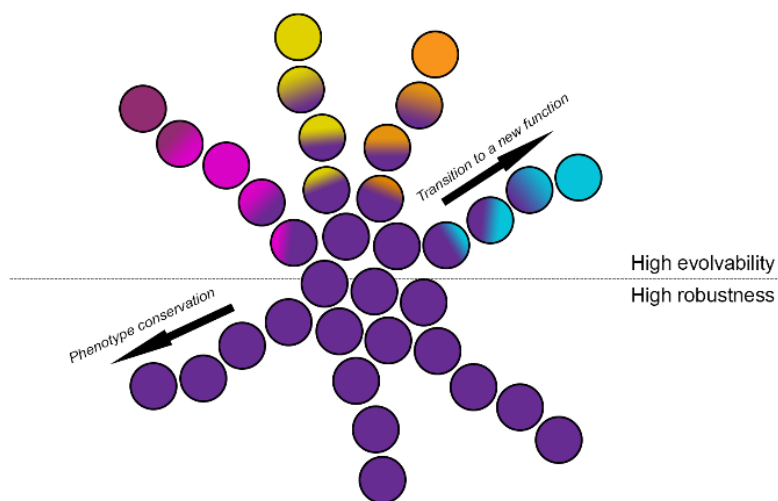


Figure 1.1. Schematic representation of evolvability and evolutionary robustness traits. Each circle represents a genotype, color represents phenotype. Mutational pathways are represented by successive genotypes radiating from the center.

Another interesting concept, which to date has not received much attention, is evolution of evolvability. It seems logical that nature would favor mutations that enhance evolvability, at least for species that have a high chance of meeting new selection pressures due to environmental changes. However, the underlying mechanisms are extremely difficult to define. So, is evolvability evolvable? Some studies oppose this concept^{20,21}, while others argue that it is plausible^{22,23}. A study by Zheng *et al.* (2020) showed that selection does indeed enhance evolvability by increasing robustness²⁴. In this study a population with yellow fluorescence protein was subjected to either strong or weak selection and then evolved toward green fluorescence. It was then demonstrated that the population under weak selection adapted the new phenotype at a higher frequency at first, however, eventually, the population under strong selection evolved more rapidly due to increased robustness and foldability in this population.

Role of stability in the evolution process

Structural stability (and foldability) of a protein is named as one of the main fitness criteria, however, generally, only marginal stability and foldability are required to obtain functional enzymes. Enzymes can therefore evolve within a “neutral” range of stability that maintains their fitness. Mutations that do not cause a large destabilizing effect are carried on. Such destabilizing mutations occur relatively often (about a third of all mutations²⁵) and are purged by negative selection. Some mutations, although rare, can increase stability too much, compromising the dynamics of the enzyme, and these mutations also do not persist.

Protein stability promotes evolutionary robustness. Stabilizing mutations do not influence fitness on their own, but they buffer the destabilizing effect of other mutations. Stabilizing

mutations can cause local or global effects, compensating for destabilizing mutations of distant residues. Most functionally beneficial mutations in enzymes are destabilizing, as active site residues must satisfy a number of constraints, such as geometry, interaction ability, and hydrophobicity. These make active site residues highly optimized for activity and, consequently, poorly optimized for stability²⁶. It was even proposed by Beadle and Shoichet that regions with relative instability or “regions where stability rules are broken” can be used as an indicator for active sites in enzymes with unknown function²⁷. Stability and activity tradeoff has been a subject of debate for decades. It was first demonstrated by Wang *et al.* that mutations leading to new functions are highly destabilizing²⁸. While some works refer to activity and stability as conflicting features^{27,29}, several studies showed that some highly stabilized enzymes can still be fully functional^{8,30}. Studies of ancestral enzymes demonstrated that these proteins were much more stable than today’s enzymes, and that the proteins lost the excess stability during evolution for the sake of new functions³¹. It was also shown that destabilized mutants with improved functions become closer to the consensus/ancestor sequence upon acquiring the stabilizing mutations. For example, many clinically isolated TEM β -lactamase mutants harbor the stabilizing mutation M182T, while for ancestral β -lactamase threonine is the canonical residue at position 182³¹. Tokuriki *et al.* (2008) indicated that although new-function mutations surely are destabilizing, the destabilization effect is not greater than that of a random destabilizing mutation³². Thus, for a new function to evolve, an enzyme must be able to cope with destabilizing mutations. In that way, general stability promotes evolvability. Multiple studies showed a link between increased stability and increased evolvability. This has been demonstrated computationally and also experimentally for cytochrome P450 by Bloom *et al.*³³. On the other hand, more stability can mean less plasticity and a more rigid protein, which generally impairs evolvability, at least in the case of enzymes. Dellus-Gur *et al.* demonstrated using TEM-1 that it is critical that the enzyme scaffold is stable but that the active site needs sufficient flexibility¹⁷.

Conserved residues

Protein evolution works via mutagenesis, and for that reason it is desirable to have a limited number of essential residues. A small number of essential residues is directly linked to evolutionary robustness, as it ensures that most mutations have a low chance of a detrimental effect on protein. Also evolvability benefits from a small number of crucial residues, because it leaves more room for new and possibly functional mutations to occur.

Mutation of an essential residue may affect the enzyme in a variety of ways (Figure 1.2), all leading to loss of enzyme function. These residues are usually highly conserved among orthologous proteins and, thus, conservation is used as a proxy for essentiality^{34–37}. Considering all the factors that are in play to create a functional protein (Figure 1.2), the number of highly conserved residues in enzymes is surprisingly low.

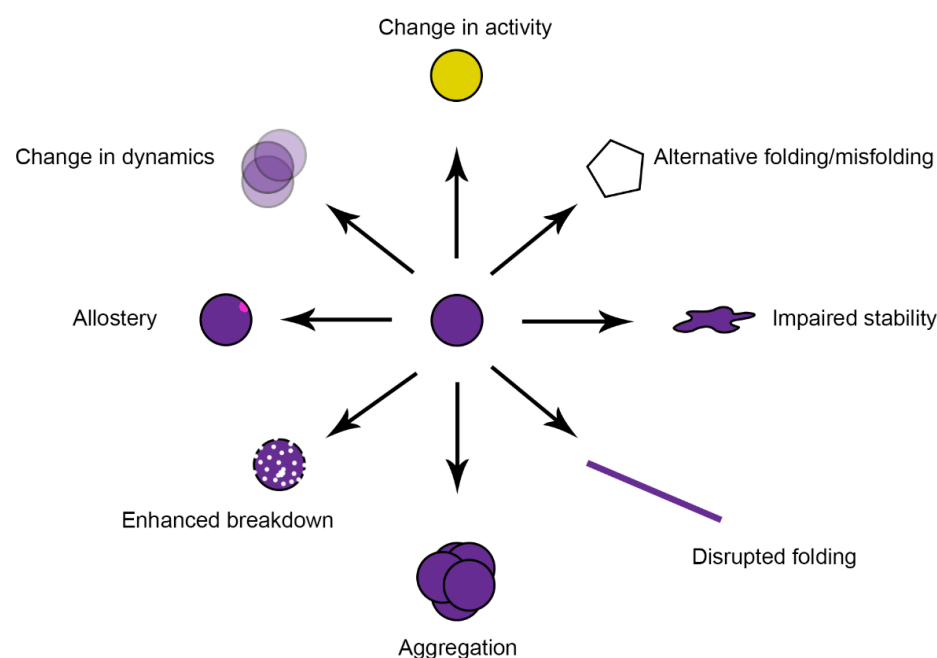


Figure 1.2. Schematic representation of possible effects of mutation of a conserved residue.

Residues involved in enzymatic catalysis, unsurprisingly, tend to be highly conserved. A link between evolution rate and the distance from the active site was demonstrated by Jack *et al.* An almost linear dependence was reported, showing decreasing conservation with increasing distance from the active site³⁸. However, even far from catalytic sites of enzymes conserved residues can be found. Often, these distant conserved residues are discussed in the context of maintaining the three-dimensional structure, i.e. the fold^{39–41}. The number of protein folds is insignificant compared to the number of reactions that can be catalyzed by enzymes. Proteins with similar fold can be involved in highly diverse reactions, for example phosphocarrier HPr protein and human carboxypeptidase A2 share the α/β plait fold⁴². Proteins with the same fold have the same secondary structure elements arranged in the same three-dimensional structure, yet the residues in these elements can vary greatly. Fold conservation is much greater than sequence conservation. Similar folds can be obtained with sequence identity as low as 10–15%⁴³. This observation suggests that the folds have a small set of “staple” residues that arrange secondary structure into three dimensions. These residues are usually highly conserved. The presence of such small number of “staple” residues aids the evolutionary robustness of a protein, as it leaves more freedom for random mutations to occur inside the secondary structure elements, while the 3D arrangement stays intact. The concept of stapling residues is discussed in more detail in Chapter 2. Conserved residues are often found to

form clusters⁴⁴. Such clusters can be found, for example, at protein-protein interfaces⁴⁵ or be involved in formation of the folding nucleus, which aids the formation of the fold⁴². In the study by Mirny and Shakhnovich the five most common folds were analyzed for detection of conserved residues that might illuminate the folding nuclei. For each of the studied folds they identified positions that are conserved in most of the protein families sharing this fold. The residues were forming clusters but the nature of interactions stabilizing these clusters were found to be different in different folds and even in different families of the same fold⁴².

Here, we divide conserved residues of enzymes into three groups based on their position in the structure. The first-shell residues form the active site, responsible for substrate binding and catalysis. The second group includes the residues outside active site but in close proximity to the residues of the active site, the residues of this group are not directly involved in the enzymatic action (second shell). Catalysis requires accurate positioning of the atoms involved in chemical reactions, so residues of the second shell can be important for the precise sub-Ångström positioning of the residues of the active site. The third group or third shell includes the residues that are located very far from the active site, spread over the protein, and without direct interactions with active site residues. This group of residues is likely to be involved in maintaining the protein fold, creating a 3D-scaffold for the active site.

Subject of the study

“The Captain of all these men of death, that came against him to take him away, was the Consumption, for it was that that brought him down to the grave”

John Bunyan, 1680

Tuberculosis

Tuberculosis (“Consumption”) is a deadly disease, a leader of all infectious diseases, which accompanied humans throughout history. Multiple studies confirm the presence of the disease in populations dating from more than 8000 years ago, as well as in many Egyptian mummies^{46–50}. Although no hard evidence is present, it has been argued that human beings fell victim to tuberculosis even earlier, since the early human migrations⁵¹. While first human populations suffered from tuberculosis incidentally, urbanization increased population density enabling tuberculosis to be spread more easily. This development, combined with the lack of a treatment, led to high mortality due to tuberculosis. The incidence of the disease peaked in the 18th-19th centuries, becoming an epidemic in Europe. Even nowadays, until the rise of coronavirus infections in 2020, tuberculosis was the leading cause of death from a single infectious agent⁵². Acknowledgement of tuberculosis as a disease can be traced also in literature throughout history, in which it is described under various names already in ancient times by Cicero, Hippocrates⁵³ and in the Old Testament⁵⁴. Later, in the 19th century, because of the wide spread of tuberculosis, it even became a fashion statement. The looks of patients with tuberculosis were romanticized for their pale faces with rosy cheeks and eyes that “sparkled as bright as diamonds”⁵⁵.

Throughout history physicians have tried to propose a cause of tuberculosis disease. The theories varied from it being hereditary to being spontaneous. In 1865, Jean-Antoine Villemin first reported that he was able to transmit tuberculosis from a human patient to a rabbit. And in 1882, Heinrich Hermann Robert Koch announced that he found a pathogen responsible for the disease, a discovery honored with the Nobel Prize in 1905. This pathogen was named *Mycobacterium tuberculosis* in 1883. *M. tuberculosis* is the main etiologic agent of tuberculosis. It has no environmental reservoir, with humans being its natural host and is believed to have co-evolved with us over millennia. For example, the ability of the pathogen to encapsulate itself inside a host and stay dormant for decades, which developed 20,000-30,000 years ago, is considered a survival strategy in response to limited contagiousity in small, widely dispersed populations of human beings⁵¹. On the other hand, the genome of humans adapted to the tuberculosis infection as well⁵⁶.

Giving the spread and lethality of tuberculosis, the human race always faced a need for prevention and remedy but attempts for treatment were for a long time ineffective. For many

years starting from ancient times fresh air, milk and sea voyages were recommended as the cure for tuberculosis and, while these recommendations are generally nice to follow and may have benefitted the general condition of the patient, they did little harm to a deadly infection. Starting from 496 and for the next several hundred years, a “royal touch” (a healing touch by a hand of a royal)⁵⁷ was commonly used in Europe to treat extrapulmonary tuberculosis condition, which, unsurprisingly, also did not work. High-altitude sanatoria became very popular in the 19th century, where the main treatment course included aero- and heliotherapy, better nutrition, and bed rest. At the same time, more harmful and unsafe methods such as bloodletting, chest massages with acetic acid, inhalation of antiseptics and even pneumonectomy and “artificial pneumothorax”⁵⁸ were implemented in a desperate search for a therapy. The big step towards the control of tuberculosis spreading was the introduction of the BCG (Bacille Calmette-Guerin) vaccine by Albert Calmette and Camille Guérin in 1921⁵⁹, which is still widely used nowadays for vaccination of newborn babies in high-risk countries, but it was only by the discovery of antibiotics later in 20th century that tuberculosis became curable. The first two drugs discovered in 1944 with a clear effect on *M. tuberculosis* were streptomycin, introduced by Selman Waksman and Albert Schatz⁶⁰ and para-aminosalicylic acid (PAS) synthesized by Jürgen Lehmann⁶¹. Although resistance to these drugs developed rather quickly, the possibility of curing tuberculosis boosted extensive research in pursuit of new compounds or to test existing compounds against *M. tuberculosis*.

Drug therapy of tuberculosis posed another issue. High mutability of *M. tuberculosis* requires the use of a combination therapy. Moreover, due to the thick cell wall of *M. tuberculosis*, its very slow generation time and its ability to become a dormant infection inside granulomas in lung tissue, the antibiotic treatment needs to be carried out for months. Modern chemotherapy of tuberculosis consists of co-administration of ethambutol, isoniazid, rifampicin, and pyrazinamide for six months. Such prolonged therapy of multiple drugs is heavily associated with poor medication compliance. Incomplete antibiotic treatments resulted in isolation of multidrug-resistant (MDR) strains in the 1990s⁶², followed by isolation of extensively drug-resistant (XDR)⁶³ and totally drug-resistant strains in the 2000s^{64–67}. Nowadays, more than half a million new MDR cases are reported each year with about 6% of them being XDR forms.

β-Lactam antibiotics

The rise of antibiotic resistance in *M. tuberculosis* puts pressure on humanity to seek new antibiotics. The process of new drug development and approval for clinical use is very complex and time-consuming. Furthermore, the perceived poor business case for new antibiotics has led to limited interest of large pharma companies to pursue their development⁶⁸. Perhaps, simplicity is the ultimate sophistication and the need for a new antituberculosis strategy can be satisfied with the existing remedies. The most widely used group of antibiotics are β-lactam antibiotics. The first antibiotic discovered in 1929 by Alexander Fleming was a β-lactam⁶⁹, nowadays this

group of antimicrobials counts multiple subgroups with numerous compounds in each⁷⁰ (Figure 1.3). β -Lactam antibiotics are well-researched and there are many advantages of the use of this group of drugs, such as low toxicity, low cost, and a simple delivery method. However, β -lactam antibiotics are not generally used in antituberculosis therapy because *M. tuberculosis* produces a β -lactamase, which makes the bacteria resistant to this group of antibiotics⁷¹. The production of β -lactamases is the most common mechanism of resistance to β -lactam antibiotics⁷², and it was overcome by the introduction of β -lactamase inhibitors. β -Lactamase inhibitors are compounds that bind to β -lactamases, rendering the enzyme inactive, thus allowing β -lactam antibiotics to act. The combination of β -lactamase inhibitors with β -lactam antibiotics was shown to be effective against *M. tuberculosis* in multiple studies^{73–76} and has been recommended as a treatment of last resort by the WHO^{77,78}. It is still possible for β -lactamases to gain resistance against inhibitors through sequence modifications. Many inhibitor-resistant variants of *Escherichia coli* β -lactamases were clinically isolated⁷⁹. Despite evidence once suggesting that resistance against β -lactamase inhibitors is not likely to arise due to mutations in β -lactamase in *M. tuberculosis*⁸⁰, inhibitor inactivation due to synergistic double mutations in BlaC has since been observed⁸¹, as well as a few single mutants less susceptible to inhibitors^{82–85}.

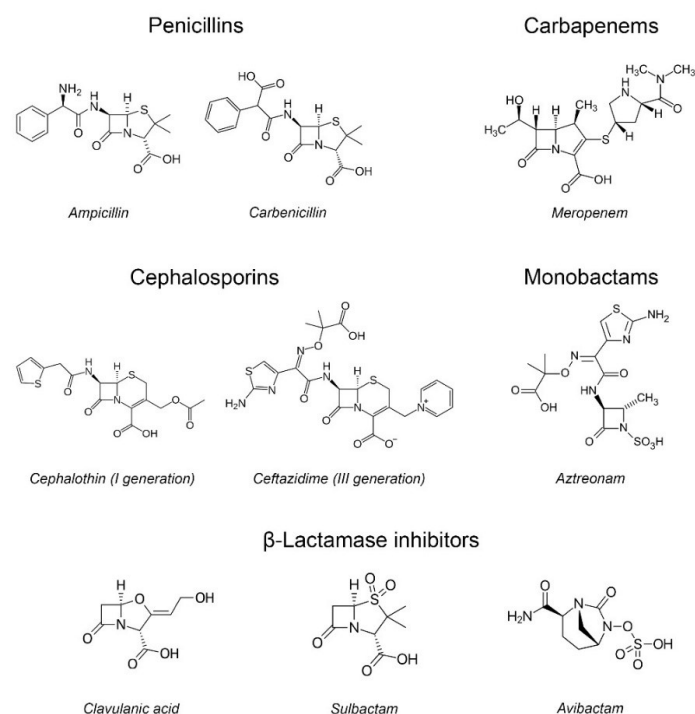


Figure 1.3. Structures of the main groups of β -lactam antibiotics with examples and structures of β -lactamase inhibitors. Clavulanic acid and sulbactam are β -lactam β -lactamase inhibitors and avibactam is a non- β -lactam β -lactamase inhibitor. All shown compounds except for aztreonam were used in this study.

Thus, the resistance against β -lactam antibiotics and β -lactamase inhibitors can routinely occur via mutations in β -lactamases. In such conditions the design of new drugs might be only a temporary solution. However, most of the mutations clinically found in resistant variants were in non-essential amino acids. So, what if we take advantage of the fact that mutations in certain essential residues cannot take place easily? Will it be possible to design an inhibitor to which resistance cannot evolve because it would require a change in an essential residue? This is an exciting idea that can be brought to life only with the comprehensive study of such essential residues and the evolutionary pathways an enzyme has taken and can take.

β -Lactamases, BlaC

β -Lactamases are the enzymes that are able to inactivate β -lactam antibiotics. They were first detected in 1940⁸⁶, interestingly already before the wide use of β -lactam antibiotics in the clinic. The introduction of β -lactam compounds as therapy intensified the process of β -lactamase evolution, and nowadays the β -lactamase family counts more than a thousand unique enzymes with various substrate profiles⁸⁷. β -Lactamases are present in the periplasmic space of Gram-negative bacteria. In Gram-positive bacteria they are found to be bound to the cytoplasmic membrane or excreted⁸⁸.

All β -lactamases are generally classified by two main classification systems. β -Lactamases can be divided in four classes based on their primary sequence homology (Ambler classification)⁸⁹. Classes A, C and D contain serine-proteases, which use a serine residue in the active site^{90,91}. The Ser70 hydroxyl group is involved in the nucleophilic attack on the carbonyl carbon atom in the β -lactam ring⁹². Class B enzymes are metallo- β -lactamases and require one or two zinc ion(s) in the active site^{93,94}. Despite having low sequence identity, different classes still have a similar fold, with two domains, an α -domain and an α/β -domain (Figure 1.4a and 1.4b) or 2 α/β -domains (class B). β -Lactamases also share structural similarity with penicillin-binding proteins (PBPs), transpeptidases that are responsible for the final stages of cell-wall synthesis in bacteria^{95,96}. They are the main target of β -lactam antibiotics and are believed to be the ancestors of β -lactamases⁹⁷.

The Bush-Jacoby classification uses substrate profiles to distinguish three or four groups. Group 1 consists of cephalosporinases and matches class C β -lactamases. Group 2 is defined by its susceptibility to inhibition by clavulanic acid, and includes β -lactamases from molecular classes A and D. It is further divided in subgroups based on the preferred substrate. Group 3 contains class B metallo- β -lactamases with various substrate specificity (mostly carbapenemases) and group 4 includes penicillinases which are not prone to clavulanate inhibition. However, this group sometimes is not included in classification due to unknown enzyme structure^{98–100}.

The β -lactamase from *M. tuberculosis*, BlaC, is a broad-spectrum class A β -lactam degrading enzyme that is encoded by a chromosomal gene¹⁰¹. Although known for years, it was first purified and characterized only in 1998⁷¹ and the first crystal structure of it was obtained in 2006¹⁰¹. BlaC is classified in Bush-Jacoby group 2 and belongs to the extended spectrum β -lactamases (ESBL)¹⁰², as it was shown to degrade penicillins, cephalosporins and several carbapenems^{101,103}, although less effectively than other β -lactamases.

Conserved residues of β -lactamases

Class A β -lactamases are the largest group of β -lactamases, and they have been extensively studied structurally and mechanistically. A sequence alignment of class A β -lactamases done by a ConSurf server^{108,109} indicate that around 15% of the amino acids are identical in >90% of the sequences (Figure 1.4b and 1.4c, more on conserved residues can be found in Chapter 2 of this work). The conserved residues are concentrated in and around the active site but are also found throughout the enzyme structure.

Active site

The process of β -lactam antibiotic hydrolysis starts with substrate binding in the active site, which is followed by nucleophilic attack on the β -lactam carbonyl group (acylation step) (Figure 1.5a). The protonation of the β -lactam nitrogen results in formation of an acyl-enzyme intermediate, which is then hydrolyzed due to a second nucleophilic attack by an activated water molecule, to yield the resting state enzyme and inactivated antibiotic molecule (deacylation step). In 1992, it was shown by Strynadka and colleagues that the acyl-enzyme intermediate is formed by a substrate covalently bound to Ser70 in a deacylation-defective β -lactamase mutant. Thus, Ser70 was recognized as the attacking nucleophile in the acylation step¹¹⁰. The authors also proposed a role for Lys73 as the general base in this process. However, still today debate is ongoing over the involvement of Glu166, the active site water, and Ser130 in Ser70 activation^{79,111}. In 1993, a study by Knox *et al.*¹¹² proposed a role of Glu166 in deacylation step but not in acylation step, but later other research groups showed the possibility of Glu166 together with a water molecule to act as the general base^{113,114}. It cannot be excluded that the hydrogen transfer pathways differ among different β -lactamases.

Hence, even though the exact mechanisms of proton shuffling, and the initial activation remain controversial, the composition of an active site in class A β -lactamases is well established. The first crystal structure of PC1 β -lactamase derived from *Staphylococcus aureus* solved in 1987 (refined later in 1991 to 2 Å) by Osnat Herzberg allowed to identify the position of the active site residues^{115,116}. The active site of class A β -lactamases consists of Ser70, Lys73, Ser130, Glu166 as the catalytic residues and several residues involved in substrate binding (Figure 1.5b). The conservation of the catalytic residues is extreme, residues 70, 73 and 130 are invariable, and residue 166 is almost invariable with only a few natural substitutions occurring (for example, in some *Nocardia* species, which were isolated from soil in China¹¹⁷, but no crystal structure or substrate information is available for those enzymes). Mutational studies on the catalytic residues allowed for capturing various adducts inside the active site, making the catalysis process clearer. The conservation of the substrate-interacting residues, however, is lower, even though it is still extremely high for some of them. This room for substitutions is likely important for adaptability of the active site for new substrates. For

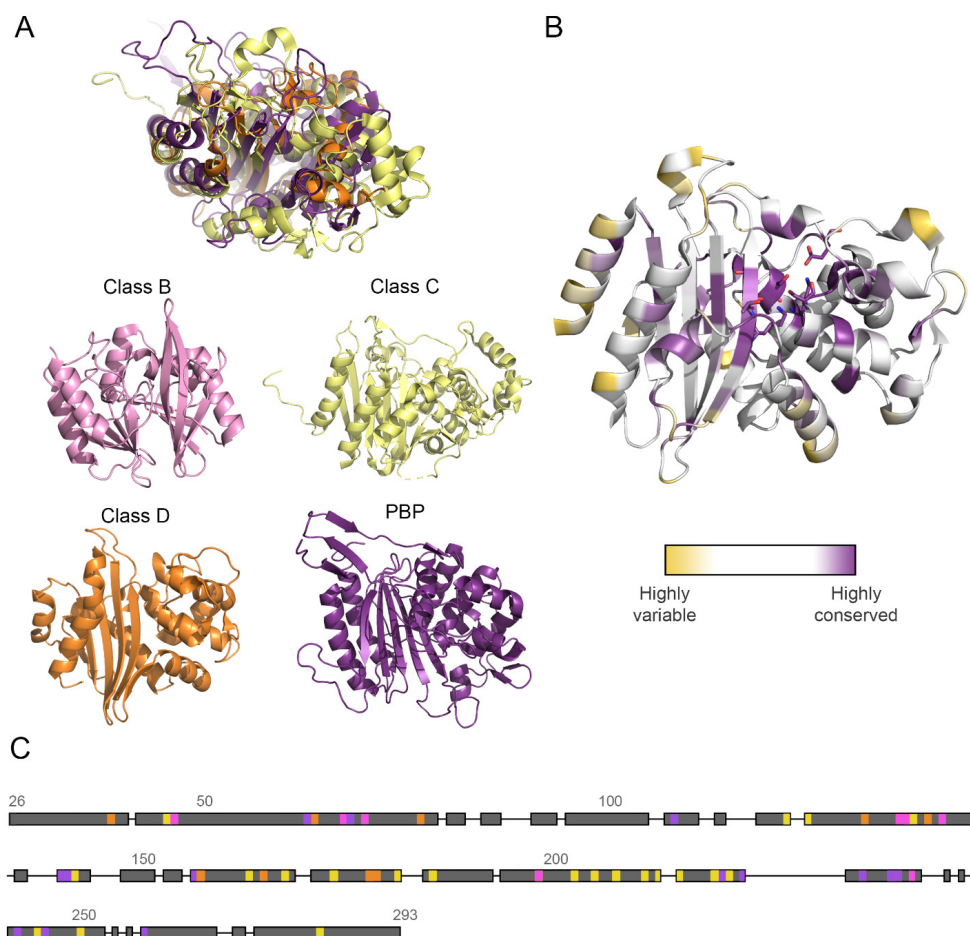


Figure 1.4. (A) Examples of classes B (4D1T¹⁰⁴), C (5K1D¹⁰⁵), D (1K57¹⁰⁶) β -lactamases and PBP (2Z2L¹⁰⁷). At the top the overlay of class C, D and PBP structures is shown; (B) BlaC (class A, 2GDN¹⁰¹) colored by conservation of amino acid residues. Active site residues are shown in sticks; (C) Consensus sequence of class A β -lactamases with Ambler numbering. Residues that are 100%, >99%, >95% and >90% conserved are shown in pink, orange, purple and yellow, respectively, thin lines show the gaps in consensus sequence.

example, the residue at position 234 is generally lysine and was shown to act as an anchor for the C3 carboxylate of penicillins¹¹⁸. Arginine 234 is found in most carbenicillinases from class A and is experimentally associated with carbenicillinase activity and decreased clavulanate sensitivity^{83,120-123}. Another example of variability in the active site residues is residue 105, which canonically is an aromatic residue (tryptophan or phenylalanine), while in BlaC it is isoleucine. This residue hangs over the active site pocket and regulates the accessibility of the active site for substrates. Due to its small size in BlaC, this “gatekeeper” residue results in a wider active site entrance, which may be one of the reasons for the broader substrate range of BlaC⁸⁰.

Around active site

The group of residues around the active site also received some attention, as they directly influence the position or orientation of active site residues. Extensive research was done on the “gatekeeper” loop (residues 103-106), which includes “gatekeeper” residue 105 (Figure 1.5c). It was shown, for example, for residue Asn106 in CTX-M β -lactamase, that mutation leads to an increased thermostability of the protein, however, it dramatically decreases activity against cefotaxime, due to altered positions of active site residues¹²³. The highly conserved residue Asn136 was demonstrated to have a crucial effect on activity upon mutation, as mutations lead to a displacement of a catalytic residue, Glu166¹²⁴. Several studies showed the importance of the invariable residue Asp131 for folding and formation of a stable protein^{125,126}. Another key element of β -lactamase, the Ω -loop (Figure 1.5c) was researched thoroughly as well. The Ω -loop contains the catalytic residue Glu166 and was demonstrated to be important for substrate recognition. One of the Ω -loop residues, Asn179, is highly conserved, and its mutation altered the substrate profile in TEM and KPC-2¹²⁷⁻¹³⁰. In many β -lactamases Asn179 makes an interaction with Arg164 and the disruption of this interaction is believed to contribute to a changed substrate profile.

Far from active site

Conserved residues far from the active site have received limited attention, probably because they do not contribute to a possible novel activity and therefore are not of great interest. It was shown that the conserved Trp229 might be involved in the modulation of an allosteric site^{131,132}. Meneksedag *et al.* showed that β -lactamase inhibitor protein caused changes in the flexibility of TEM-1 regions away from the main binding site, thus pointing toward the binding to the alternative site. Such an alternative binding site contained Trp229 and the authors discussed the importance of Trp229 for the modulation of the allosteric communication between the main and alternative binding sites¹³². A similar conclusion was made in another study on TEM-1, where the importance of Trp229 for regulation of an allosteric site was discussed together with Pro226, another highly conserved residue¹³¹.

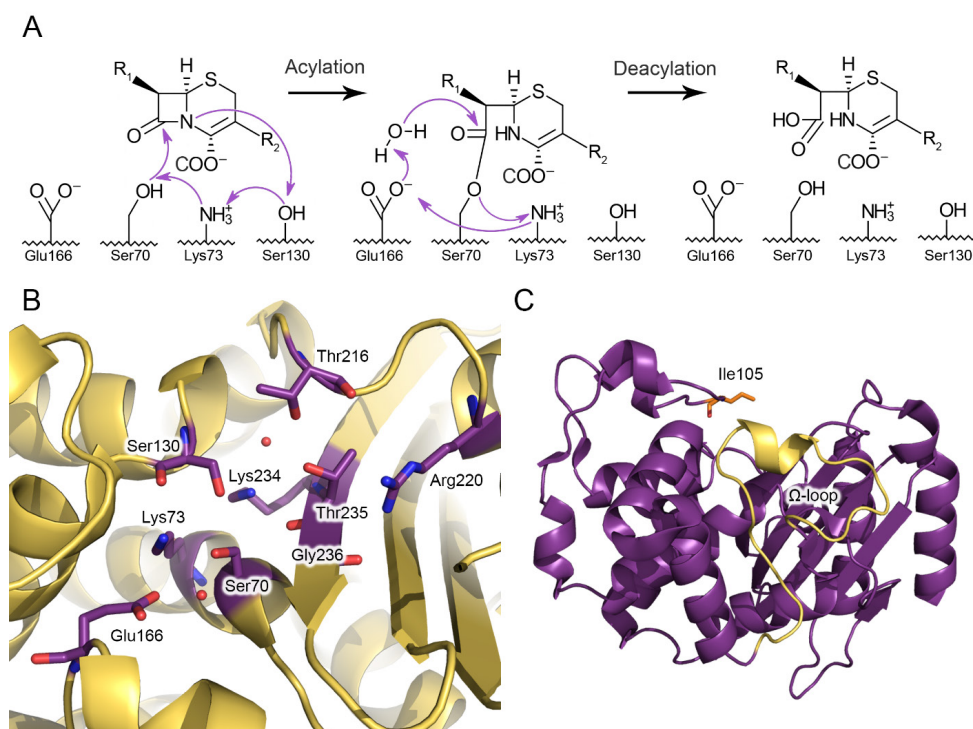


Figure 1.5. (A) Schematic representation of the proposed catalytic mechanism of class A β -lactamases; (B) Active site of BlaC (2GDN) with important residues shown in sticks and waters as red spheres; (C) BlaC structure with the gatekeeper residue 105 in orange sticks and the Ω -loop (in yellow).

Research question and thesis overview

The aim of this research was to better understand evolutionary processes in enzymes, specifically in β -lactamases, in terms of the patterns of residue conservation. Under the assumption that enzymes under heavy and varying selection pressures, such as is the case for β -lactamases, will minimize the number of essential residues to increase evolutionary robustness and evolvability, the question of which critical roles the remaining essential residues play, is highly relevant. Understanding these roles in relation to the location in the structure (first, second and third shell) can provide insight into the relationship between structure, dynamics, activity and evolution of β -lactamases and enzymes in general. While most research is focused on catalytic residues, the conserved residues of second and third shells also convey an interesting message. We have formulated possible roles of such conserved residues and attempted to test these hypotheses with extensive mutational studies to serve a basis for understanding molecular mechanisms involved in enzyme evolution.

Chapter 1 of this thesis provides relevant background information in the fields of protein evolution and β -lactamases, as well as an overview of questions discussed in this work. A large-scale mutational study, including *in vivo* and *in vitro* characterization is described in *chapter 2*, where the roles of all second-shell and third-shell conserved residues are discussed. It is shown that second-shell residues contribute to the arrangement of the active site residues, while residues from the third shell are mostly responsible for the folding process and stability. Interesting observations on the structural effects of second-shell mutations are described and various roles in the folding process are proposed. The general observations and patterns presented in this chapter are supported with in-depth discussions of specific mechanisms of function for several second- and third-shell residues in the next chapters. *Chapter 3* gives an insight into the exact roles of several second-shell residues. It is proposed that mutations in these residues create a mobile part displacing the substrate-binding residues. Moreover, this chapter demonstrates co-evolution of residues because comparison of the sequences reveals a surprising pattern in the position of a substrate binding residue. In *chapter 4* a thorough discussion of several third-shell residues is presented. Two residues very far from active site are shown to be involved in different aspects of the folding of β -lactamase. *Chapter 5* touches on some characteristics of residues that exhibit unexpected results upon mutation. While it is expected that conserved residues are essential, for some of them mutations are not only non-damaging but, in some cases, even advantageous. In *chapter 6*, crystal structures of a variety of BlaC mutants which were found in directed evolution studies are discussed. This chapter reveals possible changes that can occur in a protein upon gaining an improved phenotype. *Chapter 7* concludes this work with a general discussion and an outlook on further research.

Chapter 2

The roles of highly conserved, non-catalytic residues in class A β -lactamases

Based on the research article:

Aleksandra Chikunova, Marcellus Ubbink (2022). The roles of highly conserved,
non-catalytic residues in class A β -lactamases, *Protein Science*, accepted

Abstract

Evolution minimizes the number of highly conserved amino acid residues in proteins to ensure evolutionary robustness and adaptability. The roles of all highly conserved, non-catalytic residues, 11% of all residues, in class A β -lactamase were analyzed by studying the effect of 146 mutations on *in vivo* and *in vitro* activity, folding, structure and stability. Residues around the catalytic residues (second shell) contribute to fine-tuning of the active site structure. Mutations affect the structure over the entire active site and can result in stable but inactive protein. Conserved residues farther away (third shell) ensure a favorable balance of folding vs. aggregation or stabilize the folded form over the unfolded state. Once folded, the mutant enzymes are stable and active and show only localized structural effects. These residues are found in clusters, stapling secondary structure elements. The results give an integral picture of the different roles of essential residues in enzymes.

Introduction

In the cause of evolution, organisms need to adapt to changing environmental conditions, so new enzyme functions must evolve, requiring changes in amino acid sequences. If such changes have a high chance of causing loss of function, the organism is less likely to adapt. Thus, evolution not only selects for functionality but also for evolvability. The potential to gain a new function is limited by the adaptability of the amino acid sequence. It is evolutionary disadvantageous to have many essential amino acid residues, because mutations in these residues will often render a protein inactive. Therefore, evolution forces tend to minimize the number of essential residues.

Conservation of amino acid residues within or among protein families serves as a proxy for essentiality^{5,34,133,134}. If an amino acid residue is highly conserved, it is assumed that evolution has selected against its substitution to prevent loss of function of an enzyme³⁴⁻³⁷. Such a loss can have many causes, including impaired folding, enhanced misfolding, translocation problems, poor stability, enhanced breakdown, and poor function. Given all these possible causes of function loss, the number of highly conserved residues in enzymes is surprisingly low. Broadly, three groups of highly conserved residues can be distinguished, based on their location. The first-shell residues are in the active site and involved in the catalytic function of the enzyme, so substrate binding and catalysis. Substitution of these residues will affect enzymatic function. Second-shell residues surround active site but are not directly involved in catalysis. It is assumed that these residues are important to ensure the exact positioning, to sub-Ångström precision, of the first-shell residues, which is required to enable catalysis of a chemical reaction. Third-shell residues are farther from the active site and, thus, are less likely to affect activity, except in the case of allosteric interactions. Conservation of such residues is expected to be related to a role in folding, prevention of misfolding and/or stability of the three-dimensional structure.

β -Lactamases, enzymes responsible for the breakdown of β -lactam antibiotics¹³⁵, exhibit high evolvability¹³⁶. Over the past decades bacteria managed to respond to the high and constantly changing antibiotic selection pressures by evolving β -lactamases able to degrade novel antibiotics. New β -lactam resistant strains are frequently reported, with sometimes only one point mutation in the enzyme leading to a new catalytic function^{82,137-139}. This room for evolution in β -lactamases is reflected in the low amino acid conservation. A sequence alignment of the β -lactamase from *Mycobacterium tuberculosis* (Mtb), BlaC, the object of this study, with 493 other class A β -lactamases shows 49% - 81% identity^{108,109,140}. Fifteen percent of the residues is extremely conserved, with the same residue type among more than 92% of the sequences. Figure 2.1 shows the degree of conservation mapped on the crystal structure of BlaC. Highly conserved residues are found not only in the active site but widely

spread over the three-dimensional structure. While the roles of the conserved residues from the first shell have been studied extensively^{81,83,84,118,141–144}, the residues from the other two shells received less attention^{124,131,145,146}. In this study, our aim was to establish the roles of the highly conserved residues in the second and third shells of BlaC and to test the general idea that conserved second-shell residues ensure the precise formation of the active site, whereas conserved third-shell residues are important in folding and stability. Evolvability against new antibiotics and β -lactamase inhibitors is related to the conservation of residues, so knowledge of which roles highly conserved residues play will aid in understanding evolutionary pathways toward new enzymatic functions.

We introduced single point mutations for all these conserved residues and characterized the activity, stability, and structure of the enzyme variants. The results of this study support the models formulated above and allow us to assign roles to the highly conserved residues. The structural analysis shows an interesting difference between second and third shell residues in the extend of structural changes caused by the mutation. Surprisingly, for some variants folding, stability and activity are not affected, raising the question as to why these residues are conserved.

Results

Several highly conserved residues can be mutated without activity loss.

An overlay of the amino acid sequences of 494 class A β -lactamases revealed 40 (15%) amino acid residues to be conserved in more than 92% of the sequences with the conservation score 9 (Figure 2.1, Table S2.1). Conserved residues in BlaC were divided in first, second and third shell based on their proximity and association with the positioning of the active site (Figure 2.1). The first shell comprises eight conserved residues involved in catalysis and substrate binding. Residues that have at least one atom located within 4 Å of a first-shell residue, were considered second shell and included 8 residues. Residues that have at least one atom of their side chain within 4 Å of those second-shell residue were also considered second shell and counted 4 residues. The other 19 conserved residues that are located outside this sphere of direct influence on the positioning of the active site residues are defined as third shell. The Ca of third-shell conserved residues were found up to 25 Å away from the Ca of active site residue Ser70.

To establish the roles of the conserved residues in β -lactamases, the second and third shell residues were mutated separately to several amino acid types, and the variant enzymes were extensively characterized, both *in vivo*, using an *Escherichia coli* expression system, and *in vitro*, using cell lysates with overexpressed BlaC. To make the number of mutants manageable, the variants were selected judiciously to vary the size, charge, and polarity of the side chain (Table S2.2), resulting in 146 variants for 31 highly conserved residues (11% of all residues) in the second and third shells. Two residues, at positions 132 and 164, were not included in the study, as BlaC is exceptional in that it carries non-conserved amino acid residues at these positions.

In vivo β -lactamase activity was tested on LB-agar plates with ampicillin and carbenicillin using a construct in which wild type BlaC is produced in low quantity and transported to the periplasm of *E. coli*, to mimic the location in Mtb¹⁴⁷. Compared to ampicillin, carbenicillin only carries an extra carboxyl group. Despite this subtle change in structure, minimal inhibitory concentrations (MIC) of ampicillin and carbenicillin differ by ten-fold for wild type BlaC in *E. coli*, being 100 μ g/mL and 1000 μ g/mL respectively. Most mutants exhibit decreased or no activity for both substrates (Figure 2.2a), but twelve mutants show activity comparable to that of wild type BlaC. Interestingly, these comprise mutations to another of the five amino acid groups (non-conservative mutations), including T71V, T71L, N214A, N214S, and N245H, and some positions were able to tolerate all mutations that were introduced. Moreover, mutants D179N and N245H displayed MICs higher than for wild type BlaC.

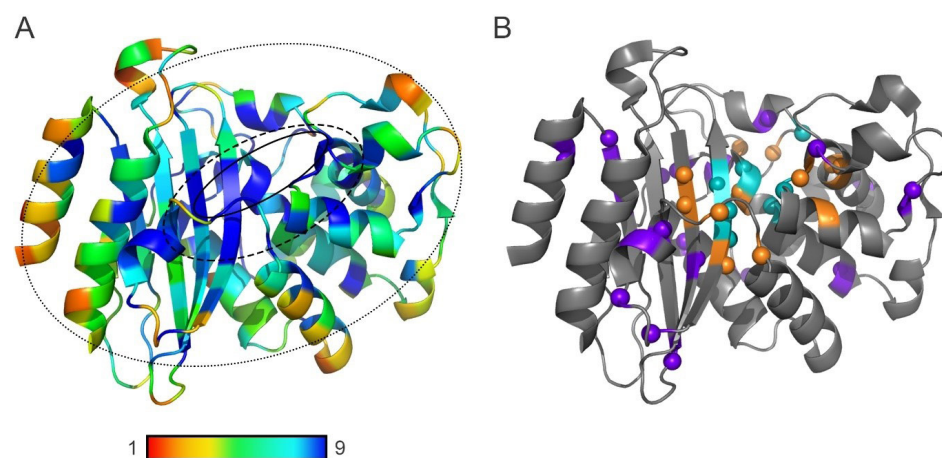


Figure 2.1. (A) Structure of β -lactamase from Mtb (PDB entry 2GDN¹⁰¹) colored by sequence conservation as determined by ConSurf^{108,109,140} with 1 being highly variable and 9 being highly conserved. Solid line, dashed line and dotted line show the area of the first, second and third shells, respectively; (B) Highly conserved residues (>92% with conservation score 9) in BlaC (PDB entry 2GDN). Residues of the first, second and third shell are colored cyan, orange or purple, respectively; backbone nitrogens are shown as spheres.

Many of the conserved residues are critical to obtain folded protein.

The enzyme production level in a cytoplasmic *E. coli* overexpression system was monitored using gel electrophoresis. Production levels of the mutants were found to be close to the wild type, however, for more than half of the mutants, most protein was not soluble. These mutants also show no or very low ampicillin resistance in the low-level expression, periplasmic system (Figure 2.2, panels a and b), indicating that both systems are at least to some extent comparable. It is noted that the periplasmic system is based on Tat-translocation, in which the folded protein is moved towards the periplasm. Thus, low solubility is likely to affect also the quantity of enzyme in the periplasm. This finding suggests that almost half of the conserved residues have a role in correct folding or avoiding misfolding.

All soluble mutants were further analyzed for their fold, stability, and activity. Because of the overproduction systems, these assays could be performed on cell lysates, not requiring the purification of each separate enzyme. Circular dichroism (CD) spectroscopy was used to determine the amount of folded enzyme relative to a wild type BlaC cell lysate and this value was used in determining the activity of the mutant relative to that of wild type BlaC. Example data are shown in Figure S2.2. The chromogenic substrate nitrocefin was used to assay activity (Figures S2.3-S2.4). For some mutants little or no activity was detected due to the protein being unfolded, which was confirmed with both CD and NMR spectroscopies. Interestingly, most mutants for which soluble protein was obtained showed nitrocefin activity comparable to that of wild type BlaC (Figure 2.2c). That was observed also for the mutations that greatly affected the amount of folded protein. Correct folding was hindered by the mutation but once folded, the enzyme behaves mostly as wild type enzyme. For others, such as N136, all variants gave protein yields comparable or better than that for wild type BlaC, yet each had lost activity, as expected for second-shell residues. A thermal shift assay was used to evaluate thermal stability of mutant proteins. The majority of mutants show a slight decrease of melting temperature of 2-3 °C (Figure 2.2c, Figure S2.5). BlaC N245Q showed the largest decrease, by 7 °C. Some mutations increased the thermostability slightly, and for most of these activity was still close to that of wild type BlaC. This observation indicates again that, once folded, the enzyme resembles wild type BlaC, although many residues that are important for folding also contribute to the thermal stability of the folded enzyme.

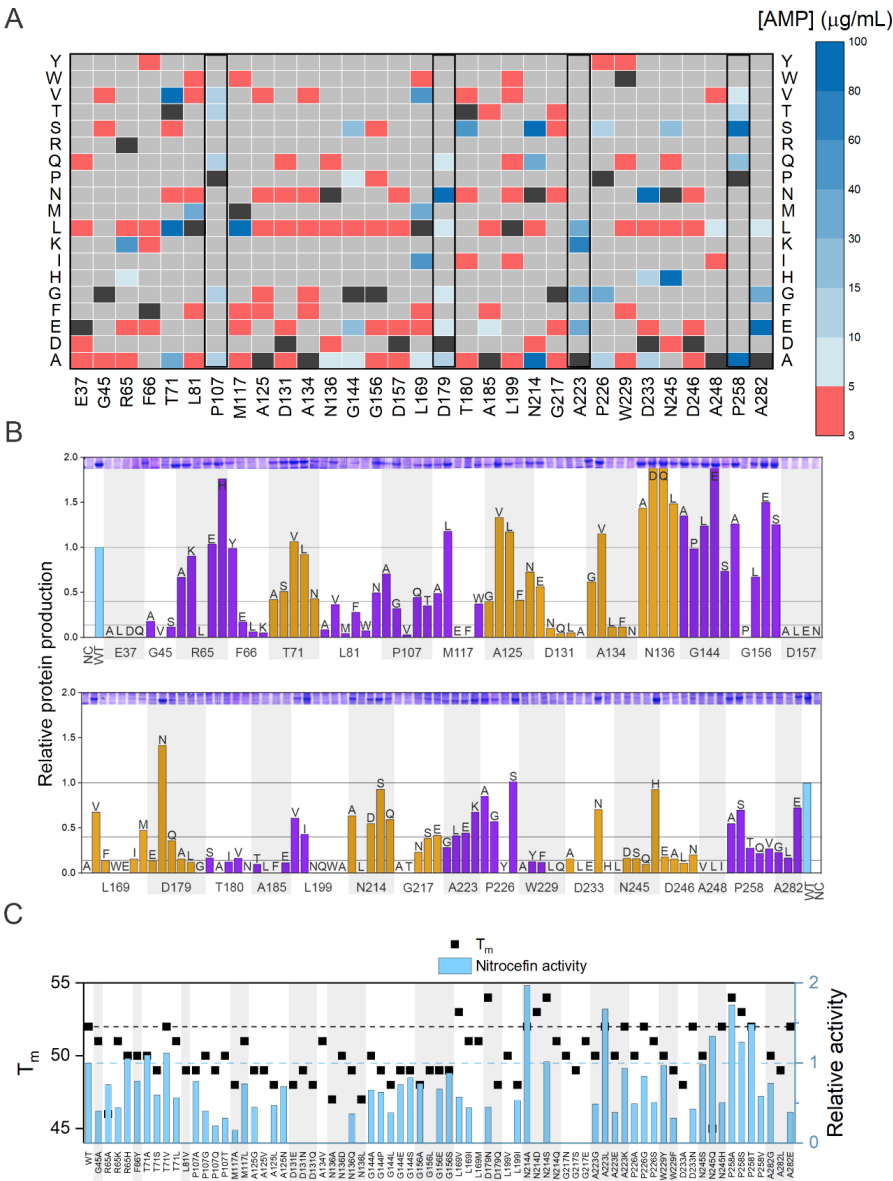


Figure 2.2. Activity, stability, and amount of soluble enzyme of BlaC variants. (A) MICs based on an ampicillin activity plate assay, with substitutions shown vertically. Wild type BlaC is indicated with a black box in each column and grey represents mutations that were not generated. Black rectangles show residues for which all generated mutations were tolerable; (B) Amount of BlaC found in soluble cell fraction of an *E. coli* cytoplasmic overexpression system relative to wild type BlaC, by comparison of the gel band intensity (shown on top of the histograms, full gels can be found in Figure S2.1). Each BlaC band was scaled to the *E. coli* protein band at 40 kDa from the same culture. NC, negative control, the vector without the blaC gene. The third-shell mutants are shown in purple, the second-shell mutants are shown in orange. The horizontal bars indicate cutoffs for good/poor/no soluble protein production; (C) Melting temperatures and relative activity in nitrocefin conversion of soluble mutants in cell lysate (see Materials and Methods for details). Horizontal dashed lines show the wild type BlaC values. The precision of the T_m is 0.5 degree. Mutants that did not yield folded enzyme sufficient for T_m and activity determination are not shown, mutants with a T_m but lacking an activity bar show no detectable activity for nitrocefin.

Second-shell variants cause more wide-spread structural changes than third-shell.

NMR TROSY spectra of the soluble fraction of the lysates were acquired to evaluate the fold of BlaC variants and the changes in structure that occur upon mutation. For many soluble BlaC variants the intensities of well-dispersed peaks were low, pointing to a low amount of folded protein, and often intense signals in the region from 8.0 to 8.5 ppm indicated the presence of a fraction of unfolded protein (Figure 2.3a). For other mutants, the spectra were suitable for tentative peak assignment, which was done by comparison to a spectrum of wild type BlaC in lysate. Figure 2.3a shows an overlay of the spectra of His-tagged enzyme in lysate and purified and His-tag cleaved BlaC. Most resonances derived from BlaC nuclei can readily be identified¹⁴⁸. In general, NMR spectra of second-shell mutants aligned worse with that of wild type BlaC than spectra of third-shell mutants (Figure 2.3a). Significant chemical shift perturbations (CSPs), defined here as > 0.03 ppm, were found for 17% and 6% of assigned peaks for second-shell and third-shell variants, respectively (Figure 2.3b). For second-shell variants, CSPs were mostly found for the same set of residues, spread throughout and around the active site (Figure 2.4). The CSPs were also observed for mutants exhibiting only moderate change in activity or stability. For the third shell residues, CSPs were mostly localized around mutation site. This interesting observation is general for all variants with good NMR spectra and suggests that the interactions that third-shell residues make have low correlation with those further away in the protein (local structural effects only), whereas second-shell mutations cause structural effects that are felt throughout the active site, showing correlation over a longer distance. The effects of the second-shell mutations were similar for both core and surface localized residues (Figure S2.8). Only for two second-shell residues in Ω -loop, L169 and D179, CSPs were found to be spread somewhat less extensively than for the rest of the second-shell residues, however, changes still involved active site and regions around it (Figure 2.4b).

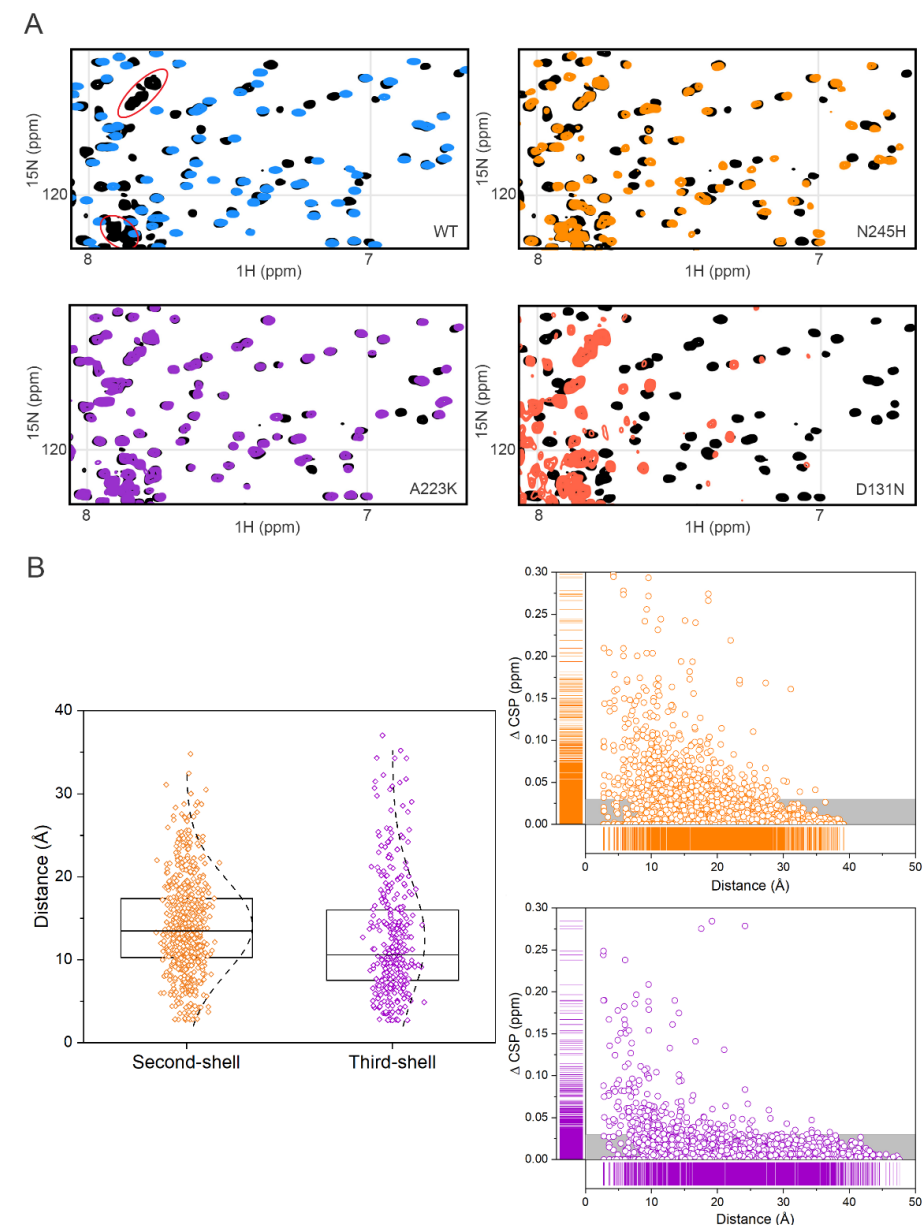


Figure 2.3. NMR TROSY spectra and CSPs. (A) Examples of details of NMR spectra (full spectra in Figures S2.6-S2.7). Wild type BlaC spectrum from whole lysate is shown in black; purified wild type BlaC is shown in blue; spectra of well-folded second-shell (N245H) and third-shell (A223K) mutants are shown in orange and purple respectively; the spectrum of a poorly folded mutant (D131N) is shown in salmon. Red ovals indicate peaks from *E. coli* proteins. (B) All CSPs from all mutant spectra from second (orange) and third (purple) shell are presented on the right against distance from the mutation site (backbone amide to amide). Grey bars represent insignificant CSP (< 0.03 ppm). On the left CSPs above 0.03 ppm are shown for all assigned peaks of all mutants against the distance of the amide nitrogen relative to the Ca atom of the mutated residue. The boxes represent 25th-75th percentile, lines inside the boxes represent the medians, dashed lines represent distribution by count. The median of the second-shell residues is significantly larger ($p < 0.01$) than that of the third-shell residues.

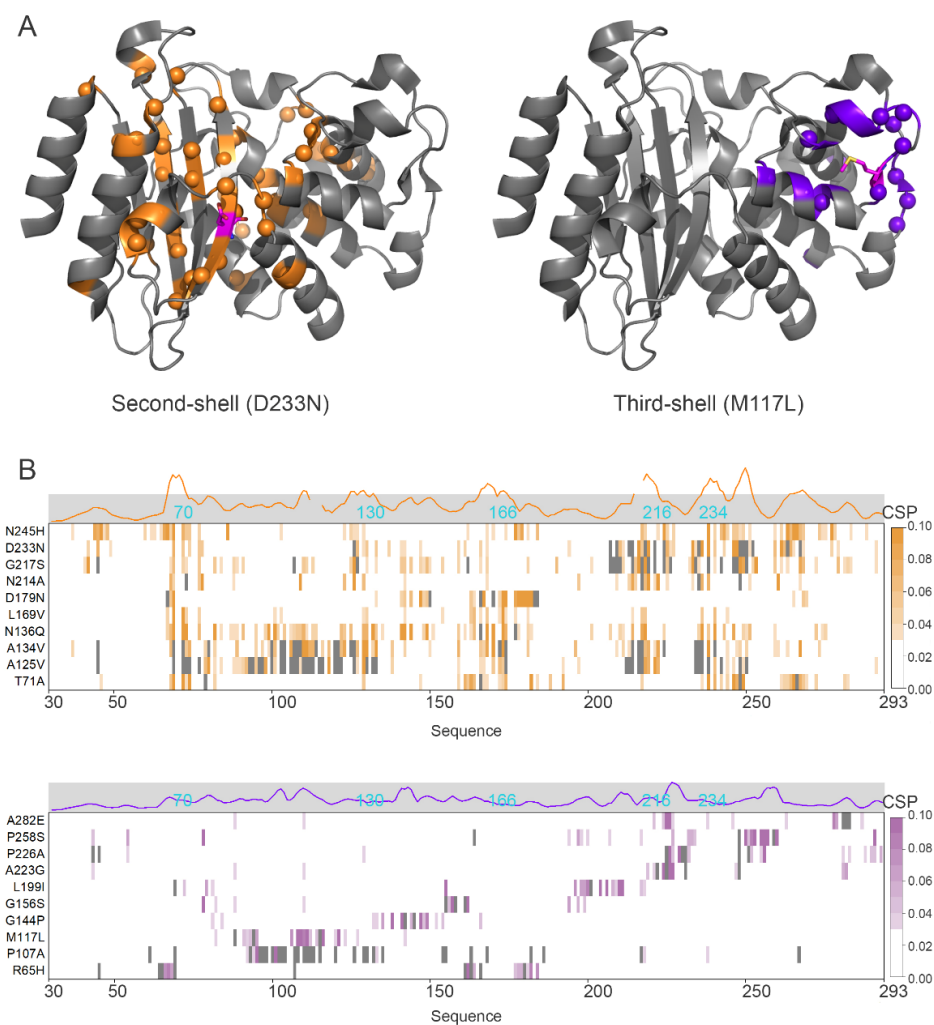


Figure 2.4. Changes in structure observed upon mutations. (A) Examples of the location of nuclei with significant CSP in a second-shell (left) and third-shell mutant (right). CSPs are spread far from mutation site in the second-shell mutant D233N and are localized around the mutation site in the third-shell mutant M117L. The mutated residue is shown in magenta sticks. PDB entry 2GDN¹⁰¹. (B) CSPs of some mutants plotted on the amino acid sequence. Residues for which no data are available are shown in grey. The positions of several first-shell residues are indicated in cyan. For most second-shell mutants large CSPs are found for the same residues, in regions around residues 67-72, 110-112, 125-132, 162-169, 213-217, 232-238, 242-248, 261-266. Third-shell mutants show CSP mostly close to the site of mutation. Traces above the graph represent averaged CSPs for all mutants, curves are smoothed using Savitzky-Golay filter to aid the visualization.

Conservative mutations can be more detrimental than non-conservative ones.

Conservative mutations of conserved third-shell residues always had an equal or less detrimental effect on BlaC, as compared to non-conservative mutations. For several variants of second-shell residues, however, conservative mutations performed worse than non-conservative ones, indicating that slight changes in the functional group have a more negative effect than replacement with a side chain that cannot maintain any interaction. Examples of such residues are Thr71 and Asn214. The conservative mutant T71S displayed *in vivo* activity, thermal stability, as well as the quality of NMR spectrum that was worse than those of T71 substituted by Leu, Val or Ala. Mutants N214D and N214Q performed much worse *in vivo* than mutants N214A or N214S (Figure 2.5, Table S2.2).

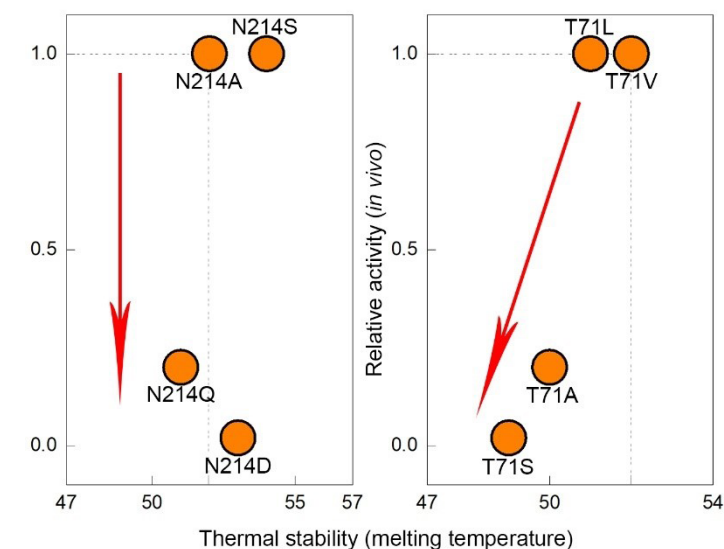


Figure 2.5. Schematic representation of the effect of mutations in residues Thr71 and Asn214 relative to WT. Dashed lines show the WT values. The red arrows show worsening of the mutation effect. For residue Asn214 activity is affected more with conservative substitutions to Gln and Asp compared to non-conservative Ala and Ser. For residue Thr71 conservative substitution to Ser displays the worst activity and stability.

Discussion

In general, we observed three types of mutation effects. Mutations in group A result in strongly reduced amounts of soluble protein and proportionally more in the insoluble fraction. The proteins in the soluble fraction of these BlaC variants exhibit near normal stability, structure and activity. These observations suggest that for these proteins, the mutation has shifted the balance between folding and formation of aggregates to the latter. Considering that folding into the soluble three-dimensional structure is kinetically driven, it implies that the mutation either slows the folding rate or accelerates the aggregation rate (Figure 2.6, blue effect). Thus, these residues were most likely conserved by the evolutionary process to select against misfolding¹⁴⁹. The second group (B) concerns variants that yield substantial amounts of soluble protein of which a fraction remains unfolded, as demonstrated by the NMR spectra. The mutants in this group often have a reduced melting temperature. We hypothesize that in this case the thermodynamic balance between folded and unfolded protein is affected. That implies that the conserved residue contributes to the stability of the folded form, relative to the unfolded state (Figure 2.6, red effect). The third group (C) are mutations that do not affect the production of a folded and stable enzyme but yield a non-native form of the enzyme with reduced activity (Figure 2.6, magenta effect). We conclude that in this case, the conserved residue is critical to obtain the active conformation, within the ensemble of conformations that the enzyme can visit within the folded form. The major effect of mutations on protein production, stability of the native form or activity was also demonstrated for other proteins. The mutational studies on two PER-ARNT-SIM domain proteins showed that many of conserved residues contributed to the production of soluble protein^{150,151}. For glutathione-S-transferase mutations in conserved motifs resulted in decreased stability and refolding rate, as well as in altered activity¹⁵². The destabilizing effect of mutations in conserved positions was also demonstrated for acyl-coenzyme A binding protein⁴⁰.

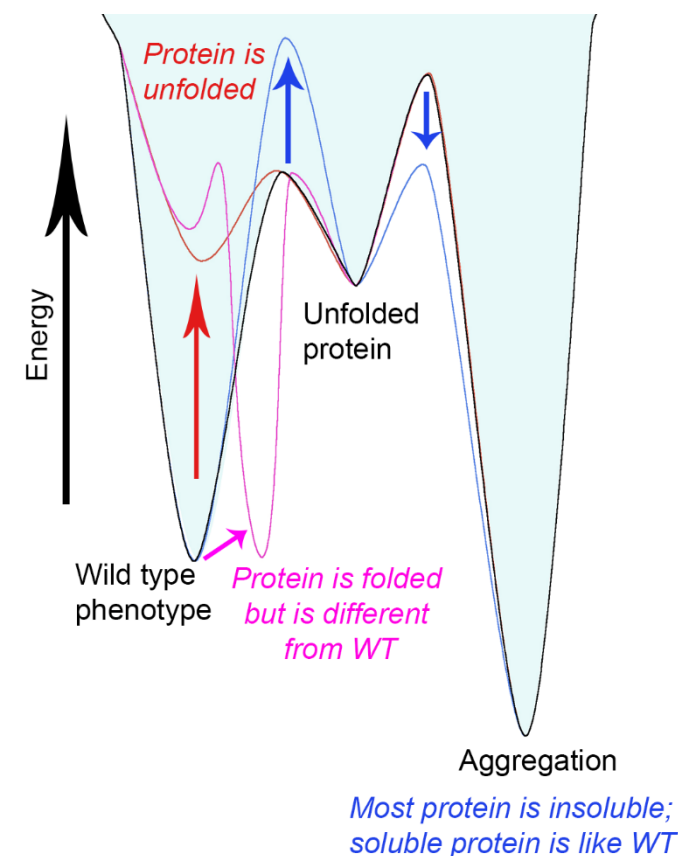


Figure 2.6. The free energy landscape of protein forms. The free energy landscape for wild type BlaC is shown with the black line. The effects of mutations described in the text for groups A, B and C are shown in blue, red and magenta lines, respectively.

The effect of group A is mainly represented by conserved residues far from the active site (third-shell residues). They are important for obtaining the correct three-dimensional fold, because for many of them mutation leads to a strong reduction in the amount of soluble protein (Figure 2.2, Table S2.2). Many are localized near the edges of the secondary structure elements (Figure 2.7a) and have interactions with nearby conserved residues, creating clusters. Such clusters are critical for the three-dimensional structure by “stapling” the secondary structure elements together. Mutations diminish the folding efficiency and protein stability, but the fraction that is folded resembles the wild type enzyme structurally and kinetically¹⁴⁵. Protein stability and ability to fold are a well-known selection forces^{153–155}.

Mutations elsewhere outside from the active site area in most cases are not detrimental as long as the secondary structure elements are formed and stapled by these essential residues. This principle results in a low number of essential residues outside the active site and thus a high evolutionary robustness of the protein. The effect of conserved residues clustering was shown for different folds⁴², where such clusters play a role in ensuring native form integrity of enzymes.

The group B effect was shown for some second-shell residue mutants. The soluble protein coexisted with the unfolded form, which could be detected with NMR (Figure 2.3a, Figure S2.7). Highly rigid proteins tend to unfold slowly, and active sites have a destabilizing effect on proteins because they require a degree of dynamics or expose hydrophobic interaction sites^{156,157}. Mutation of these group B residues thus could increase the unfolding rate and shift the balance of folding and unfolding toward the latter by destabilizing the folded form.

The activity change observed for group C mutants was evident to different degrees. Subtle effects (group C1) were observed for a group of third-shell residues containing glycines, prolines and alanines, found mostly in solvent-exposed loops (Table 2.1). These residues might be important for protein dynamics^{158,159}. Very low activity (group C2) was displayed by 12 well-folded and stable mutants of second-shell residues. These residues are located in places that ensure exact positioning of the residues involved in catalysis. Examples of such residues can be seen in figure 7b. Residue Ala134 is located in α -helix 8 (Figure S2.9) and its side chain points towards α -helix 7. Introducing a larger side chain is likely to interfere with the relative positions of these helices, dislocating active site residue Ser130. Residue Asn136 is also found in α -helix 8, making two hydrogen bonds to backbone atoms of catalytic residue Glu166 and ensuring the cis conformation of the peptide bond between Glu166 and Pro167¹²⁴.

An interesting observation was made for a group of second-shell residues for which the effect of the mutation is dependent on the nature of the new side chain. For these residues, variants with substitutions that remove the functional group are performing better than mutants with conservative substitutions. This observation emphasizes that the functional enzyme, especially around the active site, consists of a complex and extensive web of interactions. The presence of such a web is also supported by the NMR data, showing CSPs spreading far from the mutation site for the second shell residues. CSP can represent minute structural changes that are not easily picked up in crystal structures yet may have catalytic consequences if they cause small changes in the atom positions of catalytic residues or polarity changes in the active site. Mutations that influence the interactions of the side chain cause changes in the whole web of interacting residues and result in a dysfunctional protein. Substitutions that simply eliminate the interactions of the side chain apparently make it possible for other

residues to compensate for the lost interaction. For example, residue Thr71 probably aids the precise positioning of catalytic residue Ser70, by providing a H-bond between the Oy1 and the carbonyl oxygen of Phe68 (Figure 2.7c). Substitution T71S, which is likely to modify the length of this H-bond, yields less stable protein with somewhat decreased activity against nitrocefin *in vitro* and no activity against ampicillin and carbenicillin *in vivo*. However, substitutions to Leu, Val or Ala, which eliminate this H-bond completely, result in protein that resembles wild type BlaC better.

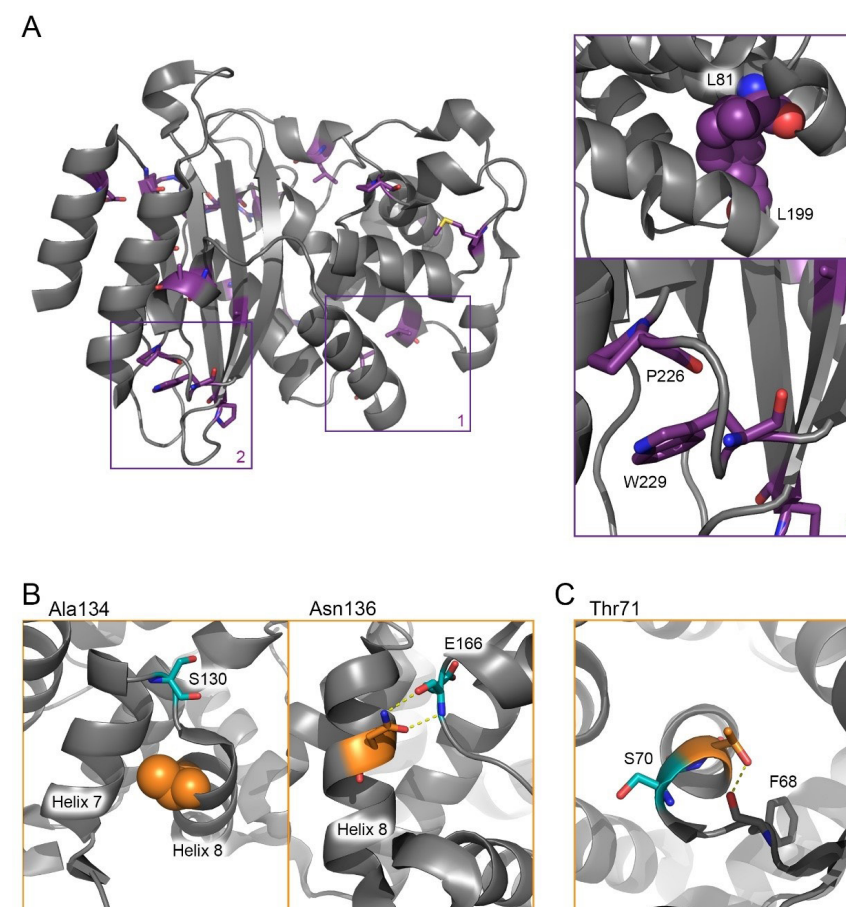


Figure 2.7. (A) Third-shell residues localized around the edges of the secondary structure elements (shown in purple sticks or spheres) and zoom-in of examples of interacting residues; (B) Examples of second-shell residues (shown in orange) influencing the position of the first-shell residues (shown in cyan) by ensuring the tight packing (Ala134) or making direct bonds to an active site residue (Asn136); (C) Environment of the second-shell residue Thr71 (in orange).

All analyzed residues had conservation higher than 92%. Such high conservation of a residue suggests that the exact nature of the side chain is extremely important. Nevertheless, a few mutants demonstrated behavior close to that of wild type BlaC. Two mutants, BlaC N245H and D179N exhibit in fact *in vivo* activity higher than wild type BlaC, accompanied by a melting temperature that is the same or higher. One would expect to find these residues in natural variants of β -lactamases as often as the conserved residues, yet the extreme conservation shows the preference towards the native residue. A few explanations can be given for this phenomenon. First, our experiments could only characterize a limited set of protein properties, activity against two specific antibiotics and nitrocefin, protein production, thermal stability and structural changes. It is possible that these mutants have lost a trait not tested within this research. One such trait is the evolvability of the protein^{15,23,160,161}. Microorganisms are under strong selection pressure of β -lactam antibiotics, so β -lactamases must be highly evolvable. Counterintuitively, it is possible that some residues might be conserved to preserve this trait, allowing residues around them to be able to undergo changes. In this vein, mutations in these residues could be a “epistatic dead end” by making other residues less evolvable. A second explanation is that not all amino acid substitutions can appear equally often. The transition/transversion bias can contribute to the lower chance of some mutations to occur in nature¹⁶². One example of such substitution can be the mutant N245H, which requires a change from adenine to cytosine. Furthermore, some amino acid substitutions require two nucleotide changes. For example, substitutions T71V or T71L that happen via consecutive point mutations can only occur via T71P, T71A, T71M or T71I. We have no data about the effects of T71P, T71I and T71M on the protein, but based on the position of Thr71 it is possible to assume that at least substitutions to Pro and Met will have a negative effect on the protein function. A third explanation is that a residue is essential in most β -lactamases but not in BlaC. In that case, the residue in BlaC is an evolutionary rudiment. For example, the variant D179N outperforms wild type BlaC in terms of *in vivo* activity, stability and protein level (*in vitro* activity is somewhat reduced). However, in TEM-1 this variant shows reduced fitness against ampicillin selection pressure^{128,129}. Thus, it can be that Asp179 is essential for many class A β -lactamases but for BlaC a mutation to Asn would not be detrimental, perhaps even an improvement for the fitness.

The results of this study led us to formulate a hypothetical function for each conserved second and third shell residue in BlaC (Table 2.1).

In conclusion, this work offers an explanation of general trends of conservation in serine β -lactamases. Conserved residues of the first shell form a catalytic center of a protein, conserved residues of the second shell establish a functional core of the protein and the third-shell residues ensure the overall fold. For the third-shell residues, the interactions they make in a final form of a protein or during folding process are extremely important. For that

reason, many of them do not tolerate any mutations and others can only undergo conservative substitutions. Residues of the third-shell contribute to a high evolutionary robustness of the protein by limiting conservation to a few clusters that are essential to staple secondary structure elements correctly. The second-shell residues form a web of interactions around the active site, fine-tuning the structure of the active site. In that way residues of the second shell contribute to a high evolvability of the protein. The conserved residues of the second shell ensure overall integrity of the active site, while random mutations can accumulate around the active site, potentially leading to a new trait.

Table 2.1. Effect of mutations and possible functions of conserved residues of the second and third shells.

Residue	Conservation among 494 sequences (%)	Other natural variants (%)	Effect of mutations (Group)	Hypothetical role	Shell
E37	99.2	A, D, Q, S (0.2)		Ensures correct folding by priming the position of the first β -strand ^a	III
G45	100			Allows the side chain of conserved residue F66 to occupy its position	III
R65	96.2	A (1.6), T, P (0.6), L (0.4), H, K, C (0.2)		Stapling function, stabilizes the position of Ω -loop via interaction with conserved residue T180	III
F66	99.8	Y (0.2)	Mutations cause loss of <i>in vivo</i> activity due to production of either insoluble or soluble unfolded protein; for some residues conservative mutations lead to production of soluble protein in low quantities, with a phenotype comparable to wild type. (A/B)	Locks $\beta 6$ on $\beta 1$ via interaction with residue 43	III
L81	99.2	M, V (0.4)		Is involved in hydrophobic interactions between $\alpha 3$, $\alpha 7$ and $\alpha 13$	III
M117	92.5	L (6.8), P (0.6), I (0.4)		Fills hydrophobic cavity between $\alpha 6$, $\alpha 7$ and $\alpha 8$	III
D157	99.2	N (0.8)		Is involved in stabilization of Ω -loop	III
T180	99.6	S, I (0.2)		Stabilizes the Ω -loop via interaction with conserved residue R65	III
A185	94.3	S (2.2), T (1.2), V, E (0.6), Q (0.4), R, N, G (0.2)		Fills small space between $\alpha 12$ and $\alpha 13$, allowing for correct positioning of side chain of conserved residue D157	III
L199	100			Keeps bend between $\alpha 12$ and $\alpha 13$ inside the hydrophobic cavity	III
W229	98	S (0.8), A (0.6), Y, C, F (0.2)		Contributes many hydrophobic and stacking interactions	III
A248	74.5	G (25.5)		Fills small space inside the core of the protein	III
P107	98.6	A (0.8), V, Q, T (0.2)		Is involved in a formation of a loop. Can be important for protein dynamics.	III
G144	99	D (0.6), S, N (0.2)		Is involved in a formation of a loop. Can be important for protein dynamics.	III
G156	97.8	N, D (0.6), E, S (0.4), R (0.2)		Makes a turn allowing for correct position of conserved residue D157	III
A223	97	K (1.2), V, S (0.4), E, R, M, T, G (0.2)	Slight effect on stability and/or activity. (C1)	Points in the solvent together with conserved residue A282, might be involved in protein-membrane interaction	III
P226	98.4	Q, A (0.6), L, D (0.2)		Is involved in stapling the turn between $\alpha 13$ and $\beta 7$ via interaction with conserved residue W229	III
P258	98	A, S, T (0.6), Q (0.2)		Allows for a bend between $\beta 8$ and $\beta 9$	III
A282	94.2	E (1.3), S, T (1.1), K (0.9), G (0.7), V (0.4), R (0.2)		Points in the solvent together with conserved residue A223, might be involved in protein-membrane interaction	III
A134	99.4	S (0.4), G (0.2)		Fills small space between $\alpha 6$, $\alpha 7$ and $\alpha 8$ together with conserved residue A125, allowing for correct positioning of active site Ser130	II
N136	100		<i>In vitro</i> activity loss with or without effect on folding. (C2)	Reduces mobility of the first-shell residue E166 via two H-bonds; stabilizes <i>cis</i> bond between E166 and P167 ^c	II
G217	94.3	S (5), N (0.4), T (0.2)		Makes a turn aiding the correct position of the first-shell residue T216	II
D246	96.4	N (1.4), T (1), A (0.6), I (0.4), E (0.2)		Pulls $\alpha 14$ to $\beta 8$; might orient conserved residue D233 for its bond with conserved residue N214	II
T171	98.2	S (0.6), A, V, L (0.4)		Reduces mobility of the active site residue S70 via H-bond to residue 68	II
A125	99.8	G (0.2)		Fills small space between $\alpha 6$, $\alpha 7$ and $\alpha 8$ together with conserved residue 134, allowing for correct positioning of active site Ser130	II
L169	95	I (2.6), M (1.6), V (0.8)	Various effects on protein stability and/or activity; effect is dependent on type of substitution. (B/C)	Stabilizes position of the first-shell residue T216 via bond to a conserved residue D233; affects active site residue K234 via water	II
N214	92.9	S (3.6), T (1.4), C (1), A, G (0.4), V (0.2)		Interacts with conserved residues D246 and N214, influencing the first-shell residues T216 and K234	II
D233	96.8	E (2), G, H (0.4), S (0.2)		Makes an interaction with residue 68, allowing it to position precisely for an interaction with conserved residue T71	II
N245	92.5	A (1.8), H, L, G (1.6), S (0.6), I (0.2)		Plays role in protein stability; holds together $\alpha 6$, $\alpha 7$ and $\alpha 8$, positioning active site S130; via bonds to residues V108, A109, A125, T133, A134, A135 ^b	II
D131	100		All mutations caused production of unfolded or partly folded protein. (B)		
D179	99.8	G (0.2)	Mutation D179N had a positive effect on stability, the other mutations affected protein folding and activity. (B/C)	Stabilizes the Ω -loop via bonds with residues D172, D163, A164; might be involved in stabilization of active site S70 via bond with residue 68	II

^a Chikunova, A. *et al.* Conserved residues Glu37 and Trp229 play an essential role in protein folding of β -lactamase. *FEBS J.* **288**, 5708–5722 (2021)

^b Swarén, P. *et al.* Electrostatic analysis of TEM1 β -lactamase: effect of substrate binding, steep potential gradients and consequences of site-directed mutations. *Structure* **3**, 603–13 (1995)

^c Banerjee, S. *et al.* Probing the non-proline *cis* peptide bond in β -lactamase from *Staphylococcus aureus* PC1 by the replacement Asn136 \rightarrow Ala. *Biochemistry* **36**, 10857–10866 (1997).

Materials & Methods

Conservation analysis

Sequence conservation among β -lactamases was determined using the ConSurf server¹⁰⁹. The BlaC sequence from Wang, Cassidy & Sacchettini¹⁰¹ (PDB ID: 2GDN) was used to find homologs using a PSI-BLAST algorithm with five iterations. Parameters for minimum and maximum sequence homology were set to 35 and 95%. An alignment of 494 sequences¹⁶³ was generated using the MAFFT algorithm¹⁶⁴ and the level of conservation of each amino acid residue position was calculated.

Mutagenesis

Site-directed mutagenesis was performed using two vectors as template. For *in vivo* studies mutants were created in a pUK21 (pUC21 based plasmid with kanamycin resistance) plasmid carrying the *blaC* gene, encoding a Tat signal peptide for transmembrane transport^{147,165}. The plasmid pET28a+ carrying the *blaC* gene with the code for a cleavable N-terminal His(6)-tag¹⁶⁶ was used as overproduction system and to determine the amount of soluble protein. Mutagenesis was performed using the QuikChange (Agilent) method. The presence of the mutations was confirmed by sequencing. Primer sequences can be found in Table S2.3.

To establish the localization of mature protein BlaC WT with the signal peptide for Tat-system was overexpressed in pET28a+ vector confirming that the protein was in membrane, while most protein was found in cytoplasm for BlaC WT expressed without Tat-system signal peptide (Figure S2.10).

In vivo activity studies

The survival of the *E. coli* cells carrying pUK-based plasmids with wild type or mutant *blaC* genes was tested on LB-agar plates with antibiotics. All plates contained 50 $\mu\text{g mL}^{-1}$ kanamycin and 1 mM isopropyl β -D-1-thiogalactopyranoside (IPTG). Cells were plated as 10 μL drops with OD_{600} values of 0.3. In the first round of *in vivo* studies, the plates contained ampicillin (3 $\mu\text{g mL}^{-1}$ or 15 $\mu\text{g mL}^{-1}$) or carbenicillin (20 $\mu\text{g mL}^{-1}$ or 200 $\mu\text{g mL}^{-1}$). Mutants that did not grow on the lowest concentrations of antibiotics were not used in the following test rounds; growth of mutants surviving the lowest concentrations but not the highest was tested on intermediary concentrations of ampicillin (5 $\mu\text{g mL}^{-1}$ and 10 $\mu\text{g mL}^{-1}$) and carbenicillin (50 $\mu\text{g mL}^{-1}$ and 100 $\mu\text{g mL}^{-1}$). For mutants surviving the highest concentrations, growth was tested on plates with 30, 60 and 100 $\mu\text{g mL}^{-1}$ ampicillin and 500, 1000 and 2000 $\mu\text{g mL}^{-1}$ carbenicillin. All tests were performed with two biological replicates. In case of disagreement between replicates mutants were tested separately again. *E. coli* cells expressing the gene of BlaC S70A was used as negative control, because these cells produce intact but inactive BlaC.

BlaC presence in *E. coli* cells

For recombinant production of mutant proteins, *E. coli* strain BL21pLysS (DE3) was used in combination with the pET28a+ based plasmids. Cells were cultured in LB medium at 37 °C until the OD_{600} reached 0.6-1.0, at which point protein production was induced with 1 mM IPTG, followed by incubation of the cultures at 18 °C for 16 hours. Of overnight bacterial cultures 100 μL were tested for nitrocefin activity and 500 μL were centrifugated and resuspended in 50 μL B-PER (Thermo Scientific) for lysis. After 30 minutes incubation at room temperature, 20 μL was treated with SDS-PAGE cracking buffer (20 mM Tris/HCl pH 6.8, 5 mM EDTA, 0.5% SDS, 0.1% β -mercaptoethanol) and the rest was centrifugated for separation of soluble and insoluble fractions. The soluble fraction was tested for nitrocefin activity and treated with SDS-PAGE cracking buffer. Whole lysate and soluble fraction samples were analyzed using SDS-PAGE and gels were stained with Coomassie Brilliant Blue. The signal intensity of the band corresponding to BlaC for each mutant was compared to signal intensity of the *E. coli* protein at 40 kDa using ImageLab software (BioRad). The experiment was done with four replicates and the gels were compared to each other, only one replicate was used to calculate the relative expression.

Mutants that showed a clear band on the gel for the soluble fraction were analyzed *in vitro*. Cultures of 10 mL were induced and incubated overnight at 18 °C and lysed with B-PER for 30 min at room temperature. After centrifugation the supernatant containing the soluble protein fraction of the lysate was diluted 100-fold.

Thermal stability

Thermal stability of the proteins was analyzed with a thermal shift assay with SYPRO Orange dye (Invitrogen). The measurements were performed in triplicate using the CFX 96 Touch Real-Time PCR Detection System (Bio-Rad) with the temperature range 20-80 °C. Melting temperatures were determined from averaged signal of three measurements. The technical error is 0.5 °C.

Circular dichroism

CD profiles were recorded at 25 °C using a Jasco J-815 spectropolarimeter with a Peltier temperature controller (Jasco, MD). Spectra were acquired in 1 mm quartz cuvette at a scan rate of 50 nm/min. The negative control spectrum was used as a background spectrum of *E. coli* proteins and subtracted from all mutant and wild type spectrum (Figure S2.2). The CD signal at 222 nm was then used as a measure for the amount of folded BlaC for calculating activity of mutants relative to wild type BlaC.

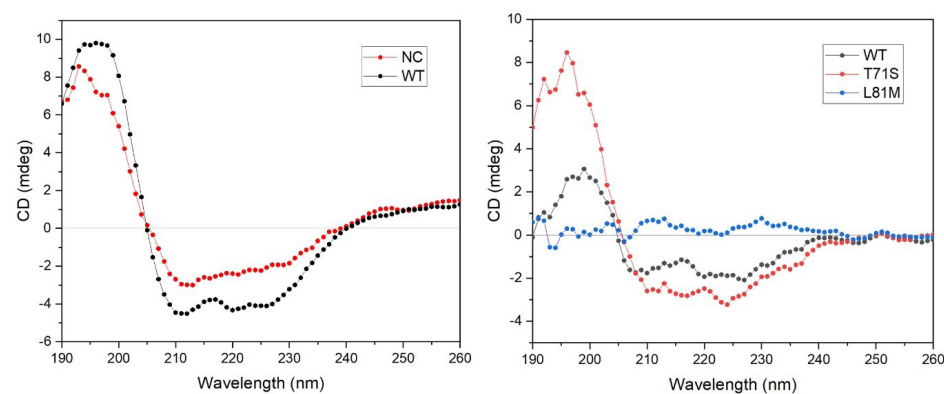


Figure S2.2. Example of CD spectra acquired for negative control (NC) and wild type (WT) (left panel); spectra of wild type, a poorly produced mutant (L81M) and a folded mutant (T71S) after background correction (right panel)

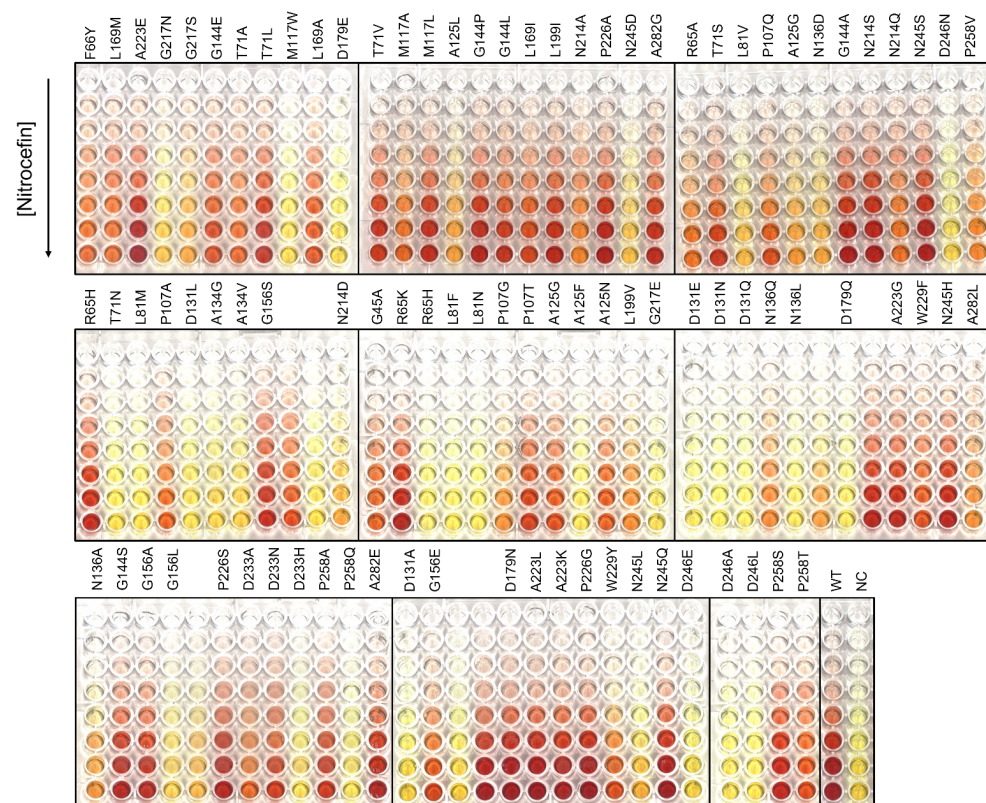


Figure S2.3. Plates with the range of nitrocefin concentration and whole lysates containing BlaC variants after 5 minutes of reaction. Non-labeled wells contain mutants of residues with lower percent conservation, thus not discussed within this study.

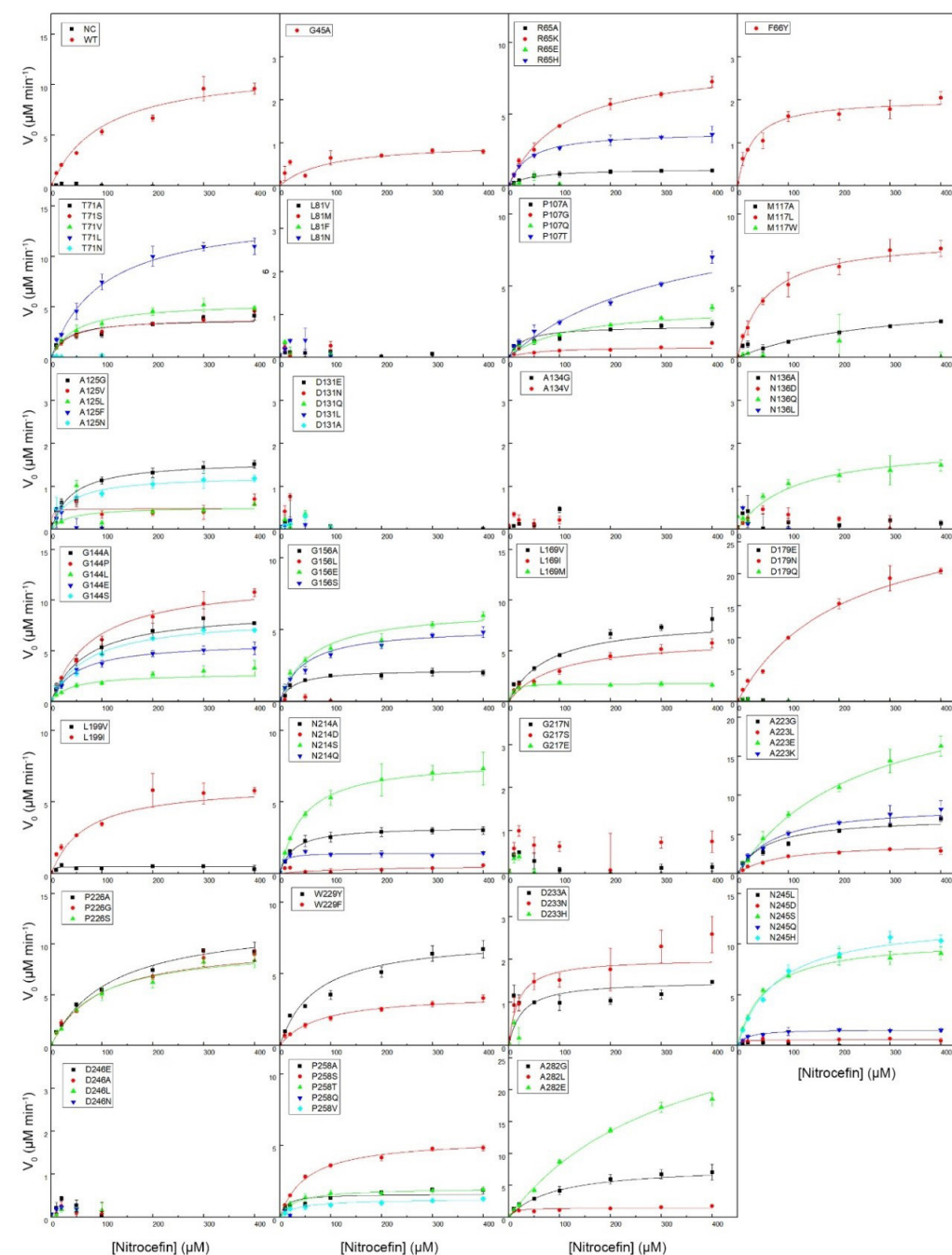


Figure S2.4. Nitrocefin kinetic curves. Error bars represent the standard deviation of a triplicate measurement. Lines represent the Michaelis-Menten fit.

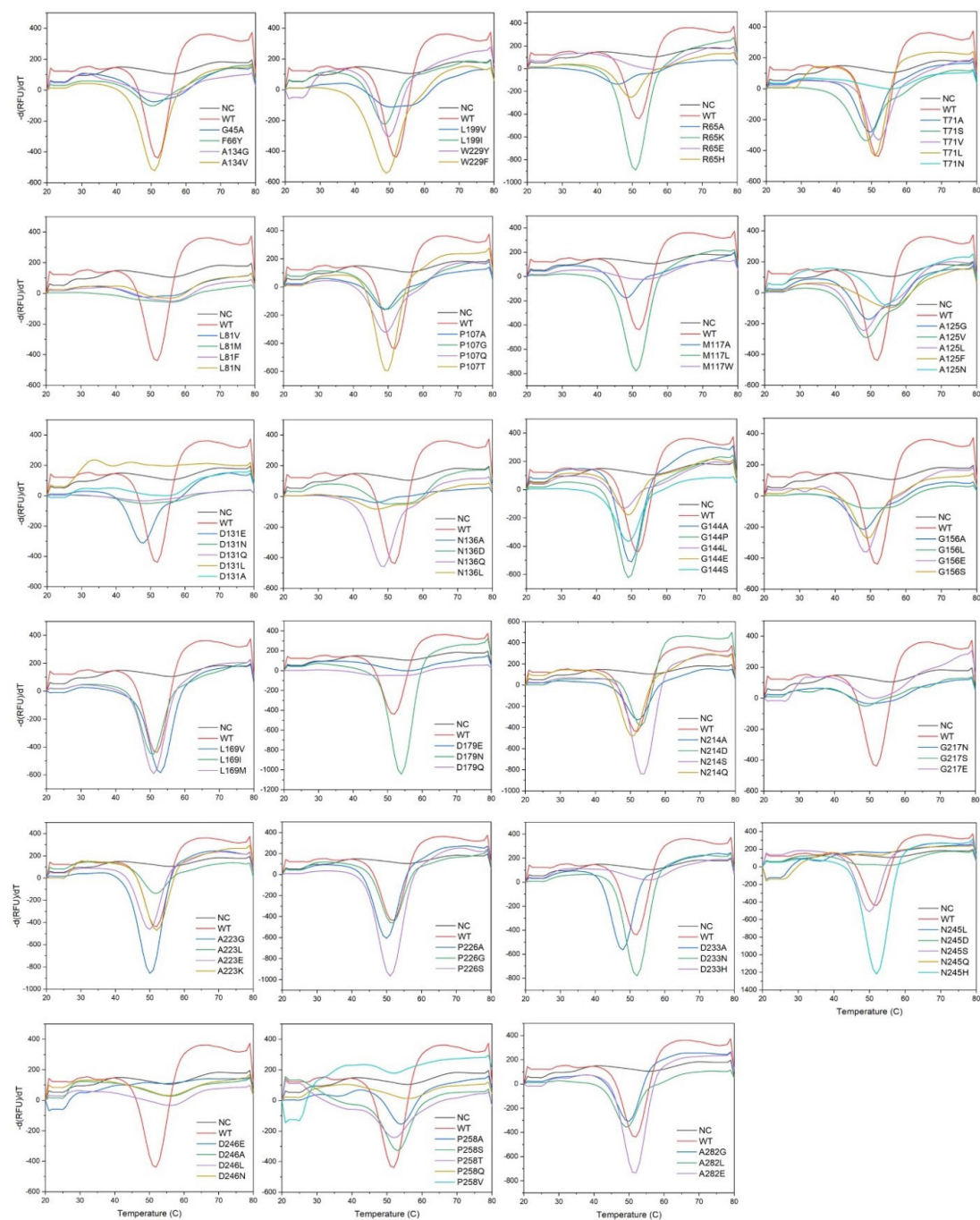


Figure S2.5. Negative derivative of the RFU signal from thermal shift assay for WT and mutant BlaC.

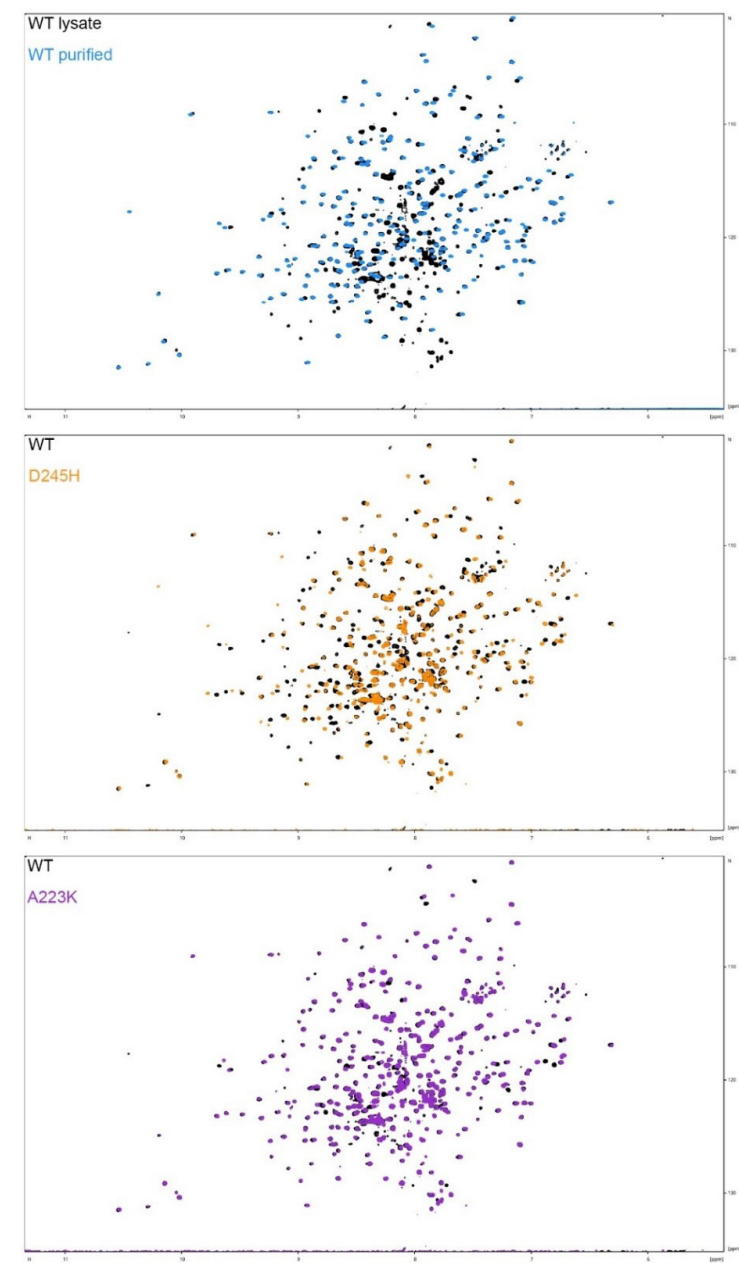


Figure S2.6. Examples of NMR spectra of cell lysates. The upper panel displays overlay of purified wild type in phosphate buffer pH 6.4 (in blue) and the soluble fraction of cell lysate of a culture expressing the wild type blaC gene (in black). The middle and bottom panels display the overlays of the cell lysate spectra of the second-shell mutant D245H (in orange) with wild type BlaC (in black) and of the third-shell mutant A223K (in purple) with wild type BlaC (in black).

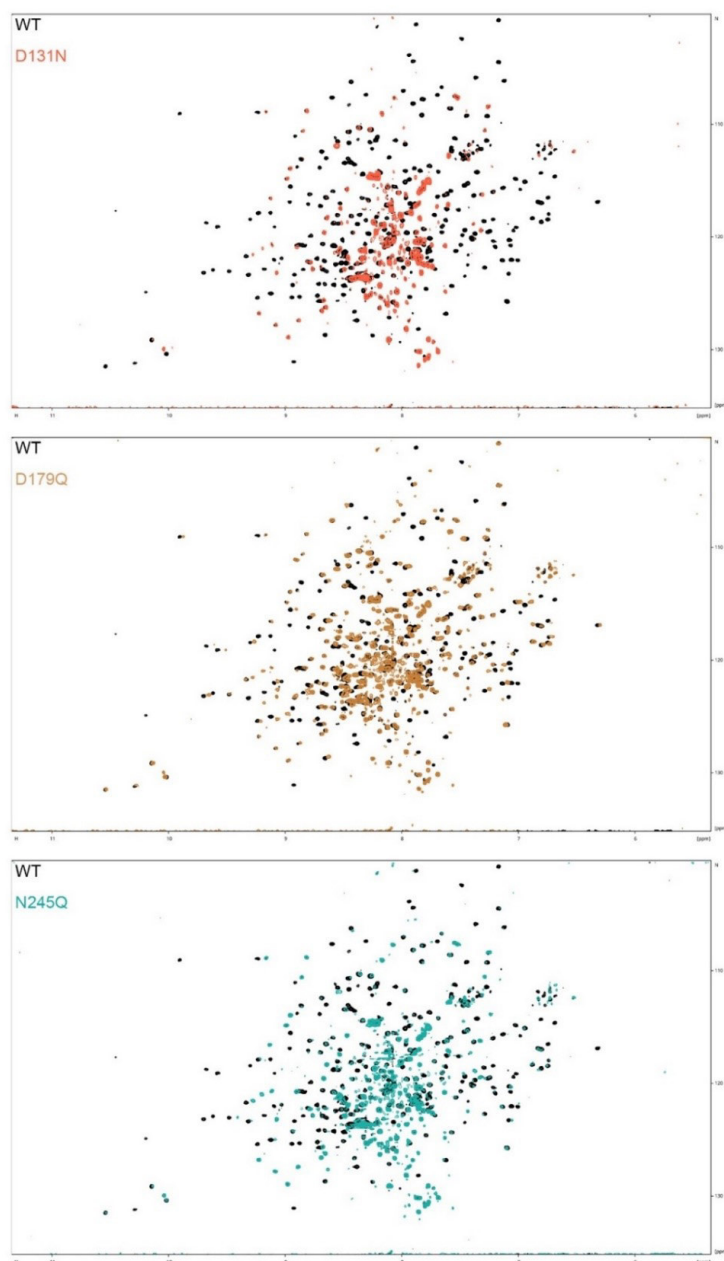


Figure S2.7. Examples of NMR spectra of cell lysates with unfolded protein. The panels display the overlays of spectra of the soluble fraction of cell lysates of mutants D131N (in pink, top), D179Q (in brown, middle) and N245Q (in turquoise, bottom) with that of wild type BlaC (in black).

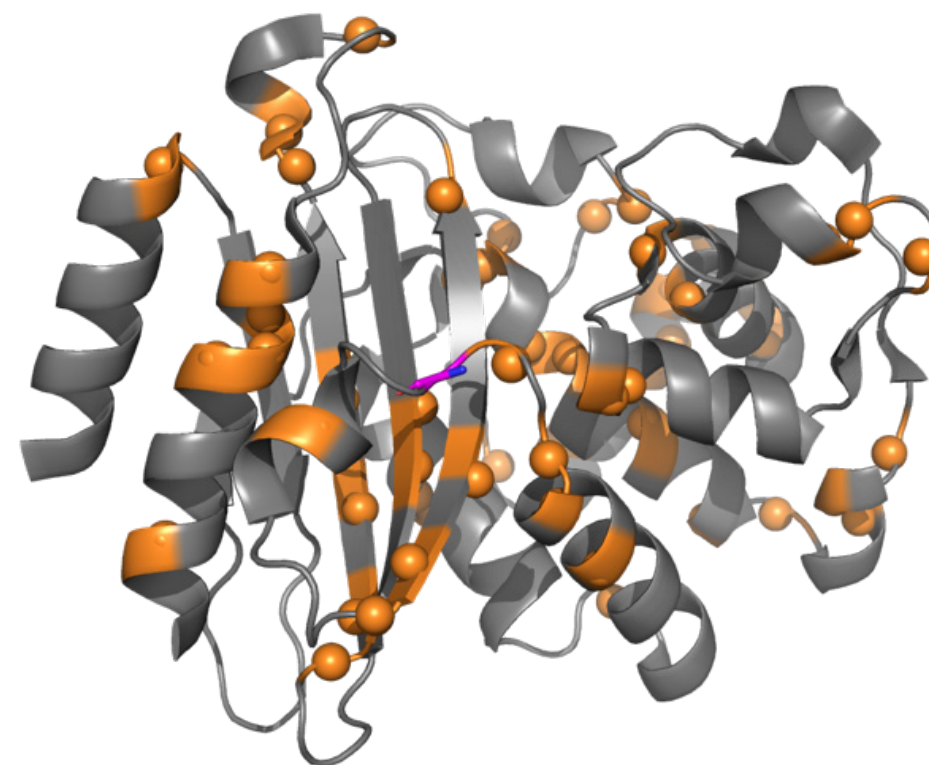


Figure S2.8. Example of the location of nuclei with significant CSP in a second-shell mutant (G217S) located on the protein surface. The mutated residue is shown in magenta sticks.

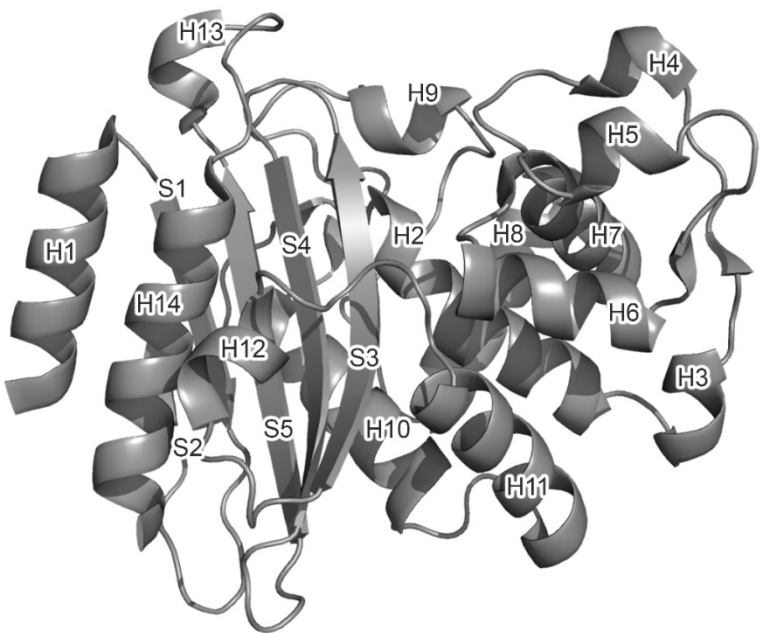


Figure S2.9. BlaC structure (2GDN¹⁰¹) with all α -helices and β -strands labeled.

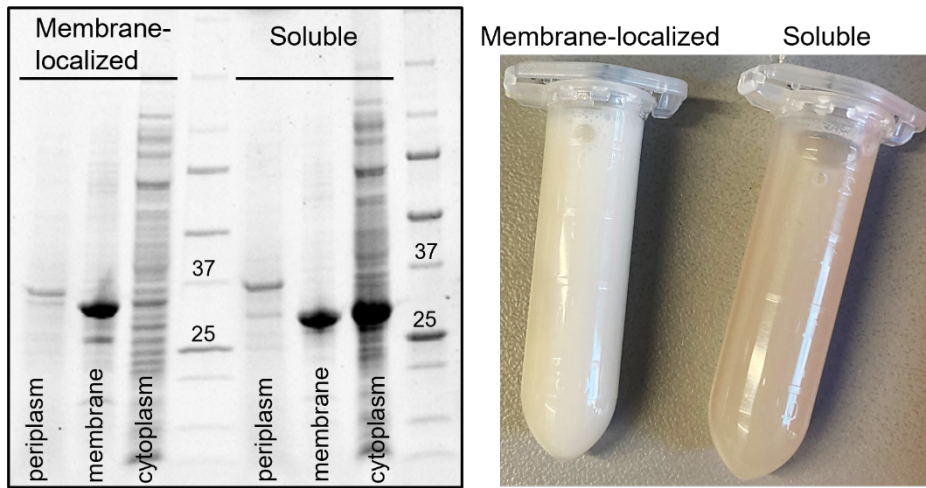


Figure S2.10. Detection of BlaC location after overexpression with and without a signal peptide for membrane localization. Most protein is found in membrane in construct with the signal peptide, which is shown on gel (left) and by the lighter color of the cells (right). Most protein is found in cytoplasm after expression in construct without the signal peptide with some protein detected in the membrane fraction, which can be possibly attributed to inclusion bodies formation due to overexpression (membrane fraction and inclusion bodies were not separated).

Supplementary tables

Table S2.1. BlaC sequence with ConSurf grades and percentages of the most occurring residue per position.

Position (Ambler)	ConSurf Grade	Residue in BlaC	The most occurring residue (%)	Position (Ambler)	ConSurf Grade	Residue in BlaC	The most occurring residue (%)
28	1	Asp	D (29.48)	65	9	Arg	R (96.154)
29	1	Leu	L (40.417)	66	9	Phe	F (99.798)
30	1	Ala	DE (16.242)	67	7	Ala	A (57.895)
31	1	Asp	R (17.812)	68	6	Phe	Y (29.96)
32	1	Arg	E (21.495)	69	6	Cys	C (54.453)
33	5	Phe	F (50.947)	70	9	Ser	S (100)
34	1	Ala	A (44.05)	71	9	Thr	T (98.178)
35	1	Glu	E (24.33)	72	7	Phe	F (71.862)
36	8	Leu	L (88.525)	73	9	Lys	K (100)
37	9	Glu	E (99.187)	74	4	Ala	A (51.215)
38	1	Arg	R (29.268)	75	5	Pro	L (65.182)
39	1	Arg	K (23.984)	76	7	Leu	A (68.016)
40	2	Tyr	F (32.657)	77	6	Val	A (65.385)
41	2	Asp	G (43.205)	78	6	Ala	A (55.466)
42	8	Ala	A (55.263)	79	6	Ala	A (73.684)
43	8	Arg	R (89.879)	80	5	Val	V (60.324)
44	8	Leu	L (92.308)	81	9	Leu	L (99.19)
45	9	Gly	G (100)	82	2	His	Q (21.457)
46	8	Val	V (87.247)	83	4	Gln	R (37.854)
47	5	Tyr	Y (48.583)	86	5	Asn	S (21.837)
48	7	Val	A (69.636)	87	5	Pro	S (25.562)
49	2	Pro	L (38.945)	88	1	Leu	L (20.654)
50	7	Ala	D (76.316)	89	2	Thr	E (33.266)
51	7	Thr	T (85.366)	90	2	His	L (21.053)
52	1	Gly	G (54.268)	91	7	Leu	L (85.83)
53	5	Thr	T (57.317)	92	1	Asp	D (49.798)
54	6	Thr	G (66.667)	93	3	Lys	R (35.223)
55	2	Ala	R (39.676)	94	5	Leu	R (46.154)
56	3	Ala	T (37.652)	95	5	Ile	I (56.275)
57	3	Ile	V (46.356)	96	1	Thr	T (39.676)
59	1	Glu	A (32.186)	97	7	Tyr	Y (82.591)
60	4	Tyr	Y (56.68)	98	1	Thr	T (33.603)
61	8	Arg	R (85.02)	99	1	Ser	K (30.567)
62	3	Ala	A (45.344)	100	1	Asp	D (32.996)
63	4	Asp	D (59.312)	101	7	Asp	D (83.401)
64	8	Glu	E (89.069)	102	7	Ile	L (81.174)

103	6	Arg	V (69.636)	144	9	Gly	G (98.988)	181	8	Thr	T (58.3)	222	8	Arg	R (92.713)
104	1	Ser	T (22.065)	145	8	Pro	P (94.737)	182	8	Thr	T (89.271)	223	9	Ala	A (96.964)
105	4	Ile	Y (64.372)	145A	1	Gly	A (31.377)	183	8	Pro	P (92.308)	224	8	Gly	G (92.51)
106	8	Ser	S (77.53)	145B	1	Gly	G (53.239)	184	2	His	R (35.83)	225	6	Phe	V (50.405)
107	9	Pro	P (98.583)	145C	6*	Gly	G (100)	185	9	Ala	A (94.332)	226	9	Pro	P (98.381)
108	5	Val	V (45.749)	145D	6*	Thr	T (100)	186	7	Ile	M (48.178)	227	1	Ala	A (26.735)
109	8	Ala	T (88.462)	146	6*	Ala	A (100)	187	6	Ala	A (71.66)	228	1	Asp	G (57.287)
110	6	Gln	E (71.255)	147	6*	Ala	A (100)	188	1	Leu	A (24.089)	229	9	Trp	W (97.976)
111	4	Gln	K (59.919)	148	5	Phe	L (42.915)	189	5	Val	S (41.296)	230	1	Lys	V (19.028)
112	7	His	H (81.579)	149	7	Thr	T (55.061)	190	6	Leu	L (74.291)	231	8	Val	V (88.664)
113	5	Val	V (69.98)	150	3	Gly	A (44.332)	191	4	Gln	R (38.866)	232	6	Ile	G (66.802)
114	1	Gln	D (35.628)	151	3	Tyr	F (35.02)	192	3	Gln	A (39.271)	233	9	Asp	D (96.761)
115	1	Thr	T (50.405)	152	6	Leu	L (55.668)	193	4	Leu	L (47.976)	234	9	Lys	K (98.178)
116	8	Gly	G (94.13)	153	7	Arg	R (82.794)	194	3	Val	V (35.425)	235	9	Thr	T (85.223)
117	9	Met	M (92.51)	154	2	Ser	S (37.247)	195	6	Leu	L (75.709)	236	9	Gly	G (100)
118	6	Thr	T (76.316)	155	4	Leu	I (46.964)	196	6	Gly	G (87.247)	237	5	Thr	T (35.425)
119	6	Ile	L (52.227)	156	9	Gly	G (97.773)	197	3	Asn	D (62.955)	238	7	Gly	G (87.652)
120	3	Gly	A (32.794)	157	9	Asp	D (99.19)	198	3	Ala	A (57.49)	240	2	Asp	D (31.984)
121	5	Gln	E (61.538)	158	1	Thr	D (20.445)	199	9	Leu	L (100)	241	6	Tyr	Y (77.393)
122	7	Leu	L (80.567)	159	1	Val	V (50.405)	200	1	Pro	P (34.615)	242	8	Gly	G (95.142)
123	5	Cys	C (69.636)	160	8	Ser	T (63.968)	201	1	Pro	A (24.494)	243	7	Arg	T (67.206)
124	6	Asp	D (38.259)	161	7	Arg	R (67.004)	202	1	Asp	A (29.352)	244	6	Ala	R (41.903)
125	9	Ala	A (99.798)	162	7	Leu	L (53.846)	203	7	Lys	K (31.377)	245	9	Asn	N (92.51)
126	7	Ala	A (71.862)	163	7	Asp	D (75.101)	204	8	Arg	R (90.283)	246	9	Asp	D (96.356)
127	4	Ile	I (41.498)	164	9	Ala	R (92.713)	205	1	Ala	A (30.972)	247	7	Ile	I (68.826)
128	8	Arg	R (47.773)	165	1	Glu	W (23.887)	206	4	Leu	Q (39.676)	248	8	Ala	A (74.494)
129	3	Tyr	Y (63.968)	166	9	Glu	E (99.595)	207	8	Leu	L (91.093)	249	6	Val	V (67.004)
130	9	Ser	S (100)	167	6	Pro	P (61.134)	208	1	Thr	T (35.425)	250	3	Val	V (37.652)
131	9	Asp	D (100)	168	3	Glu	E (51.417)	209	1	Asp	D (41.7)	251	7	Trp	W (93.725)
132	9	Gly	N (92.308)	169	9	Leu	L (94.939)	210	8	Trp	W (91.903)	252	8	Ser	P (85.425)
133	8	Thr	T (81.579)	170	9	Asn	N (87.449)	211	6	Met	L (62.955)	254	4	Pro	P (74.696)
134	9	Ala	A (99.393)	171	4	Arg	E (37.045)	212	2	Ala	K (29.96)	255	1	Thr	D (22.267)
135	6	Ala	A (49.19)	172	7	Asp	A (61.943)	213	5	Arg	G (42.105)	256	2	Gly	R (42.105)
136	9	Asn	N (100)	173	1	Pro	I (26.978)	214	9	Asn	N (92.915)	257	4	Val	A (49.393)
137	8	Leu	L (87.045)	174	8	Pro	P (94.523)	215	6	Thr	T (63.968)	258	9	Pro	P (97.976)
138	7	Leu	L (76.721)	175	6	Gly	G (87.652)	216	9	Thr	T (94.737)	259	4	Tyr	I (56.68)
139	6	Leu	L (61.741)	176	8	Asp	D (81.579)	217	9	Gly	G (94.332)	260	6	Val	V (65.385)
140	2	Ala	K (24.899)	177	1	Glu	P (39.474)	218	2	Ala	D (57.085)	261	4	Val	L (40.688)
141	2	Asp	E (23.887)	178	8	Arg	R (88.057)	219	1	Lys	A (23.732)	262	6	Ala	A (71.197)
142	4	Leu	L (62.753)	179	9	Asp	D (99.798)	220	8	Arg	R (45.842)	263	5	Val	V (51.619)
143	8	Gly	G (95.344)	180	9	Thr	T (99.595)	221	8	Ile	I (72.672)	264	7	Met	Y (42.51)

265	7	Ser	S (48.785)
266	6	Asp	T (44.332)
267	6	Arg	R (40.486)
268	1	Ala	D (23.887)
269	1	Gly	G (50)
270	4*	Gly	G (83.333)
271	1	Gly	T (20.445)
272	2	Tyr	K (33.266)
273	3	Asp	D (60.041)
274	6	Ala	A (80.652)
275	1	Glu	E (24.224)
276	1	Pro	Y (30.608)
277	4	Arg	D (40.592)
278	5	Glu	D (40.764)
279	4	Ala	A (41.957)
280	6	Leu	L (55.58)
281	6	Leu	I (60.659)
282	9	Ala	A (94.222)
283	2	Glu	E (41.111)
284	7	Ala	A (69.265)
285	6	Ala	A (53.452)
286	4	Thr	R (36.748)
287	2	Cys	IV (28.285)
288	4	Val	V (59.821)
289	3	Ala	A (32.265)
290	1	Gly	D (16.898)
291	1	Val	A (43.72)
292	4	Leu	L (70.812)
293	2	Ala	G (32.87)

Table S2.2 Data from *in vivo* and *in vitro* experiments. The orange and purple color represent the second and the third shell respectively. Color coding for the experimental data is as follows: green – (almost) as good as wild type, yellow – somewhat worse than wild type, red – considerably worse than wild type. ND – not detected.

Conserved residue	Mutations	MIC (µg mL ⁻¹)				Protein on gel		Nitrocefin reaction in cells		T _m	NMR	V _{max} /K _m in cell lysate (10 ⁻² min ⁻¹)	CD signal at 222 nm relative to WT	Relative activity
		Ampicillin	Carbenicillin	Lysate	Supernatant (Relative to WT)	Whole cell (within 10 min)	Supernatant (first minutes)							
	WT	100	1000		1					52	Folded protein	8.9 ± 0.3	1	1
	NC	3	20		ND					ND	Only <i>E. coli</i> protein peaks	ND	Used as background	ND
Glu37	E37A	3	20		0.01									
	E37L	3	20		ND									
	E37D	3	20		ND									
	E37Q	3	20		ND									
Gly45	G45A	3	20		0.18					51	Low signal	3.5 ± 1.8	1.0	0.4
	G45V	3	20		ND									
	G45S	3	20		0.12									
	R65A	3	20		0.67					46	Folded protein in low quantity	2.9 ± 0.9	0.4	0.7
Arg65	R65K	40	200		0.90					51	Folded protein	7.9 ± 0.7	2.0	0.4
	R65L	3	20		ND									
	R65E	3	20		1.04					ND	Low signal	ND	1.1	ND
	R65H	5	50		1.76					50	Folded protein	9.3 ± 0.9	1.0	1.1
Phe66	F66Y	3	20		0.99					50	Low signal	6.5 ± 1.2	0.9	0.8
	F66E	3	20		0.17									
	F66L	3	20		0.07									
	F66K	3	20		0.05									
Thr71	T71A	30	200		0.42					50	Folded protein	9.0 ± 0.2	0.9	1.1
	T71S	3	20		0.51					49	Folded protein in low quantity	8.2 ± 0.7	1.5	0.6
	T71V	80	1000		1.06					52	Folded protein	10.0 ± 0.2	1.0	1.1
	T71L	80	1000		0.92					51	Folded protein	15.6 ± 0.3	3.1	0.6
	T71N	3	20		0.43					ND	Folded and unfolded protein	ND	0.5	ND

Leu81	L81A	3	20				0.09					49	Folded and unfolded protein	ND	0.4		ND
	L81V	3	20				0.37					ND	Unfolded protein	ND	ND		ND
	L81M	30	200				0.05					ND	Low signal	ND	ND		ND
	L81F	3	20				0.28					ND					
	L81W	3	20				0.07										
Pro107	L81N	3	20				0.50					ND	Low signal	ND	ND		ND
	P107A	10	200				0.71					49	Folded protein	5.8 ± 0.2	0.8		0.8
	P107G	10	200				0.32					50	Low signal	3.4 ± 0.1	0.9		0.4
	P107V	10	200				0.03										
	P107Q	10	200				0.45					49	Folded protein	2.7 ± 0.05	1.4		0.2
Met117	P107T	10	200				0.35					50	Folded protein	2.9 ± 0.2	1.0		0.3
	M117A	3	20				0.49					48	Folded protein in low quantity	2.4 ± 0.3	1.7		0.2
	M117L	80	1000				1.18					51	Folded protein	14.0 ± 1.9	2.1		0.7
	M117E	3	20				ND										
	M117F	3	20				ND										
Ala125	M117W	3	20				0.38					ND	Low signal	ND	0.7		ND
	A125G	3	20				0.40					49	Low signal	3.7 ± 0.6	0.9		0.4
	A125V	3	20				1.33					49	Folded protein	ND	1.3		ND
	A125L	3	20				1.17					48	Folded protein	4.7 ± 1.2	1.1		0.5
	A125F	3	20				0.41					ND	Low signal	ND	0.2		ND
Asp131	A125N	3	20				0.73					ND	Folded and unfolded protein	3.9 ± 0.8	0.6		0.7
	D131E	3	20				0.56					48	Folded and unfolded protein	ND	1.0		ND
	D131N	3	20				0.10					49	Folded and unfolded protein	ND	ND		ND
	D131Q	3	20				0.04					48	Low signal	ND	ND		ND
	D131L	3	20				0.05					ND	Low signal	ND	ND		ND
Ala134	D131A	3	20				ND					ND	Low signal	ND	ND		ND
	A134G	3	20				0.62					ND	Folded protein in low quantity	ND	0.7		ND
	A134V	3	20				1.15					51	Folded protein	ND	2.0		ND
	A134L	3	20				0.12										
	A134F	3	20				0.12										
Asn136	A134N	3	20				ND										
	N136A	5	200				1.44					47	Folded protein	ND	ND		ND
	N136D	3	20				1.92					50	Folded and unfolded protein	ND	0.9		ND
	N136Q	3	100				2.10					49	Folded protein	2.3 ± 0.3	0.7		0.4
	N136L	3	20				1.48					47	Low signal	ND	ND		ND

Gly144	G144A	5	200				1.35					50	Folded protein	13.0 ± 2.0	2.2		0.7
	G144P	5	100				0.98					49	Folded protein	12.0 ± 0.7	2.1		0.6
	G144L	3	20				1.24					48	Folded protein	5.0 ± 1.4	1.5		0.4
	G144E	15	200				1.90					49	Folded protein	12.0 ± 3.0	1.8		0.7
	G144S	15	200				0.73					49	Folded protein	10.0 ± 1.3	1.4		0.8
Gly156	G156A	3	20				1.26					48	Folded protein	6.7 ± 1.1	1.0		0.7
	G156P	3	20				ND										
	G156L	3	20				0.67					49	Low signal	ND	0.3		ND
	G156E	3	20				1.50					49	Folded protein	10.0 ± 2.4	1.7		0.7
	G156S	3	20				1.25					49	Folded protein	8.4 ± 1.0	1.1		0.9
Asp157	D157A	3	20				ND										
	D157L	3	20				ND										
	D157E	3	20				ND										
	D157N	3	20				ND										
	L169A	5	20				ND										
Leu169	L169V	40	200				0.68					53	Folded and unfolded protein	10.0 ± 2.0	1.9		0.6
	L169F	3	20				0.14										
	L169W	3	20				ND										
	L169E	3	20				ND										
	L169I	40	200				0.16					51	Folded protein	6.0 ± 2.0	1.5		0.4
Asp179	L169M	30	200				0.47					51	Folded protein	ND	2.2		ND
	D179E	5	20				0.14					ND	Folded and unfolded protein	ND	0.5		ND
	D179N	100	2000				1.41					54	Folded protein	14.0 ± 1.1	3.5		0.4
	D179Q	5	20				0.36					48	Folded and unfolded protein	ND	ND		ND
	D179A	10	200				0.16										
Thr180	D179L	5	100				0.12										
	D179G	5	100				ND										
	T180S	40	500				0.17										
	T180A	3	20				ND										
	T180I	3	20				0.13										
Ala185	T180V	3	20				0.16										
	T180N	3	20				ND										
	A185T	3	20				0.10										
	A185L	3	20				ND										
	A185F	3	20				ND										
	A185E	5	100				0.12										

Leu199	L199V	3	20			0.61				50	Folded and unfolded protein	ND	ND	ND	ND
	L199I	3	50			0.43				48	Folded protein	10.0 ± 0.6	2.1		0.5
	L199N	3	20			ND									
	L199Q	3	20			ND									
	L199W	3	20			ND									
	L199A	3	20			ND									
Asn214	N214A	100	1000			0.63				52	Folded protein	14.0 ± 1.5	0.8		2.0
	N214L	3	20			ND									
	N214D	3	20			0.55				53	Folded protein	ND	2.3		ND
	N214S	100	1000			0.93				54	Folded protein	17.0 ± 2.9	1.9		1.0
Gly217	N214Q	30	200			0.59				51	Folded protein	ND	2.0		ND
	G217A	3	20			ND									
	G217T	3	20			ND									
	G217N	3	20			0.23				50	Folded protein	ND	0.8		ND
	G217S	3	20			0.39				49	Folded protein	ND	1.0		ND
	G217E	3	20			0.42				51	Folded protein	ND	0.6		ND
Ala223	A223G	30	500			0.29				50	Folded protein	8.5 ± 1.1	2.0		0.5
	A223L	30	500			0.41				52	Folded protein	5.1 ± 0.5	0.3		1.7
	A223E	30	500			0.45				50	Folded protein	10.0 ± 1.4	2.9		0.4
	A223K	60	1000			0.68				52	Folded protein	11.0 ± 1.4	1.3		0.9
	P226A	10	200			0.85				50	Folded protein	11.0 ± 0.8	2.5		0.5
	P226G	30	500			0.57				52	Folded protein	9.8 ± 0.5	1.3		0.8
Pro226	P226Y	3	20			ND									
	P226S	10	200			1.01				51	Folded protein	9.7 ± 0.6	2.2		0.5
	W229A	3	20			ND									
Trp229	W229Y	3	50			0.13				50	Folded protein in low quantity	8.0 ± 0.3	0.9		1
	W229F	3	50			0.12				49	Folded protein in low quantity	4.3 ± 0.5	1.5		0.3
	W229L	3	20			ND									
	W229Q	3	20			ND									
Asp233	D233A	10	200			0.16				48	Folded protein	ND	2.2		ND
	D233L	3	20			ND									
	D233E	3	20			ND									
	D233N	100	500			0.71				52	Folded protein	9.3 ± 2.4	2.4		0.4
	D233H	10	200			ND				ND	Folded protein in low quantity	ND	0.7		ND

Asn245	N245L	3	20			ND				ND	Unfolded protein	ND	ND	ND	ND
	N245D	3	20			0.16				ND	Folded protein	ND	0.8		ND
	N245S	15	200			0.16				50	Folded protein	21.0 ± 1.0	2.4		1.0
	N245Q	3	20			0.10				45	Folded and unfolded protein	7.8 ± 0.6	0.7		1.3
	N245H	100	2000			0.93				52	Folded protein	16.0 ± 0.5	3.6		0.5
	D246E	3	20			0.18				ND	Folded protein in low quantity	ND	0.2		ND
Asp246	D246A	3	20			0.16				ND	Folded protein in low quantity	ND	0.6		ND
	D246L	3	20			0.11				ND	Low signal	ND	0.5		ND
	D246N	3	20			0.20				ND	Folded protein in low quantity	ND	0.9		ND
	A248V	3	20			ND									
Ala248	A248L	5	50			ND									
	A248I	3	20			ND									
	P258A	80	1000			0.55				54	Folded protein in low quantity	5.5 ± 1.3	0.4		1.7
Pro258	P258S	80	1000			0.70				53	Folded protein	11.0 ± 0.1	1.0		1.3
	P258T	10	200			0.28				52	Low signal	8.7 ± 2.0	0.7		1.5
	P258Q	15	200			0.22				ND	Low signal	ND	0.3		ND
	P258V	5	50			0.27				ND	Low signal	3.4 ± 1.1	0.7		0.6
	A282G	30	500			0.23				50	Folded protein in low quantity	9.7 ± 0.6	1.5		0.7
Ala282	A282L	5	50			0.17				49	Folded protein in low quantity	ND	0.9		ND
	A282E	80	1000			0.72				52	Folded protein	11.0 ± 0.5	3.2		0.4

Table S2.3. Primers used to introduce mutations to the *blaC* gene. Only forward primer is presented.

Mutation	Forward primer 5'-3'	Mutation	Forward primer 5'-3'
E37A	G GCA GAT CGT TTT GCA GAA CTG GCG CGT CGT TAT GAT GCA CG	L169A	GAT GCA GAA GAA CCG GAA GCG AAT CGT GAT CCG CCT GGT
E37D	G GCA GAT CGT TTT GCA GAA CTG GAT CGT CGT TAT GAT GCA CG	L169V	GAT GCA GAA GAA CCG GAA GTG AAT CGT GAT CCG CCT GGT
E37L	G GCA GAT CGT TTT GCA GAA CTG CTG CGT CGT TAT GAT GCA CG	L169F	GAT GCA GAA GAA CCG GAA TTC AAT CGT GAT CCG CCT GGT
E37Q	G GCA GAT CGT TTT GCA GAA CTG CAG CGT CGT TAT GAT GCA CG	D179E	G CCT GGT GAT GAA CGT GAA ACC ACC ACA CCG CAT GCC ATT
G46A	CGT CGT TAT GAT GCA CGT CTG GCG GTT TAT GTT CCG GCA ACC	D179N	G CCT GGT GAT GAA CGT AAT ACC ACC ACA CCG CAT GCC ATT
G46V	CGT CGT TAT GAT GCA CGT CTG GTG GTT TAT GTT CCG GCA ACC	D179Q	G CCT GGT GAT GAA CGT CAG ACC ACC ACA CCG CAT GCC ATT
G46S	CGT CGT TAT GAT GCA CGT CTG TCT GTT TAT GTT CCG GCA ACC	D179A	G CCT GGT GAT GAA CGT GCA ACC ACC ACA CCG CAT GCC ATT
R65A	GCA ATT GAA TAT CGT GCA GAT GAA GCG TTT GCA TTT TGC AGC ACC	D179L	G CCT GGT GAT GAA CGT CTT ACC ACC ACA CCG CAT GCC ATT
R65K	GCA ATT GAA TAT CGT GCA GAT GAA AAA TTT GCA TTT TGC AGC ACC	D179G	G CCT GGT GAT GAA CGT GGT ACC ACC ACA CCG CAT GCC ATT
R65L	GCA ATT GAA TAT CGT GCA GAT GAA CTG TTT GCA TTT TGC AGC ACC	T180S	G CCT GGT GAT GAA CGT GAT AGC ACC ACA CCG CAT GCC ATT
R65E	GCA ATT GAA TAT CGT GCA GAT GAA GAA TTT GCA TTT TGC AGC ACC	T180A	G CCT GGT GAT GAA CGT GAT GCA ACC ACA CCG CAT GCC ATT
R65H	GCA ATT GAA TAT CGT GCA GAT GAA CAT TTT GCA TTT TGC AGC ACC	T180I	G CCT GGT GAT GAA CGT GAT ATT ACC ACA CCG CAT GCC ATT
F66Y	CGT GCA GAT GAA CGT TAC GCA TTT TGC AGC ACC TTT AAA GCA CCG C	T180V	G CCT GGT GAT GAA CGT GAT GTT ACC ACA CCG CAT GCC ATT
F66E	CGT GCA GAT GAA CGT GAG GCA TTT TGC AGC ACC TTT AAA GCA CC	T180N	G CCT GGT GAT GAA CGT GAT AAT ACC ACA CCG CAT GCC ATT
F66L	CGT GCA GAT GAA CGT CTC GCA TTT TGC AGC ACC TTT AAA GCA CC	A185T	GAT ACC ACC ACA CCG CAT ACC ATT GCA CTG GTT CTG CAG
F66K	CGT GCA GAT GAA CGT AAG GCA TTT TGC AGC ACC TTT AAA GCA CCG C	A185L	GAT ACC ACC ACA CCG CAT CTG ATT GCA CTG GTT CTG CAG
T71A	CGT TTT GCA TTT TGC AGC GCG TTT AAA GCA CCG CTG GTT GCA GCC	A185F	GAT ACC ACC ACA CCG CAT TTC ATT GCA CTG GTT CTG CAG
T71S	CGT TTT GCA TTT TGC AGC TCT TTT AAA GCA CCG CTG GTT GCA GCC	A185E	GAT ACC ACC ACA CCG CAT GAA ATT GCA CTG GTT CTG CAG
T71V	CGT TTT GCA TTT TGC AGC GTG TTT AAA GCA CCG CTG GTT GCA GCC	L199V	CTG GTT CTG GGT AAT GCA GTG CCT CCG GAT AAA CGT GCA
T71L	CGT TTT GCA TTT TGC AGC CTG TTT AAA GCA CCG CTG GTT GCA GCC	L199I	CTG GTT CTG GGT AAT GCA ATG CCT CCG GAT AAA CGT GCA
T71N	CGT TTT GCA TTT TGC AGC AAC TTT AAA GCA CCG CTG GTT GCA GCC	L199N	CTG GTT CTG GGT AAT GCA AAC CCT CCG GAT AAA CGT GCA
L81A	CTG GTT GCA GCC GTT GCG CAT CAG AAT CCG CTG ACC CAT CTG	L199Q	CTG GTT CTG GGT AAT GCA CAG CCT CCG GAT AAA CGT GCA
L81V	CTG GTT GCA GCC GTT GTG CAT CAG AAT CCG CTG ACC CAT CTG	L199W	CTG GTT CTG GGT AAT GCA TGG CCT CCG GAT AAA CGT GCA
L81M	CTG GTT GCA GCC GTT ATG CAT CAG AAT CCG CTG ACC CAT CTG	L199A	CTG GTT CTG GGT AAT GCA GCG CCT CCG GAT AAA CGT GCA
L81F	CTG GTT GCA GCC GTT TTT CAT CAG AAT CCG CTG ACC CAT CTG	N214A	CTG ACC GAT TGG ATG GCA CGT GCG ACC ACC GGT GCC AAA CGT
L81W	CTG GTT GCA GCC GTT TGG CAT CAG AAT CCG CTG ACC CAT CTG	N214L	CTG ACC GAT TGG ATG GCA CGT CTG ACC ACC GGT GCC AAA CGT
L81N	CTG GTT GCA GCC GTT AAC CAT CAG AAT CCG CTG ACC CAT CTG	N214D	CTG ACC GAT TGG ATG GCA CGT GAT ACC ACC GGT GCC AAA CGT
P107A	GAT ATC CGT AGC ATT AGT GCG GTT GCA CAG CAG CAT G	N214S	CTG ACC GAT TGG ATG GCA CGT TCT ACC ACC GGT GCC AAA CGT
P107G	GAT ATC CGT AGC ATT AGT GGC GTT GCA CAG CAG CAT G	N214Q	CTG ACC GAT TGG ATG GCA CGT CAG ACC ACC GGT GCC AAA CGT
P107V	GAT ATC CGT AGC ATT AGT GTG GTT GCA CAG CAG CAT G	G217A	CTG ACC GAT TGG ATG GCA CGT AAT ACC ACC GCG GCC AAA CGT
P107Q	GAT ATC CGT AGC ATT AGT CAG GTT GCA CAG CAG CAT G	G217T	CTG ACC GAT TGG ATG GCA CGT AAT ACC ACC ACC GCC AAA CGT
P107T	GAT ATC CGT AGC ATT AGT ACC GTT GCA CAG CAG CAT G	G217N	CTG ACC GAT TGG ATG GCA CGT AAT ACC ACC AAC GCC AAA CGT
M117A	CAG CAG CAT GTT CAG ACC GGT GCG ACC ATT GGT CAG CTG	G217S	CTG ACC GAT TGG ATG GCA CGT AAT ACC ACC TCT GCC AAA CGT
M117L	CAG CAG CAT GTT CAG ACC GGT CTG ACC ATT GGT CAG CTG	G217E	CTG ACC GAT TGG ATG GCA CGT AAT ACC ACC GAA GCC AAA CGT
M117E	CAG CAG CAT GTT CAG ACC GGT GAA ACC ATT GGT CAG CTG	A223G	ACC ACC GGT GCC AAA CGT ATT CGT GGC GGT TTT CCG GCA GAT
M117F	CAG CAG CAT GTT CAG ACC GGT TTC ACC ATT GGT CAG CTG	A223L	ACC ACC GGT GCC AAA CGT ATT CTG CTG GGT TTT CCG GCA GAT
M117W	CAG CAG CAT GTT CAG ACC GGT TGG ACC ATT GGT CAG CTG	A223E	ACC ACC GGT GCC AAA CGT ATT CGT GAA GGT TTT CCG GCA GAT
A125G	GGT ATG ACC ATT GGT CAG CTG TGT GAT GGC GCA ATT CGT	A223K	ACC ACC GGT GCC AAA CGT ATT CTG AAA GGT TTT CCG GCA GAT
A125V	GGT ATG ACC ATT GGT CAG CTG TGT GAT CTG GCA ATT CGT	P226A	CGT GCA GGT TTT GCG GCA GAT TGG AAA GTT ATT GAT AAA ACC
A125L	GGT ATG ACC ATT GGT CAG CTG TGT GAT CTG GCA ATT CGT	P226G	CGT GCA GGT TTT GCG GCA GAT TGG AAA GTT ATT GAT AAA ACC
A125F	GGT ATG ACC ATT GGT CAG CTG TGT GAT TTC GCA ATT CGT	P226Y	CGT GCA GGT TTT TAC GCA GAT TGG AAA GTT ATT GAT AAA ACC
A125N	GGT ATG ACC ATT GGT CAG CTG TGT GAT AAC GCA ATT CGT	P226S	CGT GCA GGT TTT TCT GCA GAT TGG AAA GTT ATT GAT AAA ACC
D131E	GCA ATT CGT TAT AGT GAA GGC ACC GCA GCC AAT CTG CTG CTG	W229A	CGT GCA GGT TTT CCG GCA GAT GCG AAA GTT ATT GAT AAA ACC
D131N	GCA ATT CGT TAT AGT AAC GGC ACC GCA GCC AAT CTG CTG CTG	W229Y	CGT GCA GGT TTT CCG GCA GAT TAT AAA GTT ATT GAT AAA ACC
D131Q	GCA ATT CGT TAT AGT CAG GGC ACC GCA GCC AAT CTG CTG CTG	W229F	CGT GCA GGT TTT CCG GCA GAT TTC AAA GTT ATT GAT AAA ACC
D131L	GCA ATT CGT TAT AGT CTG GGC ACC GCA GCC AAT CTG CTG CTG	W229L	CGT GCA GGT TTT CCG GCA GAT CTG AAA GTT ATT GAT AAA ACC
D131A	GCA ATT CGT TAT AGT GCG GGC ACC GCA GCC AAT CTG CTG CTG	W229Q	CGT GCA GGT TTT CCG GCA GAT CAG AAA GTT ATT GAT AAA ACC
A134G	GCA ATT CGT TAT AGT GAT GGC ACC GGC GCC AAT CTG CTG CTG	D233A	CCG GCA GAT TGG AAA GTT ATT GCT AAA ACC GGT ACG GGT G
A134V	GCA ATT CGT TAT AGT GAT GGC ACC GTG GCC AAT CTG CTG CTG	D233E	CCG GCA GAT TGG AAA GTT ATT GAA AAA ACC GGT ACG GGT G
A134L	GCA ATT CGT TAT AGT GAT GGC ACC CTG GCC AAT CTG CTG CTG	D233H	CCG GCA GAT TGG AAA GTT ATT CAT AAA ACC GGT ACG GGT G

A134F	GCA ATT CGT TAT AGT GAT GGC ACC TTG GCC AAT CTG CTG CTG	D233L	CCG GCA GAT TGG AAA GTT ATT CTG AAA ACC GGT ACG GGT G
A134N	GCA ATT CGT TAT AGT GAT GGC ACC AAC GCC AAT CTG CTG CTG	D233N	CCG GCA GAT TGG AAA GTT ATT AAC AAA ACC GGT ACG GGT G
N136A	CGT TAT AGT GAT GGC ACC GCA GCC GCG CTG CTG CTG GCC	N245A	ACG GGT GAT TAT GGT CGT GCA GCG GAT ATT GCA GTT GTT TGG
N136D	CGT TAT AGT GAT GGC ACC GCA GCC GAT CTG CTG CTG GCC	N245L	ACG GGT GAT TAT GGT CGT GCA CTG GAT ATT GCA GTT GTT TGG
N136Q	CGT TAT AGT GAT GGC ACC GCA GCC CAG CTG CTG CTG GCC	N245D	ACG GGT GAT TAT GGT CGT GCA GAT GAT ATT GCA GTT GTT TGG
N136L	CGT TAT AGT GAT GGC ACC GCA GCC CTG CTG CTG CTG GCC	N245S	ACG GGT GAT TAT GGT CGT GCA TCT GAT ATT GCA GTT GTT TGG
G144A	CTG GCC GAT CTG GGT GCG CCG GGT GGT GGT ACA GCA GCC TTT	N245Q	ACG GGT GAT TAT GGT CGT GCA CAG GAT ATT GCA GTT GTT TGG
G144P	CTG GCC GAT CTG GGT CCG CCG GGT GGT GGT ACA GCA GCC TTT	N245H	ACG GGT GAT TAT GGT CGT GCA CAT GAT ATT GCA GTT GTT TGG
G144L	CTG GCC GAT CTG GGT CTG CCG GGT GGT GGT ACA GCA GCC TTT	D246A	GGT GAT TAT GGT CGT GCA AAT GCT ATT GCA GTT GTT TGG AGC
G144E	CTG GCC GAT CTG GGT GAA CCG GGT GGT GGT ACA GCA GCC TTT	D246E	GGT GAT TAT GGT CGT GCA AAT GAA ATT GCA GTT GTT TGG AGC
G144S	CTG GCC GAT CTG GGT TCT CCG GGT GGT GGT ACA GCA GCC TTT	D246L	GGT GAT TAT GGT CGT GCA AAT CTG ATT GCA GTT GTT TGG AGC
G156A	GGT TAT CTG CGT AGC CTG GCG GAT ACC GTT AGC CGT CTG GAT	D246N	GGT GAT TAT GGT CGT GCA AAT AAC ATT GCA GTT GTT TGG AGC
G156P	GGT TAT CTG CGT AGC CTG CCG GAT ACC GTT AGC CGT CTG GAT	A248V	GGT CGT GCA AAT GAT ATT GTG GTT GTT TGG AGC CCG ACC
G156L	GGT TAT CTG CGT AGC CTG CTG GAT ACC GTT AGC CGT CTG GAT	A248L	GGT CGT GCA AAT GAT ATT CTG GTT GTT TGG AGC CCG ACC
G156E	GGT TAT CTG CGT AGC CTG GAA GAT ACC GTT AGC CGT CTG GAT	A248I	GGT CGT GCA AAT GAT ATT ATG GTT GTT TGG AGC CCG ACC
G156S	GGT TAT CTG CGT AGC CTG TCT GAT ACC GTT AGC CGT CTG GAT	P258A	GTT TGG AGC CCG ACC GGT GTT GCG TAT GTT GTT GCA GTT ATG
D157A	GGT TAT CTG CGT AGC CTG GGT GCG ACC GTT AGC CGT CTG GAT	P258S	GTT TGG AGC CCG ACC GGT GTT TCC TAT GTT GTT GCA GTT ATG
D157L	GGT TAT CTG CGT AGC CTG GGT CTG ACC GTT AGC CGT CTG GAT	P258T	GTT TGG AGC CCG ACC GGT GTT ACC TAT GTT GTT GCA GTT ATG
D157E	GGT TAT CTG CGT AGC CTG GGT GAA ACC GTT AGC CGT CTG GAT	P258Q	GTT TGG AGC CCG ACC GGT GTT CAG TAT GTT GTT GCA GTT ATG
D157N	GGT TAT CTG CGT AGC CTG GGT AAC ACC GTT AGC CGT CTG GAT	P258V	GTT TGG AGC CCG ACC GGT GTT GTG TAT GTT GTT GCA GTT ATG
L169W	GAT GCA GAA GAA CCG GAA TGG AAT CGT GAT CCG CCT GGT	A282G	CGT GAA GCA CTG CTG GGC GAA GCA GCA ACC TGT GTT GCC
L169E	GAT GCA GAA GAA CCG GAA GAA AAT CGT GAT CCG CCT GGT	A282L	CGT GAA GCA CTG CTG GAA GCA GCA ACC TGT GTT GCC
L169I	GAT GCA GAA GAA CCG GAA ATC AAT CGT GAT CCG CCT GGT	A282E	CGT GAA GCA CTG CTG GAA GAA GCA GCA ACC TGT GTT GCC
L169M	GAT GCA GAA GAA CCG GAA ATG AAT CGT GAT CCG CCT GGT		

Table S2.4. M9 medium composition per liter.

KH ₂ PO ₄	13.0 g
K ₂ HPO ₄	10.0 g
Na ₂ HPO ₄	9.0 g
Na ₂ SO ₄	2.4 g
¹⁵ NH ₄ Cl	0.3g
Glucose	4.0 g
Thiamine	30 mg
MgCl ₂	2 g
Biotin	1 mg
Choline chloride	1 mg
Folic acid	1 mg
Niacinamide	1 mg
D-pantothenate	1 mg
Pyridoxal	1 mg
Riboflavin	0.1 mg
FeSO ₄ *7H ₂ O	10 mg
CaCl ₂ *2H ₂ O	60 mg
MnCl ₂ *4H ₂ O	12 mg
CoCl ₂ *6H ₂ O	8 mg
ZnSO ₄ *7H ₂ O	7 mg
CuCl ₂ *2H ₂ O	3 mg
H ₃ BO ₃	0.2 mg
EDTA	50 mg

Chapter 3

**The N214-D233-D246 motif is essential
for correct positioning of the active site
residues in BlaC**

Abstract

Evolutionary adaptability is restricted by essential amino acid residues, therefore their number in proteins is minimized. Highly conserved residues around active site of enzymes are believed to play an essential role in the precise positioning of the active site residues. Here, we examined a triad of the second-shell residues of the β -lactamase BlaC, Asn214-Asp233-Asp246. Introducing substitutions in these residues allowed to probe their involvement in activity and stability of the protein. It is shown that all variants affect the activity of the enzyme. NMR data suggests the presence of two conformations that are differently populated, depending on the mutation. We propose that the triad is responsible for the positioning of active site residue Thr216 and Arg220 and that substitutions in this motif increase dynamics and lead to displacements of these substrate-binding residues.

Introduction

Enzymes consist of a three-dimensional frame of secondary structure elements to arrange the positions of catalytic amino acid residues very precisely in the active site. Enzymes achieve this with a relatively small number of essential amino acids, residues that cannot be replaced without a detrimental effect on protein. The conservation of a residue among orthologous proteins is often used as a proxy for essentiality^{34–36,108}. High conservation is generally observed for amino acids in the active site, because they are crucial for ligand binding and catalysis. Some residues in the layer around an active site (the second shell) are also conserved (see chapter 2).

The work described in this chapter focuses on a triad of highly conserved second-shell residues, Asn214, Asp233 and Asp246, which we believe play an important role in the function of β -lactamases. The active site of class A β -lactamases contains essential amino acids Ser70¹⁶⁸, Lys73 and Glu166^{115,169} (Figure 3.1). Ser70 acts as nucleophile in the acylation reaction and Lys73 and Glu166 act as proton donor/acceptors during the reaction. Also the motifs S130-D131-(N/G)132¹²⁵ and K234-(T/S)235-G236^{118,119} are conserved because of their role in regulation of the hydrolysis of β -lactam antibiotics (Figure 3.1a). Furthermore, several other residues are involved in making interactions with substrates.

Asn214 is a residue with a conservation of 93% among 494 class A β -lactamases (Chapter 2). It is found in a small loop between two α -helices (Figure 3.1b). In β -lactamase BlaC from *Mycobacterium tuberculosis*, this residue makes a hydrogen bond with another conserved residue, Asp233, as well as with Thr216, which is involved in substrate binding. Asn214 also interacts with an active site residue Lys234 via a water molecule. The homologous protein TEM-1, originating from *Escherichia coli*, has an Asp in position 214 instead. It was shown for TEM-1 that the interaction between Asp214 and Asp233 is important for a stability of the enzyme, while the water bridged by residues Asp214, Lys234 and Thr235 plays a role in activity¹⁷⁰. In PER β -lactamases residue 214 is a threonine^{171,172}.

Residue Asp233 is 97% conserved and is located in a β -sheet¹⁷³ (Figure 3.1c). Next to the H-bond with Asn214, it forms an H-bond with the conserved residue Asp246. In TEM-1, Asp233 makes a salt bridge with Arg222, contributing to protein stability¹⁷⁰. In some class A β -lactamases glutamate (GES β -lactamases^{174–178}) and histidine (CepA from *Bacteroides fragilis*¹⁷⁹, DES-1 from *Desulfovibrio desulfuricans*¹⁸⁰ and PER β -lactamases^{171,172}) are found as natural variants at position 233.

Residue Asp246 is 96% conserved. It is part of the same β -sheet as Asp233, located in the neighboring strand (Figure 3.1c). These two residues are known to have a carboxyl-

carboxylate interaction^{181,182} forming a low-barrier H-bond that was hypothesized to play a role in protein stability¹⁸³. Furthermore, Asp246 interacts with the amide nitrogen of Ile221.

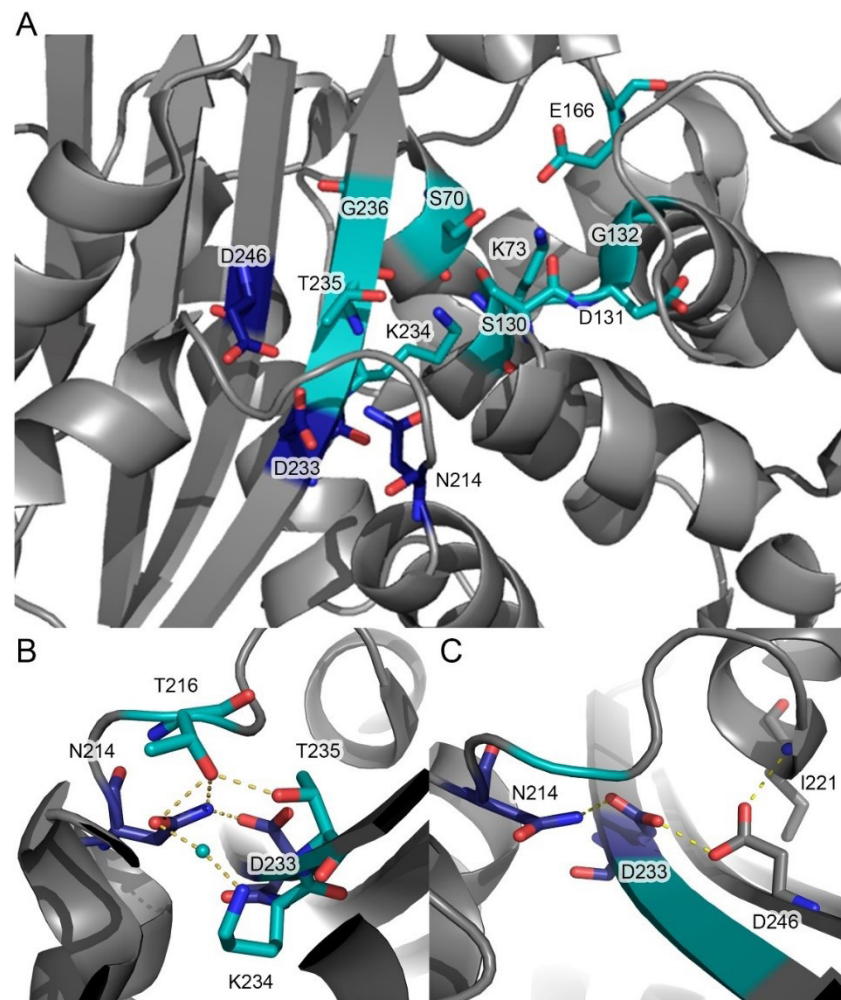


Figure 3.1. (A) The active site residues (in cyan) and the Asn214-Asp233-Asp246 triad (in dark blue) in BlaC (PDB entry 2GDN¹⁰¹); (B) Interactions made by the side chain of Asn214 shown in yellow dashed lines; (C) Interactions made by Asp233 and Asp246 shown in yellow dashed lines.

The residues Asn214, Asp233 and Asp246 form a triad of residues interacting *via* a chain of hydrogen bonds in the protein core (Figure 3.1c). Given the high conservation of these interactions we wondered what the function of the triad is. As this motif is found just outside the active site, it is hypothesized that it is crucial for enzyme activity. This study aimed to investigate the structural and functional role of this conserved motif by mutagenesis and characterization of the variants *in vivo* and *in vitro*. The contribution of the triad to the precise positioning of important residues is discussed, and it is argued that in enzymes in which the triad is not conserved, such as TEM-1, adaptations are made to ensure the positioning of the catalytic residues in another way.

Results

In order to understand the roles of interactions between the conserved residues Asn214, Asp233 and Asp246, single point mutations were introduced to these residues. Substitutions were chosen to sample various scenarios, in which interactions are modified due to modified length or polarity of the side chain or abolished entirely.

Wild type BlaC and variants were first tested for their activity against ampicillin and carbenicillin in cells by spotting cell cultures as drops of different dilutions on agar plates containing various concentrations of antibiotics. BlaC mutant S70A, which produces intact enzyme that is catalytically dead, was used as a negative control. Cell cultures producing BlaC mutants showed different degrees of activity loss (Figure 3.2, Figure 3.3a, Figure S3.1). BlaC D233N, N214A and N214S show activity comparable to the wild type BlaC, whereas BlaC N214Q and D233A/E/H exhibited a 5-to-10-fold reduction in activity. None of the D246 mutants was able to hydrolyze these antibiotics, and neither were BlaC variants N214D, N214L and D233L.

All BlaC variants were recombinantly produced in *E. coli* and purified, except for BlaC D233H that did not yield sufficient soluble protein to proceed with *in vitro* characterization. The degree of folding was determined by CD spectroscopy. Most mutants are folded and have a secondary structure composition comparable to the wild type protein. BlaC D233E, D233L and N214L are partially unfolded (Figure 3.3b) and these variants were not included in further *in vitro* studies. The thermal stability of BlaC variants was analyzed with a thermal shift assay using hydrophobic fluorescent dye SYPRO Orange¹⁸⁴ (Figure 3.3c, Table 3.1). All N214 mutants displayed a melting temperature similar to that of wild type BlaC. In contrast, BlaC D233A and all D246 mutants showed a decrease in melting temperature, up to 8 degrees.

Table 3.1. Kinetic parameters for the hydrolysis of nitrocefin and melting temperatures of wild type BlaC and BlaC variants. SD – standard deviation of triple measurements. NA – no activity detectable.

	Nitrocefin activity			Thermal stability	
	k_{cat} (SD) (s ⁻¹)	K_M (SD) (μM)	k_{cat}/K_M (SD ^a) (x10 ⁵ M ⁻¹ s ⁻¹)	T_{melt}^b (°C)	ΔT_{melt}^c (°C)
Wild type	95 (3)	296 (18)	3.2 (0.2)	52	-
N214A	60 (8)	177 (49)	3.4 (1.0)	52	0
N214D	NA	NA		53	1
N214Q	19 (1)	47 (10)	4.0 (0.9)	50	-2
N214S	37 (4)	138 (38)	2.7 (0.8)	53	1
D233A	58 (2)	263 (17)	2.2 (0.2)	47	-5
D233N	24 (2)	102 (21)	2.3 (0.5)	52	0
D246A	8 (1)	134 (16)	0.6 (0.1)	47	-5
D246E	NA	NA		44	-8
D246L	NA	NA		46	-6
D246N	25 (4)	145 (30)	1.7 (0.5)	44	-8

^a Propagated standard deviation; ^b Error 0.5 °C; ^c Error 0.7 °C

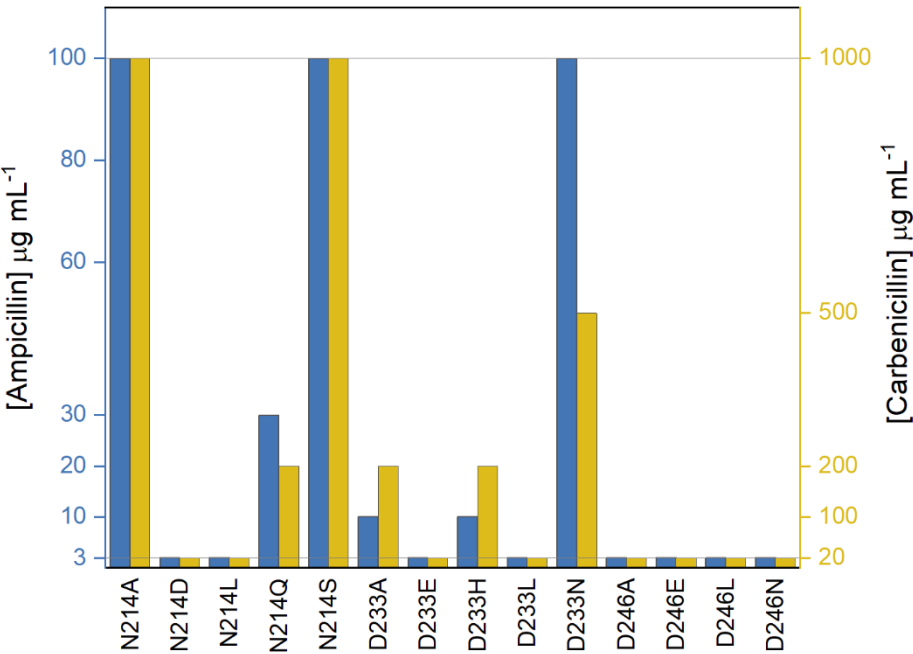


Figure 3.2. MICs of ampicillin and carbenicillin for BlaC variants. The horizontal lines represent MIC of wild type BlaC and BlaC S70A used as a negative control.

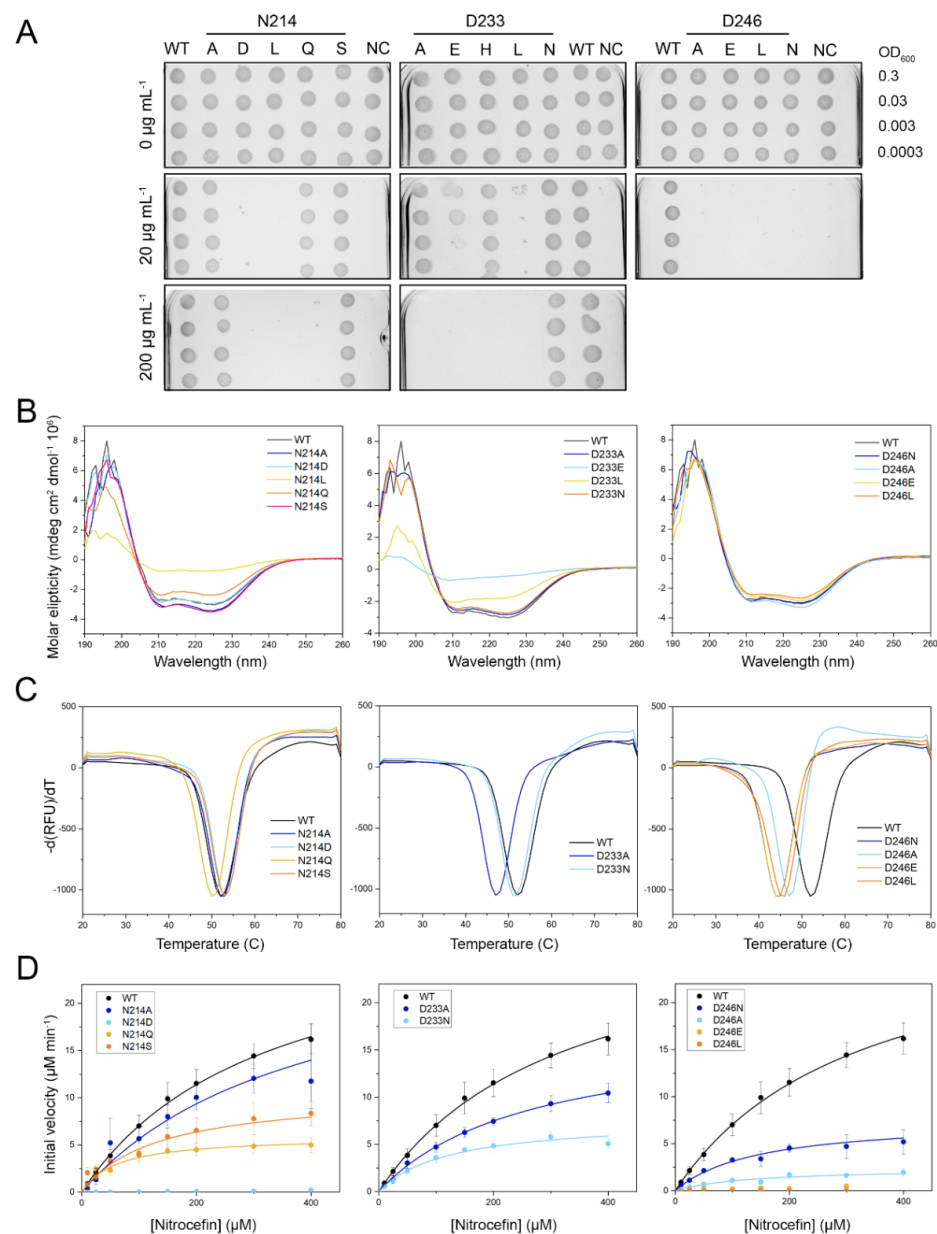


Figure 3.3. (A) Plates showing growth at 37 °C of *E. coli* cells expressing wild type (WT) or mutant *blaC* genes (negative control, NC is the mutant S70A) with no antibiotics, 20 or 200 µg mL⁻¹ of carbenicillin (MIC for wild type BlaC is 1000 µg mL⁻¹); (B) Circular dichroism profiles of wild type BlaC and mutants of Asn214, Asp233 and Asp246. D233L, D233E and N214L are partially unfolded; (C) Normalized negative derivatives of thermal shift assay (SYPRO orange binding). The minimum in the curve represents melting temperature; (D) Michaelis-Menten kinetic curves of reaction with nitrocefin. The lines represent the fits to Michaelis-Menten equation. Error bars represent the standard deviations of triple measurements.

The catalytic efficiency of wild type BlaC and its variants was determined using the chromogenic substrate nitrocefin (Figure 3.3d, Table 3.1). The kinetic parameters demonstrate that all mutants suffer from activity loss to some extent. BlaC N214A and D233A exhibit a turn-over rate constant, k_{cat} , that is 35% lower than that of the wild type enzyme, while BlaC N214Q, N214S, D246N and D233N display a reduction of 60-83%. No activity could be measured for two Asp246 mutants and BlaC N214D. The specificity constant k_{cat}/K_M was reduced up to about 2-fold for the mutants showing activity. Only for BlaC D246A, the reduction was 6-fold.

Interestingly, the mutations modifying the length of the side chain cause a larger effect on enzyme than the mutations that completely remove the functional group of the side chain. For Asn214, the mutations to Ala and Ser were less damaging than the mutation to Gln, as both BlaC N214A and BlaC N214S were shown to be more thermostable and more active *in vivo* than BlaC N214Q. The same effect can be noted for the Asp246, as BlaC D246A is more active and stable than BlaC D246E.

To probe the effects of the mutations on the structure of the protein, TROSY-HSQC spectra were recorded with ¹⁵N labeled mutants. All mutants show changes in chemical environment of the backbone amides not only surrounding the mutation site but throughout the whole protein with prominent changes around catalytically important residues (Figure S3.2). For some amide groups in Asn214 and Asp233 mutants two resonances were present, indicating that there is a second state present for these mutants (Figure 3.4). An interesting observation was made for Asp246 mutants. The CSPs of some amide hydrogen and nitrogen resonances increased approximately with the same ratio for the different mutants, placing peaks on a vector, in the order WT-D246N-D246A-D246E-D246L (Figure 3.5a). The activity loss of Asp246 mutants followed a similar trend but with different magnitude (Figure 3.5b). These findings suggest the existence of a second state, which is most likely catalytically inactive, and which is populated by the mutants to a different degree. The linear trend was visible for many residues throughout the structure (Figure 3.5c). For many other amides, mostly localized around the active site and right above the mutation site, peaks could not be assigned

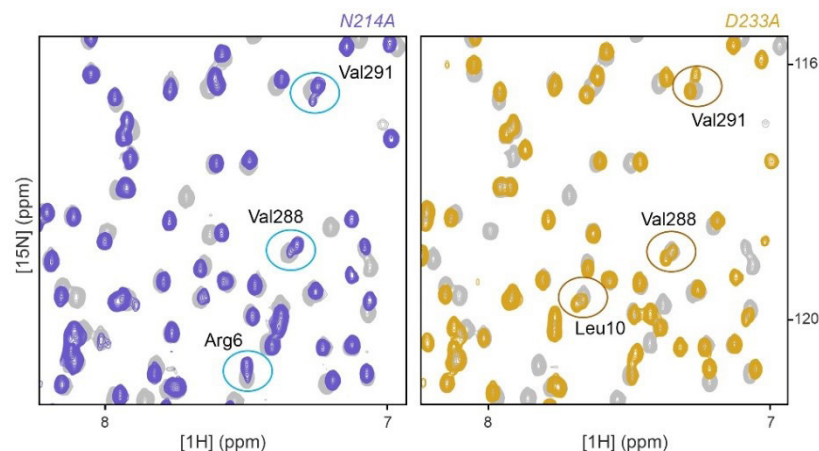


Figure 3.4. A few examples of double peaks found in NMR spectra of BlaC N214A/S (left) and BlaC D233A/N (right). Spectra of wild type BlaC are in grey.

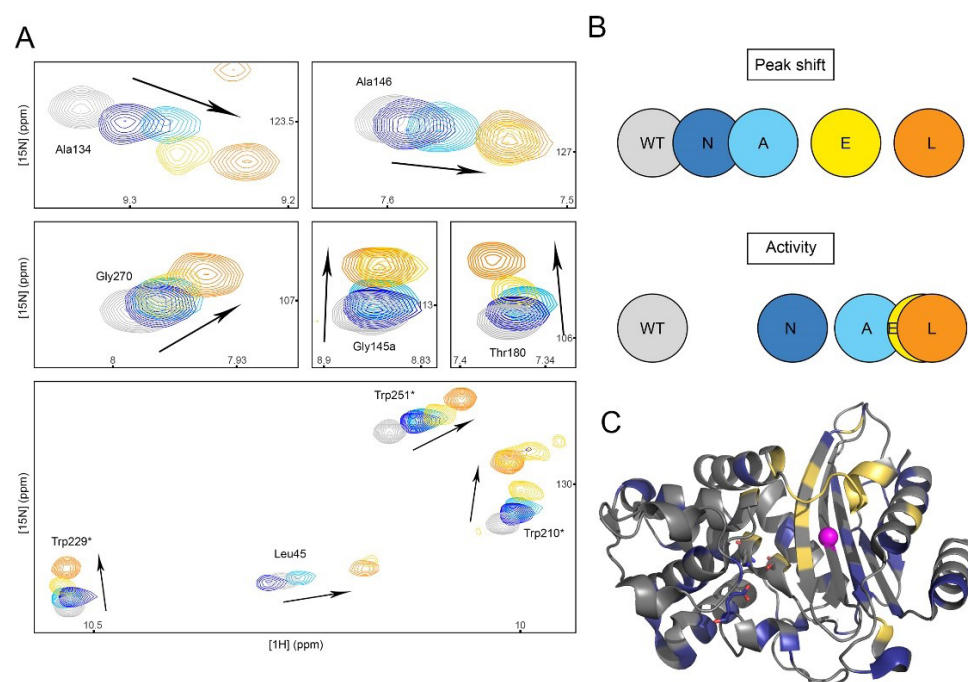


Figure 3.5. (A) Examples of the dependence of the peak shift from mutation in Asp246; (B) Schematic representation of the effect of the mutations in Asp246 on NMR spectrum and activity (k_{cat}/K_M); (C) Residues for which peaks are following the trend from panel A are shown in blue, residues for which peaks could not be assigned for all variants are shown in yellow. Ca of Asp246 is shown in magenta sphere. Active site residues are shown in sticks.

Discussion

The triad Asn214-Asp233-Asp246 is conserved in most class A β -lactamases. Our data indicate that this motif plays crucial role in the catalytic activity of the protein. Many mutations lead to activity *in vivo* and *in vitro*. All Asp214 mutants displayed little or no change in melting stability and secondary structure, while Asp246 and Asp233 mutants were more affected. That is not surprising, giving that Asn214 is located on the surface of the protein and Asp233 and Asp246 are buried. However, that means that the H-bond between residues 214 and 233 that was shown to be essential for protein stability in TEM¹⁷⁰, is not essential in BlaC, as N214A is not able to make that interaction and N214S is unlikely to, due to the expected increased distance between the Ser214 and Asp233 side chains. Most likely, residue Asp233 contributes to enzyme stability by maintaining the interactions with the loop on top of it. The thermal stability data indicated that the length of the residue at position 233 is of great importance, because only the mutation to Asn did not affect the melting temperature. At the same time mutation to Glu, yielding a side chain that is only one carbon atom longer, has a dramatic effect on stability. Mutation to Ala decreased melting temperature, also indicating a less stable tertiary structure. Thus, even though conservation of interactions is preferable, the complete removal of the side chain is less detrimental than its elongation. The same trend was observed for the other residues. For Asp246 all mutants showed stability and activity loss, however mutation to Glu resulted in the least stable protein, as judged by NMR spectroscopy and thermal shift assay. Out of all soluble Asn214 mutants BlaC N214Q displayed the lowest melting temperature, however, catalytically it performed better than BlaC N214D. This observation indicates that the exact nature of the side chain is vital for residue 214, but length and charge are important for different reasons.

We believe that the Asn214-Asp233-Asp246 motif is responsible for two features of BlaC. First, Asp246 in BlaC and many other β -lactamases makes a hydrogen bond with the backbone amide of Ile221. Ile221 is located in a small helix that is placed directly above the β -sheet domain. Another variation of this motif that is found in TEM and SHV β -lactamases is Asp214-Asp233-Ile246. As can be seen in Figure 3.6a the α -helix in structures with Ile246 is placed at least 1.9 Å further away than this helix in structures with Asp246, due to lost 246-221 connection. The same helix shift can be observed in a β -lactamase from *Vibrio*, which also carries Ile246 naturally. This small helix in BlaC contains a residue important for substrate/inhibitor binding – Arg220¹⁸⁵. In TEM and SHV Arg244 plays this role. The guanidine group of Arg244 in TEM or SHV occupies the same space as Arg220 in BlaC (Figure 3.6b). It was shown for TEM that mutations in Arg244 result in a lower affinity for inhibitors and thus a higher resistance. Also penicillin hydrolysis is compromised¹⁸⁶. Exactly the same effect was shown for Arg220 in PER-2¹⁸⁷. It has been proposed for both Arg244 and Arg220 that they make interactions with the substrate^{80,188,189}. That suggests that for TEM,

the precise positioning of the small α -helix is not as crucial, because residue 244, not 220 is involved in substrate binding, thus conservation of an aspartic acid in position 246 is not required for TEM and SHV β -lactamases.

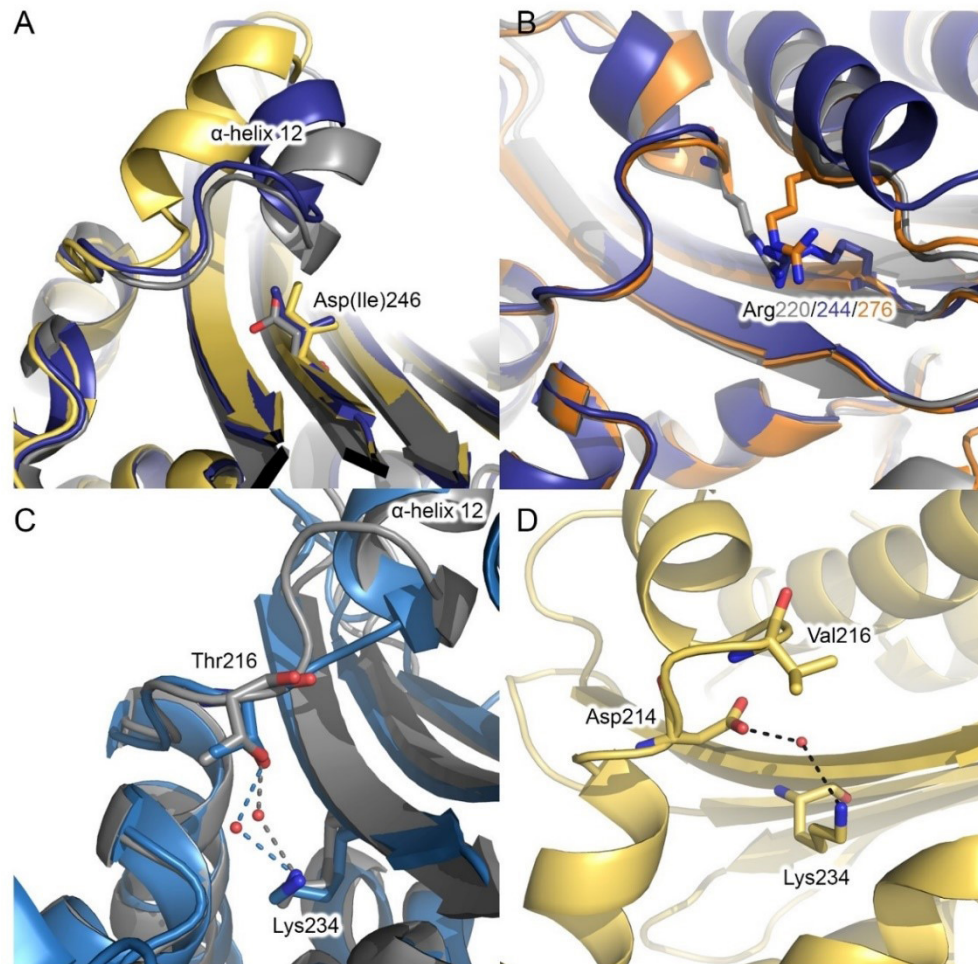


Figure 3.6. (A) Structural alignment of BlaC in grey (2GDN¹⁰¹), SHV in yellow (2ZD8¹⁹⁰) and TEM in blue (1BTL¹⁹¹). Residues at position 246 are shown in sticks, label represents residues in BlaC with residues in TEM and SHV in brackets; (B) Guanidino group of Arg220 in BlaC, Arg244 in TEM and Arg276 in Toho-1 (in orange, 1IYS¹⁹²) occupy the same space; (C) Position of Thr216 in BlaC and β -lactamase from *Mycobacterium fortuitum* (in light-blue, 2CC1¹⁹³). Despite different length of the linker to α -helix 12, Thr216 occupies the same place, allowing it to interact with the conserved water (shown as spheres); (D) Structure of SHV. Asp214 and Val216 are present instead of Asn214 and Thr216 but the water position is still conserved.

The second feature that we believe is ensured by Asn214-Asp233-Asp246 motif is “locking” Thr216 residue in place. Residue Thr216 in BlaC and many other β -lactamases is involved in a chain of H-bonds involving Thr216-Asn214-water-Lys234. Lys234 is part of the active site KTG motif (Figure 3.1b). Most likely, the precise position of Thr216 is influenced by both the H-bonds between Asn214 and Asp233 and between Asp246 and Ile221, discussed above. The position of Thr216 is very conserved (94%) among many class A β -lactamases. Even in case of β -lactamase from *Mycobacterium fortuitum*, which has a shorter linker between α -helices 11 and 12 α -helix 12 is mounted on top of the β -sheet in the same fashion as in BlaC and Thr216 is locked in place, allowing it to interact with Lys234 via a water molecule (Figure 3.6c). A few β -lactamases, however, do not carry threonine at position 216. Interestingly, these enzymes have Asp rather than Asn at position 214 (Figure 3.6d). It seems that water bridging in such structures can be achieved solely by Asp214. However, as shown in this study, in BlaC mutation N214D results in completely inactive protein. We believe that this effect appears because of repulsion between Asp214 and Asp233, shifting Thr216 away from its natural site. The repulsion effect was demonstrated before for TEM, in MD simulations performed for a fully deprotonated Asp214-Asp233 pair¹⁷⁰.

Thus, in summary, the motif Asn214-Asp233-Asp246 ensures the correct positioning of Thr216 and Arg220, which are important for catalysis. The combination of this motif together with Thr216 is a conserved feature. Another variant of this motif is Asp214-Asp233-Ile246, which occurs less frequently and is coupled with no threonine at position 216 and no arginine at position 220.

Marciano and colleagues performed an extensive analysis of β -lactamase sequences in order to determine the evolution of the positive charge near an active site. They discussed the presence of arginine either at position 220, or 244, or 276 and named Arg220 as an ancestral position¹⁸⁹. To link the position of arginine to the nature of residue at position 246, we built a phylogenetic tree using 310 class A β -lactamase sequences (Figure 3.7). The evaluation of the phylogenetic tree revealed that arginine at position 220 was initially coupled with the aspartate at the position 246. A switch to arginine 244 or arginine 276 appeared at some point independently in non-related branches. However, these sequences still carried Asp246 (Asn in some rare cases) as well as Thr216. The only exception was a relatively small group of sequences including TEM, SHV and β -lactamase from *V. parahaemolyticus*, which carry Arg244 and lost both Asp246 and Thr216.

Based on results presented in this research together with structural studies, we propose a model in which mutations in residue 246 lead to the loss of the connection between the β -sheet and α -helix 12. This lost connection introduces dynamics in which the helix is mobile, and activity is reduced, due to changed Thr216 and Arg220 positions. However, the protein

still populates the native state for a fraction of the time that differs for different mutants. This conformational freedom leads to chemical exchange in the NMR resonances of backbone amides, resulting in the linear pattern of the CSPs. To characterize the exchange, CPMG experiments were performed with BlaC D246A, however, no significant differences were observed with the wild type protein. Most likely, the exchange is occurring with a rate that is too fast to detect ($k_{ex} > 1000 \text{ s}^{-1}$). The linear shift of the peaks upon mutation was observed before by multiple research groups. Jensen and colleagues reported linear correlation between the chemical shifts of the wild type and two variants of SH3 domain of JIP1¹⁹⁴. They proved that the variants are in fast to intermediate exchange between two conformations governed by an aromatic ring flipping inside the protein core. Schütz, Rennella, and Kay showed a peak position of one of the p97 residues titrating as a function of mutation in a near linear fashion indicating a rapid exchange between two conformers¹⁹⁵. A similar trend was observed in TEM β -lactamase Zimmerman et al., where resonances were found to display a linear shift pattern from the wild type protein and the least stable variants to the most stable variants¹⁹⁶. The authors propose that chemical shifts close to the wild type represent nuclei in a more loosely packed interface and those closer to the stabilized variants represent nuclei in a more tightly packed interface. Although the packing of the structure and strength of interaction do not directly explain the shift of the amide resonances in a linear manner, it is possible that the effect observed by Zimmerman and colleagues also indicates the interconversion between different states. In this case, however, the wild type enzyme is the one that undergoes these changes.

It was shown for TEM¹⁷⁰ that the pair Asp214-Asp233 share a proton, but most of the time, Asp214 is protonated in this pair. Analogously, in BlaC, the pair Asp233-Asp246 needs to share a proton to avoid repulsion. Considering our results, we propose that predominantly Asp246 is protonated.

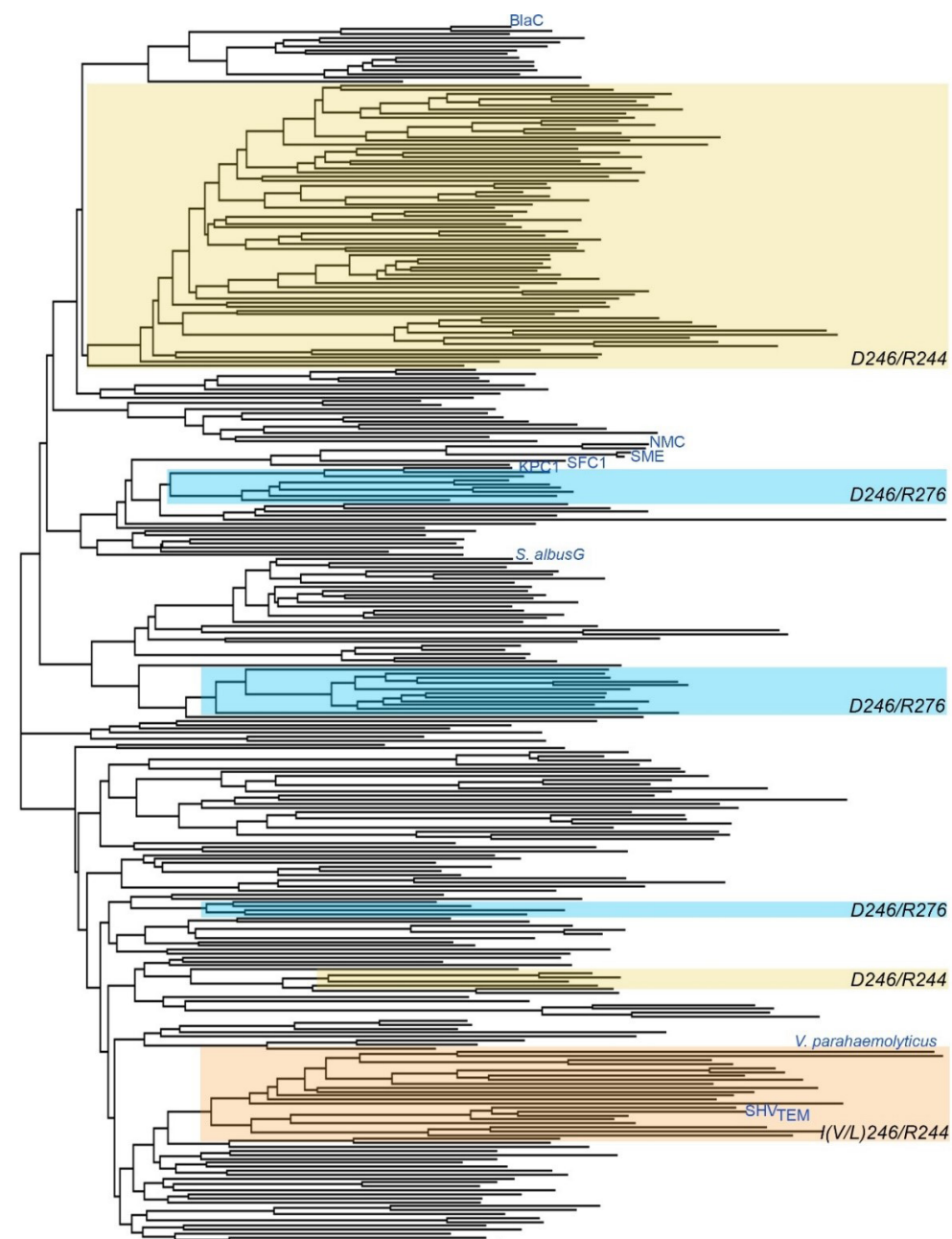


Figure 3.7. Phylogenetic tree of class A β -lactamases. A total of 310 sequences were used to compose a tree. Some well-known β -lactamases and structures discussed in the text are labeled. Blue highlights represent enzymes that carry Asp246 together with Arg276; yellow represents sequences with Asp246 and Arg244; orange color represents sequences with Ile(Val/Leu)246 and Arg244. All the rest carry Asp(Asn)246 and Arg220. Only sequences in orange do not carry Thr216.

Materials and Methods

Production of BlaC variants

Site-directed mutagenesis was performed using whole plasmid site-directed mutagenesis. The primer sequences can be found in Table S2.3. Wild type and mutant proteins were produced in *E. coli* BL21 (DE3) pLysS strain transformed with pET28a plasmids containing the *blaC* gene with an N-terminal His-tag and TEV cleavage site. Cells were cultured in LB medium at 250 rpm at 37 °C until the optical density at 600 nm reached 0.6, at which point protein production was induced with 1 mM isopropyl β-D-1-thiogalactopyranoside (IPTG), followed by incubation of the cultures at 18 °C for 16 hours. For the production of isotope labeled proteins for NMR experiments, M9 medium was used with ¹⁵N ammonium chloride as the sole nitrogen source for ¹⁵N-labeled samples. Components of the M9 medium can be found in Table S2.4. Cells were harvested by centrifugation and lysed with French Press in 20 mM Tris-HCl buffer, pH 7.5 with 500 mM NaCl. The first purification was conducted with 5 mL HisTrap Nickel column (GE Healthcare) in 20 mM Tris-HCl buffer, pH 7.5 with 500 mM NaCl. Protein was eluted with the same buffer with 125 mM imidazole. Proteins carried an N-terminal His-tag that was removed by overnight incubation with 0.2 mg mL⁻¹ His-tagged Tobacco Etch Virus (TEV) protease at 4 °C in 25 mM Tris-HCl buffer, pH 8.0 with 100 mM NaCl, 1 mM EDTA and 5 mM DTT. After cleavage the enzyme was purified further by another run over a HisTrap Nickel column.

In vivo activity studies

For *in vivo* experiments in *E. coli* cells proteins encoded on pUK21 were produced with an *E. coli* twin arginine transporter (Tat)-signal at the N-terminus, to ensure translocation to the periplasm, mimicking the location of the protein in *M. tuberculosis*¹⁴⁷. The survival of the *E. coli* cells carrying pUK-based plasmids with wild type or mutant *blaC* genes was tested on LB-agar plates with various concentrations of ampicillin or carbenicillin. All plates contained 50 µg mL⁻¹ kanamycin and 1 mM IPTG. Cells were applied on the plates as 10 µL drops with OD₆₀₀ values of 0.3, 0.03, 0.003 or 0.0003 and incubated for 16 h at 37 °C before photography.

Circular dichroism

CD profiles were recorded using Jasco J-815 spectropolarimeter with a Peltier temperature controller (Jasco, MD). Measurements were performed at 25 °C with 10 µM protein in 100 mM sodium phosphate buffer, pH 6.4. Spectra were acquired in 1 mm quartz cuvette at a scan rate of 50 nm/min.

Thermal stability

Thermal stability of the proteins was analyzed by thermal shift assay (TSA) with SYPRO Orange dye (Invitrogen). The measurements were performed in triplicate in two independent

experiments using the CFX 96 Touch Real-Time PCR Detection System from Bio Rad with 2x dye and 10 µM protein in 100 mM sodium phosphate buffer, pH 6.4 with the temperature range 20-80 °C. Melting temperatures were determined as an average of 6 measurements.

Kinetics

Determination of the Michaelis-Menten kinetic constants was done by measuring the absorption change at 486 nm for nitrocefin ($\Delta\epsilon = 11300 \text{ M}^{-1}\text{cm}^{-1}$ ¹⁴⁵) in a PerkinElmer Lambda 800 UV-Vis spectrometer at 25 °C in 100 mM sodium phosphate buffer, pH 6.4. All measurements were performed in triplicate. The reactions were carried out at various concentrations of substrates and 5 nM of BlaC, and initial rates of the hydrolysis were plotted against concentration of substrate and fitted separately for each experimental set to the Michaelis-Menten equation 3.1 using OriginPro 9.1, where v_0 is the initial reaction rate, $[S]_0$ the initial substrate concentration, V_{\max} the maximum reaction rate and K_M the Michaelis-Menten constant. v_0 and $[S]_0$ are the dependent and independent variables, respectively, and K_M and V_{\max} are the fitted parameters. $V_{\max} = k_{\text{cat}}[E]$, k_{cat} is the rate-limiting conversion rate, and $[E]$ is the concentration of BlaC.

$$v_0 = \frac{V_{\max}[S]_0}{[S]_0 + K_M} \quad (3.1)$$

NMR spectroscopy

TROSY-HSQC spectra of all BlaC variants were recorded on a Bruker AVIII HD 850 MHz spectrometer at 25 °C in 100 mM phosphate buffer (pH 6.4) with 6% D₂O. Data were processed in Topspin 3.2 (Bruker). Spectra were analyzed with CCPNmr Analysis V3¹⁶⁷ software. Peaks of the mutant spectra were assigned by comparison to peaks in the wild type BlaC spectrum and average chemical shift perturbations (CSP), $\Delta\delta$, of the ¹H ($\Delta\omega_1$) and ¹⁵N ($\Delta\omega_2$) resonances of backbone amides were calculated using equation 3.2. Peaks that could not be assigned with certainty were assigned based on the smallest possible CSP (Figure S3.2).

$$\Delta\delta = \sqrt{\frac{1}{2}\left(\Delta\omega_1^2 + \left(\frac{\Delta\omega_2}{5}\right)^2\right)} \quad (3.2)$$

Supplementary materials

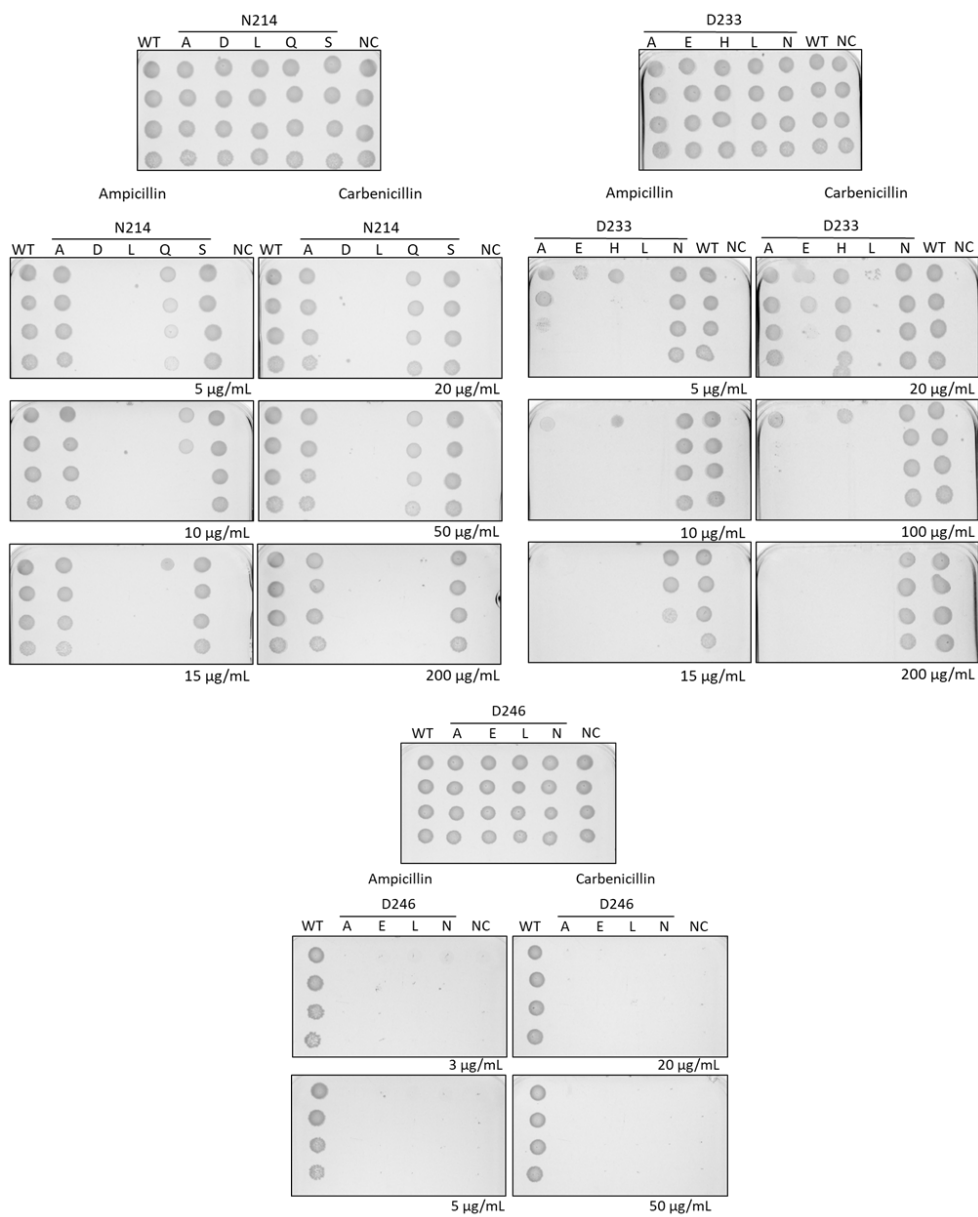


Figure S3.1. Plates showing growth at 37 °C of *E. coli* cells expressing wild type (WT) or mutant blaC (negative control, NC is the S70A mutant) with no antibiotics or various concentration of ampicillin and carbenicillin (MICs for wild type BlaC are 100 $\mu\text{g/mL}$ and 1000 $\mu\text{g/mL}$ respectively).

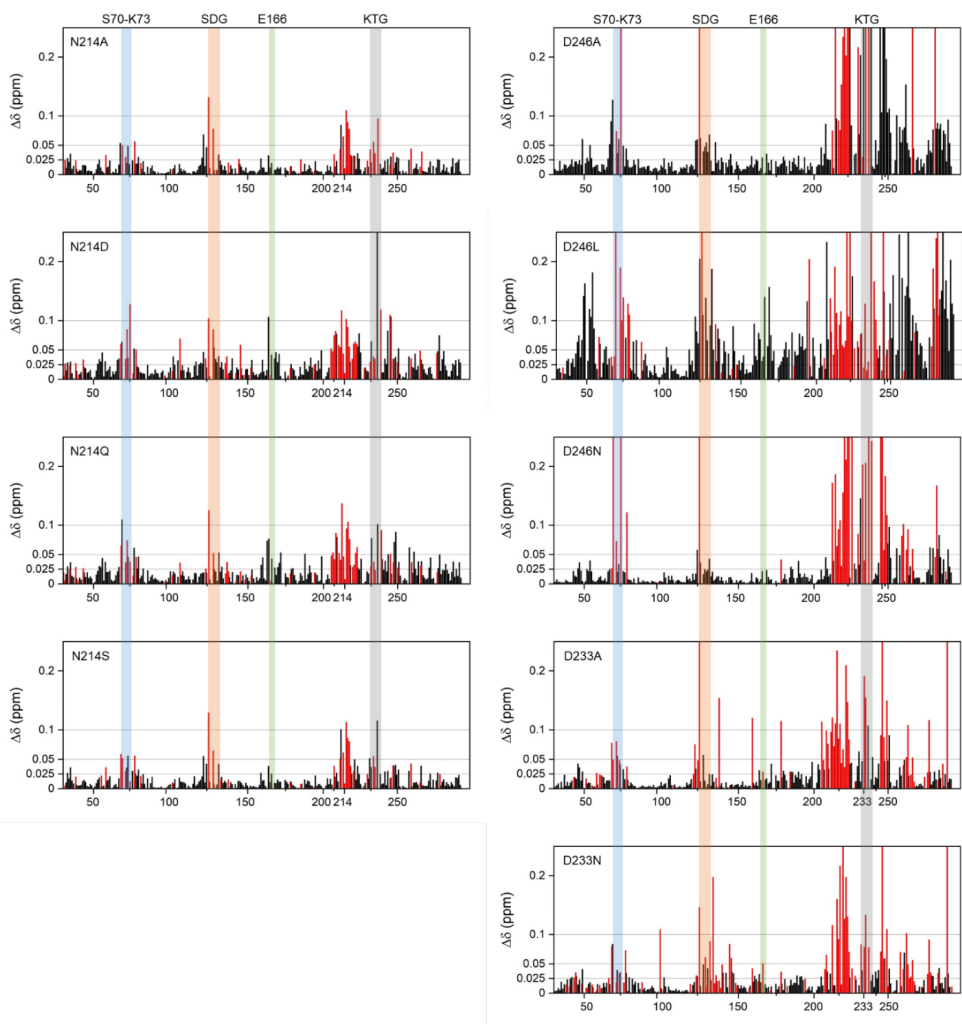


Figure S3.2. Average CSP for the backbone amides of the BlaC mutants. Residue numbers refer to Ambler numbering. Black bars represent CSP for residues assigned with certainty. Red bars show CSP calculated as the minimal possible CSP. Important catalytic residues and residues next to them are shown with colored highlights.

Chapter 4

Conserved residues Glu37 and Trp229 play an essential role in protein folding of β -lactamase

Based on the research article:

Aleksandra Chikunova, Max P. Manley, Misbha Ud Din Ahmad, Tuğçe Bilman, Anastassis Perrakis, Marcellus Ubbink (2021). Conserved residues Glu37 and Trp229 play an essential role in protein folding of β -lactamase, *FEBS J.* 288(19): 5708-5722

Abstract

Evolutionary robustness requires that the number of highly conserved amino acid residues in proteins is minimized. In enzymes, such conservation is observed for catalytic residues but also for some residues in the second shell or even further from the active site. β -lactamases evolve in response to changing antibiotic selection pressures and are thus expected to be evolutionarily robust, with a limited number of highly conserved amino acid residues. As part of the effort to understand the roles of conserved residues in class A β -lactamases, we investigate the reasons leading to the conservation of two amino acid residues in the β -lactamase BlaC, Glu37 and Trp229. Using site-directed mutagenesis, we have generated point mutations of these residues and observed a drastic decrease in the levels of soluble protein produced in *Escherichia coli*, thus abolishing completely the resistance of bacteria against β -lactam antibiotics. However, the purified proteins are structurally and kinetically very similar to the wild type enzyme, only differing by exhibiting a slightly lower melting temperature. We conclude that conservation of Glu37 and Trp229 is solely caused by an essential role in the folding process, and we propose that during folding Glu37 primes the formation of the central β -sheet and Trp229 contributes to the hydrophobic collapse into a molten globule.

Introduction

Most proteins are under evolutionary pressure to minimize the number of essential residues, yielding evolutionary robust proteins. Proteins for which the function depends on the exact nature of many amino acid residues are prone to be rendered inactive by random mutations. Nevertheless, in many proteins the conservation of some residues is high, and it is not always obvious why that is the case. In enzymes, the few residues involved in ligand binding and catalysis are generally highly conserved for obvious reasons. However, also other residues, surrounding the active site or even at more distant locations, are conserved. Conservation is taken as a proxy for functional relevance and is extensively used in research for the prediction of functionally important regions^{34–36,108}, yet it is often not evident what the function of such residues is. Many factors contribute to the proper functioning of proteins, such as rapid and correct folding, a stable three-dimensional structure, precise positioning of the catalytic residues in the active site, correct dynamic properties, targeting to the correct location in the cell and post-translational modifications. We have started an effort to determine the functions of all conserved residues in β -lactamases and establish whether high conservation equates functional necessity. Specifying the roles of all conserved residues in an enzyme can contribute to a better understanding of the evolutionary robustness of proteins. β -lactamases catalyze the reaction of hydrolysis of β -lactam antibiotics, the largest group of antibiotics, providing bacteria with resistance against these compounds¹⁹⁷. The current study focuses on the relevance of two of the highly conserved residues in the β -lactamase from *Mycobacterium tuberculosis*, BlaC. This enzyme is a broad-spectrum class A β -lactamase encoded by a chromosomal gene¹⁰¹. The presence of BlaC in this pathogen is the reason that β -lactam antibiotics are not normally used for tuberculosis treatment⁷³.

Residue Glu37 (Ambler numbering⁸⁹) is present in 99% of class A β -lactamases^{109,140,173,198} (across 494 sequences) and has not been reported to be involved in protein function in this class. In class B (metallo- β -lactamases) this residue is also conserved and mutations lead to lower activity^{199,200}. The C α of this residue is located 20 Å away from the C α of the active site Ser70. In BlaC Glu37 interacts with Ala42, Leu44, Tyr60 and Arg61 (Figure 4.1). Alanine, aspartate, glutamine or serine were also found at this position in 1% of sequences.

Residue Trp229 is 98% conserved in class A β -lactamases. In TEM-1, another class A β -lactamase, mutations at this position significantly decrease enzyme activity¹³¹. Trp229 is in close proximity to an allosteric site in TEM-1, where two non-competitive inhibitors have been shown to bind²⁰¹. Trp229 is situated 24 Å away from the active site serine, and in BlaC Trp229 interacts with Phe225, Tyr259, Pro254 and Pro226 (Figure 4.1). Alanine, phenylalanine, tyrosine, serine or cysteine are found at position 229 in 2% of sequences.

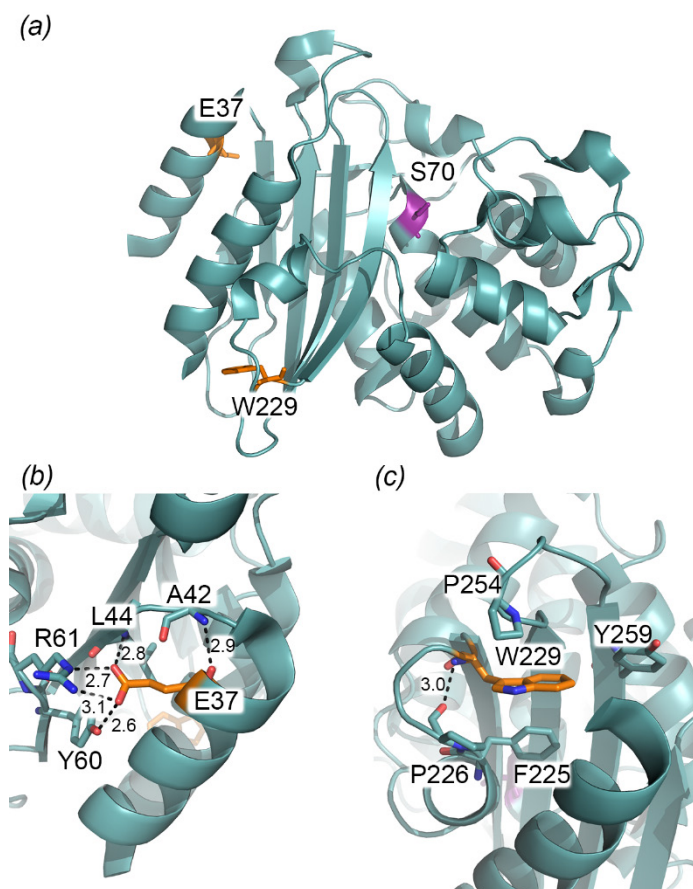


Figure 4.1. Location of Glu 37 and Trp229 in BlaC. (A) Structure of BlaC (PDB entry 2GDN¹⁰¹) with residues Glu37 and Trp229 shown in orange sticks and the catalytic residue Ser70 in violet; (B) Detail of the structure surrounding Glu37. Interactions involving Glu37 are drawn in black dashed lines; (C) Detail of the structure surrounding Trp229. Interaction involving backbone of Trp229 is drawn in black dashed line.

To reveal the reason for conservation of these residues in class A β -lactamases, site-directed mutagenesis was performed, replacing Glu37 and Trp229 with a range of amino acids with different properties. We report that the production levels are strongly reduced, indicating that both residues are important for correct folding. Apart from a moderate decrease in thermal stability, revealed by thermal shift assays, the mutations have surprisingly little effect on the structure and activity of the enzyme, as probed with kinetic measurements, CD and NMR spectroscopy and X-ray crystallography. The possible roles of Glu37 and Trp229 in the folding process are discussed.

Results

To investigate the role of Glu37 in BlaC, it was mutated to Ala, Asp, Leu and Gln. The mutation to Ala was chosen to ensure that all interactions involving the side chain (Figure 4.1) are no longer possible. The Asp mutant maintains the functional group but reduces the size, probing interactions in which exact positioning is critical. The mutation to Leu introduces a side chain of the exact same surface area²⁰² as the wild type residue but with non-polar nature. Gln is a mimic that eliminates the charge but maintains size, polarity and ability to form hydrogen bonds, while allowing to also donate a hydrogen in such interactions.

The aromatic nature of Trp229 was mimicked with mutations to Phe and Tyr. The latter also resembles the amphipathic nature of Trp with its hydroxyl group. The other mutants were Leu, Gln and Ala. Properties of the side chains of these residues are in Table 4.1.

E37 and W229 are essential for function

The survival of BlaC wild type and variants in *Escherichia coli* was tested by applying cells cultures of different dilution on agar plates containing various concentrations of ampicillin and carbenicillin. A catalytically inactive mutant with active site serine 70 replaced by alanine was used as a negative control. Cells producing wild type protein are able to grow with 100 $\mu\text{g mL}^{-1}$ of ampicillin and 500 $\mu\text{g mL}^{-1}$ of carbenicillin, whereas mutant producing cells have very low survival in the analyzed antibiotic concentration range (Figure 4.2a, Figure S4.1).

Cultures that produce BlaC Glu37 mutants do not perform better than the negative control with minimal inhibitory concentrations (MIC) of 3 $\mu\text{g mL}^{-1}$ and 20 $\mu\text{g mL}^{-1}$ for ampicillin and carbenicillin, respectively. Only W229F and W229Y mutants do slightly better and are not able to grow at 5 $\mu\text{g mL}^{-1}$ and 50 $\mu\text{g mL}^{-1}$ of ampicillin and carbenicillin, respectively. Interestingly, cultures producing W229A, W229L and W229Q were outperformed by the negative control at 2 $\mu\text{g mL}^{-1}$ of ampicillin (Figure 4.2b). The observed effect could be explained by increased production of toxic protein, induced by the presence of antibiotic in mutant producing cultures, an effect previously described for some proteins²⁰³. In cultures incubated at 25 °C Glu37 mutants still show no activity against antibiotics. However, for the mutants W229F and W229Y improved growth was observed at 25 °C both on plate and in liquid cultures (Figure 4.2c, Figures S4.2-S4.3), suggesting that the mutant proteins can be formed in reasonable amounts but have reduced thermostability.

Table 4.1. Amino acid residues properties

Residue	Side-chain ASA (Å ²)	Side chain polarity	Charge	Aromaticity
Glu37	Glu	138	+	Negative
	Ala	67	-	Neutral
	Asp	106	+	Negative
	Leu	137	-	Neutral
	Gln	144	+	Neutral
	Trp	217	-	+
Trp229	Ala	67	-	-
	Phe	175	-	+
	Leu	137	-	-
	Gln	144	+	-
	Tyr	187	+	+

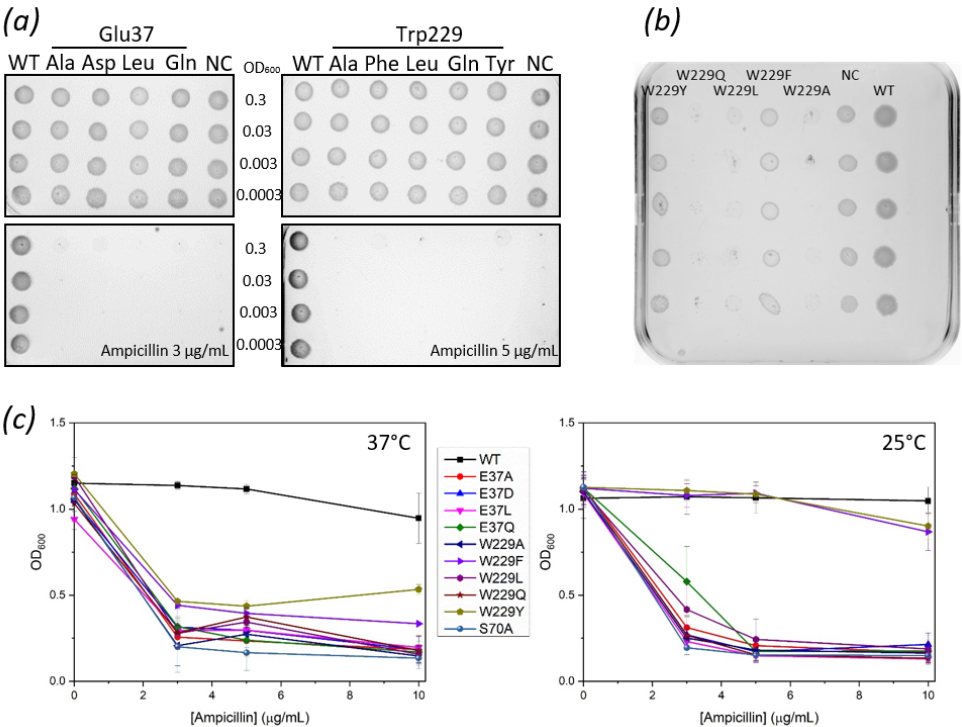


Figure 4.2. Glu37 and Trp 229 mutants are mostly inactive *in vivo*. (A) Plates showing growth at 37 °C of *E. coli* cells expressing wild type (WT) or mutant BlaC (negative control, NC is the S70A mutant) with no antibiotics (top) or a low concentration of ampicillin (bottom, MIC for wild type BlaC > 100 mg mL⁻¹); (B) Plate with 2 µg mL⁻¹ ampicillin. The growth of W229A, W229L and W229Q mutant producing cultures is inhibited, whereas the negative control (S70A mutant) still grows; (C) End point OD₆₀₀ values (15 hours at 37 °C and 25 hours at 25 °C) of *E. coli* cultures expressing wild type and mutant blaC genes as a function of ampicillin concentration. Error bars represent standard deviation of three replicates.

Mutants of E37 and W229 yield less soluble enzyme

For *in vitro* characterization, the genes for the mature wild type and variants BlaC were over-expressed without signal sequence to obtain cytosolic soluble protein. Production of soluble protein was checked using SDS-PAGE. The results (Figure 4.3a) show a large decrease in the amount of soluble protein for Glu37 mutants. The total amount of protein, however, remains similar.

For protein quantification the signal intensities were compared to each other and to samples with known protein concentrations (Figure S4.4) using ImageLab software (BioRad). For all variants, the BlaC total yield varied from 138 µg mL⁻¹ to 206 µg mL⁻¹ of cell culture, while the soluble fraction contained 70-86% of protein for wild type and only up to 12% for Glu37 mutants. For BlaC E37L, W229A, W229L and W229Q no soluble protein was detected. For

BlaC W229F and W229Y 60-69% of soluble protein was present, however, after purification most of it turned out to be unfolded.

To check the effect of additional chaperones in the cell, expression was also carried out in a strain, in which the production of chaperones could be induced (JM109(DE3) pGKEJ-8). Two chaperone combinations were used, namely the DnaK-DnaJ-GrpE combination and GroES-GroEL. In the presence of chaperones, slightly less insoluble protein was found for the mutants and wild type. However, the amount of BlaC in the soluble fractions did not increase, as judged by SDS-PAGE and an activity test based on nitrocefin conversion in the culture (Figure 4.3b-4.3c).

E37 and W229 mutants are active *in vitro* but have reduced thermostability and refolding ability

Insofar mutants yielded soluble BlaC, the enzymes were purified for *in vitro* characterization. The far-UV circular dichroism (CD) spectra showed that folded fractions of all mutant proteins display a secondary structure similar to wild type BlaC, with two peaks at around 210 nm and 222 nm, characteristic of a predominantly helical protein (Figure 4.4a).

Melting temperatures were determined using a thermal shift assay, following the fluorescence signal of SYPRO Orange dye, which increases upon binding to hydrophobic areas of the protein that become exposed during thermal unfolding (Figure 4.4b; Table 4.2). These mutations decrease the thermal stability of BlaC by 2-4 °C. Specificity constants of nitrocefin conversion for BlaC variants were shown to be only marginally smaller than that of wild type BlaC (Table 4.2, Figure 4.4c), suggesting that the inability of *E. coli* cells expressing mutants to grow in the presence of β -lactams was due to a lack of sufficient folded, soluble protein rather than inactivity of the mutant enzymes.

A refolding experiment was carried out to compare the extent of refolding of WT BlaC and mutants after denaturation by the chaotropic agent guanidinium and dilution to various final concentrations of this agent. The fraction of refolded, active enzyme was probed by the rate of nitrocefin conversion. BlaC E37A is much more sensitive to the presence of the chaotropic agent than wt BlaC. The sensitivity of BlaC W229F is similar to wt BlaC but refolding is slower (Figure 4.4d).

Table 4.2. Melting temperatures and specificity constants of wild type and mutant BlaC.

	T_{melt}^a (°C)	ΔT_{melt}^b ($T_{\text{melt}}[\text{mutant}] - T_{\text{melt}}[\text{WT}]$, °C)	k_{cat}/K_M ($\times 10^5 \text{ M}^{-1}\text{s}^{-1}$)	K_M (μM)	k_{cat} (s^{-1})
C-terminal His-tag					
WT	52	-	4.4 ± 0.5	212 ± 17	107 ± 12
E37A	48	-4	3.1 ± 0.9	146 ± 24	44 ± 8
E37D	50	-2	2.8 ± 0.4	217 ± 36	60 ± 9
E37Q	49	-3	4.5 ± 0.9	176 ± 25	67 ± 13
No His-tag					
WT	52	-	4.7 ± 0.5	281 ± 18	133 ± 7
W229F	49	-3	3.2 ± 0.1	403 ± 51	129 ± 10
W229Y	49	-3	3.4 ± 0.6	284 ± 48	98 ± 2

^a Error 0.5 °C; ^b Error 0.7 °C

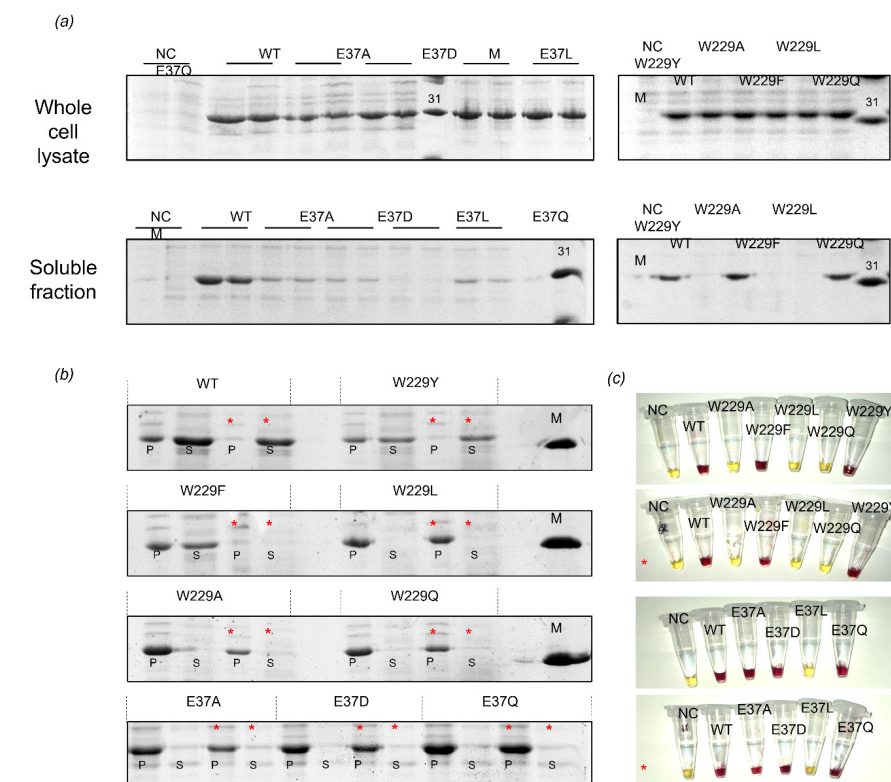


Figure 4.3. (A) Production levels of total BlaC and soluble fraction for wild type (WT) and variants. SDS PAGE showing whole cell lysate and soluble fraction after induction of gene expression. Negative control (NC) indicates non-induced cell culture for the wild type BlaC. M, markers with the 31 kDa band indicated; (B) SDS PA-gels showing pellet (P) and supernatant (S) content of lysed cultures grown with and without chaperones expression. Samples from cultures with chaperones are marked with asterisk. Note that the induction of W229F culture with chaperones failed. M corresponds to the marker band of 31 kDa. The amount of protein in the pellet is reduced in the presence of chaperones, the amount of protein in supernatant, however, is not affected; (C) Nitrocefin activity test for BlaC presence in the supernatant of lysed cultures. Cultures producing chaperones are marked with an asterisk.

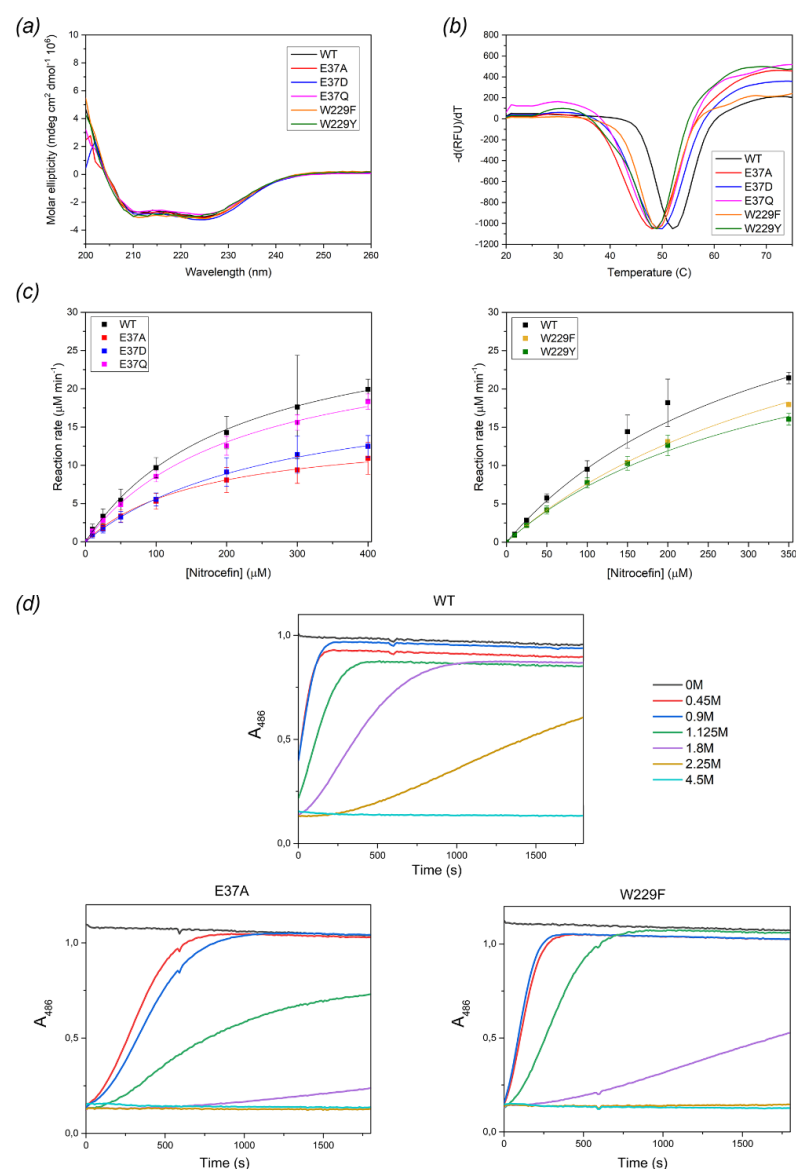


Figure 4.4. Secondary structure and thermostability of WT and mutant BlaC. (A) CD spectra of wild type and soluble BlaC mutants; (B) Normalized negative derivative of thermal shift assay (SYPRO orange binding). The minimum in the curve represents the melting temperature; (C) Kinetics curves of BlaC wild type and mutants for nitrocefin. Experiments were performed at 25 °C in 100 mM sodium phosphate buffer, pH 6.4. Error bars represent the standard deviation of five measurements for E37D and E37Q mutants and three measurements for all other samples. A His-tag is present at the C-terminus for E37 variants and wild type at the left panel. No His-tag is present for W229 variants and wild type at the right panel. Experimental data were fitted to the Michaelis-Menten equation (equation 2); (D) Refolding assay for BlaC wt and E37A and W229F. Samples were denatured in 4.5 M Gdn for 20 min on ice and then diluted into the Gdn concentration indicated in the graph with a buffer that also contained nitrocefin (100 mM final concentration). The final enzyme concentration was 0.9 μM. The conversion of the substrate was followed over time at 486 nm and 25 °C. The enzyme used for the curves at 0 M Gdn was not unfolded. The curves are averages of three replicate experiments.

E37 and W229 mutations only cause local changes in structure

Chemical shifts perturbations (CSPs) are an indication of the extent of structural changes caused by point mutations. Figure 4.5 shows the backbone amide CSP maps obtained from TROSY-HSQC NMR²⁰⁴ spectra of the ¹⁵N labelled BlaC variants plotted on the crystal structure of wild type BlaC (Figure 4.5). Two features stand out. Firstly, significant CSPs are only localized to regions nearby the mutations, as most clearly shown by W229F and W229Y BlaC. This observation is in line with the CD results that indicate that the secondary structure is unaffected. In combination with the fact that the mutants are capable of converting nitrocefin, it is likely that the three-dimensional structures of the mutants are very similar to that of the wild type BlaC. Indeed, the crystal structure of the E37A mutant we determined at 1.5 Å resolution, does not show large differences compared to the wild type (Table 4.3, Figure 4.6).

The loss of hydrogen bond ability of residue 37 seems to be compensated by a well-ordered water molecule that is not present in the structure of the wild type enzyme (Figure 4.6a). The structures of wild type and E37A BlaC superimpose with an average root-mean-square deviation (RMSD) between Ca atoms of 0.29 Å and the position of catalytic residues match with the great precision (Figure 4.6b). We were unable to crystallise any W229 mutants.

The CSP maps for the three E37 mutants (E37A, E37D and E37Q) are similar, as are the ones for W229F and W229Y. This finding suggests that the mutations disrupt specific interactions that are not or not completely rescued by the mutant side chain. For example, the similarity of the maps of E37A and E37Q indicates that the alanine and glutamine side chains cause the same changes in the chemical environments of the involved amides, relative to a glutamate side chain. Also an aspartate, which is expected to maintain the negative charge present on the glutamate side chain, causes similar CSPs. Thus, both length and charge of the glutamate appear to be critical in wild type BlaC. Similarly, but perhaps less surprisingly, neither tyrosine nor phenylalanine can completely replace the indol of W229.

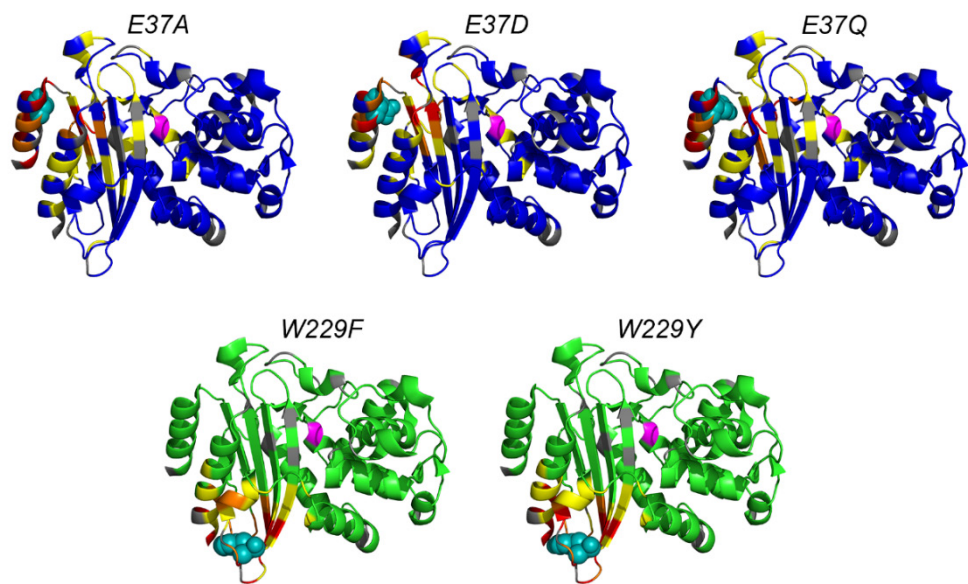


Figure 4.5. Structural effects of the single point mutations. The backbone amide CSP, as defined in the Materials and Methods section, observed for E37A, E37D, E37Q, W229F and W229Y relative to wild type BlaC are plotted on the structure (PDB 2GDN¹⁰¹). Blue/green, $\Delta\delta < 0.025$ ppm; yellow $0.025 < \Delta\delta < 0.050$ ppm; orange $0.050 < \Delta\delta < 0.100$ ppm; red, $\Delta\delta > 0.1$ ppm; grey, no data. The mutated residue is modelled and shown as a teal space fill. The location of the catalytic residue S70 is shown in magenta.

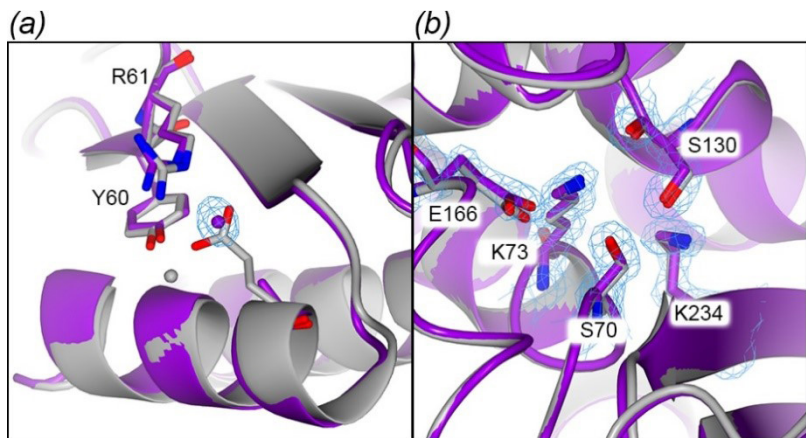


Figure 4.6. Overlay of E37A mutant crystal structure in violet (7A5U) and wild type BlaC in grey (PDB 2GDN6). (A) Mutation site close-up. Residues 37, Tyr60 and Arg61 are shown in sticks. Water found on the surface in wild type structure (grey sphere) is found to be buried in the mutant structure (violet sphere). The 2mFo-DFc electron density corresponding to this water is shown in blue chicken wire; (B) Active site close-up. Catalytic residues are shown in sticks. Blue chicken wire shows the 2mFo-DFc electron density of catalytic residues in mutant structure.

Table 4.3. Data collection and refinement statistics for the structures of BlaC E37A, PDB entry 7A5U.

Data Collection	7A5U
Wavelength (Å)	0.966
Resolution (Å)	54.30-1.50 (1.53-1.50)
Space group	P 1 21 1
Unit cell a, b, c (Å)	38.56, 54.74, 54.51
α, β, γ	90.00, 94.99, 90.00
CC _{1/2}	99.9 (76.8)
R _{pim} (%)	2.3 (35.8)
I/σI	9.1 (1.5)
Completeness (%)	91.5 (97.0)
Multiplicity	2.5
Unique reflections	33194
Refinement	
Atoms protein/ligands/water	2021/9/148
B-factors protein/ligands/water (Å ²)	16/20/31
R _{work} /R _{free} (%)	12.5/17.6
Bond lengths RMSZ/RMSD (Å)	0.998/0.014
Bond angles RMSZ/RMSD (°)	1.065/1.772
Ramachandran plot preferred/outliers	247/2
Ramachandran plot Z-score	-0.51
Clash score	2.23
MolProbity score	1

Discussion

The results presented in this work show that BlaC variants of both Glu37 and Trp229, once folded, behave like the wild type protein. NMR spectra do not show major changes compared to the wild type BlaC spectrum, and most CSPs are found in the vicinity of the mutation site. Also, the kinetic parameters of nitrocefin hydrolysis are comparable to those of the wild type enzyme. However, cells producing mutated protein were not able to grow even on the lowest concentrations of antibiotics. In each case, a large fraction or even all of the mutant protein was insoluble and found in the pellet.

Residue Glu37 is 20 Å away from the active site, yet it is 99% conserved^{109,140}. In BlaC Glu37 makes a hydrogen bond with the side chain of Tyr60 and two hydrogen bonds with Arg61, fixing the turn in between two β-strands. Furthermore, it makes a side chain-to-backbone interaction with Leu44 and backbone-to-backbone interaction with Ala42, which “staples” the first α-helix to the first β-strand. Whereas the backbone-to-backbone interaction can be achieved with any other residue, the remaining hydrogen bonds require a polar side chain. Multiple-sequence alignment shows that residues Tyr60 and Arg61 are present in only 56% and 85% of the sequences, respectively. However, the nature of these residues remains conserved. In position 60 mostly aromatic residues are found and position 61 is occupied exclusively by amino acids that contain an amide, amine or guanidinium group in the side chain. Furthermore, in multiple structures the guanidinium group of arginine is located 3.4-4.2 Å from the aromatic ring of residue 60, which makes it possible to form a cation-π interaction. This suggests that for Arg, His or Lys at position 61 such cation-π interaction is also plausible, and a N-H-π interaction could be present for Asn or Gln residues (Figure 4.7)²⁰⁵. The hydrogen bond between Tyr60 and Glu37 is not conserved because position 60 is not always a Tyr residue^{84,101,190,191,206,207}. On the other hand, a hydrogen bond between Glu37 and residue 61 is conserved and the 60-61 N-H-π or cation-π interaction also seems to be present in all β-lactamases of class A, and we propose that the loss of these hydrogen bonds is the cause of the 3 °C decrease in melting temperature of BlaC upon mutation of Glu37.

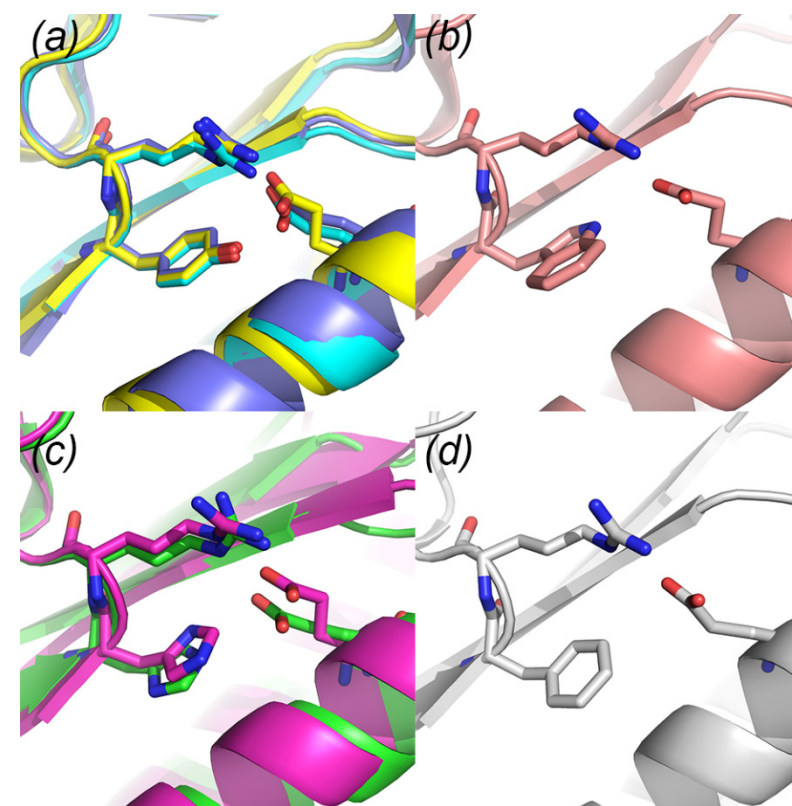


Figure 4.7. Structural overlay of some of the β-lactamase crystal structures, residues 37, 60 and 61 are represented with sticks. (A) Tyr60 containing structures: BlaC - purple (2GDN¹⁰¹), β-lactamase from *Streptomyces albus* - yellow (1BSG), BS3 from *Bacillus licheniformis* - cyan (1I2S²⁰⁶); (B) Trp60: SHV1 from *Klebsiella pneumoniae* - salmon (2ZD8¹⁹⁰); (C) His60: GES1 from *Klebsiella pneumoniae* - green (2QPN¹⁷⁵), β-lactamase from *Mycobacterium abscessus* - magenta (4YFM⁸⁴); (D) Phe60: TEM1 from *Escherichia coli* - white (1BTL¹⁹¹).

Our results show that both charge and exact location of the carboxyl group are important because neither Asp nor Gln performs better than Ala in replacing the Glu. Thus, the Glu at position 37 contributes to stability but at the same time is not critical for enzymatic activity, as mutants exhibit activity at a level similar to wild type BlaC. *In vivo*, however, Glu37 mutants confer no resistance against β-lactam antibiotics at all and the amount of soluble protein is very low. Clearly, Glu37 also has a critical role in protein folding. We propose that Glu37 is involved in the early stages of the folding process, through formation of an intermediate that facilitates formation of the central β-sheet. The sheet consists of two β-strands from stretches of amino acids located close the N-terminus and three that are close to the C-terminus (Figure 4.8). The multiple interactions of Glu37 with residues 42, 44, 60 and 61 could prime the formation of the β-sheet by stimulating the interactions between the first and second β-strand (in blue in Figure 4.8). *In vitro* the E37A variant is clearly hampered in refolding in the presence of low concentrations of Gdn. This result is an indication that Glu37 is relevant

for folding, but it is noted that cellular folding differs from *in vitro* refolding in the presence of a chaotropic agent. In prokaryotic cells, folding already starts on the ribosome^{208,209}, so formation of this interaction may happen very early on, even before the remaining part of the protein has emerged from the ribosome channel.

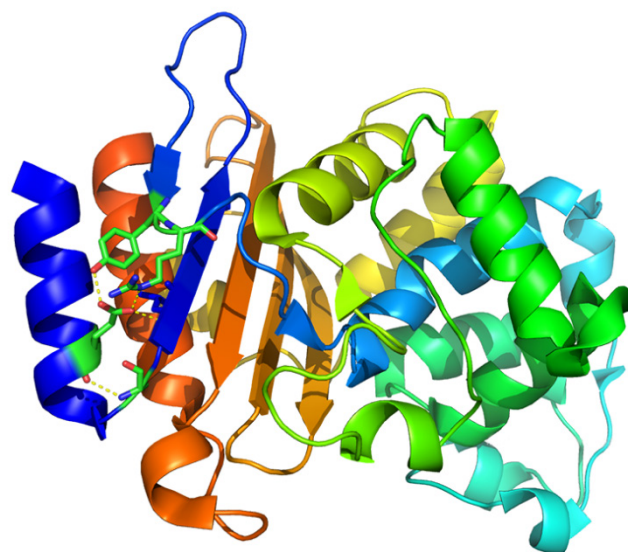


Figure 4.8. The potential role of Glu37 interactions for folding. The structure of BlaC (PDB 2GDN)¹⁰¹ is shown in cartoon representation with rainbow colours, from blue (N-terminus) to orange (C-terminus). Glu37 and the residues to which it forms hydrogen bonds (dashed lines) are shown in sticks, with carbons, oxygens and nitrogens in green, red and blue, respectively. It is proposed that the interactions of Glu37 prime the formation of the two blue β -strands, required for formation of the β -sheet with the remaining three β -strands that are distant in the primary structure.

Residue Trp229 is 98% conserved in class A β -lactamases. It is located in a turn between α -helix 12 and β -sheet 3 (Figure S2.9) and, just like Glu37, is found more than 20 Å away from the active site Ser70. In BlaC Trp229 makes a backbone-to-backbone interaction with Pro226 and a number of stacking interactions, including a perpendicular π -stacking interaction with Phe225, shifted parallel π -stacking interaction with Tyr259, and a stack-like interaction with Pro254. Pro226 most likely interacts with Trp229 via an L-shaped CH- π interaction (Figure 4.9)^{210–212}. These residues are not highly conserved in β -lactamases, with the exception of Pro226. Interestingly, even though β -lactamases are conserved structurally, the sequence as well as the precise structure of the loops differ considerably in this region. A consensus is that other aromatic residues play the same roles as Phe225 and Tyr259 in BlaC (Figure 4.9). Thus, in the folded protein, Trp229 facilitates staple interactions and occupies a large volume inside the hydrophobic pocket. Tryptophan has been shown to perform this role in multiple proteins^{213,214}.

For the class A β -lactamase TEM-1, it was reported that mutation of Trp229 to Ala, Phe or Tyr drastically decreases the yield but also reduces the activity of the enzyme¹³¹. Another aromatic residue at the position 229 can still form stacking interactions inside the hydrophobic pocket, although those with Pro226 and Pro254/252 are likely to be weaker, because the indol π -cloud is more electron rich²¹¹. Due to the smaller size of Phe and Tyr, the van der Waals interactions will be sub-optimal. Together, these effects can explain the slightly lower melting temperatures obtained for W229Y and W229F BlaC. The insolubility of three mutants and low yields of two Trp229 mutants coupled with their poor *in vivo* performance indicate that Trp229 is essential for mediating correct and efficient folding of BlaC. Aromatic mutants are able to confer resistance to β -lactam antibiotics at reduced growth temperatures (25 °C), indicating that the balance of misfolding and productive folding can easily be shifted in this case. Analogous to the Glu37 mutants, once folded, the mutant proteins show an overall fold and activity similar to those of the wild type BlaC. It is less obvious why Trp229 is critical for the folding process, because many of the surrounding residues are not conserved to a high degree and, unlike Glu37, Trp229 is not involved in stapling distant parts of the primary structure together. Trp229 is part of the large hydrophobic core of the protein formed by the three C-terminal β -strands that stabilizes the entire $\alpha\beta$ domain of the β -lactamases and thus could play a role in ensuring a rapid hydrophobic collapse and formation of the molten globule state^{215–217}, which then evolves to the folded state.

The yield of soluble, folded protein did not improve by increasing the concentration of chaperones for either Glu37 or Trp229 mutants. Despite seeing a decrease in the amount of protein within the pellet, the yield of soluble protein did not increase. It is plausible that chaperones help misfolded BlaC to undergo proteolysis, a process which has been well documented in eukaryotic systems^{218–220} and *E. coli*^{221,222}. Apparently, the chaperones do not enhance correct folding.

In summary, we find that residues Glu37 and Trp229 are not only conserved but also essential residues. Mutations dramatically reduces the yield of soluble, folded protein. In the case of Glu37, this reduction is proposed to be attributable to a role in the early folding process by priming the formation of the central β -sheet, which consists of parts of the protein widely separated in the primary structure. Given its large size and hydrophobic and aromatic interactions, Trp229 could be involved in the hydrophobic collapse and the formation of the molten globular state. Interestingly, though in the folded state both residues are engaged in interactions that affect the thermostability to some degree, they are not critical for the overall structure and activity.

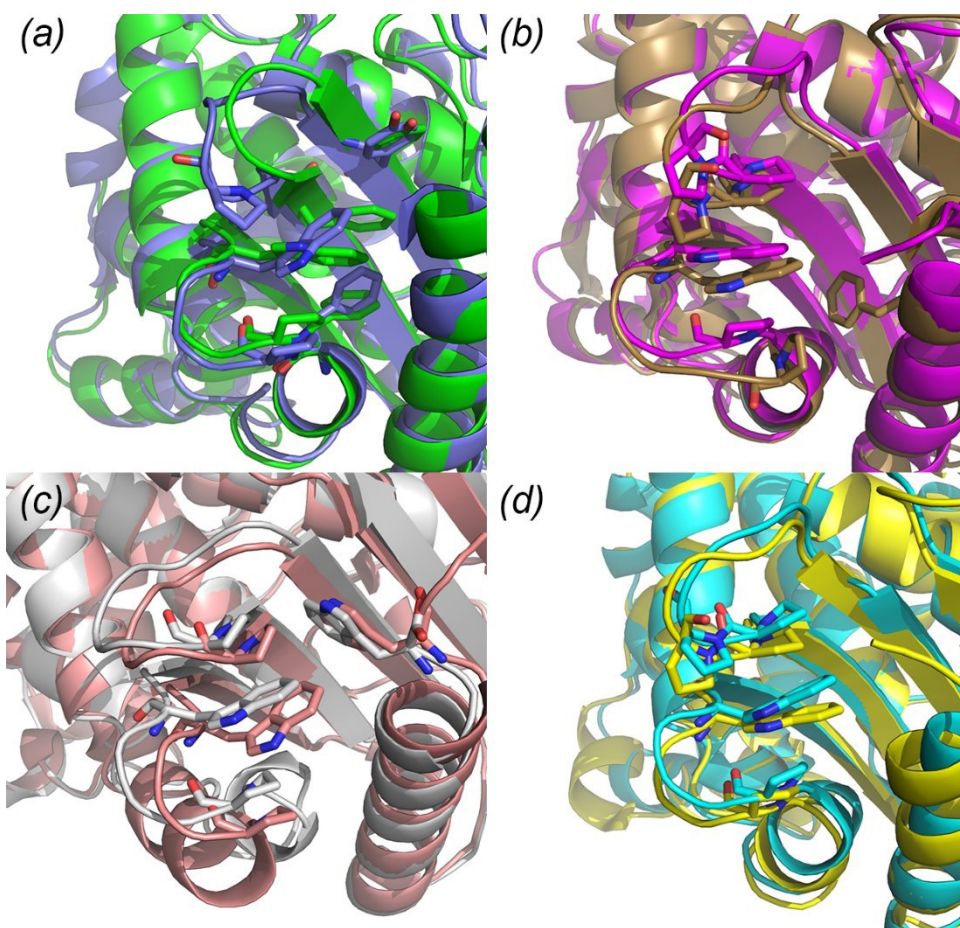


Figure 4.9. Structural overlay of some of the β -lactamase crystal structures, residues 229, 226, 254 and aromatic residues from hydrophobic pocket are represented with sticks. (A) Phe225-Pro226-Trp229-(Phe249)-(Pro254)-Tyr259 chain: BlaC - purple (2GDN¹⁰¹), GES1 from *Klebsiella pneumoniae* - green (2QPN¹⁷⁵); (B) Pro226-Trp229-Pro251-Pro252-(Phe287) chain: β -lactamase from *Burkholderia phymatum* - gold (5VPQ), β -lactamase from *Mycobacterium abscessus* - magenta (4YFM⁸⁴); (C) Pro226-Trp229-Pro252-Trp290 chain: TEM1 from *Escherichia coli* - white (1BTL¹⁹¹), SHV1 from *Klebsiella pneumoniae* - salmon (2ZD8¹⁹⁰); (D) Pro226-Trp229-Pro251-Pro252 chain: β -lactamase from *Streptomyces albus* - yellow (1BSG), BS3 from *Bacillus licheniformis* - cyan (112S²⁰⁶).

Materials and methods

Production of BlaC variants

Site-directed mutagenesis was performed using whole plasmid site-directed mutagenesis. Plasmid pUK21 carrying the *blaC* gene, encoding a signal peptide for transmembrane transport or the plasmid pET28a+ carrying the *blaC* gene with the code for a N-terminal or C-terminal His(6)-tag was used as template. Sequences of the primers were designed to introduce single amino acid substitutions (Table S2.3). Mutated plasmids were transformed into competent *E. coli* KA797 cells. Colonies were selected on LB agar plates containing 50 $\mu\text{g mL}^{-1}$ kanamycin. The presence of the mutations was confirmed by sequencing, performed by Baseclear BV.

For recombinant production of mutant proteins, *E. coli* strain BL21pLysS (DE3) was used in combination with the pET28 based plasmids. Cells were cultured in LB medium at 37 °C until the optical density at 600 nm reached 0.6, at which point protein production was induced with 1 mM isopropyl β -D-1-thiogalactopyranoside (IPTG), followed by incubation of the cultures at 18 °C for 16 hours. For the production of isotope labeled proteins for NMR experiments, M9 medium was used, instead of LB, with ¹⁵N ammonium chloride as the sole nitrogen source. Components of the M9 medium can be found in Table S2.4. Proteins carried a N-terminal (Trp229 mutants) or C-terminal (Glu37 mutants) His-tag. The C-terminal His-tag was chosen for Glu37 mutants to avoid possible influence of the tag on folding due to the close proximity of mutation site to the N-terminus. Wild type protein was produced in both tag variants and there was no observable difference between the yields. Cells were harvested by centrifugation and lysed with French Press in 20 mM Tris-HCl buffer, pH 7.5 with 500 mM NaCl. The first purification was conducted with 5 mL HisTrap Nickel column (GE Healthcare) in 20 mM Tris-HCl buffer, pH 7.5 with 500 mM NaCl, protein was eluted with the same buffer with 125 mM imidazole. N-terminal His-tags were removed by overnight incubation with 0.2 mg mL⁻¹ His-tagged Tobacco Etch Virus (TEV) protease at 4 °C in 25 mM Tris-HCl buffer, pH 8.0 with 100 mM NaCl, 1 mM EDTA and 5 mM DTT followed by an additional HisTrap Nickel column purification to separate BlaC without His-tag from uncleaved BlaC and TEV protease. SDS-PAGE analysis revealed single bands of similar sizes for all variant enzymes. Protein concentration was determined by absorption at 280 nm, using the theoretical extinction coefficient 29 910 M⁻¹cm⁻¹ 223.

Protein quantification in cultures

Overnight bacterial cultures induced with 1 mM IPTG were normalized to the same optical density at 600 nm and treated either with SDS PAGE sample buffer or with lysis buffer (25 mM Tris-HCl, 100 mM NaCl, pH 8.0 with 1 mM EDTA and 1 mg mL⁻¹ lysozyme) to separate soluble and insoluble fractions. Whole lysate, soluble and insoluble fraction samples were

analyzed using SDS PAGE. Gels were stained with Coomassie Brilliant Blue. The signal intensities were compared to each other and to samples with known protein concentrations using ImageLab software (BioRad).

***In vivo* activity studies**

The survival of the *Escherichia coli* cells carrying pUK-based plasmids with wild type or mutant BlaC genes was tested on LB-agar plates with various concentrations of antibiotics. The sequence for the mature protein was coupled to a signal sequence for the Tat-system, because under physiological conditions BlaC is produced in the cytoplasm and translocated through the cell membrane¹⁶⁵. All plates contained 50 µg mL⁻¹ kanamycin and 1 mM IPTG. Cells were applied on the plates as 10 µL drops with OD₆₀₀ values of 0.3, 0.03, 0.003 or 0.0003.

Circular dichroism

CD profiles were recorded using Jasco J-815 spectropolarimeter with a Peltier temperature controller (Jasco, MD). Measurements were performed in triplicate at 25 °C with 10-15 µM protein in 100 mM sodium phosphate buffer, pH 6.4. Spectra were acquired in 1 mm quartz cuvette at a scan rate of 50 nm/min and later normalized for concentration.

Thermal stability

Thermal stability of the proteins was analyzed by thermal shift assay (TSA) with SYPRO Orange dye (Invitrogen). The measurements were performed in triplicate in two independent experiments using the CFX 96 Touch Real-Time PCR Detection System from Bio Rad with 2x dye and 10 µM protein in 100 mM sodium phosphate buffer, pH 6.4 with the temperature range 20-80 °C. Melting temperatures were determined as an average of 6 measurements with standard deviation.

Kinetics

Determination of the Michaelis-Menten kinetic constants was done by measuring the absorption change at 486 nm for nitrocefin ($\Delta\epsilon = 11300 \text{ M}^{-1}\text{cm}^{-1}$) in a PerkinElmer Lambda 800 UV-Vis spectrometer at 25 °C in 100 mM sodium phosphate buffer, pH 6.4; all measurements were performed in triplicate. The $\Delta\epsilon$ was calculated by measuring a dilution series, which yielded a calibration line of absorption against concentration, with the concentration of the stock determined by quantitative NMR against 2.0 mM trimethylsilylpropanoic acid (TSP). The reactions were carried out at various concentrations of substrates and 2 nM or 5 nM concentration of BlaC, and initial rates of the hydrolysis were plotted against concentration of substrate and fitted separately for each experimental set to the Michaelis-Menten equation 4.1 using OriginPro 9.1, where v_0 is the initial reaction rate, $[S]_0$ the initial substrate concentration, V_{\max} the maximum reaction rate and K_m the Michaelis-Menten constant. v_0 and $[S]_0$ are the dependent and independent variables, respectively, and K_m and V_{\max} are the fitted parameters. $V_{\max} = k_{\text{cat}}[E]$, k_{cat} is the rate-limiting conversion rate, and $[E]$ is the concentration of BlaC.

$$v_0 = \frac{V_{\max}[S]_0}{[S]_0 + K_m} \quad (4.1)$$

Refolding experiments

For refolding experiments initial unfolding of BlaC proteins was done using thermal denaturation and chemical denaturation. Thermal denaturation was found to be irreversible in analyzed temperature range (data not shown). For chemical denaturation 45 µM of BlaC WT and mutants were incubated for 20 minutes on ice with 4.5 M guanidinium chloride in 100 mM phosphate buffer (pH 6.4). Refolding was then initiated by dilution of samples with the same buffer containing 2.25 M, 1.8 M, 1.125 M, 0.9 M or 0.45 M guanidinium chloride with 100 µM nitrocefin. Untreated BlaC in 100 mM phosphate buffer was used as a positive control. The hydrolysis of nitrocefin was measured at 486 nm on a TECAN Infinite® M1000PRO plate reader. In each measurement the final BlaC concentration was 0.9 µM. Experiments were carried out in triplicate.

NMR Spectroscopy experiments

TROSY-HSQC spectra were recorded on a Bruker AVIII HD 850 MHz spectrometer at 25 °C in 100 mM phosphate buffer (pH 6.4) with 6% D₂O. Data were processed in Topspin 3.2 (Bruker). Spectra were analyzed with CCPNmr Analysis software. Peaks of the mutant spectra were assigned by comparison to peaks in the wild type BlaC spectrum and average chemical shift perturbations (CSP), $\Delta\delta$, of the ¹H ($\Delta\omega_1$) and ¹⁵N ($\Delta\omega_2$) resonances of backbone amides were calculated using equation 4.2. Peaks that could not be assigned with certainty were assigned based on the smallest possible CSP (Figure S4.5).

$$\Delta\delta = \sqrt{\frac{1}{2} \left(\Delta\omega_1^2 + \left(\frac{\Delta\omega_2}{5} \right)^2 \right)} \quad (4.2)$$

Crystallization

Crystallization conditions for BlaC at a concentration of 10-15 mg mL⁻¹ were screened for by the sitting-drop method using the JCSG+, PACT premier (Molecular Dimensions) and Index HT (Hampton Research) screens at 20 °C with 200 nL drops with 1:1 protein to screening condition ratio²²⁴. Crystals for BlaC E37A grew within four days in 0.1 M sodium acetate buffer pH 5, 0.2 M magnesium chloride and 20% w/v PEG 6K as precipitant). The crystals were mounted on cryoloops in mother liquor and 30% glycerol as cryo-protectant and vitrified by plunging in liquid nitrogen.

X-ray data collection, processing and structure solving

Diffraction data to 1.5 Å resolution of BlaC E37A crystals were collected at the European Synchrotron Radiation Facility on the MASSIF beamline²²⁵. The data were integrated using XDS²²⁶ and scaled using Aimless²²⁷ and data to 1.5 Å resolution were kept for structure solution and refinement. Overall completeness of this dataset is somewhat low (91.5%) due to the presence of ice rings. The structures were solved by molecular replacement using MOLREP²²⁸ from the CCP4 suite²²⁸ using PDB entry 2GDN¹⁰¹ as a search model. Subsequently, building and refinement were performed using Coot and REFMAC²²⁸. Waters were added in REFMAC during refinement; we have modeled double conformation for residues N110, R128, D240 and V263. The final model falls on the 100th percentile of MolProbity²²⁹ and showed that 98.85% of all residues were within the Ramachandran plot favoured regions with two outliers. The model was further optimized using the PDB-REDO webserver^{230,231}. Data collection and refinement statistics can be found in Table 4.3. The data have been deposited in the Protein Data Bank, entry 7A5U.

Supporting Information

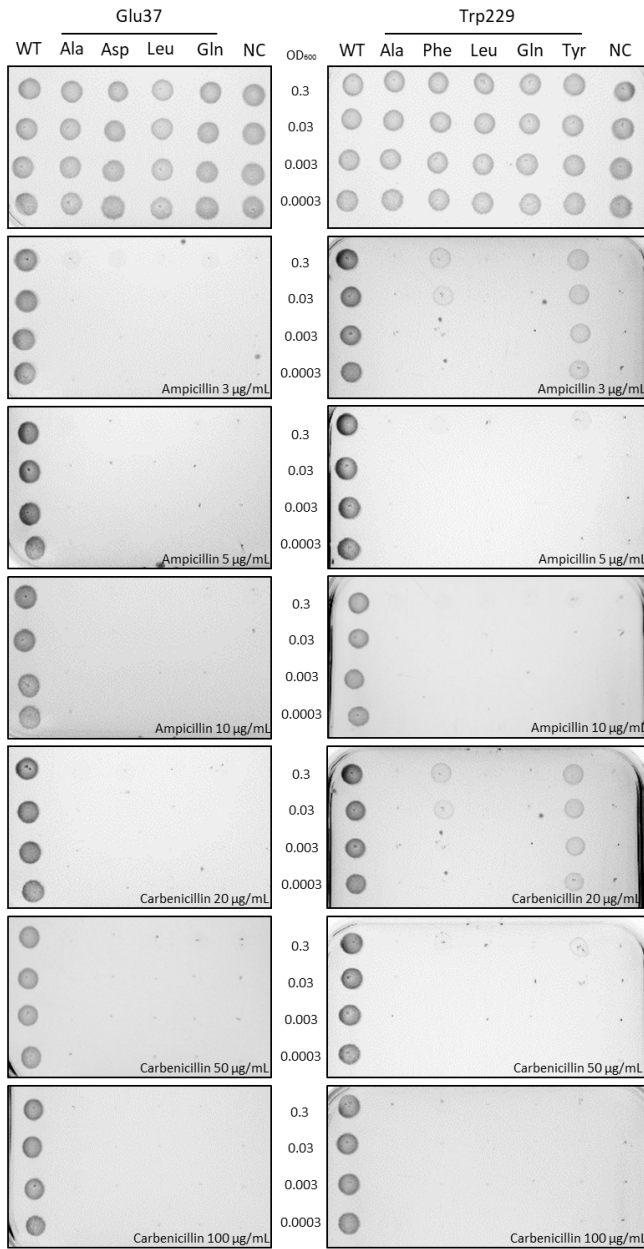


Figure S4.1. Plates showing growth of *E. coli* cells expressing wild type (WT) or mutant proteins (negative control, NC is the S70A mutant) with no antibiotics or various concentrations of antibiotics. Cultures were applied as the drops with OD shown in between the plates.

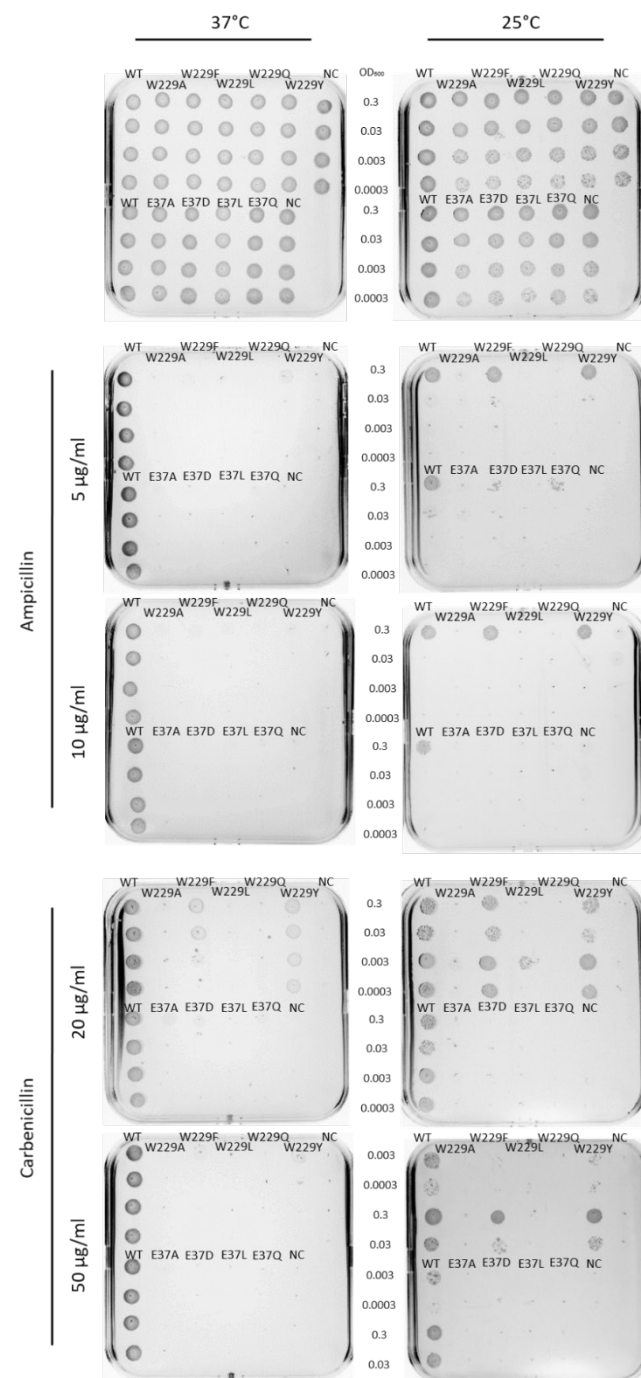


Figure S4.2. Plates with ampicillin or carbenicillin incubated at 37°C or 25°C. Cultures producing wild type (WT) or mutant BlaC (negative control, NC is the S70A mutant) were applied as the drops with OD shown in between the plates. For W229F and W229Y BlaC growth is better at 25 °C.

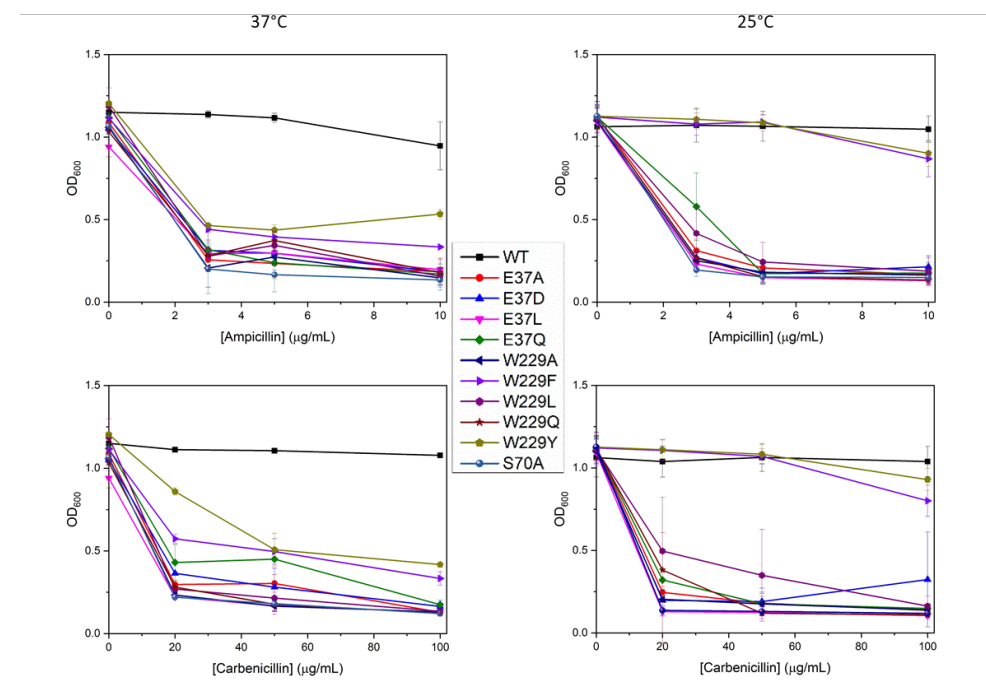


Figure S4.3. The end point (15 hours at 37 °C or 25 hours at 25 °C) of OD₆₀₀ of wild type and mutant cultures growth with various concentrations of antibiotics. For W229F and W229Y BlaC growth is better at 25°C. Error bars represent the standard deviation of three measurements.

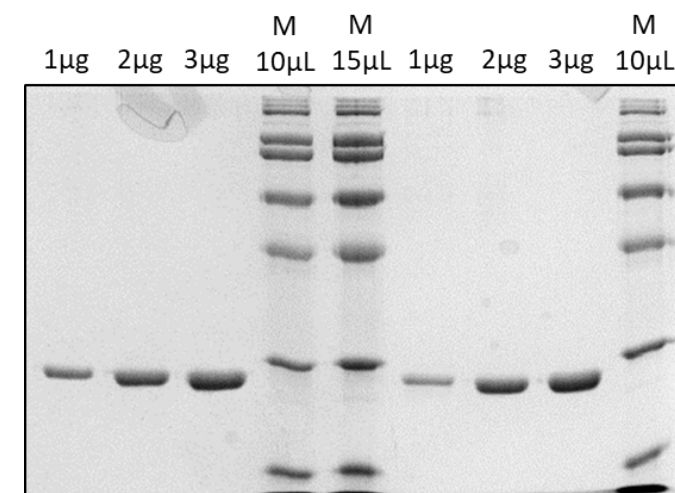


Figure S4.4. SDS PA-gel for determination of protein amounts in Marker (BioRad). Purified BlaC with known concentration was used in quantities shown on the figure. Analysis of the band intensities was performed with ImageLab software (BioRad).

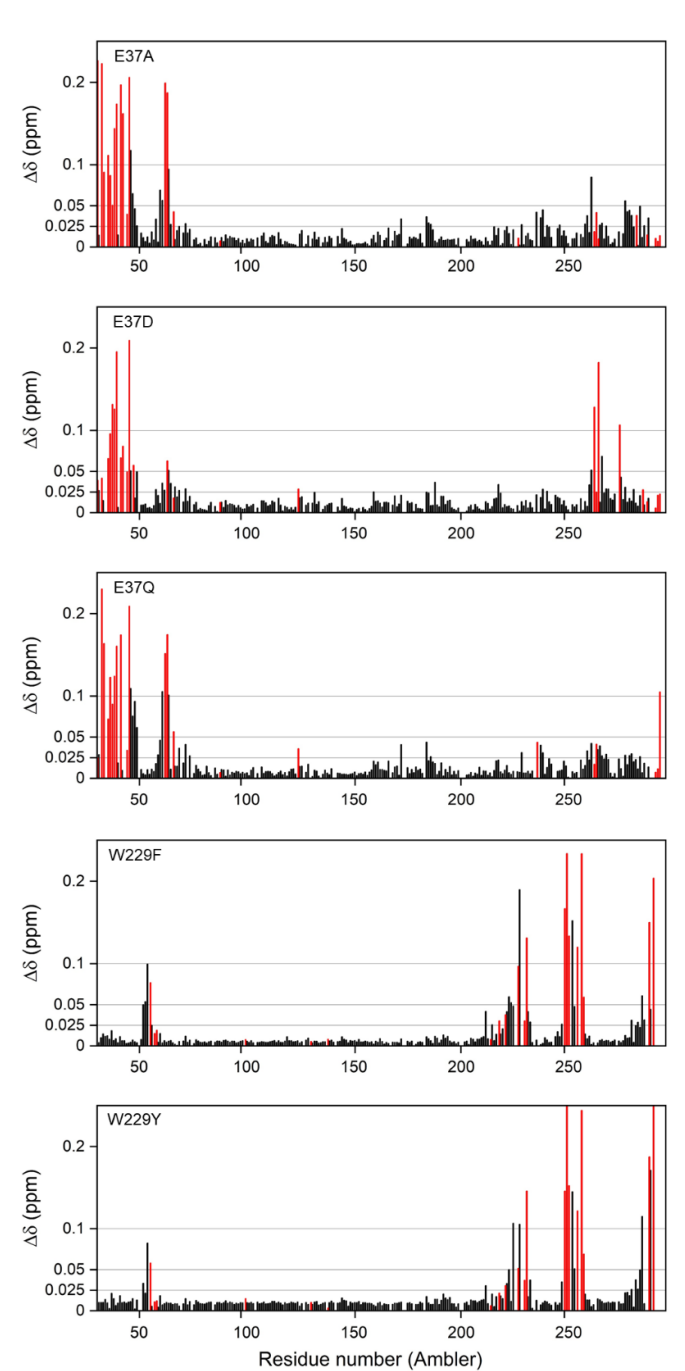


Figure S4.5. Average CSP for the backbone amides of the BlaC mutants. Residue numbers refer to Ambler numbering⁸⁹. Black bars represent CSP for residues assigned with certainty. Red bars show CSP calculated as the minimal possible CSP.

Chapter 5

**Mutations in two highly conserved
residues are beneficial for BlaC**

Abstract

Conserved residues are often considered essential, thus substitutions in such residues are expected to have negative influence on properties of a protein. However, mutations in a few highly conserved residues of BlaC were shown to have only a limited negative effect on the enzyme. Two mutants, D179N and N245H, displayed increased antibiotic resistance *in vivo* and were investigated further. For BlaC D179N higher survivability can be attributed to a more stable enzyme. The crystal structure reveals subtle structural changes in the Ω -loop as compared to the structure of wild type BlaC. The mutation N245H leads to an increased catalytic activity. Several substitutions of Asn245 give rise to elevated resistance to the β -lactamase inhibitor avibactam, which can be the consequence of the altered binding site. Possible reasons for why these residues are conserved yet not optimal are discussed.

Introduction

Each family of proteins contains a set of highly conserved amino acid residues that are essential for the general function that these proteins exhibit as a group. If a residue is conserved, it is often used as a proxy for its essentiality and therefore, mutations in such a residue are expected to have a negative effect on the function. If the protein has multiple functions, for example, an enzyme that converts several substrates, improvement of one trait is likely correlated with decline of another. However, as discussed in chapter 2, some conserved residues display virtually no change upon mutation and sometimes mutations even benefit the enzyme. Two such residues of BlaC, Asp179 and Asn245 (Ambler numbering⁸⁹), are discussed here. The mutations N245H and D179N exhibited the most interesting results, yielding mostly positive effects and limited negative downsides.

Asp179 is a highly conserved residue (99.8%, Chapter 2), located in the Ω -loop. In BlaC its side chain makes hydrogen bonds to the side chain of the Asp172 and to the backbone Ala164. Recent literature has described substitutions of Asp179 in other β -lactamases. In the β -lactamases TEM, KPC-2 and SHV^{232,233,127} a salt bridge interaction is present between Asp179 and Arg164 (Figure 5.1a)²⁸. Disruption of this salt bridge was related to increased activity against ceftazidime (Figure 1.3). In BlaC, this salt bridge is absent because the residue at position 164 is an alanine. PER β -lactamases have an asparagine at position 179, but comparison is complicated because the amino acid sequence in general and the conformation of the Ω -loop in particular in PER enzymes differ considerably from other class A β -lactamases (Figure 5.1b). Two other conserved amino acid residues discussed within this chapter are Asp163 and Leu169 (Figure 5.1a).

Asn245 is located in the β -sheet. This residue is 93% conserved in class A β -lactamases (Chapter 2). The side chain of this residue makes two interactions, with the backbone atoms of Ala67 and Phe68 (Figure 5.2). Due to close proximity of the latter residues to Ser70, these interactions are likely to be important for its positioning or orientation, suggesting that Asn245 has a role in fine-tuning the active site structure.

To understand the reason for conservation further, mutants of Asp179 and Asn245 were analysed for their thermal stability and activity against various substrates *in vivo*. The initial focus on D179N and N245H yields more understanding of the good performance of these mutants, as they exhibited increased stability and increased activity, respectively. Additionally, the BlaC variants D179G and N245S were analysed in detail, as they displayed increased ceftazidime and avibactam resistance, respectively.

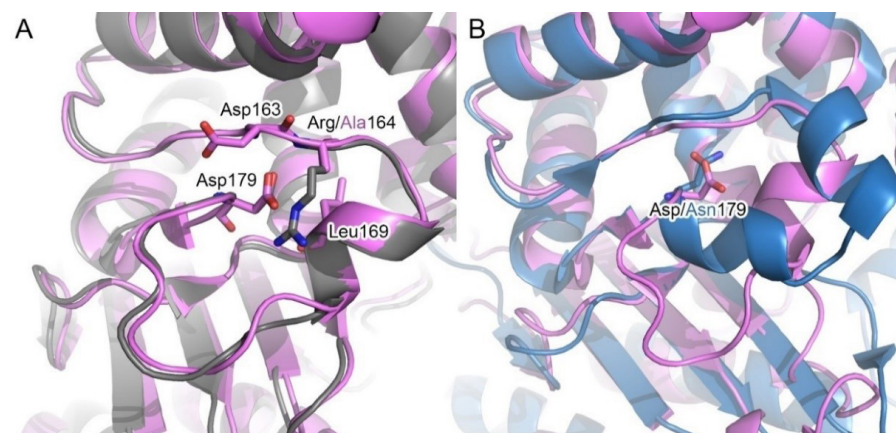


Figure 5.1. Overlay of the structures of BlaC (2GDN¹⁰¹, in pink) and TEM-1 (1YT4²³⁴, in gray) (A), and PER-2 (4D2O¹⁷¹, in blue) (B), showing the region around residue 179.

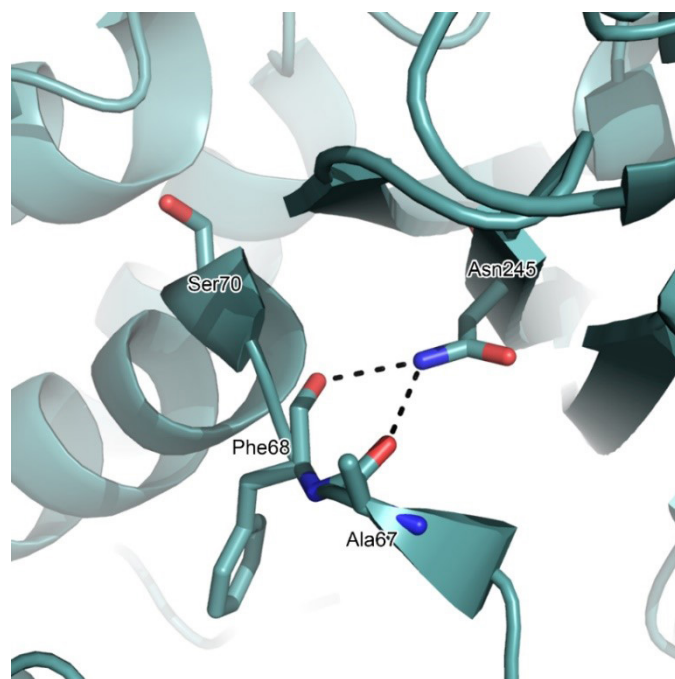


Figure 5.2. Interactions of Asn245 in BlaC (2GDN¹⁰¹). Residues Asn245, Ala67, Phe68 and the active site Ser70 are shown in sticks. The dashed lines indicate potential H-bonds.

Results

Activity increase for D179N and N245H is observed *in vivo* for different classes of β -lactam antibiotics

Mutants D179N and N245H were found to perform better than wild type BlaC *in vivo* against ampicillin and carbenicillin (chapter 2). Often increased activity against one substrate leads to decreased activity against another, therefore *E. coli* cultures producing Asp179 and Asn245 mutants were tested for resistance against other compounds. To determine the minimum inhibitory concentrations (MIC), drops of cell culture diluted 10 - 10,000-fold were applied on agar plates, containing the penicillins ampicillin, carbenicillin or penicillin G, the third-generation cephalosporin ceftazidime or the carbapenem meropenem (Figure 1.3). For evaluation of β -lactamase inhibitor susceptibility, 100 $\mu\text{g mL}^{-1}$ carbenicillin was used in combination with β -lactam β -lactamase inhibitor sulbactam and non- β -lactam β -lactamase inhibitor avibactam.

The results indicated that almost all tested Asp179 mutants outperformed wild type against ceftazidime. D179G mutant was shown to be the most effective, with more than 6-fold increase in MIC (Figure 5.3a). However, only cells producing BlaC D179N displayed increased survival in presence of other β -lactam antibiotics (Table 5.1). Meropenem is a very poor substrate for BlaC, with the wild type enzyme not outperforming a negative control (BlaC S70A) in our screens, thus even the subtle increase in meropenem degradation for D179N mutant (Figure 5.3b). The moderately higher survivability of BlaC D179N with meropenem was shown in liquid culture as well. Previously it was detected that the increase of antibiotic in liquid cultures causes longer horizontal phase (e.g. Figure S5.1), which can be attributed to a degradation of antibiotic by an active enzyme. BlaC D179N variant exhibits shorter horizontal phase than wild type BlaC in presence of meropenem (Figure 5.3b). BlaC D179N also showed somewhat higher resistance to sulbactam and avibactam, which probably can be attributed to an increased conversion of carbenicillin that was used in combination with inhibitors (Figure 5.3c). The increased ceftazidime resistance observed for almost all mutants is remarkable. TEM and KPC β -lactamases^{129,130,138} mutants of Asp179 showed the same effect, however, that was attributed to the mutant's inability to form the salt bridge with Arg164. In BlaC this salt bridge is absent due to a R164A substitution, yet we also observe an increase in ceftazidime hydrolysis activity upon mutation of Asp179. In relation to this finding, mutants of two other conserved residues from Ω -loop were analysed for their activity against ampicillin and ceftazidime (Table 5.1) to check if the effect of increased ceftazidime activity is specific to substitutions in Asp179. Mutants of Asp163 (75% conservation) exhibited lost ampicillin activity together with maintained ceftazidime activity at wild type level and most mutants of Leu169 (95% conservation) displayed a loss in ampicillin activity coupled with increased ceftazidime activity (Figure S5.2). These results indicated that the effect of increased ceftazidime activity can be attributed to many modifications in Ω -loop.

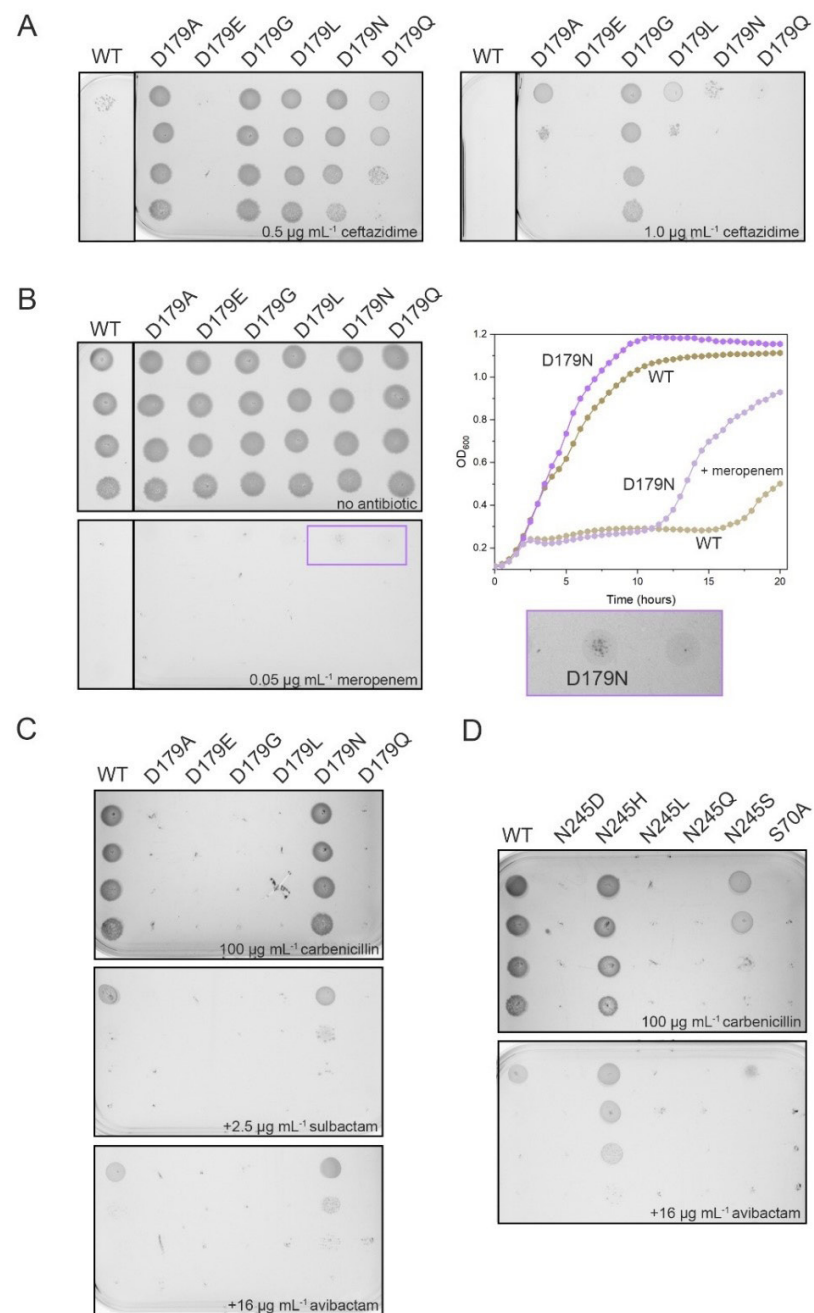


Figure 5.3. (A) Plates and growth curves of BlaC Asp179 variants growing with meropenem. BlaC D179N still exhibits growth on plate with 0.05 $\mu\text{g mL}^{-1}$ meropenem. On the right growth curves of wild type BlaC and BlaC D179N are presented without meropenem and with 0.1 $\mu\text{g mL}^{-1}$ meropenem; (B) Almost all Asp179 variants have higher survivability with ceftazidime than wild type BlaC; (A)-(B) Wild type BlaC panels are from the same LB-agar plates as BlaC variants; (C)-(D) Plates showing growth of Asp179 (C) and Asn245 (D) variants with inhibitors.

Mutations in Asn245 lead to poor ampicillin and ceftazidime degradation for all mutants except for BlaC N245H. Carbenicillin and penicillin G activity suffered to a various degree in Asn245 mutants, however, for BlaC N245H a slightly increased MIC was observed for these substrates as well (Table 5.1). The avibactam and sulbactam inhibition of BlaC N245H was comparable to wild type. For BlaC N245S, sulbactam inhibited growth at 2.5 $\mu\text{g mL}^{-1}$ which is two times lower than for wild type, but N245S also exhibited 2-fold lower MIC against carbenicillin (Table 5.1). With avibactam, however, BlaC N245S was only marginally less sensitive than wild type despite reduced carbenicillin activity (Figure 5.3d). That observation points to a possibly increased avibactam resistance of N245S mutant.

Table 5.1. MIC values of various β -lactams and β -lactamase inhibitors for wild type and mutant BlaC accessed with the droplet test. All MIC values are in $\mu\text{g mL}^{-1}$. Catalytically inactive BlaC S70A is used as a negative control.

BlaC variant	Ampicillin	Ceftazidime	Meropenem	Carbenicillin	Penicillin G	Avibactam ^a	Sulbactam ^a
WT	80	0.8	0.05	1000	120	>16	5
S70A	20	0.2	0.05 ^b	100 ^b	40	0	0
D179A	20	2	0.05	500	80	0	0
D179E	20	0.2	0.05	500	40	0	0
D179G	20	5	0.05	500	40	0	0
D179L	20	2	0.05	100	40	0	0
D179N	120	2	0.1	>1500	>120	>16	7.5
D179Q	20	1	0.05	100	40	0	0
N245D	20	0.2	0.05	100	40	0	0
N245H	80	2	0.05	1500	>120	>16	5
N245L	20	0.2	0.05	100	40	0	0
N245Q	20	0.2	0.05	100	40	0	0
N245S	20	0.2	0.05	500	120	>16	2.5
D163A	20	0.8					
D163E	40	0.8					
D163N	20	0.8					
D163Q	20	0.8					
L199A	20	1					
L169E	20	1					
L169F	20	1					
L169M	40	1					
L169V	80	0.8					

^a Inhibitors were used together with 100 $\mu\text{g mL}^{-1}$ carbenicillin; ^b The minimum concentration tested

Asn245 contributes more to proper folding but less to thermostability than Asp179

The genes of BlaC variants of Asp179 and Asn245 were overexpressed, and the proteins purified. The yield of soluble BlaC D179E, N245D, N245L and N245Q was up to 20 mg of protein from one litre of cell culture. For these mutants, most protein was found in the pellet. Other mutants as well as the wild type BlaC yielded between 40 and 60 mg of soluble protein per litre. BlaC D179N production on the other hand resulted in an increased production of soluble protein with a yield of 150 mg per litre of cell culture. Most but not all mutants exhibited the correct proper fold, as judged by CD spectroscopy (Figure 5.4). Mutants with a low yield also gave aberrant CD spectra.

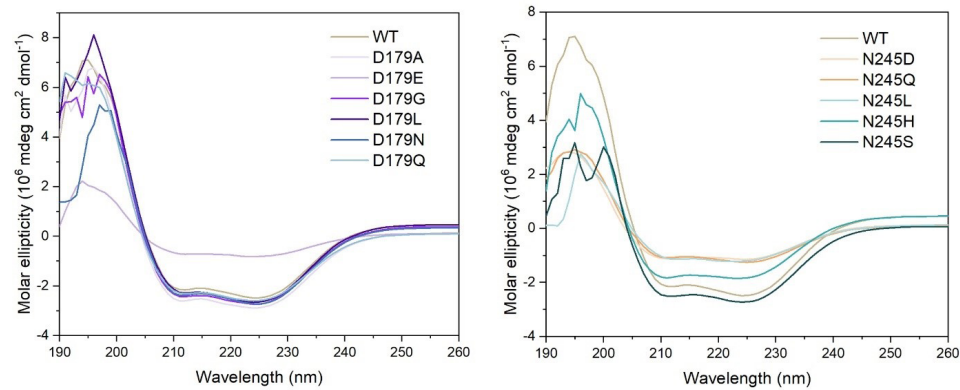


Figure 5.4. CD spectra of BlaC Asp179 and Asn245 mutants.

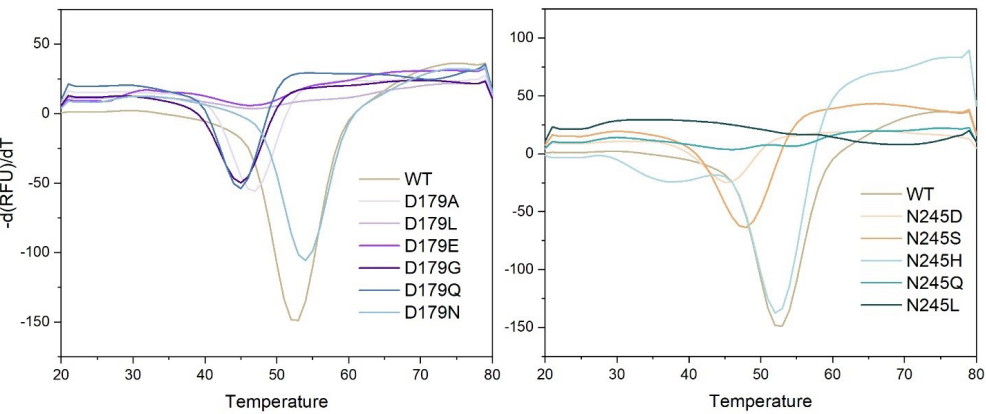


Figure 5.5. Negative derivative of signal from thermal shift assay with the hydrophobic dye SYPRO orange of BlaC Asp179 and Asn245 mutants.

To establish the thermal stability of the BlaC variants, denaturation experiments were performed. Both tryptophan fluorescence and thermal shift assay with hydrophobic dye were used for melting temperature assessment, as these methods might yield structure specific results. The melting temperature of BlaC N245H is close to that of wild type BlaC (Table 5.2, Figure 5.5), whereas for BlaC N245S the melting temperature is 4-5 degrees lower and poorly folded BlaC N245D, N245L and N245Q showed a very gradual unfolding profile upon thermal denaturation, thus melting temperature could not be determined with certainty.

Mutation of Asp179 influenced thermostability more (Table 5.2, Figure 5.5). Substitution with asparagine resulted in 1.5 °C increase in melting temperature, whereas substitutions to glycine, glutamine and alanine significantly lowered melting temperature. Due to sample quality, the melting temperature analysis of D179E and D179L was not possible.

Table 5.2. Differences in melting temperature for BlaC variants compared to wild type BlaC. SD standard deviation of three measurements.

BlaC variant	ΔT_m (tryptophan fluorescence) \pm SD	ΔT_m (hydrophobic dye) ^a
D179A	-6.3 \pm 0.1	-5
D179G	-10.9 \pm 0.4	-7
D179N	1.40 \pm 0.05	1.5
D179Q	-15.2 \pm 1.1	-7
N245D	-6.6 \pm 0.1	-7
N245H	-1.2 \pm 0.1	0
N245S	-4.50 \pm 0.05	-4

^a Error 0.7 °C

Increased in vivo activity of BlaC D179N and N245H has different origins

The kinetic parameters of nitrocefin hydrolysis of BlaC D179N and N245H (Table 5.3, Figure 5.6a) were measured using purified enzymes. BlaC N245H displayed somewhat increased activity. D179N mutant on the other hand, exhibited nitrocefin activity very close to that of wild type BlaC, therefore we attribute the slight increase in activity against most antibiotics *in vivo* of this variant to an elevated production of more stable protein.

Table 5.3. Michaelis-Menten kinetic parameters for nitrocefin hydrolysis. Reactions were carried out in 100 mM sodium phosphate buffer (pH 6.4) at 25 °C. Standard deviations (SD) are calculated from triplicate measurements.

BlaC variant	$K_M \pm \text{SD}$ (μM)	$k_{\text{cat}} \pm \text{SD}$ (s^{-1})	$k_{\text{cat}}/K_M \pm \text{SD}$ ($10^5 \text{ M}^{-1}\text{s}^{-1}$)
WT	263 ± 17	106 ± 5	4.0 ± 0.3
D179N	297 ± 24	98 ± 6	3.3 ± 0.3
N245H	245 ± 8	144 ± 4	5.9 ± 0.2

Asn245 mutants are more avibactam resistant than wild type BlaC

An inhibition assay of nitrocefin hydrolysis using avibactam was performed with wild type enzyme, and BlaC D179N, N245H and N245S. These variants displayed resistance to avibactam *in vivo* at wild type levels or slightly higher. The results indicated that while D179N mutant is inhibited by avibactam similarly to wild type enzyme, both Asn245 mutants are less sensitive to inhibition as they were able to convert relatively more nitrocefin in presence of avibactam (Figure 5.6b). This is clearly visible at 500 μM avibactam at which the mutants N245H and N245S still retain 51% and 47% of initial hydrolysing ability respectively, while for wild type enzyme only 32% of activity is detected. Observation of the nitrocefin hydrolysis over time reveals that the wild type is fully inhibited within 15 min, but N245H and N245S still generate product after 20 min, indicating that full inhibition is not achieved (Figure 5.6c).

Asp179 mutants exhibit changed substrate profile

To address the large increase in ceftazidime MIC coupled with decreased MIC of other compounds for D179G mutant, this variant, together with wild type BlaC and BlaC D179N, were evaluated for their ability to degrade nitrocefin and ceftazidime *in vitro*. The data indicated that BlaC D179G does not display any nitrocefin activity (Figure 5.7a). Ceftazidime degradation with BlaC variants displays two phases (Figure 5.7b). Two-phase ceftazidime hydrolysis was explained before for KPC-2 β -lactamase with the burst phase, caused by rapid acylation and the following linear phase caused by slow deacylation²³⁵. This explanation does not apply to BlaC, as the amplitude of the burst phase indicates that the enzymes perform more than a single turnover and is substrate concentration dependent. Here, we used the second phase to calculate the “initial” velocities of the reaction (Figure 5.7c). Ceftazidime activity benefits from both the Asp \rightarrow Asn and Asp \rightarrow Gly substitution. The catalytic efficiency in the second phase of the reaction for wild type BlaC and BlaC D179N was found to be $46 \pm 3 \text{ M}^{-1} \text{ s}^{-1}$ and $160 \pm 6 \text{ M}^{-1} \text{ s}^{-1}$ respectively. For BlaC D179G the value could not be calculated with certainty due to the unusual behaviour of this variant with the substrate. It is probable that BlaC D179G exists in two forms with one form responding to a substrate presence slower than the other.

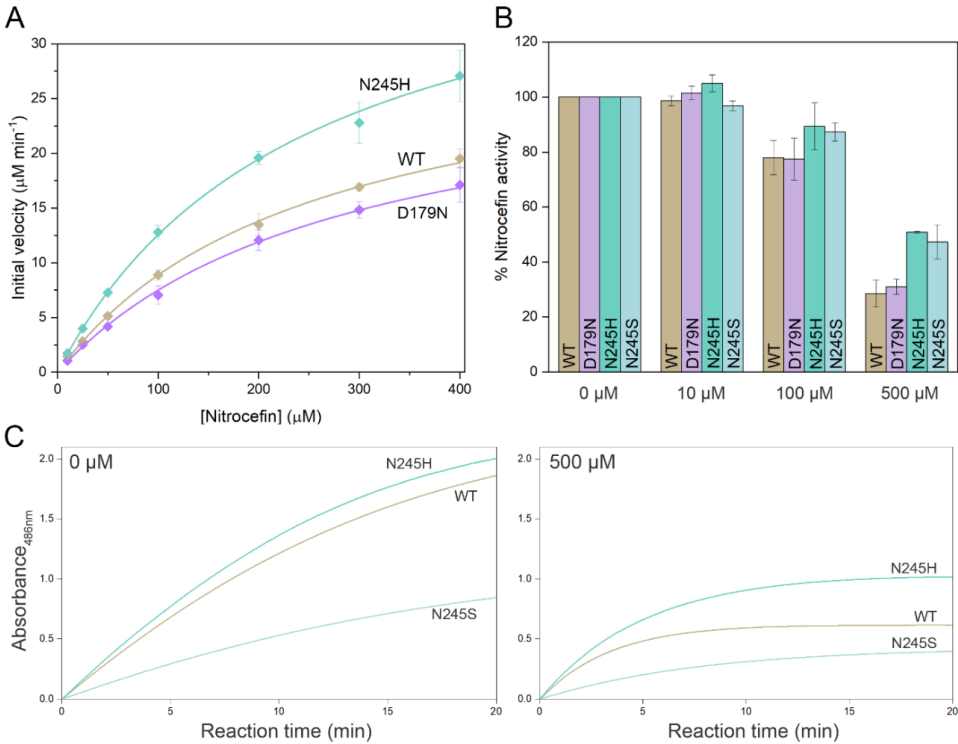


Figure 5.6. (A) Michaelis-Menten curves for reaction with nitrocefin of wild type BlaC, D179N and N245H. Error bars represent standard deviations of triplicates and curves represent the fit to the Michaelis-Menten equation; (B) Relative activity in the absence or presence of avibactam and BlaC measured as amount of hydrolyzed nitrocefin after 20 min at 25 °C. Measurements were performed in duplicate in the presence of 100 μM nitrocefin and 2.5 nM BlaC. The error bars represent one standard deviation; (C) Absorbance of the reaction product measured at 486 nm for 20 minutes without avibactam (left) and in presence of 500 μM avibactam (right).

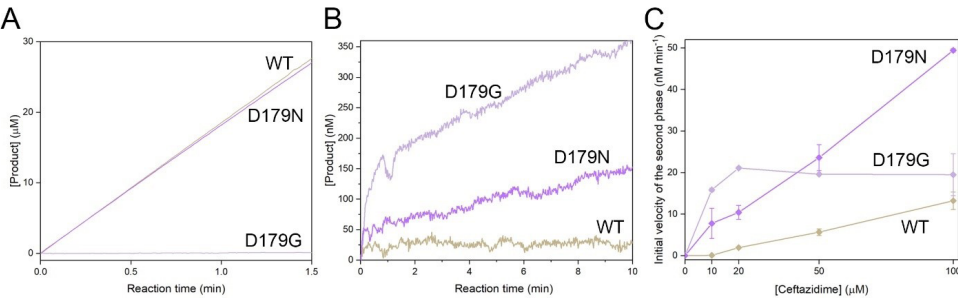


Figure 5.7. (A) Product generation over time in reaction with 400 μM nitrocefin with 5 nM wild type BlaC, BlaC D179N and BlaC D179G; (B) Product generation over time in reaction with 20 μM ceftazidime with 50 nM wild type BlaC, BlaC D179N and BlaC D179G, the burst phase can be observed in the first moments of the reaction followed by the second linear phase; (C) The initial velocity as a function of initial ceftazidime concentration of the second phase kinetics for wild type BlaC and two BlaC Asp179 variants. Error bars represent the standard deviations of duplicate experiments. Data were acquired in 100 mM sodium phosphate buffer (pH 6.4) at 25 °C.

Structural changes

^{15}N - ^1H TROSY-HSQC NMR spectra of BlaC D179N and N245H both indicate the presence of a well-folded enzyme (Figure S5.3). The CSPs of backbone amide resonances for mutant minus wild type are plotted on the crystal structure of wild type BlaC in Figure 5.8a-b. Mutation of Asn245 causes extensive CSPs, covering nearly the whole protein. For BlaC D179N, although changes are also quite spread and involve the active site, the major CSPs are observed for amides in the Ω -loop.

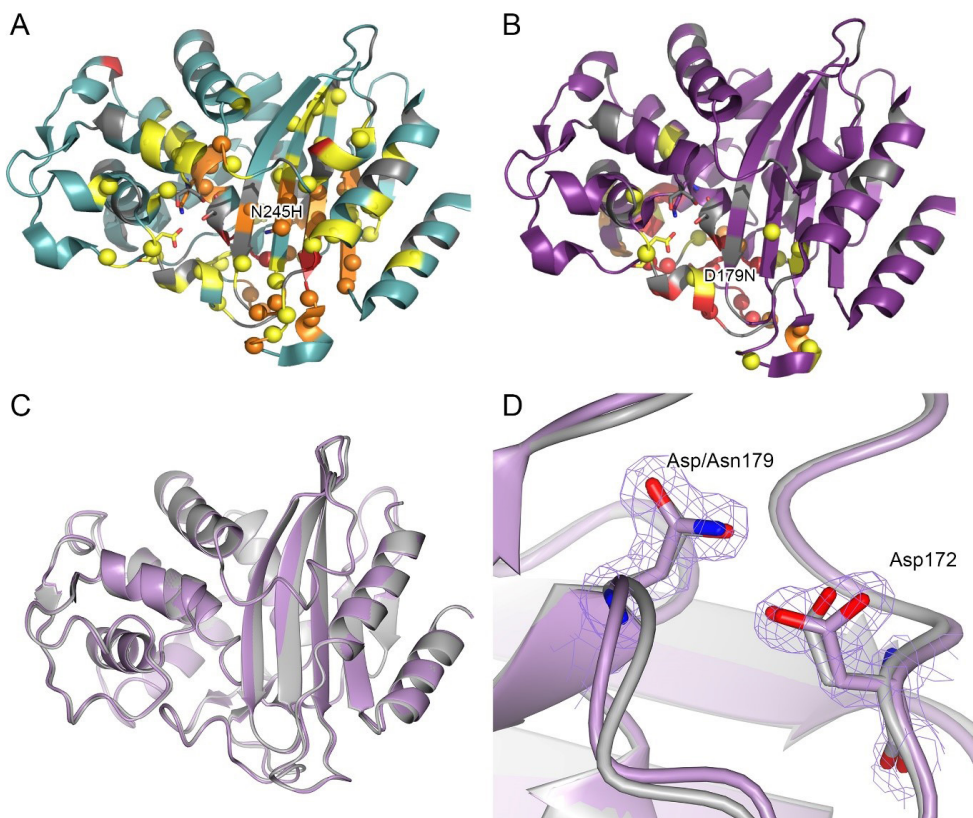


Figure 5.8. (A, B) Average chemical shift differences (CSP) between the resonances of BlaC N245H (A) or BlaC D179N (B) and wild type BlaC mapped on structure (2GDN¹⁰¹). Residues are colored yellow for CSP > 0.03 ppm; orange for CSP > 0.05 ppm and red for CSP > 0.1 ppm and gray for no data. The active site residues are shown in sticks; (C-D) Crystal structure of BlaC D179N (lilac) overlaid with wild type structure (2GDN, gray). The 2mF₀-DFc electron density map is centered on labeled residues and is shown in purple chicken wire, with contour level 1 σ and extent radius 5 Å.

The crystal structure of the BlaC D179N variant solved at 1.7 Å resolution reveals the nature of the structural changes (Table 5.4, Figure 5.8c-f). Overall, the structure of the mutant resembles the BlaC wild type structure (C α RMSD 0.31 Å, Figure 5.8c). The newly introduced asparagine occupies the same location as the side chain of aspartate (Figure 5.8d) and the interactions that D179 is involved in are conserved in D179N mutant. In the wild type structure the carboxy-carboxylate interaction requires a shared proton between Asp172 and Asp179^{181,182}, in BlaC D179N this interaction is an ordinary hydrogen bond between γ -carboxy group of Asp172 and amide group of Asn179. Thus, at near-neutral pH, replacement of one of the carboxy group with a carboxamide is expected to yield a more stable structure. Noticeable changes concern the Ω -loop of the mutant. Two peptide bonds are flipped in BlaC D179N involving Pro174-Gly175 (Figure 5.9a) and Arg178-Asn179 (Figure 5.9b). The flipped bond involving Arg178 is accompanied by the lost interaction between the side chains of Arg178 and Asp172 and Asp163 and Arg161. Asp163 turns into the solvent and the location previously occupied by its side chain carbonyl is now occupied by the backbone carbonyl of Arg178.

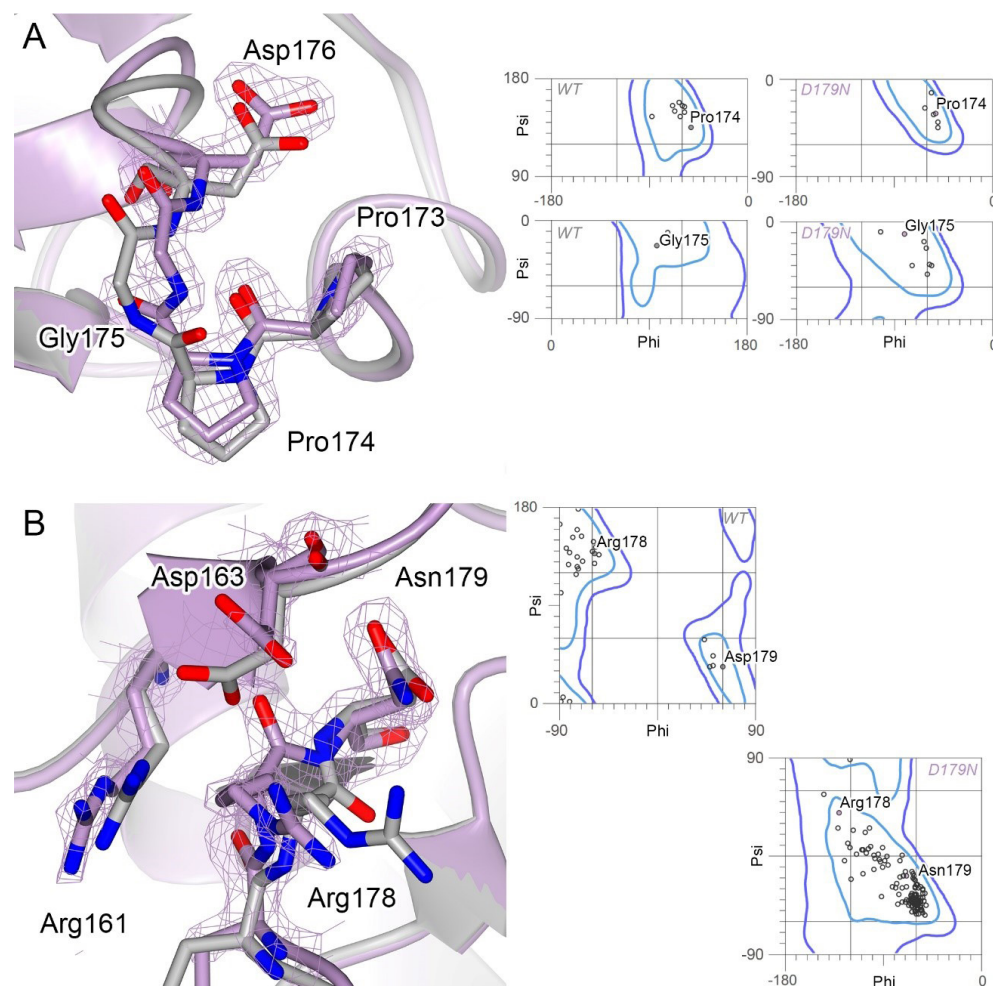


Figure 5.9. Crystal structure of BlaC D179N (lilac) overlaid with wild type structure (2GDN, gray). The 2mF0-DFc electron density map is centered on labeled residues and is shown in purple chicken wire, with contour level 1 σ and extent radius 5 Å. Panels on the right show Ramachandran plots for wild type BlaC and BlaC D179N for the phi-psi of the regions from the left panels.

Discussion

Two residues of BlaC, Asp179 and Asn245, had been identified that are very conserved, yet could be mutated without obvious detrimental effects (chapter 2). For the latter, the initial focus was on mutant N245H because this mutant showed similar or improved resistance traits compared to wild type BlaC. *In vivo* experiments also showed that N245S has increased resistance against avibactam. Also *in vitro* BlaC N245H proved to be more active than wild type and both BlaC N245H and N245S outperformed wild type in an inhibition assay. Asp245 is situated in a β -sheet, in the core of the enzyme, where it makes hydrogen bonds with backbone carbonyl oxygens of Ala67 and Phe68. A mutation from asparagine to histidine fits reasonably well in the structure of wild type BlaC if it displaces the nearby water molecule (HOH303 in 2GDN). To relieve the remaining steric clashes, slight movement of the β -strands are expected, explaining the extensive CSPs observed around the mutation site. The effects extend into the active site, which could be the cause of the changed activities. The change from Asn to His requires only a single mutation from adenine to cytosine, so it is not obvious why residue 245 is an Asn and not a His in BlaC. It is possible that the Asn is an evolutionary rudiment or the change to His is functionally near neutral.

Asp179 is one of the highly conserved residues of Ω -loop. Within this loop lies the catalytic Glu166 residue, so proper Ω -loop formation is essential for catalysis, although it was shown in Ubbink group and by Nitnai *et al.* that even in deacylation-deficient variants with Glu166 substituted to alanine slow hydrolysis of some cephalosporins can still take place²³⁶. The most common side chain interactions observed in the Ω -loop of class A β -lactamases are Arg161-Asp163, Glu166-Asn170, and Arg164-Asp179. BlaC does not carry arginine at position 164, thus this salt bridge is missing. The importance of the salt bridge was discussed in multiple studies on various class A β -lactamases. It was shown that mutations in either Arg164 or Asp179 increase resistance against ceftazidime, while decreasing the resistance to other β -lactam antibiotics^{130,137,232,235,237,238}. The same effect is observed in our study on BlaC, because almost all mutants of Asp179 showed increased *in vivo* resistance against ceftazidime, with D179G showing the largest increase of 6-fold compared to wild type BlaC, and decreased resistance to other compounds. It can be concluded that, at least in BlaC, the loss of the salt bridge is not the reason for changed substrate profile upon mutation of Asp179 because the salt bridge is not there in the first place. The same effect of increased ceftazidime resistance was also observed for mutants of Asp163 and Leu169 (this study) and a higher ceftazidime MIC was reported for mutant P167S of CTX-M²³⁹. Another interesting observation is that BlaC D179N exhibits increased MIC values against most tested antibiotics, outperforming wild type BlaC and all other tested mutants, different from what was reported for this mutation in TEM β -lactamase, where increase in ceftazidime MIC comes at a cost of other β -lactam antibiotics activity¹²⁹. However, in KPC-2, the mutation D179N was reported to

improve antibiotic profile, similar to BlaC²⁴⁰. This study used modelling to predict the changes in the Ω -loop occurring upon mutation, indicating loss of the Arg164-Asn179 interaction and increased flexibility of Ω -loop. Moreover, molecular modelling revealed changes in the position of catalytic Ser70 and Glu166. An increased flexibility of the Ω -loop is supported by a crystal structure of D179N mutant of PC1 β -lactamase from *Staphylococcus aureus*, where the Ω -loop was found to be disordered²⁴¹. In the crystal structure of BlaC D179N, the loop is highly ordered, however, and only relatively subtle changes are observed. The active site residues do not show any displacement. Two flipped peptide bonds are observed in the Ω -loop of BlaC D179N due to altered interactions between Asp172 and Asn179 and Asp163 and Arg161. The observed changes in the Ω -loop seemingly do not influence the active site or the size of the entrance to the binding site. The NMR data also show few CSPs in the active site, though effects are transmitted to the backside of the protein, probably via Ω -loop residues. It was shown for CTX-M β -lactamase that the mutation P167S causes conformational flexibility in Ω -loop and a large rearrangement of the loop in acyl-enzyme complex²³⁹. The study showed that in resting state enzyme the loop appeared structurally similar to the wild type protein, however, this mutation allowed the loop to exist in a different conformation with acylated adduct, changing the position of the adduct compared to the adduct in the wild type structure and also influencing the positions of active site residues. This conformational freedom introduced by a mutation can be the reason for its extended substrate profile. The crystal structure or the NMR spectrum of BlaC D179N do not support increased flexibility of the Ω -loop. D179N did not display higher hydrolysing efficiency with nitrocefin, so it is likely that *in vivo* performance of this mutant with antibiotics other than ceftazidime can be attributed mostly to increased stability. However, it remains unclear how the subtle changes observed in the crystal structure can be responsible for an increased ceftazidime activity. The mechanism of conformational change can still be possible in BlaC D179G. Seemingly the Ω -loop of BlaC D179G variant exists in two forms, and the exchange between these forms causes the high amplitude first phase in the ceftazidime kinetics.

The question remains why the effects of the same mutation of an extremely conserved residue differ between β -lactamases. Evolution of β -lactamases even from the same class sometimes takes different pathways. It was demonstrated for TEM and SHV, where substitution R164S in TEM increases ceftazidime activity by almost 100-fold, while in SHV R164S confers only a 2-fold increase²³⁷. In SHV and TEM, mutation D179G leads to a 5-fold and 7-fold increase in MIC, respectively, so for SHV 179 position substitutions are more beneficial than for TEM. Majiduddin and Palzkill carried out a competition experiment in which D179G mutation outcompeted R164S in SHV, but the contrary happened in TEM. So even though all four mutants provided a better phenotype, in the end only two mutations persisted²³⁷. Similarly, in clinical isolates substitutions of Asp179 have been observed in SHV²³⁸, but never in TEM. Position 164 is occupied predominantly by arginine in class A β -lactamases, while BlaC

carries alanine at this position. The H-bond between Asp172 and Asp179 in BlaC is possible due to the absence of Arg at position 164 as the side chains of Arg164 and Asp172 would clash. This subtle change might be responsible for differences observed upon mutation in Asp179 in different β -lactamases. While D179N in BlaC might aid the stability via improved interaction with Asp172, in other β -lactamases it will likely introduce a negative effect on stability due to the lost salt bridge between Asn179 and Arg164. Asp179 is highly conserved in class A β -lactamases, but so is Arg164, thus it is possible that the absence of arginine allowed BlaC to open a new evolutionary pathway with D179N variant being better, so in that way the wild type, with Asp179, might be considered not fully evolved to its fitness optimum.

Materials and methods

In vivo activity

In vivo experiments were performed with *E. coli* KA797 cells transformed with pUK21 based plasmids. For the on-plate test cells were applied on the agar plates as 10 µL drops with OD₆₀₀ values of 0.3, 0.03, 0.003 and 0.0003. All plates contained 50 µg mL⁻¹ kanamycin and 1 mM IPTG. Antibiotics and concentrations used were as follows: 20, 40, 80, 100 and 120 µg mL⁻¹ of ampicillin, 100, 500, 1000 and 1500 µg mL⁻¹ of carbenicillin, 0.2, 0.5, 0.8, 1, 2 and 5 µg mL⁻¹ of ceftazidime, 0.05 and 0.1 µg mL⁻¹ of meropenem and 20, 40, 80 and 120 µg mL⁻¹ of penicillin G. Avibactam was used in concentrations 4, 8, 12 and 16 µg mL⁻¹ and sulbactam was used in concentrations 2.5, 5, 7.5 and 10 µg mL⁻¹, both inhibitors were used in combination with 100 µg mL⁻¹ carbenicillin. The MICs were determined as the lowest concentration at which no cell dilution grew. For the soluble culture test cells with the OD₆₀₀ 0.3 were diluted x100 and incubated with at 37 °C overnight with constant shaking. Measurements were performed with Bioscreen C plate reader in duplicate.

Protein production and purification

BlaC was produced using *E. coli* BL21 (DE3) pLysS cells transformed with pET28a plasmids containing the *blaC* gene with an N-terminal His tag and TEV cleavage site. Protein was produced and purified as described in chapter 3.

Circular dichroism spectroscopy

The circular dichroism spectra were acquired in a 1 mm quartz cuvette at 25 °C with a Jasco J-815 spectropolarimeter. Samples contained 100 mM sodium phosphate buffer (pH 6.4).

Melting temperature

Thermostability of BlaC variants was determined with the use of the hydrophobic SYPRO orange dye or using tryptophan fluorescence changes. The commercially available stock of SYPRO orange dye has a x5000 concentration, x4 concentration was used in the measurements. Tryptophan fluorescence was followed using NanoTemper Tycho NT.6 at 330 nm and 350 nm and the ratio 330 nm/350 nm was used to evaluate the melting temperature. All measurements were done in triplicates in 100 mM sodium phosphate buffer (pH 6.4).

Kinetics

All kinetic experiments were performed with the use of a PerkinElmer Lambda 800 UV-vis spectrometer at 25 °C in 100 mM sodium phosphate buffer (pH 6.4). For nitrocefin kinetics 5 nM of enzyme was used with 0 µM, 10 µM, 25 µM, 50 µM, 100 µM, 200 µM, 300 µM, and 400 µM of nitrocefin. The reactions were followed at 486 nm for 90 seconds in triplicate (extinction). The initial velocities were fit to the Michaelis-Menten equation. To measure the

hydrolysis of ceftazidime, 50 nM of BlaC was used with 0 µM, 10 µM, 20 µM, 50 µM, and 100 µM ceftazidime. Product formation was measured at 260 nm for 10 minutes ($\Delta\epsilon_{260} = 8\,099\text{ M}^{-1}\text{ cm}^{-1}$). Extinction coefficient was determined with series of dilutions. Experiments were done in duplicate. Due to K_M ceftazidime being much larger than concentrations of ceftazidime used for wild type BlaC and BlaC D179N, k_{cat}/K_M value for these variants was calculated via the slope of the $v_0/[S]$ dependency. Errors presented in the text represent propagated standard deviations.

Inhibition assay

To measure the BlaC inhibition by avibactam, 2.5 nM of BlaC was used with 100 µM of nitrocefin in the presence of increasing amounts of avibactam, 0 µM, 10 µM, 100 µM, 500 µM. The reactions were followed at 486 nm for 20 minutes in duplicate.

NMR Spectroscopy experiments

¹⁵N enriched (98%) proteins were produced as described in chapter 2 of this work. TROSY-HSQC spectra were recorded on a Bruker AVIII HD 850 MHz spectrometer at 25 °C in 100 mM phosphate buffer (pH 6.4) with 6% D₂O. Data were processed in Topspin 3.2 (Bruker). Spectra were analysed with CCPNmr Analysis software V3. Peaks of the mutant spectra were assigned by comparison to peaks in the wild type BlaC spectrum and average chemical shift perturbations (CSP), $\Delta\delta$, of the ¹H ($\Delta\omega_1$) and ¹⁵N ($\Delta\omega_2$) resonances of backbone amides were calculated using equation 5.1. Peaks that could not be assigned with certainty were assigned based on the smallest possible CSP.

$$\Delta\delta = \sqrt{\frac{1}{2}\left(\Delta\omega_1^2 + \left(\frac{\Delta\omega_2}{5}\right)^2\right)} \quad (5.1)$$

Crystallization

Crystallization conditions for BlaC D179N at a concentration of 10 mg mL⁻¹ were screened for by the sitting-drop method using the JCSG+, BCS and Morpheus (Molecular Dimensions) screens at 20 °C with 200 nL drops with 1:1 protein to screening condition ratio²²⁴. The growth appeared within four days in 0.1 M ammonium acetate, 0.1 M BIS-TRIS buffer (pH 5.5) with 0.1 M ammonium acetate and 17% w/v PEG 10K. After one month the crystals were mounted on cryoloops in mother liquor and vitrified by plunging in liquid nitrogen.

X-ray data collection, processing and structure solving

Diffraction data were collected at the Diamond Light Source (DLS, Oxford, England). The data were integrated using XDS²²⁶ and scaled using Aimless²²⁷ and data to 1.7 Å resolution were kept for structure solution and refinement. The structure was solved by molecular

replacement using MOLREP²²⁸ from the CCP4 suite²²⁸ using PDB entry 2GDN¹⁰¹ as a search model. Subsequently, building and refinement were performed using Coot and REFMAC²²⁸. Waters were added in REFMAC during refinement; a double conformation was modelled for residue Asn110. The final model falls on the 99th percentile of MolProbity²²⁹ and showed that 97.72% of all residues were within the Ramachandran plot favoured regions with two outliers, Cys69 and Arg220. The model was further optimized using the PDB-REDO webserver^{230,231}. Data collection and refinement statistics can be found in Table 5.4.

Table 5.4. Data collection and refinement statistics for BlaC D179N.

Data Collection	D179N
Wavelength (Å)	0.912
Resolution (Å)	38.34-1.69 (1.73-1.69)
Space group	P 1 21 1
Unit cell a, b, c (Å)	38.37, 54.05, 53.64
α, β, γ	90.0, 93.2, 90.0
CC _{1/2}	98.8 (29.2)
R _{pim} (%)	9.7 (53.7)
I/σI	9.1 (1.5)
Completeness (%)	98.1 (95.9)
Multiplicity	1.8
Unique reflections	23953
Refinement	
Atoms protein/water	1988/169
B-factors protein/water (Å ²)	21/27
R _{work} /R _{free} (%)	19.8/22.3
Bond lengths RMSZ/RMSD (Å)	0.742/0.0189
Bond angles RMSZ/RMSD (°)	0.791/1.90
Ramachandran plot preferred/outliers	251/2
Ramachandran plot Z-score	-0.39
Clash score	5.07
MolProbity score	1.56

Supplementary materials

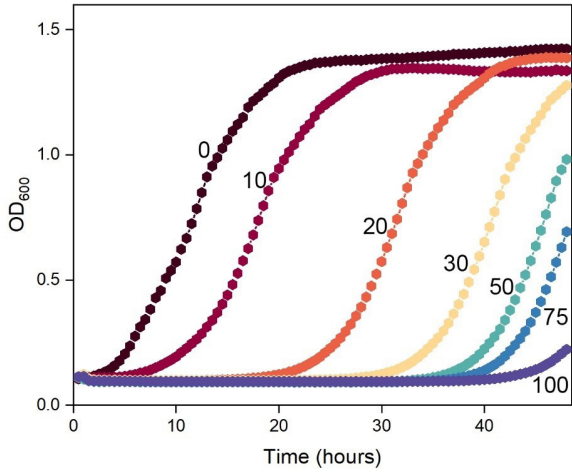


Figure S5.1. An example of the growth curves of wild type BlaC grown at 25 °C with various concentrations of ampicillin. Ampicillin concentrations presented next to the curves are in µg mL⁻¹. The duration of the horizontal phase increases upon increasing concentration of the antibiotic.

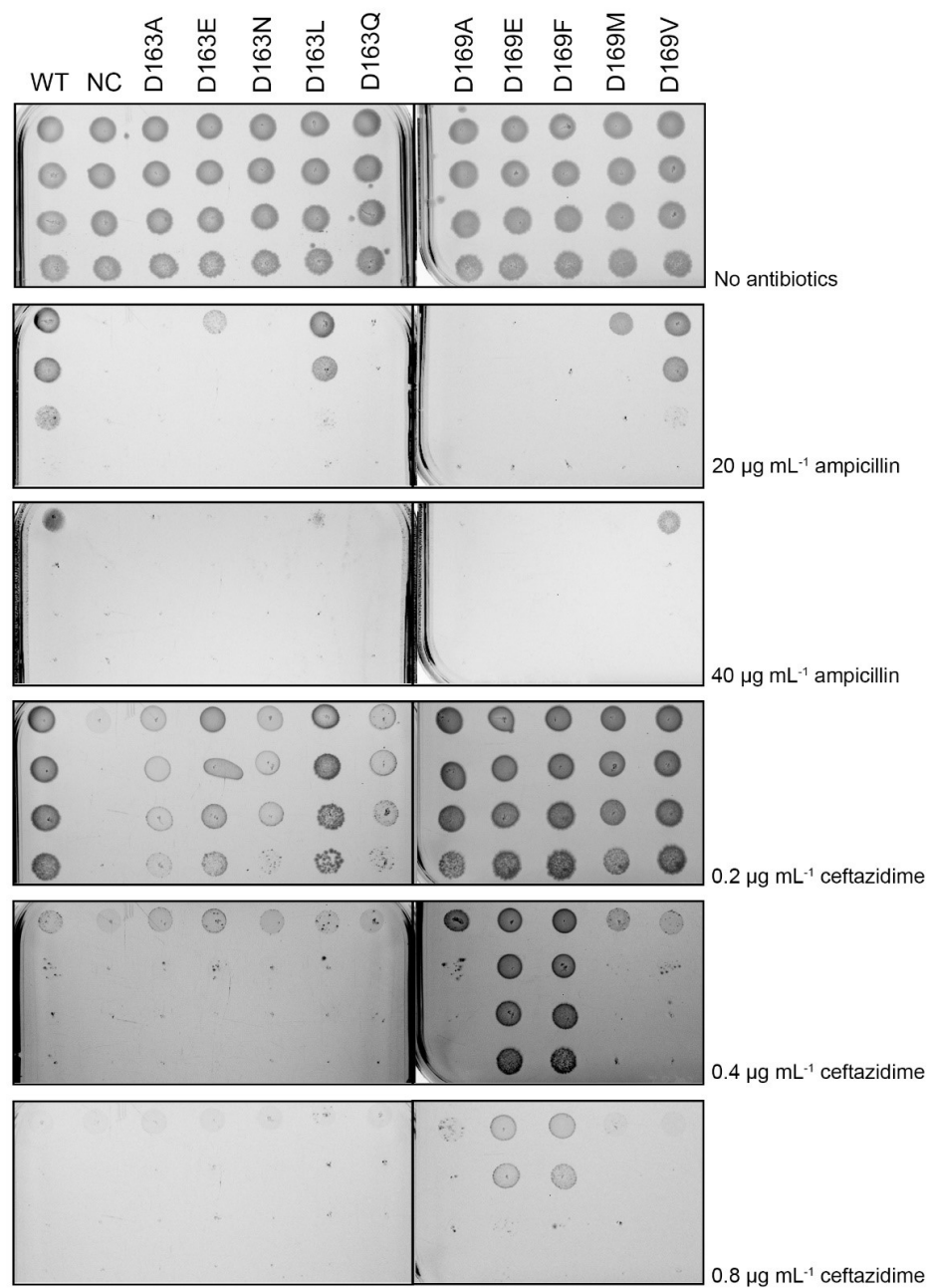


Figure S5.2. Plates showing growth of wild type BlaC and Asp163 and Leu169 variants with ampicillin and ceftazidime.

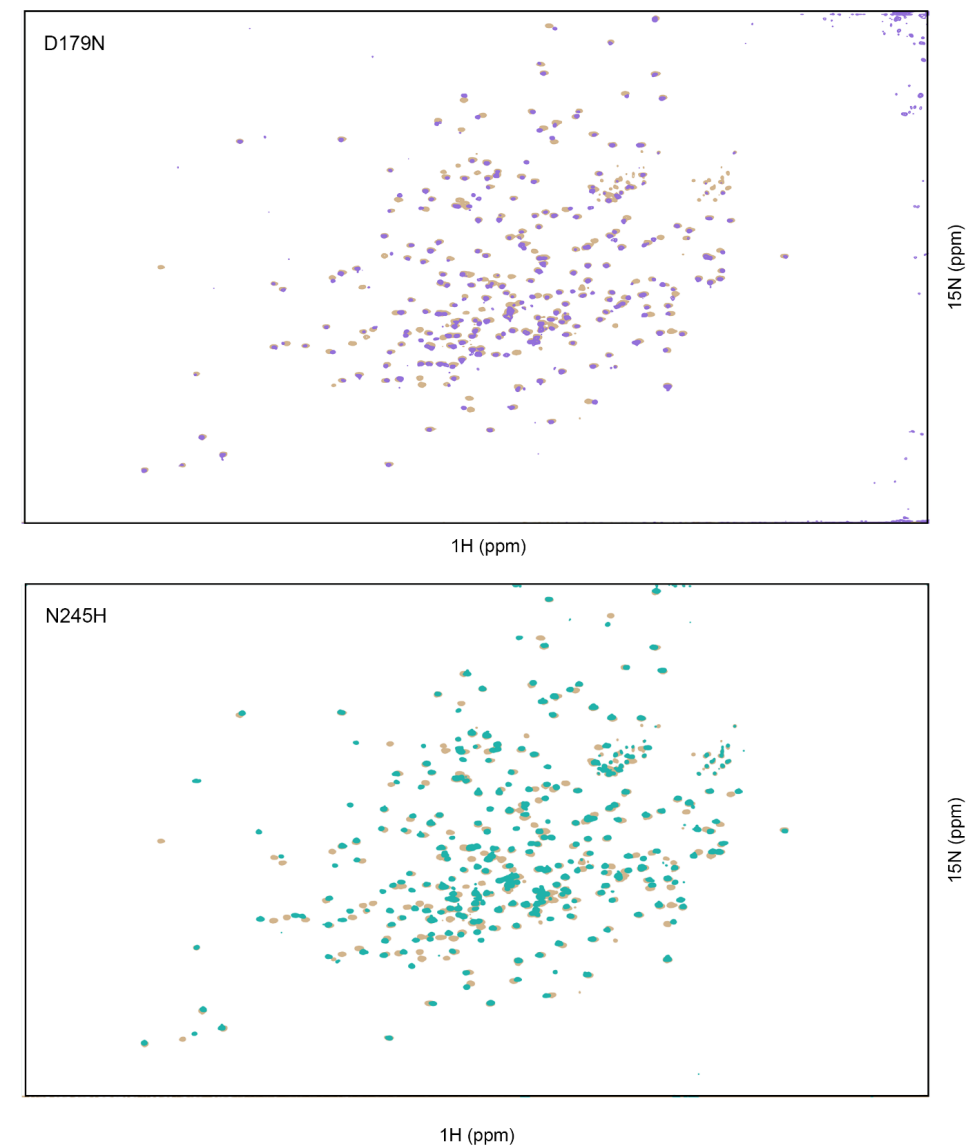


Figure S5.3. ¹⁵N-¹H TROSY-HSQC NMR spectra of BlaC D179N (in purple) and N245H (in turquoise) overlaid on the spectrum of wild type BlaC (in beige).

Chapter 6

Crystal structures of single-point mutants of BlaC

Based on the research articles:

Ilona van Alen, Aleksandra Chikunova, Adil A Safeer, Misbha Ud Din Ahmad, Anastassis Perrakis, Marcellus Ubbink (2021). The G132S Mutation Enhances the Resistance of Mycobacterium tuberculosis β -Lactamase against Sulbactam, *Biochemistry*. 60(28): 2236-2245

Wouter Elings, Aleksandra Chikunova, Danny B van Zanten, Ralphe Drenth, Misbha Ud Din Ahmad, Anneloes J Blok, Monika Timmer, Anastassis Perrakis, Marcellus Ubbink (2021). Two β -Lactamase Variants with Reduced Clavulanic Acid Inhibition Display Different Millisecond Dynamics, *Antimicrob Agents Chemother*. 65(8): e0262820

Abstract

Laboratory evolution studies on BlaC showed that reduced sensitivity to the inhibitors sulbactam and clavulanic acid can be caused by single amino acid substitutions. To understand the structural nature of the changes, several BlaC variants with reduced sensitivity for sulbactam or clavulanate were crystallized and their structures analyzed. Decreased sensitivity to sulbactam can be reached by stabilizing interactions, as shown for mutant D172N, or rearrangements in the active site, as demonstrated by BlaC G132S in complex with the adduct of sulbactam. The crystal structure of BlaC G132N, which displays reduced clavulanate sensitivity, showed a rearrangement near active site similar to BlaC G132S, with two conformations of active site residue Ser130 and formation of a cis-peptide bond in an active site loop.

Introduction

β -Lactamase inhibitors are used to overcome the resistance to β -lactam antibiotics caused by β -lactamases^{242,243}. The first discovered inhibitor, clavulanic acid²⁴⁴ (Figure 1.3), is structurally similar to penicillin and inhibits the enzyme via formation of a covalent complex that is hydrolyzed only very slowly. Another clinically approved inhibitor, sulbactam (Figures 1.3, 6.1), is a synthetic inhibitor that was developed in 1978 by Wayne E. Barth²⁴⁵. It is structurally similar to clavulanic acid and is currently used in the clinic in combination with either ampicillin or cefoperazone^{79,243}. The adducts of clavulanate and sulbactam can exist in a *trans*-enamine form. It is this form that is hydrolyzed very slowly, inhibiting the enzyme (Figure 6.1) transiently, or alternatively, the imine adduct form can acylate an additional active site nucleophile, Ser130 to yield a cross-linked enzyme, which is irreversibly inactivated^{1246,247}. The enzyme-adduct complexes of BlaC were described with mass spectrometry^{102,248} and x-ray crystallography¹⁴¹. Mass spectrometry on BlaC with clavulanate together with activity studies performed by Hugonnet and colleagues supported the conclusion that clavulanate inhibition is irreversible¹⁰². However, it was shown later that enzymatic activity recovers from inhibition with the half live for recovery of ~ 3 h, furthermore, the recovery can be accelerated by ions present in the buffer²⁴⁸. The recovery of enzymatic activity from sulbactam inhibition was observed already after 30 min¹⁰².

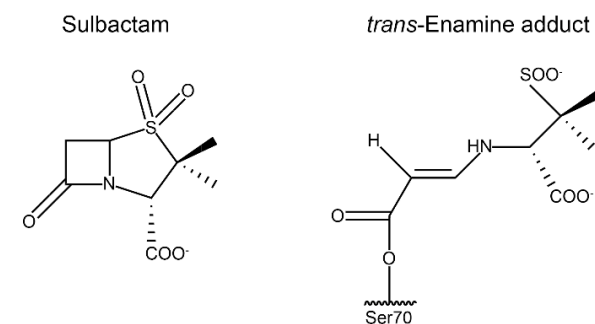


Figure 6.1. Structures of sulbactam and *trans*-enamine adduct of sulbactam covalently linked to Ser70.

One of the questions that was raised in the Ubbink research group was whether evolution against sulbactam inhibition through mutations in BlaC could easily occur. Decreased sensitivity could have a negative bearing on the effectiveness of combination therapy. For that purpose, a laboratory evolution experiment was carried out, yielding, among others, mutations A55E, G132S, and D172N mutants. BlaC A55E and D172N exhibited a slight decrease in sensitivity to sulbactam *in vivo*, but the activity of the purified enzymes was inhibited to the same degree as the wild type enzyme, suggesting changes in stability or

protein production *in vivo*⁸². Ala55 is located in a loop (Figure 6.2) and its Ca atom is 28 Å away from Ca of active site Ser70, which makes it unlikely that the mutation can affect enzyme activity, in line with the experimental findings. Asp172 is a part of an important structural element, the Ω-loop, but it is not conserved in class A β-lactamases, with alanine being the most abundant residue at this position (62% out of 494 class A β-lactamase sequences, see chapter 2 for details). BlaC D172N exhibits an increased melting temperature, in line with an increased stability that can explain the decreased sulbactam sensitivity *in vivo*⁸². Residue 132 is part of the one of the most conserved motifs in class A β-lactamase active sites – the Ser130-Asp131-Asn132 motif (SDN motif). Interestingly, BlaC harbors a glycine instead of an asparagine at position 132. BlaC G132S displayed reduced sensitivity for sulbactam, both *in vivo* and *in vitro* using an activity assay with nitrocefin as substrate. These findings indicate that G132 is involved in the interactions of sulbactam with the active site⁸².

The substitution of Asn with Gly results in an enlarged active site in BlaC as compared to other β-lactamases. At the same time, the potential for stabilizing enzyme-substrate interactions via the Asn side chain is lost. The glycine at position 132 in BlaC could be one of the reasons for its broadened substrate specificity, paired with somewhat decreased overall activity compared to other class A β-lactamases. It has been proposed that substituents at the R⁶ position (rest chain at β-lactam ring) of carbapenem (Figure 1.3) could be accommodated by this substitution²⁴⁹. For this reason, the reverse mutant G132N in BlaC was studied extensively. Soroka *et al.* showed that the G132N mutation increases the hydrolysis rate of nitrocefin, imipenem and aztreonam, while decreasing the hydrolysis rate of cephalosporins^{84,85}. It also increases the resistance of the enzyme to clavulanic acid, but at the same time increases sensitivity to another inhibitor, avibactam (Figure 1.3)⁸⁴. Elings *et al.* recently showed that BlaC G132N exists in two almost equally populated states in solution. Moreover, binding to the inhibitor influences the dynamic behavior of the enzyme, increasing the millisecond time scale chemical exchange in the active site⁸³.

To elucidate the relation between the inhibitor resistance and structural changes, the BlaC variants A55E, D172N, G132S, and G132N were crystallized, and the obtained x-ray diffraction structures were analyzed. Also, the structure of another variant, BlaC P226G, of the third-shell conserved residues discussed in chapter 2, was solved. Most structures show only subtle effects of the mutations. In the G132 variants the effects are more significant. An active site serine was found to occupy multiple orientations in G132 mutants, and an alternative conformation was found for one of the active site loops. The structures of BlaC G132S mutants were also solved with the adduct of sulbactam, which revealed a possible mechanism of inhibitor resistance.

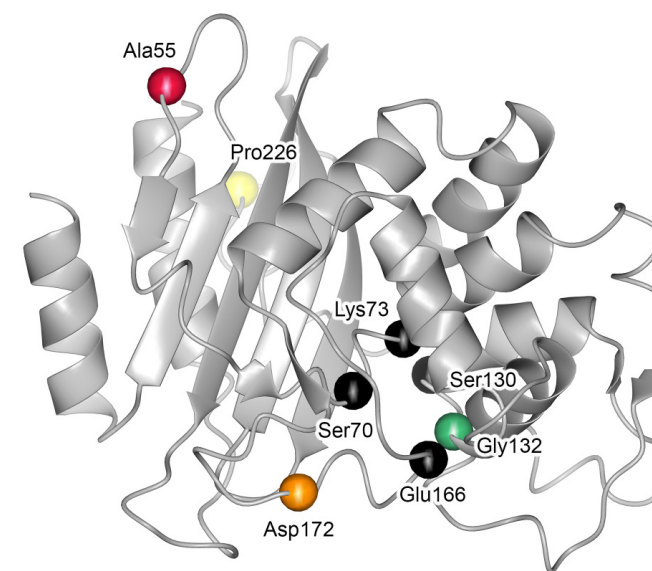


Figure 6.2. BlaC structure (2GDN¹⁰¹) with Ca atoms shown as spheres for active site residues (black) and for residues for which substitutions are discussed in this chapter (colors).

Results

To complement the findings about *in vivo* and *in vitro* activity of the variants of BlaC, the three-dimensional structures were determined using x-ray diffraction of crystals. The mutant proteins were produced in *Escherichia coli*, purified to homogeneity and crystallized as described in Material and Methods section. BlaC A55E, G132S and D172N were produced by Ilona van Alen, BlaC G132N was produced by Wouter Elings and Roeland de Wit and BlaC P226G was produced by Aleksandra Chikunova and Max Manley.

The phase problem was solved by molecular replacement with PDB entry 2GDN¹⁰¹ as a model, except for the crystal soaked with inhibitor sulbactam, in which case entry 6H2K¹⁴¹ was used. The structures had resolutions in the range of 1.6 – 1.3 Å and could be refined to high quality factors (Table 6.3). The overall structures of the variants were found to be very similar to that of wild type BlaC with average C α RMSDs for A55E, D172N, P226G, G132N, G132S and G132S with sulbactam of 0.28, 0.32, 0.34, 0.33, 0.33 and 0.36 Å, respectively. Figure 6.2 presents overlays of the structures with that of wild type BlaC.

In BlaC A55E, the δ -carboxy group of Glu55 adds an extra negative charge on the surface of the protein. In the crystal lattice, the δ -carboxyl of Glu55 engages in a hydrogen bond with the symmetry-related side chain of Arg277 (Figure 6.4a). Notably, the lattice of the A55E mutant deviates from the commonly observed primitive orthorhombic lattice observed for other structures, crystallizing in the closely related primitive monoclinic lattice, presumably largely because of this mutated side chain and the new salt bridge. The δ -carboxy group also makes two hydrogen bonds involving water molecules.

The changes for D172N are less obvious, as the side chain of Asn172 occupies the same space as the aspartic acid in the wild type protein. The carboxamide group of Asn172 forms two highly favorable hydrogen bonding interactions with the side chain carboxyl of Asp179 and the carbonyl of the peptide bond between residues 178 and 179 (Figure 6.4b). These favorable interactions, which are not observed for wild type BlaC, stabilize the loop of residues 171–180 and are likely the cause of the increased thermostability of the D172N mutant.

BlaC P226G displays virtually no differences in comparison with the structure of wild type BlaC. Surprisingly, even the loop containing residue 226 displayed no changes (Figure 6.4c). An absence of the pyrrolidine ring, however, allowed for an additional ordered water to be present in a mutant structure.

In BlaC G132N the Asn side chain that is introduced at position 132 occupies the canonical position for class A β -lactamases (Figure 6.5a). The oxygen of the side chain is hydrogen

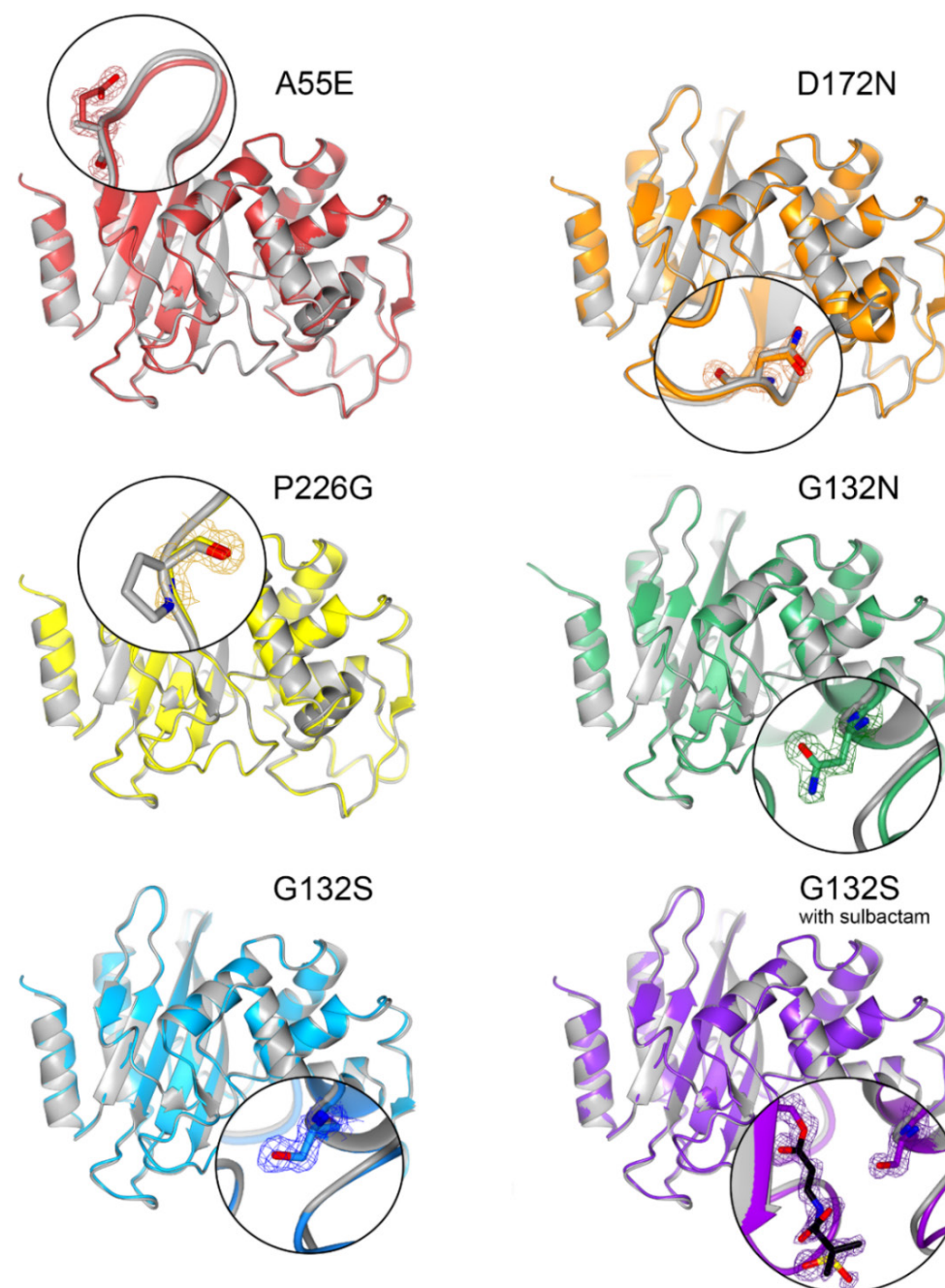


Figure 6.3. Overlay of wild type BlaC structure (2GDN¹⁰¹, in grey) and mutants (in colors). Mutation sites are shown as close-ups in circles and mutated residues are shown in sticks. The $2mF_o - DF_c$ electron density maps are shown in chicken wires with contour levels of 1 σ and extent radius of 5 Å. The electron density maps are pinned around mutated residues. The sulbactam adduct is shown in black sticks bound to the active site Ser70 (in purple sticks).

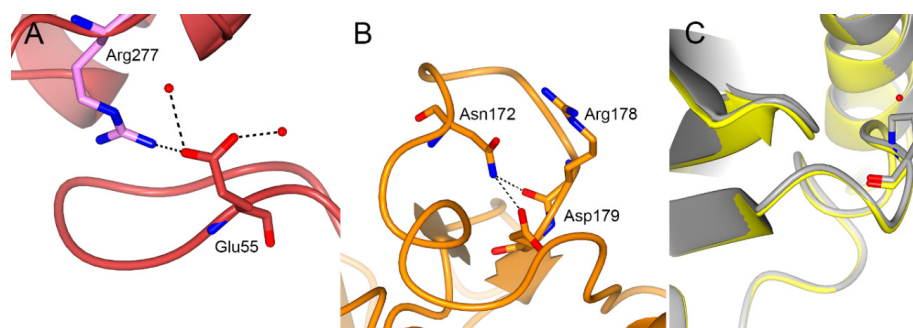


Figure 6.4. (A) Mutated residue Glu55 (in red) has an ionic interaction with symmetry-related Arg277 (in pink) and waters (red spheres); (B) Interactions of the side chain of Asn172; (C) Overlay of wild type BlaC (2GDN¹⁰¹, in grey) and BlaC P226G (7A6Z, in yellow).

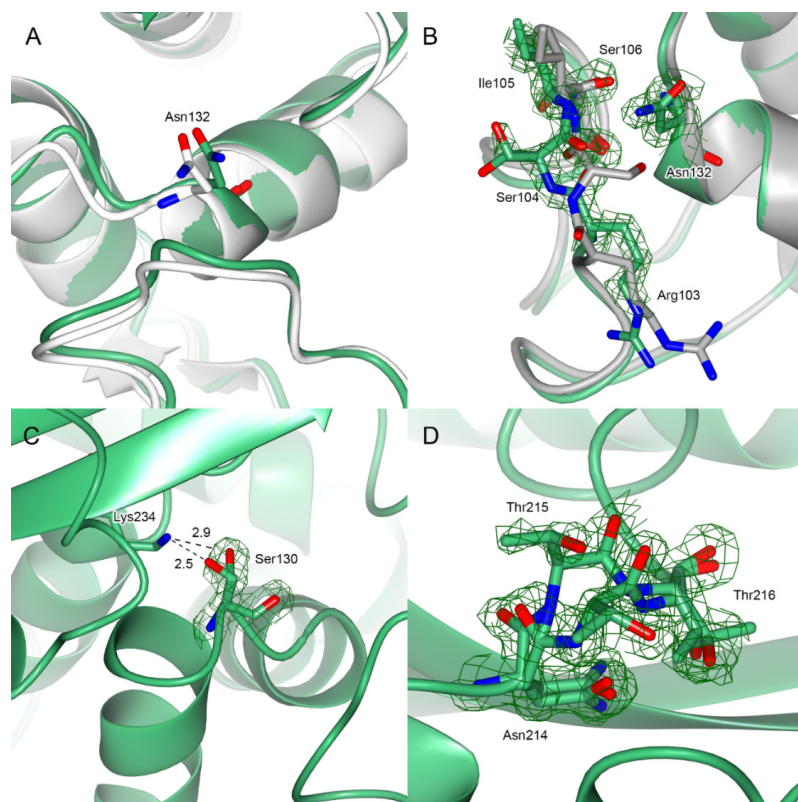


Figure 6.5. Structure of G132N mutant (7A74, in green) overlaid with TEM-76 (1YT4²³⁴, in white) or wild type BlaC (2GDN¹⁰¹, in grey). The 2mF₀-DFc electron density map is centered on the selected residues and is shown in green chicken wire, with contour level 1 σ and extent radius 5 Å. (A) Side chain of the residue Asn132 in BlaC G132N occupies a position canonical in class A β -lactamases; (B) In BlaC G132N, the side chain of residue Ser104 flips to the surface, where it can be modeled in two alternative conformations, forcing the peptide bond with Ile105 into a cis conformation; (C) Residue Ser130 in BlaC G132N exists in two conformations; (D) Region 214-216 exists in multiple conformations.

bonded (2.7 Å) with the amine of Lys73. Strikingly though, the nitrogen of the Asn132 side chain hydrogen bonds (2.8 Å) to the carbonyl oxygen of residue Ser104. This interaction flips the side chain of Ser104 from the inside to the outside of the protein, where it adopts two conformations. This conformation in turn flips the carbonyl of Ser104 and forces the peptide bond with residue 105 to a cis conformation. This is notable as this is the only cis peptide conformation in this position in all 94 homologous structures in the PDB, as revealed by the LAHMA server²⁵⁰. This change propagates to residues 102-105, which adopt conformations distinct from the wild type BlaC (Figure 6.5b).

An interesting double conformation is also observed for the side chain of Ser130 (Figure 6.5c). In the structure of BlaC G132N this side chain occupies the position that is observed in all but six homologues in the PDB, making hydrogen bonds to the active site Lys234 amine (2.9 Å). In the second conformation the hydrogen bond is maintained, with the bond to the Lys234 amine becoming shorter (2.5 Å). Multiple conformations are also supported by the electron density for the Asn214, Thr215 and Thr216 loop region, two of which were modelled (Figure 6.5d). In this case, the occupancy of each modeled conformation is not equal and current modeling can only be considered an estimate indicative of the conformational dynamics.

In the G132S mutant, the side chain moiety of Ser104 is forced away by the side chain of Ser132 (Figure 6.6a) in the same manner that is observed in G132N mutant. The side chain of Ser104 is turned toward the protein surface, and the carbonyl oxygen of its peptide bond with Ile105 engages in a hydrogen bond with the newly introduced hydroxyl group of Ser132. This hydrogen bond again causes the peptide bond between residues 104 and 105 to assume a cis conformation. Two conformers are observed for Ser130 also in this structure (Figure 6.6b).

In the structure of the mutant with the trans-enamine adduct of sulbactam, the different positioning of the residues mediated by the G132S mutation as compared to that in wild-type BlaC is maintained, allowing the hydroxyl of Ser104 to form a hydrogen bond with one of the oxygens of the sulbactam sulfonyl moiety, not observed in the adduct with wild type BlaC (PDB entry 6H2K¹⁴¹, Figure 6.6c). The interaction of the sulfonyl moiety with Arg171, observed in the latter structure, is also found in the BlaC G132S–adduct complex. This interaction reduces the rotational freedom of the sulfonyl group in the wild type enzyme to a single conformation. The side chain of Ile105 in the structure of the BlaC G132S–adduct complex is not flipped to the side of the active site entrance, as observed for the wild type BlaC–adduct complex and is likely pushing away the dimethyl group of the sulbactam adduct. Overall, the trans-enamine adduct of sulbactam has more interaction and better packing in BlaC G132S than in wild type BlaC (Figure 6.6d), which is in apparent contrast with the weakened inhibitory effect in the hydrolysis of substrates.

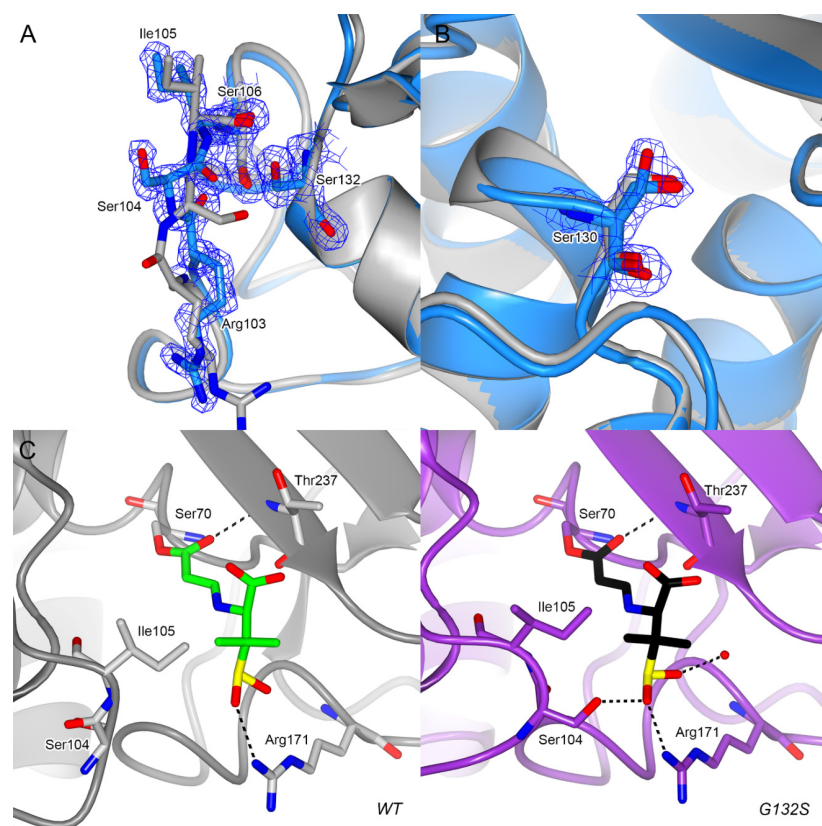


Figure 6.6. Structures of BlaC G132S. (A, B) Overlay of wild type BlaC (2GDN¹⁰¹, in grey) and BlaC G132S (7A71, in azure). Residues 103-106 (A) and Ser130 (B) are shown in sticks. The side chain of Ser104 flips to the surface, forcing the peptide bond with Ile105 to a cis conformation. Residue Ser130 in the mutant structure exists in two conformations with almost equal occupation. The 2mF_o-DF_c electron density map is centered on these residues and is shown in blue chicken wire, with contour level 1 σ and extent radius 5 Å; (C) Structure of the covalent trans-enamine adduct (in green or black) formed between sulbactam and wild type BlaC (in grey) (6H2K¹⁴¹, left) and BlaC G132S (7A72, in purple, right). More interactions are involved in stabilization of the adduct in the mutant than in the wild type enzyme, with a hydrogen bond donated by Ser104 in its new orientation.

Discussion

In this chapter the structures of several single mutants of BlaC are discussed. Two variants, A55E and D172N, found in laboratory evolution with sulbactam activity as a selection pressure⁸², displayed no mechanistic resistance to sulbactam, because they performed better than wild type enzyme against this inhibitor *in vivo*, but not *in vitro*. There can be a number of reasons for this, for example, higher activity against ampicillin, the antibiotic that was used in combination with sulbactam, or differences in the amount of active protein between the mutants, caused by differences in mRNA stability, translation, or folding, stability, or translocation of the protein. The increased stability is likely to be the reason for D172N mutant, as it was shown that this variant has a higher melting temperature than wild type enzyme⁸². The crystal structure presents a structural underpinning for increased stability of the ω -loop caused by interactions of Asn172 with residues 178 and 179. The interaction between Asn172 and Asp179 has a stabilizing effect similar to the Asp172-Asn179 interaction in D179N mutant discussed in chapter 5. Two negatively charged side chains at short distance destabilize the enzyme by repulsion. Therefore, given the short distance between Asp172 and Asp179 side chains in wild type BlaC, a hydrogen must be shared between the two carboxy groups. At near-neutral pH, replacement of one of the carboxy group (Asp) with a carboxamide (Asn) is expected to yield a more stable structure.

The mechanism of somewhat higher sulbactam resistance for A55E mutant is less obvious. The additional surface charge may contribute to a higher solubility of BlaC and thus a somewhat higher concentration of active enzyme in the periplasmic state, but this hypothesis was not tested.

A change in a conserved amino acid is expected to yield considerable effects on the structure or function of the enzyme. However, as demonstrated by P226G mutant that is not always the case. This mutant displayed marginally lower activity *in vivo* yet has biophysical properties comparable to wild type enzyme *in vitro* (Table S2.2, Table S6.1), with somewhat higher activity displayed *in vitro* but not *in vivo*. The NMR spectrum of this mutant shows changes that are limited to the region around the site of the mutation (Figure S6.1) and the crystal structure is near-identical to that of the wild type enzyme. Therefore, the high conservation of this residue cannot be explained by its importance for the traits examined within this work. It is, however, plausible that highly conserved prolines located in the loops contribute to dynamics. Stacking interaction between conserved residues Pro226-Trp229-Pro252 was proposed to be important for modulating the H10 helix mobility in TEM-1¹³².

For BlaC G132N, it was shown with NMR relaxation experiments that the substitution affects the dynamics in the active site in millisecond timescale⁸³. The crystal structure also suggests

an increase in flexibility because several residues occur in more than one conformer. The relative occupancies of the Ser104 and Ser130 conformations observed in the crystal structure match those of the states observed in the NMR experiments. Moreover, these residues are positioned right in the region of the protein where broadening and exchange were observed with NMR spectroscopy. The x-ray and NMR observations may thus represent the same phenomenon. In this case, the two conformations, which are slowly exchanging at room temperature, were captured by flash freezing of the crystal prior to x-ray analysis. The region in which the effects of conformational exchange are observed with NMR is relatively large for single side chain movements, and the exchange is relatively slow ($\sim 80 \text{ s}^{-1}$)⁸³. As discussed in chapter 2, mutation in and around the active site affects the chemical shifts of many amide groups around the active site, which is explained by assuming that there is a network of interactions through hydrogen bonding and other electrostatic interactions, also involving many water molecules.

In the resting state structure of BlaC G132S, the side chain of Ile105 has moved 1.6 Å relative to its position in the structure of wild type BlaC, partly blocking the active site. This change is brought about by the backbone rearrangement due to the introduction of the Ser at position 132. Upon formation of the adduct of sulbactam, Ile105 keeps its position, whereas in the wild type enzyme, it rotates away. Interestingly, the backbone rearrangement in BlaC G132S leads to better interactions with the adduct, including a hydrogen bond from Ser104 to the sulfonyl group. This observation seems to be in contrast with the weakened inhibition by sulbactam observed by van Alen *et al.*⁸². However, the structure of sulbactam is very different from that of the adduct. The latter is an elongated molecule without rings, whereas sulbactam has two ring structures, which place the sulfonyl group in a different position in the active site. The reduced inhibitory effect of sulbactam can be explained by decreased access to Ser70, caused by the rearrangement of the loop containing Ser104 and Ile105.

The change in the position of the loop and the cis peptide bond configuration are induced by the newly introduced side chain at position 132 for both G132N and G132S, because the introduced side chain would cause steric collisions, were Ser104 to take the same position as in wild type BlaC. The two conformers of Ser130 observed in both G132S and G132N structure are reminiscent of observations in clavulanic acid-resistant variants of SHV, PSE-4 and CTX-M-14 β -lactamases. There, MD simulations¹²¹ and x-ray crystallography^{120,122,251} have shown that the presence of Arg234 rather than Lys234 causes a displacement of the Ser130 side chain, moving it further away from the reactive Ser70. This may prevent cross-linking between Ser70 and Ser130, which could explain the increased resistance of the enzyme to clavulanic acid.

Materials and Methods

Protein expression and purification

Protein was produced using *E. coli* BL21 (DE3) pLysS cells transformed with pET28a plasmids containing the *blaC* gene with an N-terminal His tag and TEV cleavage site. Protein was produced and purified as described in chapter 3 of this work and in van Alen *et al.* and Elings *et al.*^{82,83}. PA-gel electrophoresis was used to evaluate the purity of the samples before samples were used for crystallization. Proteins were concentrated using Pierce™ (Thermo Scientific™) concentrators with cutoff 10 kDa.

Crystallization

Crystallization conditions for BlaC mutants were screened by sitting-drop vapor diffusion using the BCS, Morpheus, JCSG+ and PACT premier (Molecular Dimensions) screens at 20 °C with 100 nL drops with 1:1 ratio. The plates were pipetted by the NT8 Drop Setter (Formulatrix). Protein solutions were used with a concentration of 9 mg mL⁻¹ for A55E, G132S, and D172N in 20 mM Tris buffer with 100 mM sodium chloride (pH 7.5) and 10 mg mL⁻¹ for P226G mutant in 100 mM sodium phosphate buffer (pH 6.4). BlaC G132N was used at a concentration of 18 mg mL⁻¹ in 100 mM MES/NaOH buffer, pH 6.4. To obtain crystals, it was necessary to supplement the protein with 100 mM sodium phosphate buffer and cross-seed with crystals from another BlaC mutant (G132S). Crystals for all mutants grew within two months under various conditions.

A selection of one to five crystals for each mutant were mounted on cryoloops in mother liquor with addition of up to 25% glycerol and vitrified in liquid nitrogen for data collection. In addition, four crystals of G132S BlaC were soaked in corresponding mother liquor with 10 mM sulbactam for 40 min. The conditions yielding crystals that were used for structure determination can be found in Table 6.1.

Table 6.1. Crystallization conditions

BlaC mutant	Crystallization condition
A55E	0.8 M disodium succinate
G132S	Sodium cacodylate (pH 6.5), 0.2 M sodium chloride, 2 M ammonium sulfate
G132S with sulbactam	0.1 M sodium cacodylate (pH 5.3), 15% PEG-SB, 10% ethylene glycol, 5% TMate
G132N	0.1 M Morpheus buffer 1 (pH 6.5), 30% EDO_8K, 0.09M halogens
D172N	0.1 M Morpheus buffer 1 (pH 6.5), 30% EDO_8K, 0.09M halogens
P226G	0.2 M Sodium malonate dibasic monohydrate, 20% PEG 3350

X-ray data collection, processing, and structure solution

X-ray diffraction data were obtained from a single crystal at the Swiss Light Source (SLS, Paul Scherrer Institute, Switzerland) for the A55E, G132S, D172N and P226G mutants and at the Diamond Light Source (DLS, Oxford, England) for BlaC G132N and G132S with sulbactam. Diffraction data were recorded on a Pilatus detector for G132N and G132S with sulbactam and on an Eiger detector for the other samples. The diffraction data extended to a resolution of 1.4 Å for A55E, G132S, and D172N and to 1.3 Å for G132S with sulbactam and P226G. The crystallographic diffraction data for G132N were recorded to resolution of 1.18 Å. The resolution was set to 1.55 Å based on $|I/\sigma I|$ and $CC_{1/2}$ values. Data were processed and integrated with XDS²²⁶ and scaled with AIMLESS²²⁷. The structure was solved by molecular replacement using MOLREP²²⁸ from the CCP4 suite²²⁸ using PDB entry 2GDN²⁴⁹ as a search model, except for G132S with sulbactam, in which case the wild type structure with sulbactam adduct was used (6H2K¹⁴¹). Building and refinement were performed using Coot and REFMAC²²⁸. The model was further optimized using the PDB-REDO webserver²³⁰. Structure validation showed a RamaZ score²³¹ of -0.09, 0.11, -0.09, 0.33, 0.36, and -0.20, for G132N, P226G, A55E, G132S, G132S with sulbactam and D172N respectively; 98-99% of all residues are within the Ramachandran plot favored regions with two outliers for all structures, namely, Cys69 and Arg220. According to MolProbity²²⁹ the structure belongs to the 100th percentile for G132N and D172N, the 99th percentile for A55E and G132S with sulbactam, the 98th percentile for P226G and the 96th percentile for G132S. Data collection and refinement statistics can be found in Table 6.2. The following residues were modeled in two conformations: Arg128 and Ile186 for A55E; Ser130, Ile186, Asn197, Arg204, Lys219, Met264 and Glu283 for G132S; Arg39, Lys93, Met264 and Tyr272 for G132S with sulbactam;

Arg128, Ser130 and Met264 for D172N; Lys93, Asp100, Ser104, Ser130, Val263 and Met264 for G132N; and Asp31, Glu35, Arg128, Ile186, Gln191, Arg204 and Met264 for P226G. For G132N, G132S and G132S with sulbactam, Ser104 was found in the cis conformation. In G132N structure residues N214-T215-T216 exist in multiple conformations and were modeled in two representative conformations.

In vivo activity studies

In vivo activity of P226G mutant was evaluated within the study described in Chapter 2 and later separately as described in Chapter 3.

Thermal stability

Thermal stability of P226G mutant was accessed as described in Chapter 3.

Kinetics

Kinetic parameters of the reaction of nitrocefin hydrolysis for P226G mutant were determined as described in Chapter 4.

NMR spectroscopy

NMR experiment for P226G mutant was performed as described in Chapter 3.

Table 6.2. Data collection and refinement statistics.

Data Collection	A55E	G132S	G132S +sulbactam	G132N	D172N	P226G
PDB ID	7A5T	7A71	7A72	7A74	7A5W	7A6Z
Beamline	X06SA (SLS)	X06SA (SLS)	I04-1 (DLS)	I04-1 (DLS)	X06SA (SLS)	X06SA (SLS)
Detector	EIGER X 16M	EIGER X 16M	PILATUS 6M-F	PILATUS 6M-F	EIGER X 16M	EIGER X 16M
Wavelength (Å)	1.000	1.000	0.912	0.912	1.000	1.000
Resolution (Å)	38.19-1.40 (1.42-1.40)	44.73-1.40 (1.42-1.40)	78.20-1.30 (1.32-1.30)	45.03-1.55 (1.58-1.55)	44.80-1.40 (1.42-1.40)	44.72-1.30 (1.32-1.30)
Space group	P 1 21 1	P 21 21 21	P 21 21 21	P 21 21 21	P 21 21 21	P 21 21 21
Unit cell a, b, c (Å)	39.00, 54.36, 53.69	53.30, 54.32, 78.85	53.49, 54.66, 78.20	54.00, 54.60, 79.40	54.03, 54.47, 78.78	53.52, 54.23, 79.05
CC _{1/2}	98.5 (75.2)	98.9 (65.4)	99.9 (65.5)	99.6 (54.6)	99.7 (77.7)	99.7 (77.0)
R _{rim} (%)	7.8 (34.4)	8.3 (69.8)	3.8 (58.2)	6.0 (52.6)	4.1 (52.4)	3.4 (39.3)
I/σI	5.2 (1.7)	8.3 (2.6)	11.1 (1.3)	5.4 (1.1)	9.3 (1.8)	11.0 (1.6)
Completeness (%)	96.9 (94.2)	98.9 (97.4)	98.2 (99.8)	99.7 (99.0)	98.0 (98.0)	99.9 (99.9)
Multiplicity	2.5	3.7	5.7	1.8	3.0	6.5
Unique reflections	42718	45293	56098	34560	45377	57233
Refinement						
Atoms protein/ ligands/water	2013/59/207	2047/61/201	2034/37/221	2074/126/164	2008/29/156	2035/67/249
B-factors protein/ ligands/water (Å²)	10/22/19	8/25/20	15/24/26	15/41/30	16/28/28	10/23/24
R _{work} /R _{free} (%)	14.8/17.7	13.0/16.1	15.2/18.9	13.4/18.2	13.5/17.2	13.1/15.1
Bond lengths RMSZ/ RMSD (Å)	1.056/ 0.014	1.270/ 0.016	1.249/ 0.016	1.016/ 0.017	1.236/ 0.016	1.475/ 0.018
Bond angles RMSZ/ RMSD (°)	1.085/ 1.781	1.120/ 1.837	1.168/ 1.940	1.070/ 2.010	1.155/ 1.919	1.148/ 1.873
Ramachandran plot preferred/outliers	248/2	248/2	259/2	245/2	245/2	249/2
RamaZ scores	-0.09	0.33	0.36	-0.09	-0.20	0.11
Clash score	2.42	4.52	1.94	7.10	1.48	1.84
MolProbity score	1.02	1.23	0.96	1.39	0.89	1.08

Supplementary materials

Table S6.1. In vivo and in vitro characteristics of wild type (WT) BlaC and the P226G variant. Kinetic parameters are given for nitrocefin hydrolysis in 100 mM sodium phosphate buffer (pH 6.4) at 25 °C. Melting temperature obtained with thermal shift assay method using hydrophobic dye.

Enzyme	$k_{cat} \pm SD^a$ (s ⁻¹)	$K_M \pm SD^a$ (μM)	k_{cat}/K_M^b (x 10 ⁵ M ⁻¹ S ⁻¹)	MIC carbenicillin (μg mL ⁻¹)	Melting temperature ^c (°C)
WT	133 ± 7	281 ± 18	4.7 ± 0.5	1000	52 ± 0.5
P226G	248 ± 12	361 ± 34	6.9 ± 0.5	500	50 ± 0.5

^a Standard deviation represents the deviation of three measurements;
^b Errors represent the propagated standard deviation;
^c Values represent average of triplicate measurement with technical error.

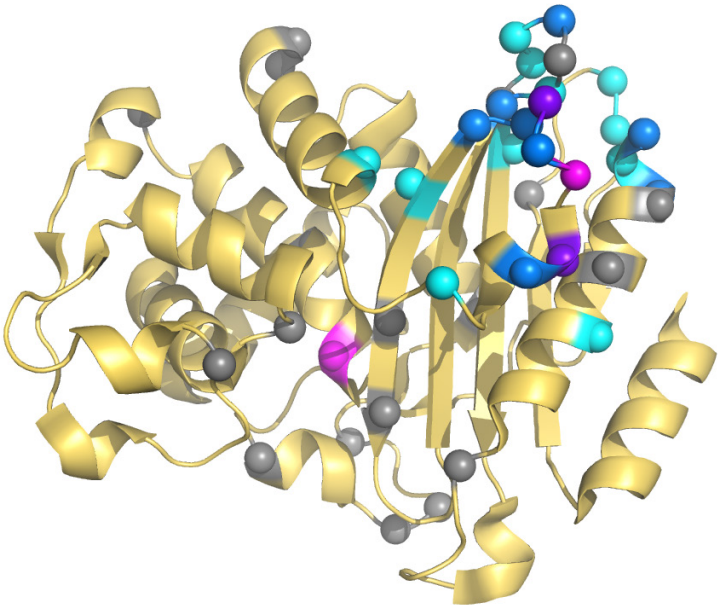


Figure S6.1. Average chemical shift differences (CSP) between the resonances of BlaC P226G and wild type BlaC mapped on structure (2GDN^[10]). Residues are colored cyan for CSP > 0.025 ppm; blue for CSP > 0.05 ppm and purple for CSP > 0.1 ppm and grey for no data. Ser70 and Gly226 are shown in magenta. Relevant backbone nitrogen atoms are shown as spheres.

Chapter 7

General conclusions

Overview and Perspectives

Changing conditions cause changing evolutionary selection pressures that lead to adaptations in organismal phenotypes. The underlying biochemical processes and thus the involved proteins need to be able to adapt to the changed environment. Proteins evolve by acquiring semi-random amino acid substitutions.

β -Lactam antibiotics are the largest and one of the best researched group of antibiotics. Due to introduction of new compounds in the clinic and cattle breeding, bacteria experience an environment with changing selection pressures. Throughout history, β -lactamases, the enzymes that are responsible for the breakdown of β -lactam antibiotics, were able to evolve and hydrolyze novel β -lactam antibiotics. These enzymes are excellent systems to study protein evolution because of their adaptability, and, furthermore, the changes in phenotype can be easily detected by antibiotic screening. For those reasons β -lactamases, especially TEM-1, often has become a focus in evolutionary studies (e.g. ^{17,127,136,237,252}). Saturation mutagenesis was performed on TEM-1, yielding the fitness effect of substitutions of every amino acid residue to all other 19 amino acids^{15,253}. These extensive works showed that robustness and evolvability of TEM-1 are dependent on the strength of purifying selective pressure¹⁵, and that mutational effects on protein thermodynamic stability shape the distribution of fitness effects of mutations²⁵³. Another study on $\sim 12,500$ single amino acid mutants of TEM pointed out the importance of epistatic interactions in the enzyme, as they showed that the frequency of mutations exhibiting epistasis increases along the evolutionary pathway²⁵⁴. The saturation mutagenesis approach differs from the approach presented in this thesis, and it might be interesting to carry out a similar study on β -lactamase BlaC in order to compare the evolutionary pathways taken by these two β -lactamases from the same class.

Evolutionary adaptability is restricted by essential amino acid residues because their substitution will likely render the protein less functional. Thus, evolution will strive to minimize the number of such essential amino acids. It is interesting to know what the exact reason for essentiality is. Being an essential residue is often linked to conservation of residue type in a sequence family^{34–36}. We set a goal to describe the roles of highly conserved residues in enzymes in relation to their position in a structure relative to the active site. Whereas catalytic residues, or the first-shell residues, are usually extensively studied and their functions known, non-catalytic residues are addressed less often. In Chapter 2, the roles of the highly conserved, non-active site residues of the BlaC were determined. β -Lactamases evolve rapidly under the constantly changing selection pressures of different classes of these compounds, yet 11% of the residues outside active site stayed unmodified throughout history. The reason for such conservation was investigated with an extensive mutational study.

We observe striking differences between the effect of mutation on second-shell residues (close to the active site) and third-shell residues (more distant from the active site). Second-shell residues are shown to influence the entire active site and mutations in the second-shell residues lead to a changes sensed throughout the entire core of the protein, which can be picked up by NMR spectroscopy as chemical shift perturbations. The spread of such changes far from the mutation site indicates a network of correlated interactions throughout the region around the active site. Second-shell residues are not significant for folding and production of mutants often yields folded but inactive enzyme. Thus, these residues are relevant for stabilizing the active conformation from within the ensemble of conformations that the enzyme can visit in its folded state. Some second-shell conserved residues are also shown to contribute to the overall thermal stability of the enzyme. Substitutions in those lead to a shift of the balance of folding and unfolding toward the latter, by destabilizing the folded form, as soluble, unfolded protein is found coexisting with the folded form.

An unexpected effect is shown for some second-shell residues for which non-conservative substitutions are preferable to conservative substitutions (Chapter 2 and Chapter 3). This observation supports the concept of a complex and extensive web of interactions inside the functional enzyme, especially around active site. Substitutions that influence the interactions of the side chain provoke changes in the whole web of interacting residues and cause a dramatic effect for the activity or stability of the protein. Substitutions that eliminate the interactions of the side chain affect the enzyme less. While the conserved second-shell residues are shown to play a role in ability of a protein to perform its function, substitutions in those residues sometimes occur and persist (Chapter 3 and Chapter 6). Such substitutions might change the substrate profile of the enzyme¹⁰¹ and some, due to the extreme importance of the residue, require a number of changes in the neighboring residues. Chapter 3 gives the example of Asn214 of said co-evolution, as in multiple β -lactamases the change in Asn214 is accompanied by a change in another conserved residue, Asp246, and a few first-shell residues. Although it is difficult to conclude what the exact order of mutation events was in the evolutionary process, the pattern in co-evolution is obvious. The role of the highly conserved triad discussed in chapter 3 needs more examination. Unfortunately, our attempts to crystallize BlaC mutants of this triad were not successful. Nevertheless, if the model of the mobile loop and helix that we describe is accurate, it is still possible that those changes would not be picked up in the crystal structure. Perhaps a better way to validate this model could be with paramagnetic NMR^{255–257}, a tool allowing for the determination of the three-dimensional structure of proteins and conformational heterogeneity.

Third-shell residues are shown to affect folding vs. aggregation rates or the thermodynamic balance between folded and unfolded (Chapter 2). Most mutations result in a heavily reduced amount of soluble protein. The folded fraction of such third-shell variants is remarkably

similar to wild type enzyme in stability, structure and activity (Chapter 4). Some mutations cause a fraction of soluble protein to remain unfolded, and the folded protein of these mutants often exhibits reduced thermostability. Effects of mutations in conserved residues on production and stability are well-known and they were also demonstrated for other proteins (e.g. ^{40,150,152}).

In contrast to the second-shell variants, substitutions in third-shell residues lead to localized structural effects, as observed both with NMR spectroscopy and crystallography. As the third-shell residues are involved in the formation of the correct three-dimensional fold, many of them are localized near the edges of the secondary structure elements and have interactions with nearby conserved residues, “stapling” the secondary structure elements together. The exact nature of the side chain of such residues is critical for the interactions they need to fulfill and, therefore, conservative substitutions in the third-shell residues are shown to be more beneficial than non-conservative ones.

Residues that were the focus of this study are highly conserved in class A β -lactamases. Harmful effects of substitutions in such essential residues were expected, still a few mutations did not cause a severe negative response in the enzyme. Two BlaC variants even displayed improved characteristics (Chapter 5). It is not obvious why these (nearly) neutral or beneficial substitutions are not found in natural variants of β -lactamases. It is possible that some residues are conserved for their essential role in most class A β -lactamases, but not necessarily all, as even closely related enzymes can take different evolutionary pathways. In that way, residues that are essential in most β -lactamases but not in BlaC can be considered an evolutionary rudiment in BlaC. Admittedly, based on our study conclusions can be made only about the effect of substitution on a limited number of enzyme properties. Furthermore, the changes in enzyme *in vitro* cannot be directly translated into changes that will take place in a living organism exposed to a pathogen carrying mutated enzyme. Zebrafish embryos are commonly used to study *Mycobacterium tuberculosis* infection (e.g. ^{258–261}), as they provide an immune response similar to that in humans. Thus, the idea to test these improved BlaC variants in a zebrafish embryo seems intriguing and most of all achievable. Such experiments are being started in the Ubbink group, in collaboration with the Meijer group at Leiden University. Moreover, it is not rare, that no change or improvement of one trait comes at a cost of another trait (e.g. ⁸²). In Chapter 2, we discuss a possibility of evolvability being one of such traits not tested within the scope of this research. For β -lactamases high evolvability is a crucial property, so high evolvability itself may have been optimized by evolution¹⁵. Some residues might be highly conserved to allow residues around it to be variable. As mentioned in Chapter 1, there is no consensus yet about the idea of evolution of evolvability. To date, it is stated that stability promotes evolvability^{24,25,33}, however, it is not known yet if the presence of specific residues can be one of the features benefiting or hindering evolvability via the

mechanism of influencing the variability of surrounding residues. That is a highly speculative idea that nevertheless is certainly interesting to test. One way to do that can be to perform laboratory evolution with wild type BlaC and an improved BlaC variant as a starting point to examine if a new function can be easier evolved in a wild type BlaC.

The work presented here offers the reasons for amino acid conservation, and it is our believe that these principles are general and applicable to essential amino acid residues in other enzymes. According to our data, the possible effects of mutations in conserved amino acid residue can be linked to their position in the structure (Figure 7.1a). Conserved residues of the first shell form a catalytic center of a protein, and therefore, substitutions are likely to result in an inactive protein or protein with changed activity. Conserved residues of the second shell establish a functional core of the protein, where they form a web of interactions around the active site, fine-tuning the structure of the active site. Changes in these residues result mostly in impaired stability, or stable enzyme with altered active site. The third-shell residues ensure the overall fold of an enzyme. Substitutions in these residues often have a dramatic negative effect on production of folded protein. Another possible effect that can be attributed to the mutations in the distant residues is an allosteric effect. The distance between allosteric ligand-binding sites and active sites was shown to range from 20 Å in hemoglobin to 60 Å in glycogen phosphorylase^{38,262}. These distances point to the third-shell residues being the ones involved in possible allostery. Activity modulation by a allosteric site was attributed to Trp229 in TEM-1 β -lactamase^{131,132}. Although the scope of this research did not concern protein dynamics, the importance of enzyme dynamics on its activity was demonstrated by various studies^{252,263,264}. A study by Elings *et al.* demonstrated how single substitutions in BlaC (in the first and the second-shell residues) can affect enzyme dynamics⁸³. And a few conserved residues from the third-shell were hypothesized to be involved in dynamics in BlaC in Chapter 2 of this work, however that requires further testing.

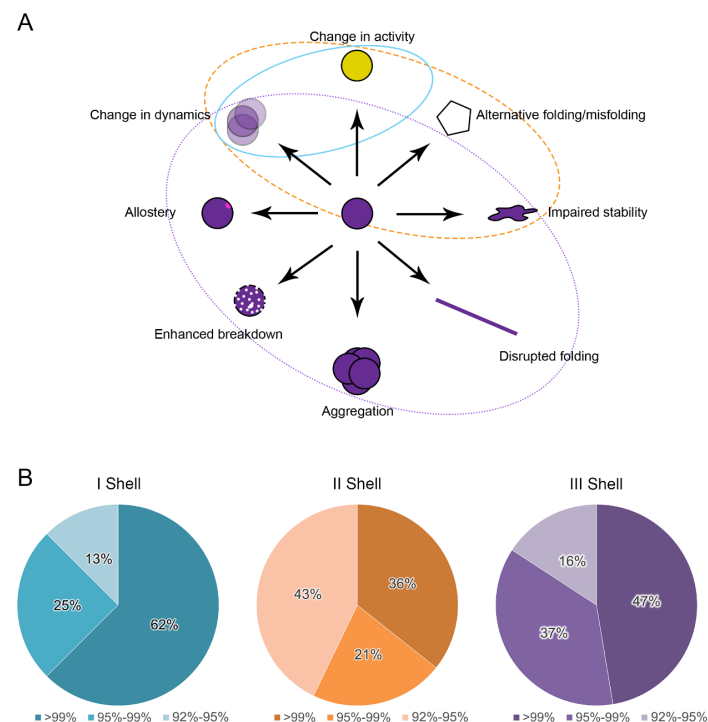


Figure 7.1. (A) Schematic representation of possible effects of mutation in a conserved residue. Circles show possible effects attributed to a mutation in the first (cyan), second (orange) and third (purple) shell; (B) Percentage of residues with conservation >99%, 95-99% and 92-95% in first (cyan), second (orange) and third (purple) shells.

Conserved residues of the second shell contribute to a high evolvability of the protein, as they protect the integrity of the active site, while random mutations can accumulate in and around the active site, possibly leading to a new trait. The conserved second-shell residues can in some instances mutate as well, leading to rearrangements in the binding site. One of the examples of such successful substitution is Gly132 in BlaC, which is believed to contribute to the broad antibiotic spectrum of this enzyme¹⁰¹, while most β -lactamases of class A carry Asn132. Conserved residues of the third-shell are frequently found at the edges of the secondary structure elements. In that way they contribute to a high evolutionary robustness of the protein, as they ensure the correct position of the secondary structure elements in three-dimensional space, allowing for substitutions to occur inside the secondary structure elements. These principles are also reflected in the conservation patterns of the residues of the different shells (Figure 7.1b). The conserved first-shell residues are mostly invariable with less conserved residues being the substrate-binding residues. While they are still highly conserved a certain degree of variability is likely responsible for adaptation of some

β -lactamases to specific substrates. The conservation of second-shell conserved residues is less extreme and as stated above that can leave some freedom for an active site evolution. The conserved third-shell residues are in general more conserved than the second-shell residues, as they are responsible for the three-dimensional frame formation, and it normally does not require any further adaptation.

Concluding remarks

The enzyme used in this study, BlaC from *Mycobacterium tuberculosis*, represents a good model system, but certainly it does not advocate for all β -lactamases. Although we consider our results as the general trend relevant for other β -lactamases and even other enzymes, this notion is based on the observed overall patterns and comparison with patterns described in literature. The results concerning the exact roles of amino acids in β -lactamases might hold some degree of ambiguity. Phenomena such as epistasis make it virtually impossible to use one enzyme to assign all specific functions of residues in related enzymes. Furthermore, experiments performed *in vivo* in this study were carried out in a model set-up in *Escherichia coli*, which clearly differs from *Mycobacterium tuberculosis*, as well as it differs from an “actual” *in vivo* set-up in a model organism. Nevertheless, the comparison of BlaC variants to unmodified BlaC made it possible to draw conclusions about the changes brought upon mutations.

The studies presented in this work serve a basis for our understanding of protein evolution. Surely such a topic cannot be fully clarified with one model system and limited set of tested properties. This thesis is merely a modest contribution to modern science, still, I believe, all small accomplishments will one day act as the building blocks for our comprehensive knowledge of such fundamental field as evolution.

References

1. Simpson, G. G. *Tempo and mode in evolution*. (New York : Columbia University Press, 1944).
2. Eldredge, N. Punctuated equilibria: an alternative to phyletic gradualism. 193–224 (1989). doi:10.1515/9781400860296.193
3. Darwin, C. R. *On the origin of species by means of natural selection, or the preservation of favoured races in the struggle for life. 5th edition*. (London: John Murray, 1869).
4. Smith, J. M. Natural selection and the concept of a protein space. *Nature* **225**, 563–564 (1970).
5. Kimura, M. & Ota, T. On some principles governing molecular evolution. *Proc. Natl. Acad. Sci. U. S. A.* **71**, 2848–2852 (1974).
6. Kimura, M. Molecular evolutionary clock and the neutral theory. *J. Mol. Evol.* **26**, 24–33 (1987).
7. Kimura, M. Preponderance of synonymous changes as evidence for the neutral theory of molecular evolution. *Nature* **267**, 275–276 (1977).
8. Bloom, J. D., Wilke, C. O., Arnold, F. H. & Adami, C. Stability and the evolvability of function in a model protein. *Biophys. J.* **86**, 2758–2764 (2004).
9. Gutin, A. M., Abkevich, V. I. & Shakhnovich, E. I. Evolution-like selection of fast-folding model proteins. *Proc. Natl. Acad. Sci. U. S. A.* **92**, 1282–1286 (1995).
10. Mélin, R., Li, H., Wingreen, N. S. & Tang, C. Designability, thermodynamic stability, and dynamics in protein folding: A lattice model study. *J. Chem. Phys.* **110**, 1252–1262 (1999).
11. Zeldovich, K. B., Chen, P. & Shakhnovich, E. I. Protein stability imposes limits on organism complexity and speed of molecular evolution. *Proc. Natl. Acad. Sci. U. S. A.* **104**, 16152–16157 (2007).
12. Govindarajan, S. & Goldstein, R. A. Evolution of model proteins on a foldability landscape. *Proteins* **29**, 461–466 (1997).
13. Bershtein, S., Goldin, K. & Tawfik, D. S. Intense neutral drifts yield robust and evolvable consensus proteins. *J. Mol. Biol.* **379**, 1029–1044 (2008).
14. Rennell, D., Bouvier, S. E., Hardy, L. W. & Poteete, A. R. Systematic mutation of bacteriophage T4 lysozyme. *J. Mol. Biol.* **222**, 67–88 (1991).
15. Stiffler, M. A., Hekstra, D. R. & Ranganathan, R. Evolvability as a function of purifying selection in TEM-1 β -lactamase. *Cell* **160**, 882–892 (2015).
16. Meini, M.-R., Llarrull, L. I. & Vila, A. J. Evolution of metallo- β -lactamases: trends revealed by natural diversity and in vitro evolution. *Antibiot. (Basel, Switzerland)* **3**, 285–316 (2014).
17. Dellus-Gur, E., Toth-Petroczy, A., Elias, M. & Tawfik, D. S. What makes a protein fold amenable to functional innovation? fold polarity and stability trade-offs. *J. Mol. Biol.* **425**, 2609–2621 (2013).
18. Draghi, J. A., Parsons, T. L., Wagner, G. P. & Plotkin, J. B. Mutational robustness can facilitate adaptation. *Nature* **463**, 353–355 (2010).
19. McBride, R. C., Ogbunugafor, C. B. & Turner, P. E. Robustness promotes evolvability of thermotolerance in an RNA virus. *BMC Evol. Biol.* **8**, 231 (2008).
20. Lynch, M. The frailty of adaptive hypotheses for the origins of organismal complexity. *Proc. Natl. Acad. Sci. U. S. A.* **104 Suppl**, 8597–8604 (2007).
21. Sniegowski, P. D. & Murphy, H. A. Evolvability. *Curr. Biol.* **16**, R831-4 (2006).
22. Draghi, J. & Wagner, G. P. Evolution of evolvability in a developmental model. *Evolution* **62**, 301–315 (2008).
23. Pigliucci, M. Is evolvability evolvable? *Nat. Rev. Genet.* **9**, 75–82 (2008).
24. Zheng, J., Guo, N. & Wagner, A. Selection enhances protein evolvability by increasing mutational robustness and foldability. *Science* **370**, eabb5962 (2020).
25. Tokuriki, N. & Tawfik, D. S. Stability effects of mutations and protein evolvability. *Curr. Opin. Struct. Biol.* **19**, 596–604 (2009).
26. Meiering, E. M., Serrano, L. & Fersht, A. R. Effect of active site residues in barnase on activity and stability. *J. Mol. Biol.* **225**, 585–589 (1992).
27. Beadle, B. M. & Shoichet, B. K. Structural bases of stability-function tradeoffs in enzymes. *J. Mol. Biol.* **321**, 285–296 (2002).
28. Wang, X., Minasov, G. & Shoichet, B. K. The structural bases of antibiotic resistance in the clinically derived mutant β -lactamases TEM-30, TEM-32, and TEM-34. *J. Biol. Chem.* **277**, 32149–32156 (2002).
29. Schreiber, G., Buckle, A. M. & Fersht, A. R. Stability and function: two constraints in the evolution of barstar and other proteins. *Structure* **2**, 945–951 (1994).
30. Arnold, F. H. How proteins adapt: Lessons from directed evolution. *Cold Spring Harb. Symp. Quant. Biol.* **74**, 41–46 (2009).
31. Risso, V. A. *et al.* Mutational studies on resurrected ancestral proteins reveal conservation of site-specific amino acid preferences throughout evolutionary history. *Mol. Biol. Evol.* **32**, 440–455 (2015).
32. Tokuriki, N., Stricher, F., Serrano, L. & Tawfik, D. S. How protein stability and new functions trade off. *PLoS Comput. Biol.* **4**, 35–37 (2008).
33. Bloom, J. D., Labthavikul, S. T., Otey, C. R. & Arnold, F. H. Protein stability promotes evolvability. *Proc. Natl. Acad. Sci. U. S. A.* **103**, 5869–5874 (2006).
34. Valdar, W. S. J. Scoring residue conservation. *Proteins Struct. Funct. Genet.* **48**, 227–241 (2002).
35. Lichtarge, O., Bourne, H. R. & Cohen, F. E. An evolutionary trace method defines binding surfaces common to protein families. *J Mol Biol.* **257**, 342–358 (1996).
36. Landgraf, R., Xenarios, I. & Eisenberg, D. Three-dimensional cluster analysis identifies interfaces and functional residue clusters in proteins. *J. Mol. Biol.* **307**, 1487–1502 (2001).
37. Del Sol Mesa, A., Pazos, F. & Valencia, A. Automatic methods for predicting functionally important residues. *J. Mol. Biol.* **326**, 1289–1302 (2003).
38. Jack, B. R., Meyer, A. G., Echave, J. & Wilke, C. O. Functional sites induce long-range evolutionary constraints in enzymes. *PLoS Biol.* **14**, 1–23 (2016).
39. Shakhnovich, E., Abkevich, V. & Ptitsyn, O. Conserved residues and the mechanism of protein folding. *Nature* **379**, 96–98 (1996).
40. Kragelund, B. B. *et al.* Conserved residues and their role in the structure, function, and stability of acyl-coenzyme A binding protein. *Biochemistry* **38**, 2386–2394 (1999).
41. Ptitsyn, O. B. & Ting, K. L. H. Non-functional conserved residues in globins and their possible role as a folding nucleus. *J. Mol. Biol.* **291**, 671–682 (1999).

42. Mirny, L. A. & Shakhnovich, E. I. Universally conserved positions in protein folds: Reading evolutionary signals about stability, folding kinetics and function. *J. Mol. Biol.* **291**, 177–196 (1999).
43. Khor, B. Y., Tye, G. J., Lim, T. S. & Choong, Y. S. General overview on structure prediction of twilight-zone proteins. *Theor. Biol. Med. Model.* **12**, 15 (2015).
44. Schueler-Furman, O. & Baker, D. Conserved residue clustering and protein structure prediction. *Proteins* **52**, 225–235 (2003).
45. Guharoy, M. & Chakrabarti, P. Conserved residue clusters at protein-protein interfaces and their use in binding site identification. *BMC Bioinformatics* **11**, 286 (2010).
46. Nerlich, A. G., Haas, C. J., Zink, A., Szeimies, U. & Hagedorn, H. G. Molecular evidence for tuberculosis in an ancient Egyptian mummy [10]. *Lancet* **350**, 1404 (1997).
47. Crubézy, E. *et al.* Identification of Mycobacterium DNA in an Egyptian Pott's disease of 5,400 years old. *C. R. Acad. Sci. III.* **321**, 941–951 (1998).
48. Donoghue, H. D. *et al.* Tuberculosis in Dr Granville's mummy: a molecular re-examination of the earliest known Egyptian mummy to be scientifically examined and given a medical diagnosis. *Proceedings. Biol. Sci.* **277**, 51–56 (2010).
49. Hershkovitz, I. *et al.* Detection and molecular characterization of 9,000-year-old Mycobacterium tuberculosis from a Neolithic settlement in the Eastern Mediterranean. *PLoS One* **3**, e3426 (2008).
50. Zink, A. R., Grabner, W., Reischl, U., Wolf, H. & Nerlich, A. G. Molecular study on human tuberculosis in three geographically distinct and time delineated populations from ancient Egypt. *Epidemiol. Infect.* **130**, 239–249 (2003).
51. O'Neill, M. B. *et al.* Lineage specific histories of Mycobacterium tuberculosis dispersal in Africa and Eurasia. *Mol. Ecol.* **28**, 3241–3256 (2019).
52. *Global tuberculosis report 2021. Geneva: World Health Organization.* (Licence: CC BY-NC-SA 3.0 IGO, 2021).
53. Major 1884-, R. H. *Classic descriptions of disease: with biographical sketches of the authors.* (Springfield, Ill. : Charles C. Thomas, 1945).
54. Daniel, V. S. & Daniel, T. M. Old Testament Biblical References to Tuberculosis. *Clin. Infect. Dis.* **29**, 1557–1558 (2002).
55. Bronte, E. *Wuthering Heights.* (Andrews UK, 2011).
56. Brites, D. & Gagneux, S. Co-evolution of Mycobacterium tuberculosis and Homo sapiens. *Immunol. Rev.* **264**, 6–24 (2015).
57. Dossey, L. The royal touch: a look at healing in times past. *Explore* **9** 3, 121–127 (2013).
58. Riva, M. A. From milk to rifampicin and back again: History of failures and successes in the treatment for tuberculosis. *J. Antibiot. (Tokyo).* **67**, 661–665 (2014).
59. Daniel, T. M. Leon Charles Albert Calmette and BCG vaccine. *Int. J. Tuberc. lung Dis. Off. J. Int. Union against Tuberc. Lung Dis.* **9**, 944–945 (2005).
60. Schatz, A., Bugle, E. & Waksman, S. A. Streptomycin, a substance exhibiting antibiotic activity against Gram-positive and Gram-negative bacteria. *Proc. Soc. Exp. Biol. Med.* **55**, 66–69 (1944).
61. Lehmann, J. E. Twenty years afterward historical notes on the discovery of the antituberculosis effect of paraaminosalicylic acid (PAS) and the first clinical trials. *Am. Rev. Respir. Dis.* **90**, 953–956 (1964).
62. Millard, J., Ugarte-Gil, C. & Moore, D. A. J. Multidrug resistant tuberculosis. *BMJ* **350**, h882 (2015).
63. Centers for Disease Control and Prevention (CDC). Emergence of Mycobacterium tuberculosis with extensive resistance to second-line drugs--worldwide, 2000-2004. *MMWR. Morb. Mortal. Wkly. Rep.* **55**, 301–5 (2006).
64. World Health Organisation. WHO | Drug-resistant TB: Totally drug-resistant TB FAQ. *WHO* (2018).
65. Rowland, K. Totally drug-resistant TB emerges in India. *Nature* (2012). doi:10.1038/nature.2012.9797
66. Velayati, A. A. *et al.* Emergence of new forms of totally drug-resistant tuberculosis bacilli: super extensively drug-resistant tuberculosis or totally drug-resistant strains in Iran. *Chest* **136**, 420–425 (2009).
67. Udawadia, Z. F., Amale, R. A., Ajbani, K. K. & Rodrigues, C. Totally Drug-Resistant Tuberculosis in India. *Clin. Infect. Dis.* **54**, 579–581 (2012).
68. Plackett, B. No money for new drugs. *Nat. Outlook* **586**, S50–S52 (2020).
69. Tan, S. Y. & Tatsumura, Y. Alexander Fleming (1881-1955): Discoverer of penicillin. *Singapore Med. J.* **56**, 366–367 (2015).
70. Fernandes, R., Amador, P. & Prudêncio, C. β -Lactams: chemical structure, mode of action and mechanisms of resistance. *Rev. Med. Microbiol.* **24**, (2013).
71. Voladri, R. K. *et al.* Recombinant expression and characterization of the major beta-lactamase of Mycobacterium tuberculosis. *Antimicrob. Agents Chemother.* **42**, 1375–1381 (1998).
72. Fisher, J. F., Meroueh, S. O. & Mobashery, S. Bacterial resistance to beta-lactam antibiotics: compelling opportunism, compelling opportunity. *Chem. Rev.* **105**, 395–424 (2005).
73. Chambers, H. F. *et al.* Can penicillins and other β -lactam antibiotics be used to treat tuberculosis? *Antimicrob. Agents Chemother.* **39**, 2620–2624 (1995).
74. Forsman, L. D. *et al.* Meropenem-clavulanic acid has high in vitro activity against multidrug-resistant Mycobacterium tuberculosis. *Antimicrob. Agents Chemother.* **59**, 3630–3632 (2015).
75. Sharma, A. K. & Vats, P. Evaluation of biochemical and molecular polymorphism in extended spectrum β -lactamases of Mycobacterium tuberculosis clinical isolates. *Indian J. Tuberc.* **66**, 92–98 (2019).
76. Li, F. *et al.* In Vitro Activity of β -Lactams in Combination with β -Lactamase Inhibitors against Mycobacterium tuberculosis Clinical Isolates. *Biomed Res. Int.* **2018**, 1–8 (2018).
77. Dinçer, I., Ergin, A. & Kocagöz, T. The vitro efficacy of β -lactam and β -lactamase inhibitors against multidrug resistant clinical strains of Mycobacterium tuberculosis. *Int. J. Antimicrob. Agents* **23**, 408–411 (2004).
78. Davies Forsman, L. *et al.* Meropenem-clavulanate has high in vitro activity against multidrug-resistant Mycobacterium tuberculosis. *Int. J. mycobacteriology* **4**, 80–81 (2015).
79. Drawz, S. M. & Bonomo, R. A. Three decades of β -lactamase inhibitors. *Clin. Microbiol. Rev.* **23**, 160–201 (2010).
80. Kurz, S. G. *et al.* Can inhibitor-resistant substitutions in the Mycobacterium tuberculosis β -lactamase BlaC lead to clavulanate resistance?: a biochemical rationale for the use of β -lactam- β -lactamase inhibitor combinations. *Antimicrob. Agents Chemother.* **57**, 6085–6096 (2013).

81. Egesborg, P., Carlettini, H., Volpato, J. P. & Doucet, N. Combinatorial active-site variants confer sustained clavulanate resistance in BlaC β -lactamase from *Mycobacterium tuberculosis*. *Protein Sci.* **24**, 534–544 (2015).
82. Alen, I. van *et al.* Mutation G132S enhances resistance of *Mycobacterium tuberculosis* β -lactamase against sulbactam. *Biochemistry* **60**, 2236–2245 (2021).
83. Elings, W. *et al.* Two β -lactamase variants with reduced clavulanic acid inhibition display different millisecond dynamics. *Antimicrob. Agents Chemother.* **65**, (2021).
84. Soroka, D. *et al.* Hydrolysis of clavulanate by *Mycobacterium tuberculosis* β -lactamase BlaC harboring a canonical SDN motif. *Antimicrob. Agents Chemother.* **59**, 5714–5720 (2015).
85. Soroka, D. *et al.* Inhibition of β -lactamases of mycobacteria by avibactam and clavulanate. *J. Antimicrob. Chemother.* **72**, 1081–1088 (2017).
86. Abraham, E. Roots: Selective reminiscences of β -lactam antibiotics: Early research on penicillin and cephalosporins. *Bioessays* **12**, 601–606 (1990).
87. Davies, J. Origins and evolution of antibiotic resistance. *Microbiologia* **12**, 9–16 (1996).
88. Nielsen, J. B. & Lampen, J. O. Membrane-bound penicillinases in Gram-positive bacteria. *J. Biol. Chem.* **257**, 4490–4495 (1982).
89. Ambler, R. P. *et al.* A standard numbering scheme for the Class A β -lactamases. *Biochem.J* **276**, 269–270 (1991).
90. Knott-Hunziker, V. *et al.* Active sites of beta-lactamases. The chromosomal beta-lactamases of *Pseudomonas aeruginosa* and *Escherichia coli*. *Biochem. J.* **201**, 621–7 (1982).
91. Pernot, L. *et al.* Crystal structures of the class D β -lactamase OXA-13 in the native form and in complex with meropenem. *J. Mol. Biol.* **310**, 859–874 (2001).
92. Sielecki, A. *et al.* Molecular structure of the acyl-enzyme intermediate in β -lactam hydrolysis at 1.7 Å resolution. *Nature* **359**, 700–705 (2003).
93. Carfi, A. *et al.* The 3-D structure of a zinc metallo-beta-lactamase from *Bacillus cereus* reveals a new type of protein fold. *EMBO J.* **14**, 4914–21 (1995).
94. Wang, Z., Fast, W. & Benkovic, S. J. On the mechanism of the metallo- β -lactamase from *Bacteroides fragilis*. *Biochemistry* **38**, 10013–10023 (1999).
95. Macheboeuf, P., Contreras-Martel, C., Job, V., Dideberg, O. & Dessen, A. Penicillin binding proteins: key players in bacterial cell cycle and drug resistance processes. *FEMS Microbiol. Rev.* **30**, 673–691 (2006).
96. Sauvage, E., Kerff, F., Terrak, M., Ayala, J. A. & Charlier, P. The penicillin-binding proteins: structure and role in peptidoglycan biosynthesis. *FEMS Microbiol. Rev.* **32**, 234–258 (2008).
97. Massova, I. & Mobashery, S. Kinship and diversification of bacterial penicillin-binding proteins and β -lactamases. *Antimicrob Agents Chemother* **42**, 1–17 (1998).
98. Bush, K. Characterization of β -lactamases. *Antimicrob. Agents Chemother.* **33**, 259–263 (1989).
99. Bush, K., Jacoby, G. A. & Medeiros, A. A. A functional classification scheme for β -lactamases and its correlation with molecular structure. *Antimicrob. Agents Chemother.* **39**, 1211–1233 (1995).
100. Bush, K. & Jacoby, G. A. Updated functional classification of β -lactamases. *Antimicrob. Agents Chemother.* **54**, 969–976 (2010).
101. Wang, F., Cassidy, C. & Sacchettini, J. C. Crystal structure and activity studies of the *Mycobacterium tuberculosis* β -lactamase reveal its critical role in resistance to β -lactam antibiotics. *Antimicrob. Agents Chemother.* **50**, 2762–2771 (2006).
102. Hugonnet, J. E. & Blanchard, J. S. Irreversible inhibition of the *Mycobacterium tuberculosis* β -lactamase by clavulanate. *Biochemistry* **46**, 11998–12004 (2007).
103. Tremblay, L. W., Fan, F. & Blanchard, J. S. Biochemical and structural characterization of *Mycobacterium tuberculosis* beta-lactamase with the carbapenems ertapenem and doripenem. *Biochemistry* **49**, 3766–3773 (2010).
104. Leiros, H.-K. S. *et al.* His224 alters the R2 drug binding site and Phe218 influences the catalytic efficiency of the metallo- β -lactamase VIM-7. *Antimicrob. Agents Chemother.* **58**, 4826–4836 (2014).
105. Na, J.-H., An, Y. J. & Cha, S.-S. GMP and IMP are competitive inhibitors of CMY-10, an extended-spectrum class C β -lactamase. *Antimicrob. Agents Chemother.* **61**, e00098-17 (2017).
106. Golemi, D., Maveyraud, L., Vakulenko, S., Samama, J. P. & Mobashery, S. Critical involvement of a carbamylated lysine in catalytic function of class D beta-lactamases. *Proc. Natl. Acad. Sci. U. S. A.* **98**, 14280–14285 (2001).
107. Yamada, M. *et al.* Crystal structure of cefditoren complexed with *Streptococcus pneumoniae* penicillin-binding protein 2X: structural basis for its high antimicrobial activity. *Antimicrob. Agents Chemother.* **51**, 3902–3907 (2007).
108. Armon, A., Graur, D. & Ben-Tal, N. ConSurf: An algorithmic tool for the identification of functional regions in proteins by surface mapping of phylogenetic information. *J. Mol. Biol.* **307**, 447–463 (2001).
109. Ashkenazy, H., Erez, E., Martz, E., Pupko, T. & Ben-Tal, N. ConSurf 2010: Calculating evolutionary conservation in sequence and structure of proteins and nucleic acids. *Nucleic Acids Res.* **38**, 529–533 (2010).
110. Strynadka, N. C. J. *et al.* Molecular structure of the acyl-enzyme intermediate in β -lactam hydrolysis at 1.7 Å resolution. *Nature* **359**, 700–705 (1992).
111. Díaz, N., Sordo, T. L., Merz, K. M. J. & Suárez, D. Insights into the acylation mechanism of class A beta-lactamases from molecular dynamics simulations of the TEM-1 enzyme complexed with benzylpenicillin. *J. Am. Chem. Soc.* **125**, 672–684 (2003).
112. Knox, J. R., Moews, P. C., Escobar, W. A. & Fink, A. L. A catalytically-impaired class A beta-lactamase: 2 Å crystal structure and kinetics of the *Bacillus licheniformis* E166A mutant. *Protein Eng.* **6**, 11–18 (1993).
113. Guillaume, G. *et al.* Site-directed mutagenesis of glutamate 166 in two beta-lactamases. Kinetic and molecular modeling studies. *J. Biol. Chem.* **272**, 5438–5444 (1997).
114. Meroueh, S. O., Fisher, J. F., Schlegel, H. B. & Mobashery, S. Ab initio QM/MM study of class A beta-lactamase acylation: dual participation of Glu166 and Lys73 in a concerted base promotion of Ser70. *J. Am. Chem. Soc.* **127**, 15397–15407 (2005).
115. Herzberg, O. & Moulton, J. Bacterial resistance to beta-lactam antibiotics: crystal structure of beta-lactamase from *Staphylococcus aureus* PC1 at 2.5 Å resolution. *Science* **236**, 694–701 (1987).
116. Herzberg, O. Refined crystal structure of β -lactamase from *Staphylococcus aureus* PC1 at 2.0 Å resolution. *J. Mol. Biol.* **217**, 701–719 (1991).

117. Bennur, T., Kumar, A. R., Zinjarde, S. & Javdekar, V. Nocardiosis species: Incidence, ecological roles and adaptations. *Microbiol. Res.* **174**, 33–47 (2015).
118. Ellerby, L. M., Escobar, W. A., Fink, A. L., Mitchinson, C. & Wells, J. A. The role of lysine-234 in beta-lactamase catalysis probed by site-directed mutagenesis. *Biochemistry* **29**, 5797–5806 (1990).
119. Lenfant, F., Labia, R. & Masson, J. M. Replacement of lysine 234 affects transition state stabilization in the active site of beta-lactamase TEM1. *J. Biol. Chem.* **169**, 17187–17194 (1991).
120. Lim, D. *et al.* Insights into the molecular basis for the carbenicillinase activity of PSE-4 β -lactamase from crystallographic and kinetic studies. *Biochemistry* **40**, 395–402 (2001).
121. Mendonça, N. *et al.* The Lys234Arg substitution in the enzyme SHV-72 is a determinant for resistance to clavulanic acid inhibition. *Antimicrob. Agents Chemother.* **52**, 1806–1811 (2008).
122. Soeung, V. *et al.* A drug-resistant β -lactamase variant changes the conformation of its active site proton shuttle to alter substrate specificity and inhibitor potency. *J. Biol. Chem.* 18239–18255 (2020).
123. Patel, M. P. *et al.* Synergistic effects of functionally distinct substitutions in β -lactamase variants shed light on the evolution of bacterial drug resistance. *J. Biol. Chem.* **293**, 17971–17984 (2018).
124. Banerjee, S. *et al.* Probing the non-proline cis peptide bond in β -lactamase from *Staphylococcus aureus* PC1 by the replacement Asn136 \rightarrow Ala. *Biochemistry* **36**, 10857–10866 (1997).
125. Jacob, F., Joris, B., Lepage, S., Dusart, J. & Frère, J. M. Role of the conserved amino acids of the ‘SDN’ loop (Ser130, Asp131 and Asn132) in a class A beta-lactamase studied by site-directed mutagenesis. *Biochem. J.* **271**, 399–406 (1990).
126. Swarén, P. *et al.* Electrostatic analysis of TEM1 β -lactamase: effect of substrate binding, steep potential gradients and consequences of site-directed mutations. *Structure* **3**, 603–613 (1995).
127. Wang, X., Minasov, G. & Shoichet, B. K. Evolution of an antibiotic resistance enzyme constrained by stability and activity trade-offs. *J. Mol. Biol.* **320**, 85–95 (2002).
128. Vakulenko, S. B., Tóth, M., Taibi, P., Mobashery, S. & Lerner, S. A. Effects of Asp-179 mutations in TEMpUC19 beta-lactamase on susceptibility to beta-lactams. *Antimicrob. Agents Chemother.* **39**, 1878–1880 (1995).
129. Vakulenko, S. B. *et al.* Effects on substrate profile by mutational substitutions at positions 164 and 179 of the class A TEM(pUC19) beta-lactamase from *Escherichia coli*. *J. Biol. Chem.* **274**, 23052–23060 (1999).
130. Castanheira, M. *et al.* Analyses of a ceftazidime-avibactam-resistant *Citrobacter freundii* isolate carrying bla (KPC-2) reveals a heterogeneous population and reversible genotype. *mSphere* **3**, (2018).
131. Avci, F. G., Altinisik, F. E., Vardar Ulu, D., Ozkirimli Olmez, E. & Sariyar Akbulut, B. An evolutionarily conserved allosteric site modulates beta-lactamase activity. *J. Enzyme Inhib. Med. Chem.* **31**, 33–40 (2016).
132. Meneksedag, D., Dogan, A., Kanlikilicer, P. & Ozkirimli, E. Communication between the active site and the allosteric site in class A beta-lactamases. *Comput. Biol. Chem.* **43**, 1–10 (2013).
133. Sitbon, E. & Pietrovski, S. Occurrence of protein structure elements in conserved sequence regions. *BMC Struct. Biol.* **7**, 1–15 (2007).
134. Saldaña, T. E., Monzon, A. M., Parisi, G. & Fernandez-Alberti, S. Evolutionary conserved positions define protein conformational diversity. *PLoS Comput. Biol.* **12**, 1–25 (2016).
135. Medeiros, A. A. β -Lactamases. *Br. Med. Bull.* **40**, 18–27 (1984).
136. Petrosino, J., Cantu, C. & Palzkill, T. β -Lactamases: Protein evolution in real time. *Trends Microbiol.* **6**, 323–327 (1998).
137. Bonomo, R. A., Rudin, S. D. & Shlaes, D. M. OHIO-1 β -lactamase mutants: Asp179Gly mutation confers resistance to ceftazidime. *FEMS Microbiol. Lett.* **152**, 275–278 (1997).
138. Vakulenko, S. & Golemi, D. Mutant TEM β -lactamase producing resistance to ceftazidime, ampicillins, and β -lactamase inhibitors. *Antimicrob. Agents Chemother.* **46**, 646–653 (2002).
139. Stürenburg, E., Kühn, A., Mack, D. & Laufs, R. A novel extended-spectrum beta-lactamase CTX-M-23 with a P167T substitution in the active-site omega loop associated with ceftazidime resistance. *J. Antimicrob. Chemother.* **54**, 406–409 (2004).
140. Berezin, C. *et al.* ConSeq: The identification of functionally and structurally important residues in protein sequences. *Bioinformatics* **20**, 1322–1324 (2004).
141. Tassoni, R., Blok, A., Pannu, N. S. & Ubbink, M. New conformations of acylation adducts of inhibitors of β -lactamase from *Mycobacterium tuberculosis*. *Biochemistry* **58**, 997–1009 (2019).
142. Lamotte-Brasseur, J. *et al.* Mechanism of acyl transfer by the class A serine β -lactamase of *Streptomyces albus* G. *Biochem. J.* **279**, 213–221 (1991).
143. Tremblay, L. W., Hugonnet, J. & Blanchard, J. S. Structure of the covalent adduct formed between *Mycobacterium tuberculosis*. *Am. Chem. Soc.* **47**, 5312–5316 (2008).
144. Juteau, J. M., Billings, E., Knox, J. R. & Levesque, R. C. Site-saturation mutagenesis and three-dimensional modelling of ROB-1 define a substrate binding role of Ser130 in class A beta-lactamases. *Protein Eng.* **5**, 693–701 (1992).
145. Chikunova, A. *et al.* Conserved residues Glu37 and Trp229 play an essential role in protein folding of β -lactamase. *FEBS J.* **288**, 5708–5722 (2021).
146. Delmas, J., Robin, F., Bittar, F., Chanal, C. & Bonnet, R. Unexpected enzyme TEM-126: Role of mutation Asp179Glu. *Antimicrob. Agents Chemother.* **49**, 4280–4287 (2005).
147. McDonough, J. A. *et al.* Identification of functional Tat signal sequences in *Mycobacterium tuberculosis* proteins. *J. Bacteriol.* **190**, 6428–6438 (2008).
148. Gronenborn, A. M. & Clore, G. M. Rapid screening for structural integrity of expressed proteins by heteronuclear NMR spectroscopy. *Protein Sci.* **5**, 174–177 (1996).
149. Lobkovsky, A. E., Wolf, Y. I. & Koonin, E. V. Universal distribution of protein evolution rates as a consequence of protein folding physics. *Proc. Natl. Acad. Sci. U. S. A.* **107**, 2983–2988 (2010).
150. Philip, A. F., Kumauchi, M. & Hoff, W. D. Robustness and evolvability in the functional anatomy of a PER-ARNT-SIM (PAS) domain. *Proc. Natl. Acad. Sci. U. S. A.* **107**, 17986–17991 (2010).
151. Zayner, J. P., Antoniou, C., French, A. R., Hause, R. J. & Sosnick, T. R. Investigating models of protein function and allostery with a widespread mutational analysis of a light-activated protein. *Biophys. J.* **105**, 1027–1036 (2013).
152. Allocati, N., Masulli, M., Pietracupa, M., Federici, L. & Di Ilio, C. Evolutionary conserved structural motifs in bacterial GST (glutathione S-transferase) are involved in protein folding and stability. *Biochem. J.* **394**, 11–17 (2006).

153. Yampolsky, L. Y. & Stoltzfus, A. The exchangeability of amino acids in proteins. *Genetics* **170**, 1459–1472 (2005).
154. Marsh, L. A model for protein sequence evolution based on selective pressure for protein stability: Application to hemoglobins. *Evol. Bioinforma.* **2009**, 107–118 (2009).
155. Tokuriki, N. & Tawfik, D. S. Chaperonin overexpression promotes genetic variation and enzyme evolution. *Nature* **459**, 668–673 (2009).
156. Karshikoff, A., Nilsson, L. & Ladenstein, R. Rigidity versus flexibility: the dilemma of understanding protein thermal stability. *FEBS J.* **282**, 3899–3917 (2015).
157. Andrews, L. D., Fenn, T. D. & Herschlag, D. Ground state destabilization by anionic nucleophiles contributes to the activity of phosphoryl transfer enzymes. *PLoS Biol.* **11**, e1001599 (2013).
158. Modi, T., Campitelli, P., Kazan, I. C. & Ozkan, S. B. Protein folding stability and binding interactions through the lens of evolution: a dynamical perspective. *Curr. Opin. Struct. Biol.* **66**, 207–215 (2021).
159. Veronica R. Moorman, Kathleen G. Valentine, Sabrina Bédard, Vignesh Kasinath, Jakob Dogan, Fiona M. Love, and A. J. W. Dynamic and thermodynamic response of the Ras protein Cdc42Hs upon association with the effector domain of PAK3. *J Mol Biol.* **426**, 3520–3538 (2015).
160. Pabis, A., Risso, V. A., Sanchez-Ruiz, J. M. & Kamerlin, S. C. Cooperativity and flexibility in enzyme evolution. *Curr. Opin. Struct. Biol.* **48**, 83–92 (2018).
161. Whitacre, J. M. Degeneracy: A link between evolvability, robustness and complexity in biological systems. *Theor. Biol. Med. Model.* **7**, 1–12 (2010).
162. Payne, J. *et al.* Transition bias influences the evolution of antibiotic resistance in Mycobacterium tuberculosis. *PLoS Biol.* **17**, (2018).
163. Consortium, T. U. UniProt: the universal protein knowledgebase in 2021. *Nucleic Acids Res.* **49**, 480–489 (2021).
164. Katoh, K., Misawa, K., Kuma, K. I. & Miyata, T. MAFFT: A novel method for rapid multiple sequence alignment based on fast Fourier transform. *Nucleic Acids Res.* **30**, 3059–3066 (2002).
165. McDonough, J. A., Hacker, K. E., Flores, A. R., Pavelka, M. S. & Braunstein, M. The twin-arginine translocation pathway of Mycobacterium smegmatis is functional and required for the export of mycobacterial β -lactamases. *J. Bacteriol.* **187**, 7667–7679 (2005).
166. Raran-Kurussi, S., Cherry, S., Zhang, D. & Waugh, D. S. Removal of affinity tags with TEV protease. *Methods Mol Biol.* **1586**, 221–230 (2017).
167. Skinner, S. P. *et al.* CcpNmr AnalysisAssign: a flexible platform for integrated NMR analysis. *J. Biomol. NMR* **66**, 111–124 (2016).
168. Cartwright, S. J., Tan, A. K. & Fink, A. L. Trapping the acyl-enzyme intermediate in β -lactamase I catalysis. *Biochem. J.* **263**, 905–912 (1989).
169. Waley, P. J. M. and S. G. b-Lactamase I from Bacillus cereus. *Biochem J* **248**, 657–662 (1987).
170. Roccatano, D. *et al.* Dynamical aspects of TEM-1 β -Lactamase probed by molecular dynamics. *J. Comput. Aided. Mol. Des.* **19**, 329–340 (2005).
171. Ruggiero, M. *et al.* Crystal structure of the extended-spectrum β -lactamase PER-2 and insights into the role of specific residues in the interaction with β -lactams and β -lactamase inhibitors. *Antimicrob. Agents Chemother.* **58**, 5994–6002 (2014).
172. Tranier, S. *et al.* The high resolution crystal structure for class A β -lactamase PER-1 reveals the bases for its increase in breadth of activity. *J. Biol. Chem.* **275**, 28075–28082 (2000).
173. Huang, W., Petrosino, J., Hirsch, M., Shenkin, P. S. & Palzkill, T. Amino acid sequence determinants of β -lactamase structure and activity. *J. Mol. Biol.* **258**, 688–703 (1996).
174. Poirel, L. *et al.* GES-2, a class A β -lactamase from Pseudomonas aeruginosa with increased hydrolysis of imipenem. *Antimicrob. Agents Chemother.* **45**, 2598–2603 (2001).
175. Smith, C. A., Caccamo, M., Kantardjieff, K. A. & Vakulenko, S. Structure of GES-1 at atomic resolution: Insights into the evolution of carbapenamase activity in the class A extended-spectrum β -lactamases. *Acta Crystallogr. Sect. D Biol. Crystallogr.* **63**, 982–992 (2007).
176. Klein, R. *et al.* Targeting the class a carbapenamase GES-5 via virtual screening. *Biomolecules* **10**, 1–10 (2020).
177. Bebrone, C. *et al.* GES-18, a new carbapenem-hydrolyzing GES-type β -lactamase from Pseudomonas aeruginosa that contains Ile80 and Ser170 residues. *Antimicrob. Agents Chemother.* **57**, 396–401 (2013).
178. Delbrück, H. *et al.* Kinetic and crystallographic studies of extended-spectrum GES-11, GES-12, and GES-14 β -lactamases. *Antimicrob. Agents Chemother.* **56**, 5618–5625 (2012).
179. Rogers, M. B., Parker, A. C. & Smith, C. J. Cloning and characterization of the endogenous cephalosporinase gene, cepA, from bacteroides fragilis reveals a new subgroup of Ambler class A β -lactamases. *Antimicrob. Agents Chemother.* **37**, 2391–2400 (1993).
180. Morin, A. S., Poirel, L., Mory, F., Labia, R. & Nordmann, P. Biochemical-genetic analysis and distribution of DES-1, an Ambler class A extended-spectrum β -lactamase from Desulfovibrio desulfuricans. *Antimicrob. Agents Chemother.* **46**, 3215–3222 (2002).
181. Sawyer, L. & James, M. N. G. Carboxyl–carboxylate interactions in proteins. *Nature* **295**, 79–80 (1982).
182. Lin, J., Pozharski, E. & Wilson, M. A. Short Carboxylic Acid-Carboxylate Hydrogen Bonds Can Have Fully Localized Protons. *Biochemistry* **56**, 391–402 (2017).
183. Nichols, D. A. *et al.* Ligand-induced proton transfer and low-barrier hydrogen bond revealed by X-ray crystallography. *J. Am. Chem. Soc.* **137**, 8086–8095 (2016).
184. Huynh, K. & Partch, C. L. Analysis of protein stability and ligand interactions by thermal shift assay. *Curr. Protoc. protein Sci.* **79**, 28.9.1-28.9.14 (2015).
185. Jacob-Dubuisson, F., Lamotte-Brasseur, J., Dideberg, O., Joris, B. & Frère, J. M. Arginine 220 is a critical residue for the catalytic mechanism of the Streptomyces albus g β -lactamase. *Protein Eng. Des. Sel.* **4**, 811–819 (1991).
186. Yang, Y., Rasmussen, B. A. & Shlaes, D. M. Class A β -lactamases - Enzyme-inhibitor interactions and resistance. *Pharmacol. Ther.* **83**, 141–151 (1999).
187. Ruggiero, M. *et al.* Impact of mutations at Arg220 and Thr237 in PER-2 β -Lactamase on conformation, activity, and susceptibility to inhibitors. *Antimicrob. Agents Chemother.* **61**, 1–8 (2017).

188. Atanasov, B. P., Mustafi, D. & Makinen, M. W. Protonation of the β -lactam nitrogen is the trigger event in the catalytic action of class A β -lactamases. *Proc. Natl. Acad. Sci. U. S. A.* **97**, 3160–3165 (2000).
189. Marciano, D. C., Brown, N. G. & Palzkill, T. Analysis of the plasticity of location of the Arg244 positive charge within the active site of the TEM-1 β -lactamase. *Protein Sci.* **18**, 2080–2089 (2009).
190. Michiyosi Nukaga, Christopher R. Bethel, Jodi M. Thomson, Andrea M. Hujer, Anne Distler, Vernon E. Anderson, James R. Knox, and R. A. B. Inhibition of Class A β -Lactamases by Carbapenems: Crystallographic Observation of Two Conformations of Meropenem in SHV-1. *Bone* **23**, 1–7 (2008).
191. Jelsch, C., Mourey, L., Masson, J. M. & Samama, J. P. Crystal structure of Escherichia coli TEM1 β lactamase at 1.8 Å resolution. *Proteins Struct. Funct. Bioinforma.* **16**, 364–383 (1993).
192. Ibuka, A. S. *et al.* Crystal structure of extended-spectrum beta-lactamase Toho-1: insights into the molecular mechanism for catalytic reaction and substrate specificity expansion. *Biochemistry* **42**, 10634–10643 (2003).
193. Sauvage, E. *et al.* Crystal structure of the mycobacterium fortuitum class a β -lactamase: Structural basis for broad substrate specificity. *Antimicrob. Agents Chemother.* **50**, 2516–2521 (2006).
194. Jensen, M. R. Capturing the structure of low-populated aromatic ring flipping intermediate. in *ICMRBS: Emerging Topics in Biomolecular Magnetic Resonance webinar 2021-05-13*
195. Schütz, A. K., Rennella, E. & Kay, L. E. Exploiting conformational plasticity in the AAA+ protein VCP/p97 to modify function. *Proc. Natl. Acad. Sci. U. S. A.* **114**, E6822–E6829 (2017).
196. Zimmerman, M. I. *et al.* Prediction of new stabilizing mutations based on mechanistic insights from Markov State Models. *ACS Cent. Sci.* **3**, 1311–1321 (2017).
197. Neu, H. C. The crisis in antibiotic resistance. *Science (80-.)*. **257**, 1064–1073 (1992).
198. Pastor, N., Piñero, D., Valdés, A. M. & Soberón, X. Molecular evolution of class A β lactamases: phylogeny and patterns of sequence conservation. *Mol. Microbiol.* **4**, 1957–1965 (1990).
199. Lim, H. M. & Pene, J. J. Mutations affecting the catalytic activity of Bacillus cereus 5/B/6 β -lactamase II. *J. Biol. Chem.* **264**, 11682–11687 (1989).
200. Little, C., Emanuel, E. L., Gagnon, J. & Waley, S. G. Identification of an essential glutamic acid residue in β -lactamase II from Bacillus cereus. *Biochem. J.* **233**, 465–469 (1986).
201. Horn, J. R. & Shoichet, B. K. Allosteric inhibition through core disruption. *J. Mol. Biol.* **336**, 1283–1291 (2004).
202. Miller, S., Janin, J., Lesk, A. M. & Chothia, C. Interior and surface of monomeric proteins. *J. Mol. Biol.* **196**, 641–656 (1987).
203. Navarro, S., Villar-Piqué, A. & Ventura, S. Selection against toxic aggregation-prone protein sequences in bacteria. *Biochim. Biophys. Acta - Mol. Cell Res.* **1843**, 866–874 (2014).
204. Pervushin, K., Riek, R., Wider, G. & Wüthrich, K. Attenuated T2 relaxation by mutual cancellation of dipole-dipole coupling and chemical shift anisotropy indicates an avenue to NMR structures of very large biological macromolecules in solution. *Proc. Natl. Acad. Sci. U. S. A.* **94**, 12366–12371 (1997).
205. Lavanya, P., Ramaiah, S. & Anbarasu, A. Cation- π interactions in β -lactamases: the role in structural stability. *Cell Biochemistry and Biophysics* **66**, 147–155 (2013).
206. Fonzé, E. *et al.* Crystal structures of the Bacillus licheniformis BS3 class a β -lactamase and of the acyl-enzyme adduct formed with cefoxitin. *Biochemistry* **41**, 1877–1885 (2002).
207. Smith, C. A., Caccamo, M., Kantardjieff, K. A. & Vakulenko, S. Structure of GES-1 at atomic resolution: Insights into the evolution of carbapenamase activity in the class A extended-spectrum β -lactamases. *Acta Crystallogr. Sect. D Biol. Crystallogr.* **63**, 982–992 (2007).
208. Kudlicki, W., Chirgwin, J., Kramer, G. & Hardesty, B. Folding of an enzyme into an active conformation while bound as peptidyl-tRNA to the ribosome. *Biochemistry* **34**, 14284–14287 (1995).
209. Javed, A., Christodoulou, J., Cabrita, L. D. & Orlova, E. V. The ribosome and its role in protein folding: Looking through a magnifying glass. *Acta Crystallogr. Sect. D Struct. Biol.* **73**, 509–521 (2017).
210. Mcgaughey, G. B., Gagne, M. & Rappe, A. K. π -Stacking interactions. Alive and well in proteins. *Biol. Chem.* **273**, 15458–15463 (1998).
211. Zondlo, N. J. Aromatic-Proline interactions: Electronically tubale CH/ π i interactions. *Acc Chem Res.* **46**, 1039–1049 (2013).
212. Lada Biedermannova, Kevin E. Riley, Karel Berka, P. H. and J. V. Another role of proline: stabilization interactions in proteins and protein complexes concerning proline and tryptophan. *Phys. Chem. Chem. Phys.* **10**, 2581–2583 (2008).
213. St-Jean, M., Izard, T. & Sygusch, J. A hydrophobic pocket in the active site of glycolytic aldolase mediates interactions with Wiskott-Aldrich syndrome protein. *J. Biol. Chem.* **282**, 14309–14315 (2007).
214. Black, K. M., Clark-Lewis, I. & Wallace, C. J. A. Conserved tryptophan in cytochrome c: Importance of the unique side-chain features of the indole moiety. *Biochem. J.* **359**, 715–720 (2001).
215. Ptitsyn, O. B. Molten globule and protein folding. *Adv. Protein Chem.* **47**, 83–229 (1995).
216. Ptitsyn, O. B. & Semisotnov, G. V. Evidence for a molten globule state as a general intermediate in protein folding. **262**, 1–5 (2001).
217. Yon, J. M. Protein folding: A perspective for biology, medicine and biotechnology. *Brazilian J. Med. Biol. Res.* **34**, 419–435 (2001).
218. Shiber, A. & Ravid, T. Chaperoning proteins for destruction: Diverse roles of Hsp70 chaperones and their co-chaperones in targeting misfolded proteins to the proteasome. *Biomolecules* **4**, 704–724 (2014).
219. Esser, C., Alberti, S. & Höhfeld, J. Cooperation of molecular chaperones with the ubiquitin/proteasome system. *Biochim. Biophys. Acta - Mol. Cell Res.* **1695**, 171–188 (2004).
220. Kettern, N., Dreiseidler, M., Tawo, R. & Höhfeld, J. Chaperone-assisted degradation: Multiple paths to destruction. *Biol. Chem.* **391**, 481–489 (2010).
221. Sherman MYu & Goldberg, A. L. Involvement of the chaperonin dnaK in the rapid degradation of a mutant protein in Escherichia coli. *EMBO J.* **11**, 71–77 (1992).
222. Kandror, O., Busconi, L., Sherman, M. & Goldberg, A. L. Rapid degradation of an abnormal protein in Escherichia coli involves the chaperones GroEL and GroES. *J. Biol. Chem.* **269**, 23575–23582 (1994).
223. Artimo, P. *et al.* ExPASy: SIB bioinformatics resource portal. *Nucleic Acids Res.* **40**, 597–603 (2012).
224. Newman, J. *et al.* Towards rationalization of crystallization screening for small- To medium-sized academic laboratories: The PACT/JCSG+ strategy. *Acta Crystallogr. Sect. D Biol. Crystallogr.* **61**, 1426–1431 (2005).

225. Svensson, O., Gilski, M., Nurizzo, D. & Bowler, M. W. Multi-position data collection and dynamic beam sizing: recent improvements to the automatic data-collection algorithms on MASSIF-1. *Acta Crystallogr. Sect. D Struct. Biol.* **74**, 433–440 (2018).
226. Kabsch, W. XDS. *Acta Crystallogr. Sect. D Biol. Crystallogr.* **66**, 125–132 (2010).
227. Evans, P. R. An introduction to data reduction: Space-group determination, scaling and intensity statistics. *Acta Crystallogr. Sect. D Biol. Crystallogr.* **67**, 282–292 (2011).
228. Winn, M. D. *et al.* Overview of the CCP4 suite and current developments. *Acta Crystallogr. Sect. D Biol. Crystallogr.* **67**, 235–242 (2011).
229. Chen, V. B. *et al.* MolProbity: All-atom structure validation for macromolecular crystallography. *Acta Crystallogr. Sect. D Biol. Crystallogr.* **66**, 12–21 (2010).
230. Joosten, R. P., Long, F., Murshudov, G. N. & Perrakis, A. The PDB-REDO server for macromolecular structure model optimization. *IUCrJ* **1**, 213–220 (2014).
231. Sobolev, O. V. *et al.* A global Ramachandran score identifies protein structures with unlikely stereochemistry. *Structure* **28**, 1249–1258.e2 (2020).
232. Vakulenko, S. B. *et al.* Effects on substrate profile by mutational substitutions at positions 164 and 179 of the class A TEM(pUC19) β -lactamase from Escherichia coli. *J. Biol. Chem.* **274**, 23052–23060 (1999).
233. Casthanheira, M. *et al.* Analyses of a ceftazidime-avibactam-resistant Citrobacter population and reversible genotype. *Mosphere* **3**, 1–8 (2018).
234. Thomas, V. L. *et al.* Structural consequences of the inhibitor-resistant Ser130Gly substitution in TEM beta-lactamase. *Biochemistry* **44**, 9330–9338 (2005).
235. Levitt, P. S. *et al.* Exploring the role of a conserved class A residue in the Ω -loop of KPC-2 β -lactamase: A mechanism for ceftazidime hydrolysis. *J. Biol. Chem.* **287**, 31783–31793 (2012).
236. Nitanaï, Y. *et al.* The catalytic efficiency (kcat/Km) of the class A β -lactamase Toho-1 correlates with the thermal stability of its catalytic intermediate analog. *Biochim. Biophys. Acta - Proteins Proteomics* **1804**, 684–691 (2010).
237. Majiduddin, F. K. & Palzkill, T. An analysis of why highly similar enzymes evolve differently. *Genetics* **163**, 457–466 (2003).
238. Winkler, M. L., Papp-Wallace, K. M. & Bonomo, R. A. Activity of ceftazidime/avibactam against isogenic strains of Escherichia coli containing KPC and SHV β -lactamases with single amino acid substitutions in the Ω -loop. *J. Antimicrob. Chemother.* **70**, 2279–2286 (2015).
239. Patel, M. P. *et al.* The drug-resistant variant P167S expands the substrate profile of CTX-M β -lactamases for oxyimino-cephalosporin antibiotics by enlarging the active site upon acylation. *Biochemistry* **56**, 3443–3453 (2017).
240. Barnes, M. D. *et al.* Klebsiella pneumoniae carbapenemase-2 (KPC-2), substitutions at Ambler position Asp179, and resistance to ceftazidime-avibactam: unique antibiotic-resistant phenotypes emerge from β -lactamase protein engineering. *MBio* **8**, (2017).
241. Herzberg, O., Kapadia, G., Blanco, B., Smith, T. S. & Coulson, A. Structural basis for the inactivation of the P54 mutant of β -lactamase from Staphylococcus aureus PC1. *Biochemistry* **30**, 9503–9509 (1991).
242. Bush, K. β -Lactamase inhibitors from laboratory to clinic. *Clin. Microbiol. Rev.* **1**, 109–123 (1988).
243. Lee, N., Yuen, K.-Y. & Kumana, C. R. Clinical role of β -lactam/ β -lactamase inhibitor combinations. *Drugs* **63**, 1511–24 (2003).
244. Reading, C. & Cole, M. Clavulanic acid: a β -lactamase-inhibiting β -lactam from Streptomyces clavuligerus. *Antimicrob. Agents Chemother.* **11**, 852–857 (1977).
245. English, A. R., Retsema, J. A., Girard, A. E., Lynch, J. E. & Barth, W. E. CP-45,899, a β -lactamase inhibitor that extends the antibacterial spectrum of β -lactams: Initial bacteriological characterization. *Antimicrob. Agents Chemother.* **14**, 414–419 (1978).
246. Scholar, E. Sulbactam. in (eds. Enna, S. J. & Bylund, D. B. B. T. C. P. R.) 1–5 (Elsevier, 2007). doi:https://doi.org/10.1016/B978-008055232-3.62687-X
247. Therrien, C. & Levesque, R. C. Molecular basis of antibiotic resistance and β -lactamase inhibition by mechanism-based inactivators: perspectives and future directions. *FEMS Microbiol. Rev.* **251**–262 (2000).
248. Elings, W. *et al.* Phosphate promotes the recovery of Mycobacterium tuberculosis β -lactamase from clavulanic acid inhibition. *Biochemistry* **56**, 6257–6267 (2017).
249. Wang, F., Cassidy, C. & Sacchettini, J. C. Crystal structure and activity studies of the Mycobacterium tuberculosis β -lactamase reveal its critical role in resistance to β -lactam antibiotics. *Antimicrob. Agents Chemother.* **50**, 2762–2771 (2006).
250. van Beusekom, L. M. J. Improving protein structure with homology-based information and prior knowledge. (Utrecht University, 2019).
251. Winkler, M. L. *et al.* Design and exploration of novel boronic acid inhibitors reveals important interactions with a clavulanic acid-resistant sulfhydryl-variable (SHV) β -lactamase. *J. Med. Chem.* **56**, 1084–1097 (2013).
252. Zou, T., Risso, V. A., Gavira, J. A., Sanchez-Ruiz, J. M. & Ozkan, S. B. Evolution of conformational dynamics determines the conversion of a promiscuous generalist into a specialist enzyme. *Mol. Biol. Evol.* **32**, 132–143 (2015).
253. Firnberg, E., Labonte, J. W., Gray, J. J. & Ostermeier, M. A comprehensive, high-resolution map of a Gene's fitness landscape. *Mol. Biol. Evol.* **31**, 1581–1592 (2014).
254. Steinberg, B. & Ostermeier, M. Shifting fitness and epistatic landscapes reflect trade-offs along an evolutionary pathway. *J. Mol. Biol.* **428**, 2730–2743 (2016).
255. Otting, G. Protein NMR using paramagnetic ions. *Annu. Rev. Biophys.* **39**, 387–405 (2010).
256. Keizers, P. H. J. & Ubbink, M. Paramagnetic tagging for protein structure and dynamics analysis. *Prog. Nucl. Magn. Reson. Spectrosc.* **58**, 88–96 (2011).
257. Clore, G. M. & Iwahara, J. Theory, practice, and applications of paramagnetic relaxation enhancement for the characterization of transient low-population states of biological macromolecules and their complexes. *Chem. Rev.* **109**, 4108–4139 (2009).
258. Commandeur, S. *et al.* Zebrafish embryo model for assessment of drug efficacy on Mycobacterial persisters. *Antimicrob. Agents Chemother.* **64**, (2020).
259. Habjan, E. *et al.* Anti-tuberculosis compound screen using a zebrafish infection model identifies an aspartyl-tRNA synthetase inhibitor. *Dis. Model. Mech.* (2021). doi:10.1242/dmm.049145

260. Cheng, T., Kam, J. Y., Johansen, M. D. & Oehlers, S. H. High content analysis of granuloma histology and neutrophilic inflammation in adult zebrafish infected with *Mycobacterium marinum*. *Micron* **129**, 102782 (2020).
261. Moreira, J. D. *et al.* Functional inhibition of host histone deacetylases (HDACs) enhances in vitro and in vivo anti-mycobacterial activity in human macrophages and in zebrafish. *Front. Immunol.* **11**, 36 (2020).
262. Changeux, J.-P. Allosteric and the Monod-Wyman-Changeux model after 50 years. *Annu. Rev. Biophys.* **41**, 103–133 (2012).
263. Petrović, D., Risso, V. A., Kamerlin, S. C. L. & Sanchez-Ruiz, J. M. Conformational dynamics and enzyme evolution. *J. R. Soc. Interface* **15**, (2018).
264. Elings, W. *et al.* β -Lactamase of mycobacterium tuberculosis shows dynamics in the active site that increase upon inhibitor binding. *Antimicrob. Agents Chemother.* **64**, (2020).

Summary

The subject of enzyme evolution has been a popular topic for decades because it conveys information about fundamental evolutionary principles and is useful for a variety of research areas, such as protein engineering and antibiotic resistance. Evolution acts via mutations in amino acid sequences, but substitution of essential amino acids can lead to a nonfunctional protein. Thus, the number of essential residues is limited by evolutionary pressure. From this notion the question arises which critical roles the remaining essential residues play. In this work an enzyme from *Mycobacterium tuberculosis*, β -lactamase BlaC, is used as a model protein to formulate the principles of amino-acid conservation. β -Lactamases are ancient proteins, which are extremely evolvable and therefore are widely used in evolutionary research. An introduction to protein evolution and β -lactamases is provided in chapter 1 of this thesis.

The roles of all non-catalytic essential residues in class A β -lactamases are discussed in chapter 2 of this thesis. It is demonstrated that residues close to the active site (second shell) and farther away (third shell) have different reasons for being essential. Substitutions introduced to the residues of the second shell are followed by the changes in stability and especially activity, showing their influence on the integrity of the active site. The active site exhibits high correlation and mutations in the second-shell residues lead to a changes sensed throughout the entire core of the protein. On the other hand, substitutions in the residues of the third shell result in a dramatic effect on the protein production, indicating the importance of these residues for the integrity of the overall protein structure. The protein frame exhibits low correlation. The structural changes are very localized and conservative mutations are preferable for the preservation of protein function.

These general patterns are supported with more focused studies of specific functions for several second- and third-shell residues. In chapter 3, a characterization of a triad of the second-shell residues of BlaC, Asn214-Asp233-Asp246 is presented. It is proposed that this triad is involved in the positioning of active site residues Thr216 and Arg220. Substitutions in Asn214, Asp233 or Asp246 affect the activity of the enzyme and lead to population of a second conformation of the enzyme, according to NMR data. We hypothesize that the substitutions enhance the mobility of a small α -helix that causes displacement of active site residues Thr216 and Arg220. Comparison of the sequences of class A β -lactamases shows that in enzymes in which the triad is not conserved adaptations are present to ensure the positioning of the active site residues in another way, a demonstration of co-evolution of residues.

The extensive characterization of the effects of the substitutions in the third-shell residues is presented in chapter 4. A severe decrease in the production of soluble, folded protein upon mutations in Glu37 and Trp229 is observed. However, the folded fraction is demonstrated to

be kinetically and structurally similar to wild type BlaC. The high conservation of these two residues is attributed to their involvement in the folding process.

Despite extreme conservation, some residues are shown to tolerate mutations. For two residues Asp179 and Asn245 some mutations are even found to improve phenotype. This is unexpected, because highly conserved residues are considered optimized by evolution. Chapter 5 provides a deeper characterization of mutants of both residues. Several substitutions of Asn245 result in elevated resistance to the β -lactamase inhibitor avibactam, which can be the consequence of an altered binding site. For BlaC D179N higher survivability can be attributed to a more stable enzyme. Thus, it appears that Asp is not the optimal residue at position 179 and may be considered an evolutionary rudiment in BlaC, because Asp179 seems to be optimal in other members of the enzyme family.

The subject of this study, BlaC, is of high medical relevance, as this enzyme from *Mycobacterium tuberculosis* is the main reason β -lactam antibiotics are not widely used to treat tuberculosis. The problem of antibiotic resistance was addressed by introduction of β -lactamase inhibitors, however, the reports of inhibitor-resistance variants found in laboratory set-up indicate the need to find a new solution. Insights into evolutionary pathways that cannot be taken by this enzyme due to essentiality of some residues, might lead to a new design of antibiotics or inhibitors to which resistance is not readily possible by mutations. Thus, understanding of inhibitor resistance mechanisms in BlaC is important. In chapter 6 of this thesis structural changes in inhibitor-resistant BlaC variants identified in the Ubbink group are discussed. Two BlaC variants displayed modifications in the binding site that are responsible for changed specificity of these mutants.

Chapter 7 offers an overview of this work and raises a few questions that remain unaddressed. This study aimed to contribute to our understanding of protein evolution and patterns of conservation of the non-essential residues. These insights are generally applicable to enzymes. In the case of β -lactamases, which are responsible for resistance against β -lactam antibiotics, understanding essentiality of residues can help prevent enzyme evolution against β -lactamase inhibitors, enhancing combination therapies.

Samenvatting

De evolutie van enzymen blijft al tientallen jaren een populair onderwerp voor onderzoek omdat het fundamentele evolutionaire principes aan het licht brengt en nuttig is voor diverse onderzoeksgebieden, zoals eiwit engineering en antibioticumresistentie. Evolutie werkt via aminozuurmutaties, maar substitutie van essentiële aminozuren kan tot een niet-functioneel eiwit leiden. Het is dus aannemelijk dat als gevolg van evolutionaire druk het aantal essentiële residuen wordt geminimaliseerd. Het is een vraag wat de rollen zijn van de residuen die geconserveerd zijn. Een enzym van *Mycobacterium tuberculosis*, β -lactamase (BlaC), wordt in dit werk gebruikt als een modeleiwit om de principes van aminozuurconservering te formuleren. β -Lactamases zijn eiwitten die lang geleden zijn ontstaan en die extreem evolueerbaar zijn en daarom vaak worden gebruikt in evolutionair onderzoek. Een inleiding tot eiwitevolutie en β -lactamases wordt gegeven in hoofdstuk 1 van dit proefschrift.

Hoofdstuk 2 beschrijft de rollen van alle niet-katalytische zeer geconserveerde residuen van klasse A β -lactamases. Er wordt aangetoond dat residuen rond de actieve plek (tweede schil) en verder weg (derde schil) verschillende redenen hebben om geconserveerd te zijn. Substituties in aminozuurresiduen van de tweede schil leiden tot veranderingen in eiwitstabiliteit en vooral activiteit, wat wijst op hun invloed op de integriteit van de actieve plek. Wijzingen in de residuen van de tweede schil worden door de gehele eiwitkern waargenomen, wat wijst op een hoge structurele correlatie in de actieve plek. Anderzijds resulteren substituties in aminozuurresiduen van de derde schil in een drastisch effect op de eiwitproductie, wat aangeeft dat deze residuen voor de integriteit van de algehele eiwitstructuur belangrijk zijn. De structurele veranderingen zijn beperkt tot de plek van de mutatie en conservatieve mutaties hebben het minste effect op de structuur. Deze resultaten geven aan dat aminozuren in de derde schil een lage structurele correlatie vertonen.

Deze algemene patronen worden ondersteund met gedetailleerd onderzoek van specifieke functies van enkele residuen van de tweede en derde schil. Hoofdstuk 3 beschrijft de karakterisering van de geconserveerde triade Asn214-Asp233-Asp246 in de tweede schil. Er wordt voorgesteld dat deze triade in BlaC een rol speelt in de juiste positionering van de actieve-plek residuen Thr216 en Arg220. Mutaties van Asn214, Asp233 of Asp246 beïnvloeden eiwitactiviteit en, volgens inzichten op grond van NMR gegevens, leiden tot populatie van een andere enzymconformatie. Als verklaring wordt voorgesteld dat de substituties de mobiliteit van een kleine α -helix versterken, met de verplaatsing van actieve-plek residuen Thr216 en Arg220 tot gevolg. Vergelijking van de sequenties van klasse A β -lactamases demonstreert dat in enzymen waarin de triade niet geconserveerd is, aanpassingen aanwezig zijn om de positionering van de actieve-plek residuen op een andere manier te verzekeren, een voorbeeld van co-evolutie van residuen.

Een uitgebreide karakterisering van effecten van substituties in de derde-schil residuen wordt gepresenteerd in hoofdstuk 4. Een grote vermindering van de productie van oplosbaar, gevouwen eiwit wordt waargenomen na het introduceren van mutaties in Glu37 of Trp229. De gevouwen fractie is qua activiteit en structuur vergelijkbaar met wildtype BlaC. De hoge conservering van deze twee residuen wordt toegeschreven aan hun rol in de eiwitvouwing.

Ondanks hun extreme conservering laten sommige residuen mutaties toe zonder functieverlies. Voor twee residuen, Asp179 en Asn245, kunnen sommige mutaties zelfs tot het verbeteren van het fenotype leiden. Dit is onverwacht, aangezien geconserveerde residuen als evolutionair geoptimaliseerd beschouwd worden. In hoofdstuk 5 wordt een uitvoeriger karakterisering van mutanten van beide residuen besproken. Sommige substituties in Asn245 leiden tot verlaagde gevoeligheid voor de β -lactamaseremmer avibactam, een mogelijke uitkomst van veranderingen in de bindingsplek. Verhoogde functionaliteit van de BlaC D179N mutant kan worden toegeschreven aan verhoogde stabiliteit van het enzym. Het is aldus mogelijk dat Asp niet een optimaal residu is op positie 179, zodat het dus als een evolutionair rudiment beschouwd moet worden, omdat Asp179 optimaal lijkt te zijn voor andere klasse A β -lactamases.

BlaC is van medisch belang, aangezien dit enzym de reden is dat β -lactam-antibiotica niet gebruikt worden voor de behandeling van tuberculose. De opkomst van antibioticaresistentie werd opgelost door introductie van β -lactamaseremmers, maar de meldingen van mutanten met remmersresistentie geven aan dat er een nieuwe oplossing nodig is. Inzichten in evolutionaire paden die vanwege de onmisbaarheid van sommige residuen niet kan worden genomen, kunnen leiden tot een nieuw antibioticumontwerp waarvoor resistentie door mutatie niet meer mogelijk is. Daarom is kennis van remmersresistentie mechanisme in BlaC zeer cruciaal. Hoofdstuk 6 van dit proefschrift presenteert structurele veranderingen in remmer-resistente mutanten van BlaC gevonden in de Ubbink groep. Twee BlaC varianten vertonen wijzigen in de actieve plek die verantwoordelijk zijn voor de veranderde specificiteit van deze mutanten.

Hoofdstuk 7 geeft een overzicht van dit onderzoek en wijst op enkele vragen die onbeantwoord blijven. Het doel van dit werk was om bij te dragen aan onze kennis van eiwitevolutie en patronen van de conservering van niet-essentiële residuen. Die inzichten gelden voor enzymen in het algemeen. In het geval van β -lactamases, die verantwoordelijk zijn voor resistentie tegen β -lactam antibiotica, is het van belang de rol van essentiële residuen te begrijpen om enzymevolutie tegen β -lactamaseremmers te voorkomen, wat combinatietherapie kan verbeteren.

Curriculum Vitae

Aleksandra Chikunova was born on January 25th 1993 in Moscow, Russia. In 2010 she started her higher education in Russian National Research Medical University, and she graduated with honors in 2016 with a Specialist's degree in Medical Biochemistry. During her education she has worked in a clinic as a laboratory assistant in a PCR department and realized that she is more interested in fundamental aspects of biochemistry rather than medical. Therefore, she started her research work in the group of Prof. dr. Mark Rosenfeld in the Institute of Biochemical Physics, where she was involved in the projects on protein coatings on magnetic nanoparticles and oxidative modification of plasma proteins. In 2016 she moved to the Netherlands and joined the group of Prof. dr. Marcellus Ubbink in Leiden University as a PhD student. For her PhD she worked on β -lactamase BlaC. Aleksandra is now a Post-doctoral researcher in the Ubbink group focusing on structural studies of BlaC and BCX.

List of Publications

Chikunova, A., Manley, M. P., Ud Din Ahmad, M., Bilman, T., Perrakis, A. and Ubbink, M. (2021) Conserved residues Glu37 and Trp229 play an essential role in protein folding of β -lactamase. *FEBS J.* 288, 5708-5722

van Alen, I., Chikunova, A., Safeer, A.A., Ud Din Ahmad, M., Perrakis, A. and Ubbink, M. (2021). The G132S mutation enhances the resistance of *Mycobacterium tuberculosis* β -lactamase against sulbactam. *Biochemistry.* 60, 2236-2245

Elings, W., Chikunova, A., van Zanten, D.B., Drenth, R., Ud Din Ahmad, M., Blok, A.J., Timmer, M., Perrakis, A., Ubbink, M. (2021). Two β -Lactamase variants with reduced clavulanic acid inhibition display different millisecond dynamics. *Antimicrob Agents Chemother.* 65, e0262820

Chikunova, A., Ubbink, M. (2022) The roles of highly conserved, non-catalytic residues in class A β -lactamases. *Protein Science*, in production. DOI: 10.1002/Pro.4328

Chikunova, A., Colle, L.M., Hensgens, M.N., Malaj, S., Ubbink, M. The N214-D233-D246 motif is essential for correct positioning of the active site residues in BlaC. **Manuscript to be submitted.**

Chikunova, A., van Alen, I., van Zanten, D.B., de Block, A.A., Ubbink, M. Mutations in two highly conserved residues are beneficial for BlaC. **Manuscript to be submitted.**

Publication from previous research work:

Vasilyeva, A.D., Bychkova, A.V., Bugrova, A.E., Indeykina, M.I., Chikunova, A.P., Leonova, V.B., Kostanova, E.A., Biryukova, M.I., Konstantinova, M.L., Kononikhin, A.S., Nikolaev, E.N., Rosenfeld, M.A. (2017). Modification of the catalytic subunit of plasma fibrin-stabilizing factor under induced oxidation. *Dokl Biochem Biophys.* 472, 40-43